

**Data Release Report for Source Physics Experiment 1
(SPE-1)
Nevada National Security Site**

April 2014

Prepared for:

U.S. Department of Energy
National Nuclear Security Administration
Defense Nuclear Nonproliferation Research and Development
National Center for Nuclear Security

Compiled by:

Margaret Townsend and Jennifer Mercadante

Underground Test Area and Boreholes Programs and Operations
National Security Technologies, LLC
Las Vegas, Nevada

DISCLAIMER STATEMENT

Reference herein to any specific commercial product, process, or service by trade name, trademark, manufacturer, or otherwise, does not necessarily constitute or imply its endorsement, recommendation, or favoring by the U.S. Government or any agency thereof or its contractors or subcontractors.

AVAILABILITY STATEMENT

Available for sale to the public, in paper, from—

U.S. Department of Commerce
National Technical Information Service
5301 Shawnee Road
Alexandria, VA 22312
Telephone: 800.553.6847
Fax: 703.605.6900
E-mail: orders@ntis.gov
Online ordering: <http://www.ntis.gov/help/ordermethods.aspx>

Available electronically at <http://www.osti.gov/bridge>.

Available for a processing fee to U.S. Department of Energy and its contractors, in paper, from—

U.S. Department of Energy
Office of Scientific and Technical Information
P.O. Box 62
Oak Ridge, TN 37831-0062
Telephone: 865.576.8401
Fax: 865.576.5728
E-mail: reports@adonis.osti.gov

Data Release Report for Source Physics Experiment 1 (SPE-1) Nevada National Security Site

Compiled by:
Margaret Townsend and Jennifer Mercadante
National Security Technologies, LLC

March 2014

Distributed by:
*Incorporated Research Institutions for Seismology
Data Management Center
1408 NE 45th Street, Suite 201
Seattle, Washington 98105 USA
www.iris.washington.edu*

The near-field data are found in Assembled Data Set 14-017, which also includes this report. The far-field data were submitted directly using the Nevada Seismological Laboratory's "SN" network code and merged directly in the IRIS archive.

Citation Reference: National Security Technologies, LLC, 2014. *Data Release Report for Source Physics Experiment 1 (SPE-1), Nevada National Security Site*. Technical Report DOE/NV/25946--2018, 197 pages. Las Vegas, NV.

Source Physics Experiment-1

Principal Investigators:

Lawrence Livermore National Laboratory

Tarabay Antoun Robert Mellors William Walter

Los Alamos National Laboratory

Christopher Bradley Wendee Brunish
Howard Patton David Steedman

Sandia National Laboratories

Robert Abbott

Defense Threat Reduction Agency

Kiran Shah

Air Force Technical Applications Center

Chandan Saikia

National Security Technologies, LLC

Catherine Snelson*

Other Major Contributors:

Lawrence Livermore National Laboratory

Sean Ford Ilya Lomov
Lew Glenn Robert Mellors
Phil Harben Artie Rodgers
J. P. Lewis Oleg Vorbiev

Los Alamos National Laboratory

David Coblenz Tom Sandoval
Earl Knight Emily Schultz-Fellenz
Esteban Rougier Aviva Sussman

Sandia National Laboratories

Scott Broome

Nevada Seismological Laboratory, University of Nevada, Reno

Ken Smith Gabe Plank

National Security Technologies, LLC

Margaret Townsend Robert White

*Now at Los Alamos National Laboratory

Executive Summary

The first Source Physics Experiment shot (SPE-1) was conducted in May 2011. The explosive source was a ~100-kilogram TNT-equivalent chemical set at a depth of 60 meters. It was recorded by an extensive set of instrumentation that includes sensors both at near-field (less than 100 meters) and far-field (more than 100 meters) distances. The near-field instruments consisted of three-component accelerometers deployed in boreholes around the shot and a set of single-component vertical accelerometers on the surface. The far-field network comprised a variety of seismic and acoustic sensors, including short-period geophones, broadband seismometers, three-component accelerometers, and rotational seismometers at distances of 100 meters to 25 kilometers. This report coincides with the release of these data for analysts and organizations that are not participants in this program. This report describes the first Source Physics Experiment and the various types of near-field and far-field data that are available.

This page intentionally left blank.

Table of Contents

Executive Summary	i
List of Appendices	iv
List of Figures	iv
List of Acronyms and Abbreviations	v
1 Introduction.....	1
1.1 Project Description.....	1
1.2 Test Description	1
1.3 Site Description.....	3
2 SPE-1 Test	3
2.1 Test Bed Construction.....	3
2.2 Geologic Characterization of the SPE-1 Test Bed.....	6
2.2.1 Geologic Setting.....	6
2.2.2 Data Collected.....	6
2.3 SPE-1 Test Description.....	8
2.3.1 Source	8
2.3.2 Diagnostic Instrumentation.....	8
2.3.3 Near-Field Instrumentation.....	8
2.3.4 Far-Field Instrumentation	11
3 Data Collection and Corrections.....	15
3.1 Near Field.....	15
3.1.1 Data Collection	15
3.1.2 Data Corrections	15
3.2 Far Field.....	17
4 Post-Experiment Procedures.....	18
4.1 Aggregation, Merging, and Archiving of SPE-1 Data.....	18
4.1.1 Data Aggregation	18
4.1.2 Merging of Data Sets	19
4.1.3 Data Archiving.....	21
5 Summary	23
6 Acknowledgements.....	23
7 References.....	23

List of Appendices

- 1 Source Hole and Instrument Hole Data
- 2 Instrument Metadata for SPE-1
- 3 Selected Metadata for SPE-1 Borehole Sensors
- 4 Selected Metadata for SPE-1 Surface Stations
- 5 *SPE-1 Baseline Shift Corrections*, LA-UR-13-23956, prepared by E. Rougier and D. Steedman, Los Alamos National Laboratory
- 6 *Review of Data from Source Physics Experiment-1: Data Corrections* (condensed version of Los Alamos National Laboratory Report LA-UR-22561 [2013] prepared by D. Steedman)

List of Figures

Number	Title	Page
1	Map Showing Location of the SPE-1 Site at the Nevada National Security Site	2
2	Aerial Photo of the SPE Phase I Test Bed Showing Locations of Source Hole and Instrument Holes	4
3	Sketch Showing Cut-Away View of SPE-1 Test Bed.....	5
4	Surface Geologic Map of the Climax Stock Area Showing Location of SPE-1 Site.....	7
5	Schematic Drawing Showing Placement of Explosives Canister and Stemming in the SPE-1 Source Hole.....	9
6	Section and Plan View Diagrams Showing Typical Gage Package Arrangement in Near-Field Instrument Holes for SPE-1	11
7	Location Map of Far-Field Instrumentation Layout	13
8	Map Showing Locations of Geophones Placed within Approximately 2 Kilometers of the SPE-1 Shot-point.....	14
9	Map Showing the Seven Infrasound Array Locations (Triangles) around Surface Ground Zero	16

List of Acronyms and Abbreviations

AFTAC	Air Force Technical Applications Center
cm	centimeter(s)
DTRA	Defense Threat Reduction Agency
E	east
ft	feet
Hz	hertz
IML-ST	Inter-Mountain Labs
IRIS	Incorporated Research Institutions for Seismology
kg	kilogram(s)
km	kilometer(s)
L	lateral
LANL	Los Alamos National Laboratory
LLNL	Lawrence Livermore National Laboratory
m	meter(s)
N	north
NNSS	Nevada National Security Site
NSL	Nevada Seismological Laboratory
PASSCAL	Program for Array Seismic Studies of the Continental Lithosphere
R	radial
SEED	Standard for the Exchange of Earthquake Data
SGZ	surface ground zero
S-HANFO	sensitized heavy ammonium nitrate and fuel oil
SNL	Sandia National Laboratories
SPC	State Plane Coordinates
SPE	Source Physics Experiment
T	tangential
TNT	trinitrotoluene
UNR	University of Nevada, Reno
Z	vertical

This page intentionally left blank.

1 Introduction

1.1 Project Description

A test bed for a series of chemical explosive tests known collectively as the Source Physics Experiment (SPE) was constructed in granitic rock of the Climax stock, in northern Yucca Flat at the Nevada National Security Site (NNSS; formerly known as the Nevada Test Site) in 2010–2011 (Figure 1). These tests are sponsored by the U.S. Department of Energy, National Nuclear Security Administration’s office of Defense Nonproliferation Research and Development. The SPE test series is designed to study the generation and propagation of seismic waves, and will provide data that will improve the predictive capability of numerical models for detecting and characterizing underground explosions (e.g., Ford and Walter, 2013; Snelson et al., 2012, 2013). These validated, improved seismic models and simulations will enhance the U.S. ability to detect and discriminate “low-yield” nuclear explosions.

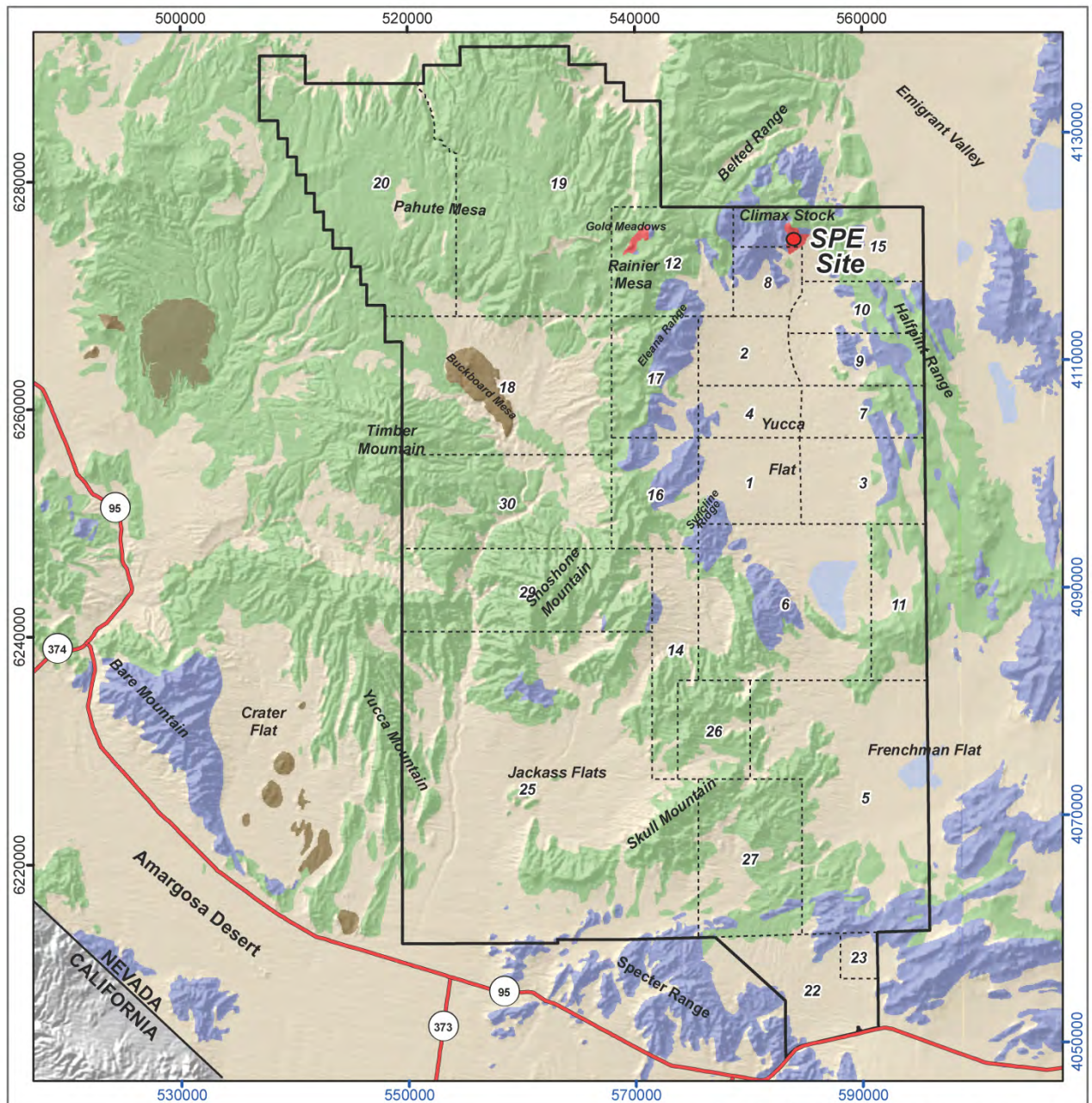
The SPE tests are designed and conducted by a consortium of organizations, including Los Alamos National Laboratory (LANL), Lawrence Livermore National Laboratory (LLNL), Sandia National Laboratories (SNL), and the Defense Threat Reduction Agency (DTRA), in conjunction with National Security Technologies, LLC (NSTec), the Management and Operations contractor at the NNSS. The University of Nevada, Reno (UNR) assisted in data collection and compilation. Other organizations, including the Air Force Technical Applications Center (AFTAC) and ENSCO, participated in data collection efforts as well.

The first SPE test (SPE-1) was conducted in May 2011. Two additional tests have since been conducted at this site, and new tests are being planned. The vast majority of data acquired under the SPE program is unclassified/unlimited but is subject to a 2-year hold, similar to the policy of the U.S. National Science Foundation. The SPE-1 time-dependent data (strong motion and seismo-acoustic) have now been released for public access. This report presents information that will aid in the proper understanding and use of the SPE-1 data sets.

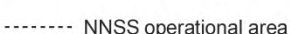
Contact Veraun Chipman, NSTec point of contact (chipmavd@nv.doe.gov), or Catherine M. Snelson, the SPE test scientist for this dataset, now at LANL (snelsonc@lanl.gov), for further information, including information about other data collected at the SPE site.

1.2 Test Description

The purpose of the SPE-1 test was to provide an initial simple shot that could serve as an approximate Green’s function for later tests. It was the first in a series of tests in the same hard-rock test bed (SPE Phase I). The test provided data for research and development of simulation capability at both near- and far-field distances. In general, the near field is expected to include inelastic nonlinear effects, while the far field can be considered primarily elastic (or visco-elastic). See a detailed description of the source in Section 2.3.



Nevada Central State Plane Projection (meters), North American Datum 1983
 Surface units from Nevada Bureau of Mines & Geology(1996)

- | | | | |
|---|---|---|-----------------------|
|  | Quaternary playa deposits |  | Highway |
|  | Pliocene & Quaternary basaltic rocks |  | NNSS boundary |
|  | Quaternary/Tertiary alluvial sediments |  | NNSS operational area |
|  | Tertiary volcanic rocks | | |
|  | Mesozoic granitic rocks | | |
|  | Paleozoic & Precambrian sedimentary rocks | | |



Black tick marks are in Nevada State Plane, Central Zone, NAD83, meters
 Blue tick marks are in Universal Transverse Mercator, NAD83, meters



April 2012

Figure 1
Map Showing Location of the SPE-1 Site at the Nevada National Security Site

A comprehensive set of strong-motion and seismo-acoustic instrumentation was deployed for SPE-1. The near-field (< 100 meters [m] from the shot point) instrumentation included high-sample-rate, three-component accelerometers deployed in boreholes. A set of single-component surface accelerometers was also installed. At distances greater than 100 m (far-field), a comprehensive set of seismic and acoustic sensors were deployed at distances up to 25 kilometers (km). The data and metadata were processed, archived, and distributed by the technical members of the Nevada Seismological Laboratory (NSL) at UNR. Records for stations at greater distances are available from the permanent UNR seismic network.

The full data set, along with associated metadata, is available from the Incorporated Research Institutions for Seismology (IRIS). The near-field data were assigned the assembled data set number 14-017 with the name “Source Physics Experiment 1.” The far-field data were submitted directly using NSL’s “SN” network code and were merged directly into the IRIS archive. This report is intended to complement the data set and provide ancillary information.

1.3 Site Description

The SPE test bed consists of a pad excavated and filled on the side of a hill that slopes to the southeast. The setting is weathered granite with a thin but variable cover of unconsolidated soil over bedrock. A 0.91-m-diameter source hole was drilled in the center of the test bed, and is surrounded by two rings of three 0.20-m diameter instrument holes. All holes were drilled to depths ranging from 57.9 to 60.7 m. The site is identified by the NNSS designator U-15n, with the source hole labeled U-15n, and instrument holes labeled U-15n#1 through U-15n#6.

The instrument holes in the inner ring (U-15n#1, #2, and #3) are each 10 m from the source hole, and positioned 120 degrees apart. The instrument holes in the outer ring (U-15n#4, #5, and #6) are each 20 m from the source hole and staggered so that they are 60 degrees off the positions of the holes in the inner ring. The placement of the instrument holes was determined from the position of a hole in the outer ring (U-15n#4), whose location was selected to coincide with one of the planned geophone lines.

2 SPE-1 Test

2.1 Test Bed Construction

The source hole was drilled to a depth of 60.7 m over a period of several months in late 2010 and early 2011. The six instrument holes were drilled in August and September 2010. See Appendix 1 for construction data for the U-15n source hole and six instrument holes. See Appendix C in Townsend et al. (2012) for detailed information about the construction of the holes at the SPE site. Figure 2 shows an aerial view of the SPE test bed with the locations of the source hole and instrument holes marked. See Figure 3 for graphic representation of the SPE-1 test bed.

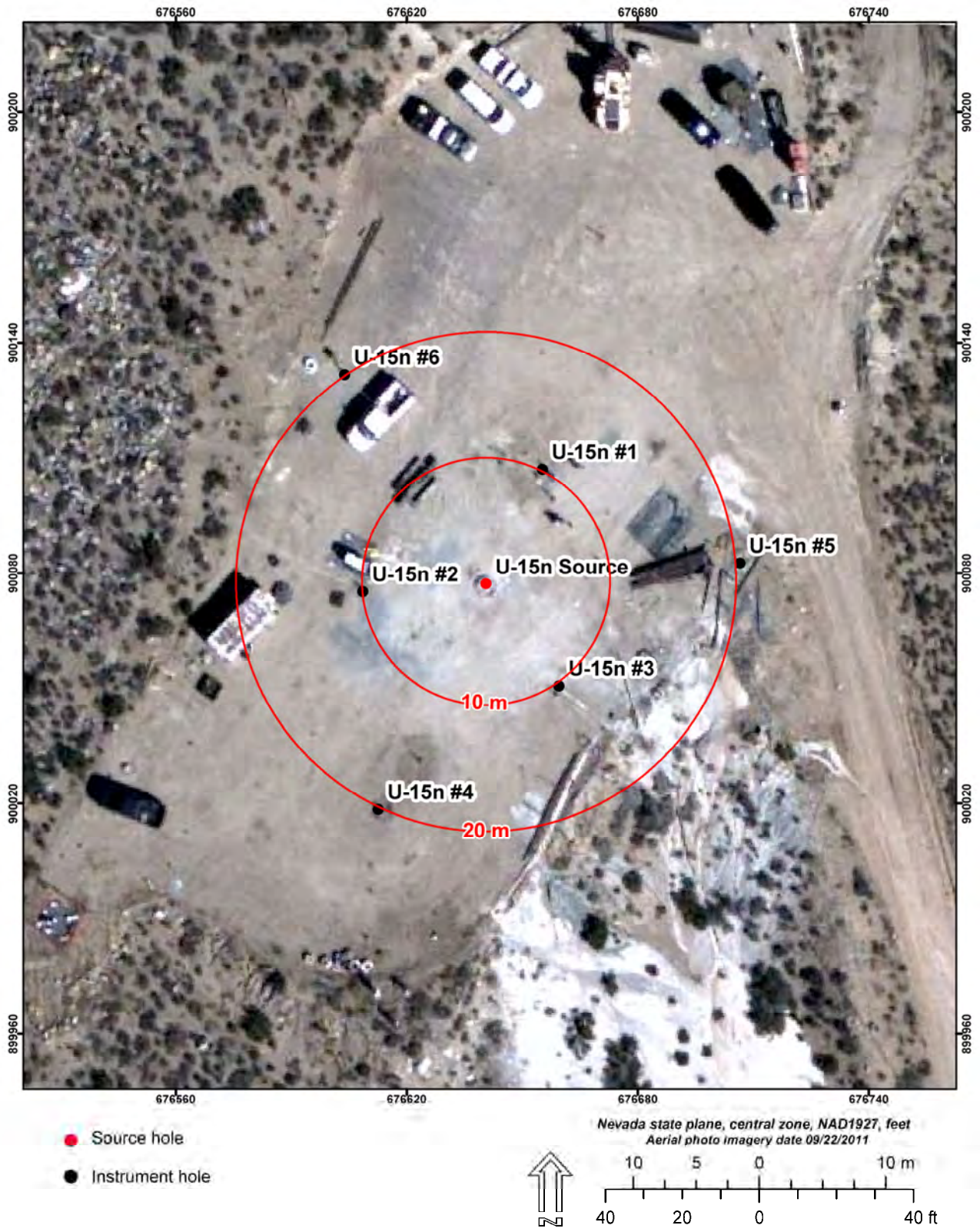


Figure 2
Aerial Photo of the SPE Phase I Test Bed Showing Locations of
Source Hole and Instrument Holes

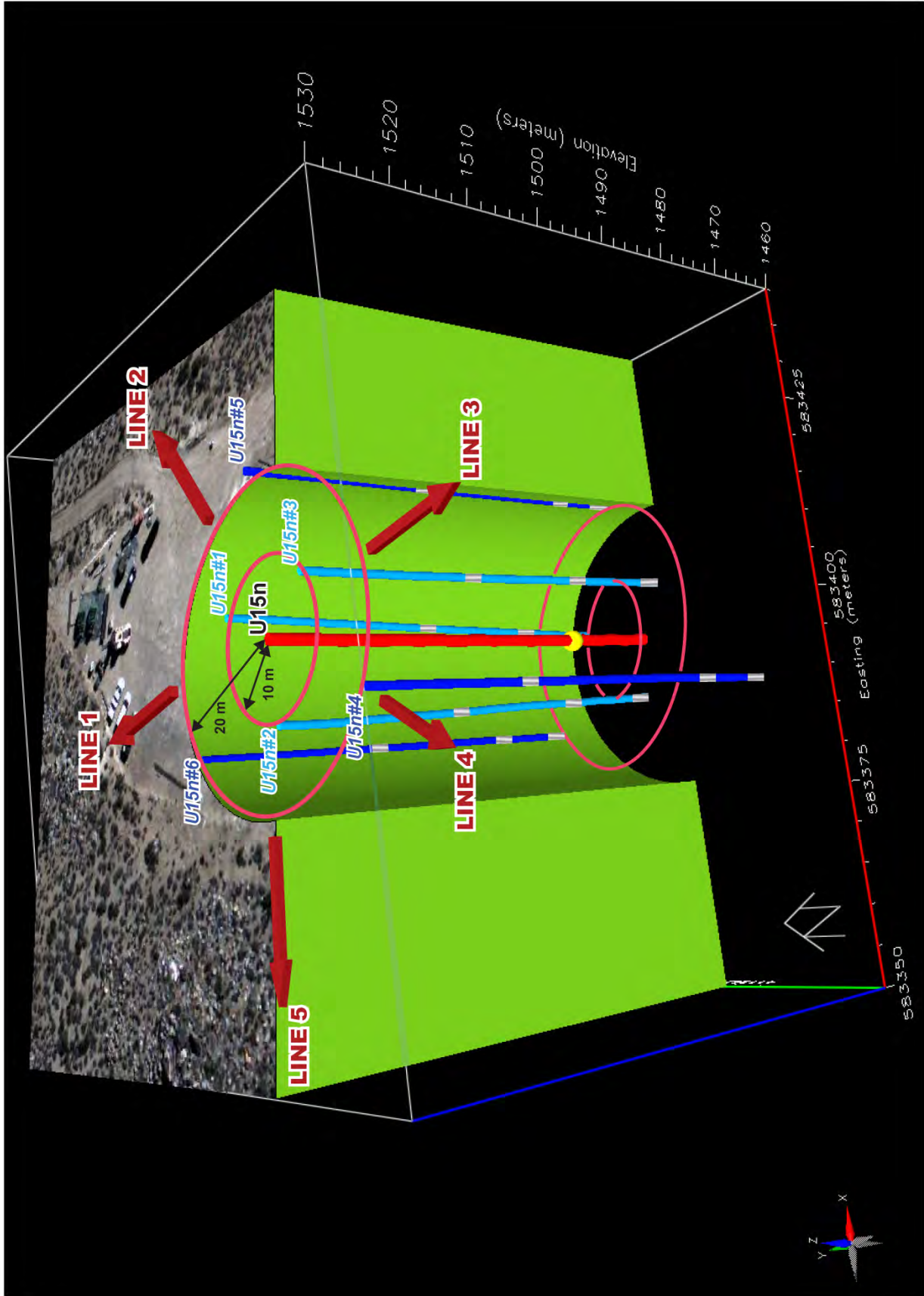


Figure 3
Sketch Showing Cut-Away View of SPE-1 Test Bed

2.2 Geologic Characterization of the SPE-1 Test Bed

The Climax stock was selected as the site of the first set of SPE tests because its granite lithology provides a relatively “homogenous” medium and because, as the site of three historical underground nuclear tests, abundant geologic, seismic, and ground shock data are available for comparison to expected SPE test data.

2.2.1 Geologic Setting

The Climax stock is a composite granitic intrusive of Cretaceous age, which intrudes sedimentary rocks of Paleozoic and Precambrian age. The granite body is exposed at the base of Oak Spring Butte, in extreme northern Yucca Flat (Figure 4). The surface exposures of the granite are weathered to depths ranging from about 7.6 to 38.1 m (Townsend et al., 2012).

The Climax stock is moderately to highly fractured. Three major faults define the structure of the Climax area, the Tippinip fault on the west and the Boundary and Yucca faults on the east and south. The SPE site is located approximately 245 m northwest, at closest approach, from the Boundary fault, which separates the surface exposure of the granitic rocks from the alluvium of the Yucca Flat basin. The Boundary fault dips steeply to the southeast, and offset on it is inferred from gravity data to be approximately 245 m down to the east near the SPE site. The offset apparently decreases to the northeast along the fault trace, as it approaches the junction with the Yucca fault to become the Butte fault (Orkild et al, 1983).

2.2.2 Data Collected

A core hole was drilled in granite (quartz monzonite) from the ground surface to the depth of 60 m at the location of the source hole, and drill cuttings were collected during drilling of the six boreholes drilled for instrumentation. Data summarized in this section is from Townsend et al. (2012), where additional information can be found.

A suite of geophysical logs (listed below) was run in the core hole and all six instrument holes to characterize the hole and surrounding rock.

- Caliper
- Deviation
- Natural Gamma
- Resistivity (core hole only)
- Full-wave Sonic/Travel Time
- Acoustic Televiewer
- Optical Televiewer (instrument holes only)

Physical and mechanical properties were measured by SNL on samples from the core hole, as listed below (Broome and Pfeifle, 2011).

- Bulk density
- Unconfined compressive strength
- Compressional and shear wave velocity
- Direct shear
- Triaxial shear
- Triaxial compression
- Dynamic Brazilian Tension

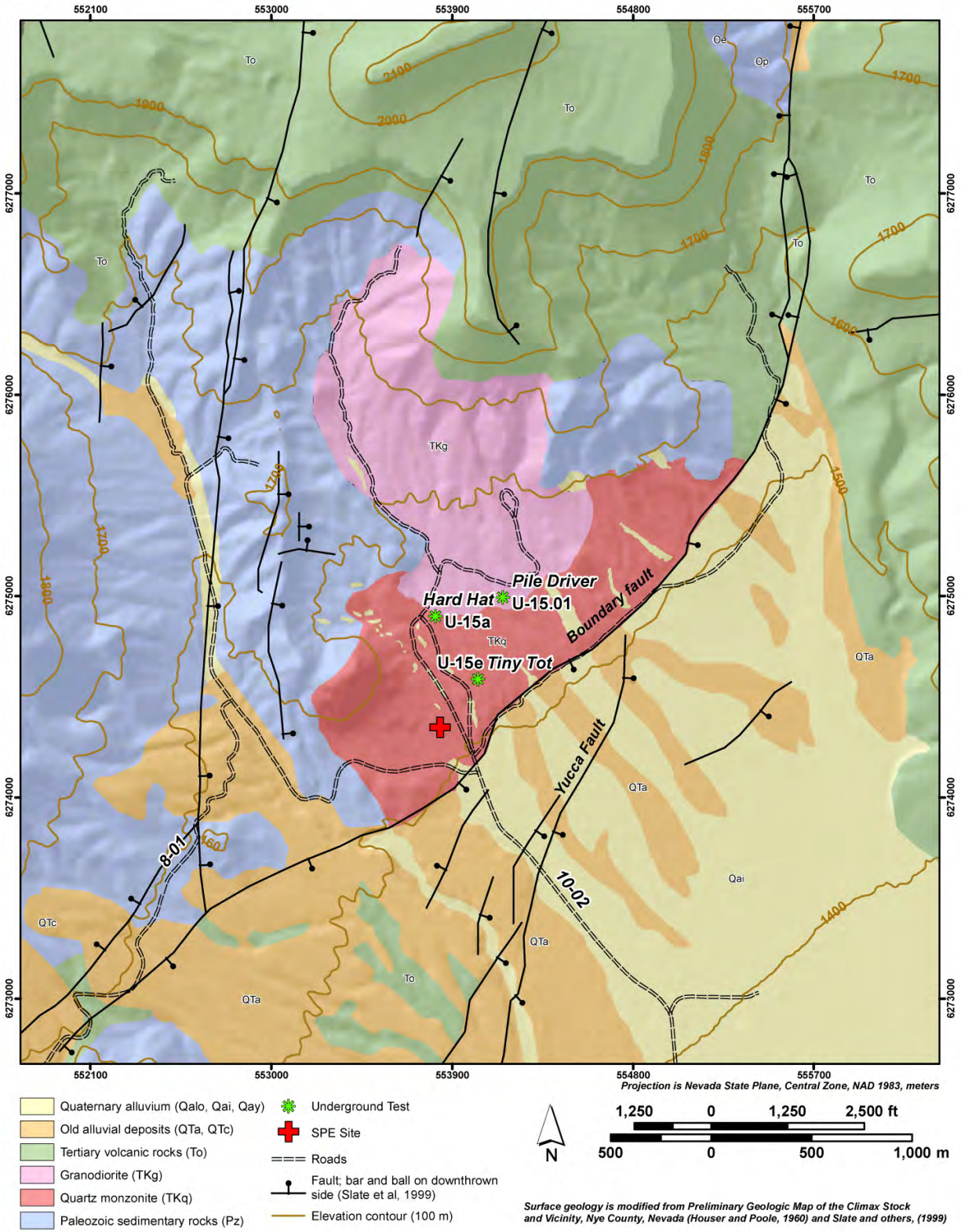


Figure 4
Surface Geologic Map of the Climax Stock Area
Showing Location of SPE-1 Site

2.3 SPE-1 Test Description

2.3.1 Source

The SPE-1 source was 87.9 kilograms (kg) of trinitrotoluene (TNT) equivalent, sensitized heavy ammonium nitrate and fuel oil (S-HANFO), with a 2.27 kg pentolite booster. The S-HANFO was loaded into a 1.27-centimeter (cm) thick aluminum canister through a 6-inch pipe after the canister had been set at the depth of 55 m in the source hole. The canister was a right circular cylinder with both a height and diameter of 51.4 cm, for a length-to-diameter equal to 1, which was intended to mimic a sphere.

The canister with the S-HANFO was cemented in place with a grout mixture up to the depth of 47.5 m below ground surface (Figure 5). Sand-filled cloth tubes were used as wadding inside the emplacement pipe after insertion of the explosives.

The shot was on May 3 (day 123), 2011, at 2200.00.01136 Greenwich Mean Time. The location was 37.221207, -116.0608674.

At the time of the shot, gas emission and minor debris fall occurred due to inadequate stemming. This appears to have had no effect on either the seismic or infrasound data.

2.3.2 Diagnostic Instrumentation

Instrumentation was installed in and on the explosives canister in the source hole to provide near-field diagnostic data for the detonation. These were CORRTEX (Continuous Reflectometry Radius versus Time Experiment), time of arrival, and velocity of detonation. These diagnostics provide a sense of the symmetry of the blast that can be used to distinguish between the blast effects and discontinuities within the formation.

2.3.3 Near-Field Instrumentation

The instrumentation included an array of near-field accelerometers to record the response of the near-field region (defined as less than 100 m from the source). Instrument holes U15n#1, #2, and #3 are on a nominally 10-m radius circle, and holes U15n#4, #5, and #6 are on a nominally 20-m radius circle (Figures 2 and 3). The inner and outer rings of instrument holes are offset from each other to maximize azimuthal coverage. Instrumentation in these holes is designed to be in place for SPE-1 and follow-on SPE tests planned for shallower depths in the same source hole; the arrangement of the gage packages reflects this purpose, as described in the following paragraphs. Appendix 2 provides information about sensors used for the SPE-1 test.

2.3.3.1 Borehole Gage Designations

Each instrument hole contained three each 3-component accelerometer gage packages set at various depths. For each hole, gage package 1 was set at the SPE-1 shot depth (55 m below ground surface), gage package 2 was set at 46 m below ground surface (the planned depth for a future test, SPE-2, in this same source hole), and gage package 3 was set at 15 m below ground surface. Each package has one radial component, one transverse component, and one longitudinal component.

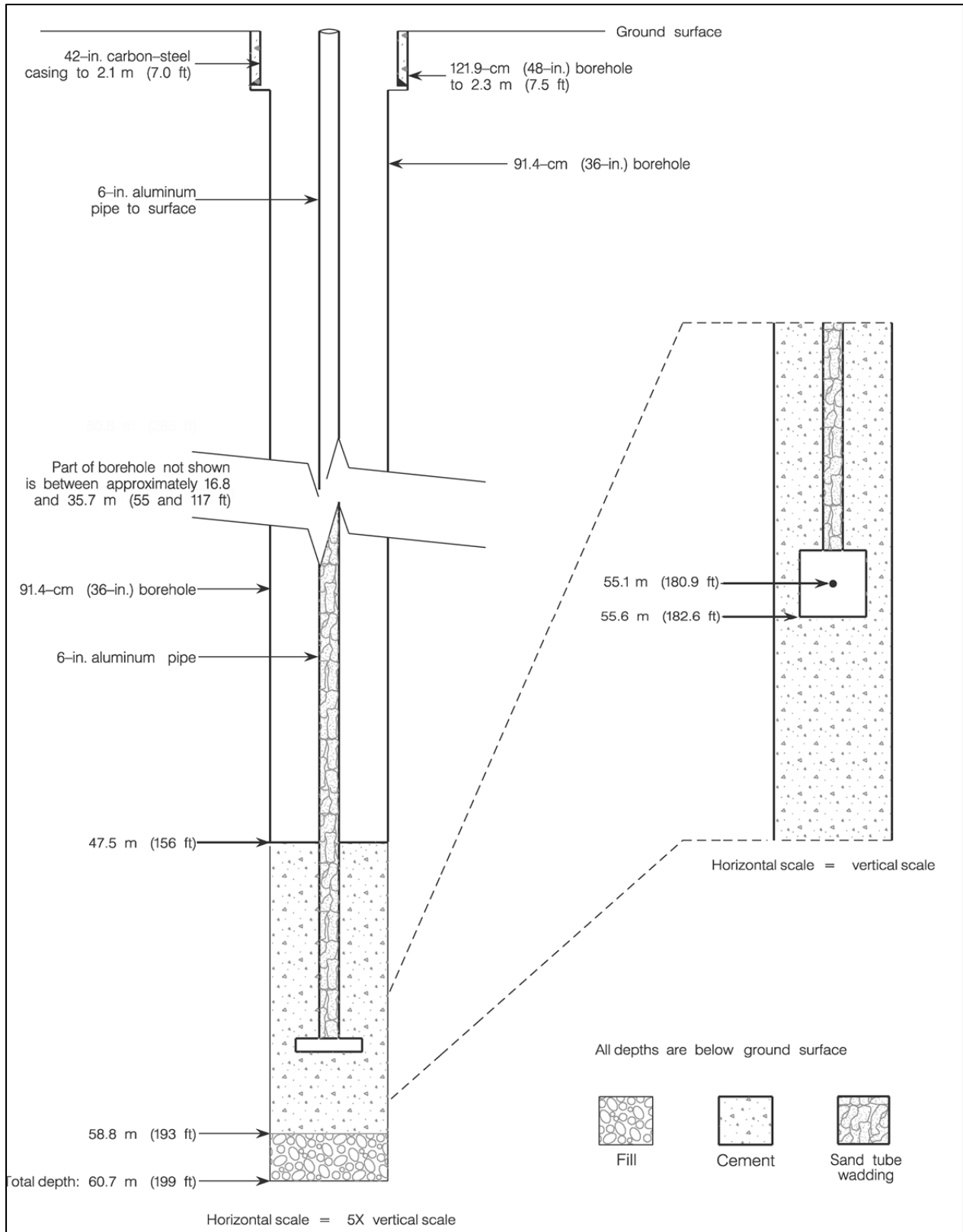


Figure 5
Schematic Drawing Showing Placement of Explosives Canister and Stemming
in the SPE-1 Source Hole

Gage packages are referred to by their respective hole and depth (e.g., package 2-1 is in hole #2 at depth 1). Further, each individual accelerometer in the package is labeled by the first letter of its component (e.g., measurement 2-1-R is the radial measurement in package 2-1). See Figure 6 for an illustration of the SPE-1 gage packages.

2.3.3.2 Near-Field Gage Placement Relative to the Source

Due to the complex deployment geometry of the test bed, these components need further description. The gage packages at depths 1 and 2 are placed in a cylindrical coordinate system about the axis of the source hole. The “radial” gages at these depths are, strictly speaking, horizontal outward measuring transducers, so for SPE-1 only the R gages at the SPE-1 depth (i.e., depth 1) are radial. For example, gage 2-1-R is a radial measurement for SPE-1. However, gage 2-2-R at the planned SPE-2 depth is more accurately described as measuring the horizontal component of the spherically propagating shock for this event. Similarly, the longitudinal component is vertical, and gage 2-1-L is a true longitudinal (or vertically oriented tangential) measurement for SPE-1, while gage 2-2-L is the vertical component of the spherically propagating shock in this test. The tangential measurement is a horizontal component normal to the R-L plane.

The gage packages at depth 3 are oriented in a spherical coordinate system with the origin at the planned SPE-2 shot point. So, the radial gage is only truly radial for that future test, but due to the geometry and distance between depth 1 and depth 3, the depth 3 “radial” gages are reasonable approximations for radial motion for the deeper SPE-1. Similarly, the longitudinal and transverse gages are orthogonal tangential measurements on a sphere centered at the planned SPE-2 shot point but are reasonable approximations to those actual components for SPE-1. See Appendix 3 for information about the borehole sensors, including locations, elevations, and type of instruments installed.

For SPE-1, there were also two sets of surface accelerometers placed at surface ground zero (SGZ) and at every 10 m out to 50 m, inline at an azimuth of west-southwest, with gages of 100- and 500-g sensitivity.

2.3.3.3 As-Built Adjustments of Near-Field Gage Positions

The description above provides nominal distances and directions between the gages and the source, as if the source hole and instrumentation boreholes were perfectly vertical. However, due to the nature of the drilling process, none of the boreholes on the SPE test bed is truly vertical. The orientation (“deviation” from vertical) of each hole was measured after drilling, and the deviation data can be used to determine the exact position of each gage position and its distance from the source. These data are included with the SPE-1 data package, and are also listed in Appendix 3 for each gage. These data should be used for determining as-built locations of both the charge and the accelerometers.

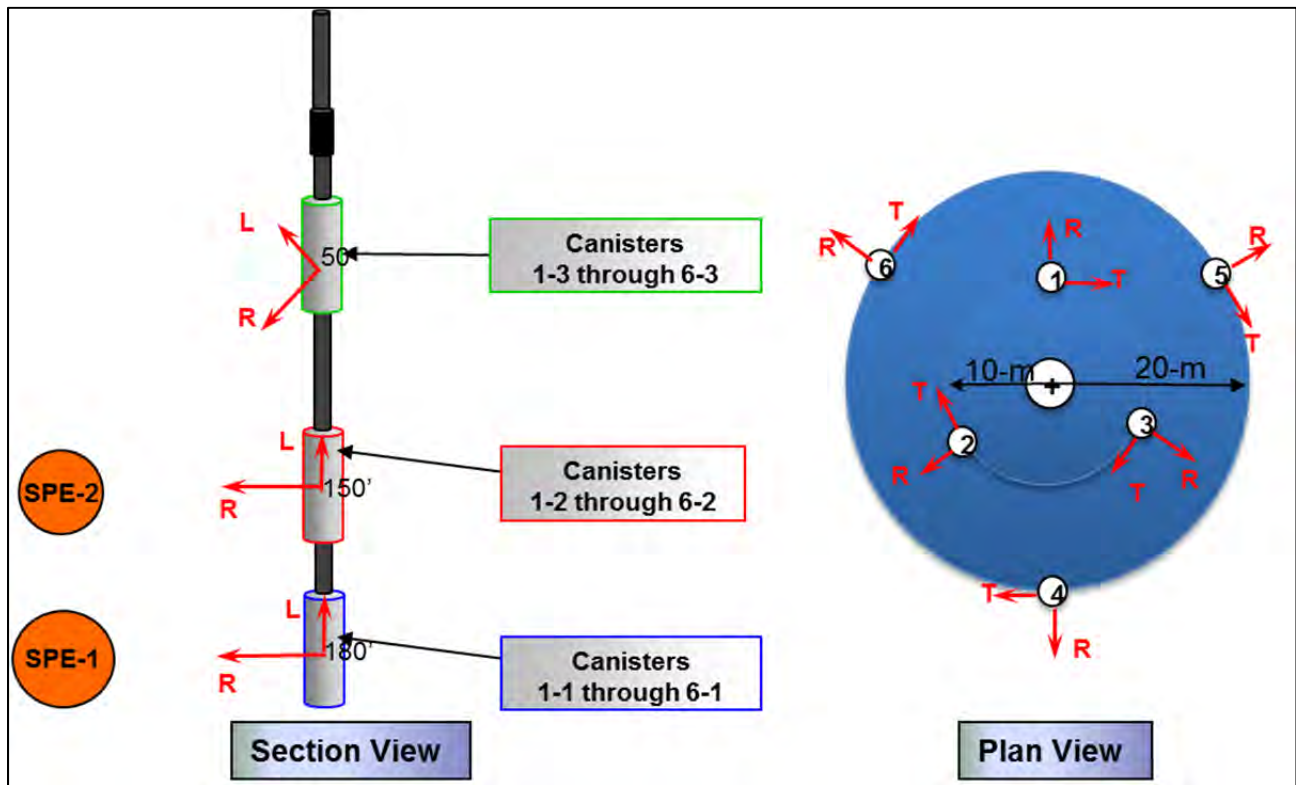


Figure 6
Section and Plan View Diagrams Showing Typical Gage Package Arrangement in Near-Field Instrument Holes for SPE-1

Canisters 1-1 through 6-1 were designed to be radial to the SPE-1 shot-point at the depth of 54.9 m (180 ft).

2.3.4 Far-Field Instrumentation

Two primary types of far-field sensors were deployed for the SPE-1 shot, seismic and infrasound, as described below.

2.3.4.1 Seismic Instrumentation

To characterize the far-field seismic wavefield (defined as 100 m or more from the source), a number of different instrument arrays were deployed starting at a distance of 100 m from the shotpoint and extending to distances as great as 25 km (Figures 7 and 8). Most seismic sensors were installed in five radial lines extending out from the source. Line 1 extends to the north and Line 2 extends to the northeast; both lines are relatively short due to proximity to the boundaries of the NNSS. Lines 3 and 4 extend to the south and southwest, while Line 5 extends roughly northwest. Instrument density on Line 5 is lower than on the other lines, because steep topographic gradients hindered deployment. Recording was done on 6-channel RefTek 130 digitizers. For the sensors within 2 km, typically several stations at different locations were recorded on one digitizer, which led to long (100 m) cable runs in some cases. The digitizers were powered by batteries trickle-charged by solar panels. Data were stored to disk and collected manually at intervals.

It is important to note that data polarity standards for geophones and seismometers differ. Geophones produce negative voltages for upward ground motion, while the seismometers and

accelerometers produce positive voltages for upward ground motion. This polarity standard is extended to three components in the case of three-component geophones. Geophone polarity follows a right-hand-rule standard with vertical pointing into the earth. The data in this collection are exactly as recorded by the sensors.

Characteristics of the instruments installed along the five geophone lines are summarized below. Exact details such as sensor type and response can be found in the metadata as well. See Appendix 4 for a summary of location and instrument information for each surface sensor site.

Geospace GS-11D 4.5-hertz (Hz) geophones were deployed in five linear arrays, radiating from SGZ from 100 m to 1.9 km. Nominal station spacing is 100 m, with some expected locations skipped due to steep topography (mostly along Line 5). Every fourth geophone in each line is a three-component sensor oriented radial, transverse, and vertical to SGZ. The remaining geophones are vertical only. The geophones are buried less than 0.5 m deep in native material, with sandbags placed on top.

Guralp CMG 40T three-component seismometers are installed at the ends of the five geophone lines, 2 km distant from SGZ. The components are oriented radial, transverse, and vertical. The Guralps are installed on a concrete pad set less than 10 cm into the soil.

Lines 1, 2, 3, and 5 each include one Kinometrics Episensor accelerometer and one Eentec R-1 rotational seismometer installed 1 km from SGZ. The instruments are mounted on an aluminum plate, which was then embedded into the concrete pad.

Lines 3, 4, and 5 are extended beyond 2 km (to a maximum of 25 km) by either six or seven Nanometrics Trillium Compact seismometers each, oriented radial north-south, east-west, and vertical (Figure 7). The instruments are installed on a concrete pad set less than 10 cm into the soil. Two stations on Line 5 (L5-28 and L5-34) were very close (centimeters) to bedrock, so at those locations the broadband instruments were covered by a sensor case in an ice chest (not barometrically sealed) covered with sandbags.

Orientation was estimated visually in the field, and the error is estimated to be less than about 5 degrees, as checked by later precise orientation measurements. At the 2 km distance and beyond, sensor orientations are set with respect to cardinal directions and not radial/tangential. This difference is denoted in the channel names. Timing was provided by a Geographic Positioning System connected to digitizer. RefTek logs were reviewed for timing errors during data compilation.

In addition to this instrumentation, AFTAC deployed instruments at nine sites. Two sites were within 2 km and were equipped with Kinometrics Episensors and CMG 40 T broadband instruments. The remaining sites were at distances up to 15 km and varying azimuths and equipped with PMD SP400U3. Two of the PMD sites also had Episensor accelerometers. All sites were equipped with Chaparral infrasound sensors. All sensors were oriented to north (N), east (E), and vertical (Z) and recorded on Reftek digitizers.

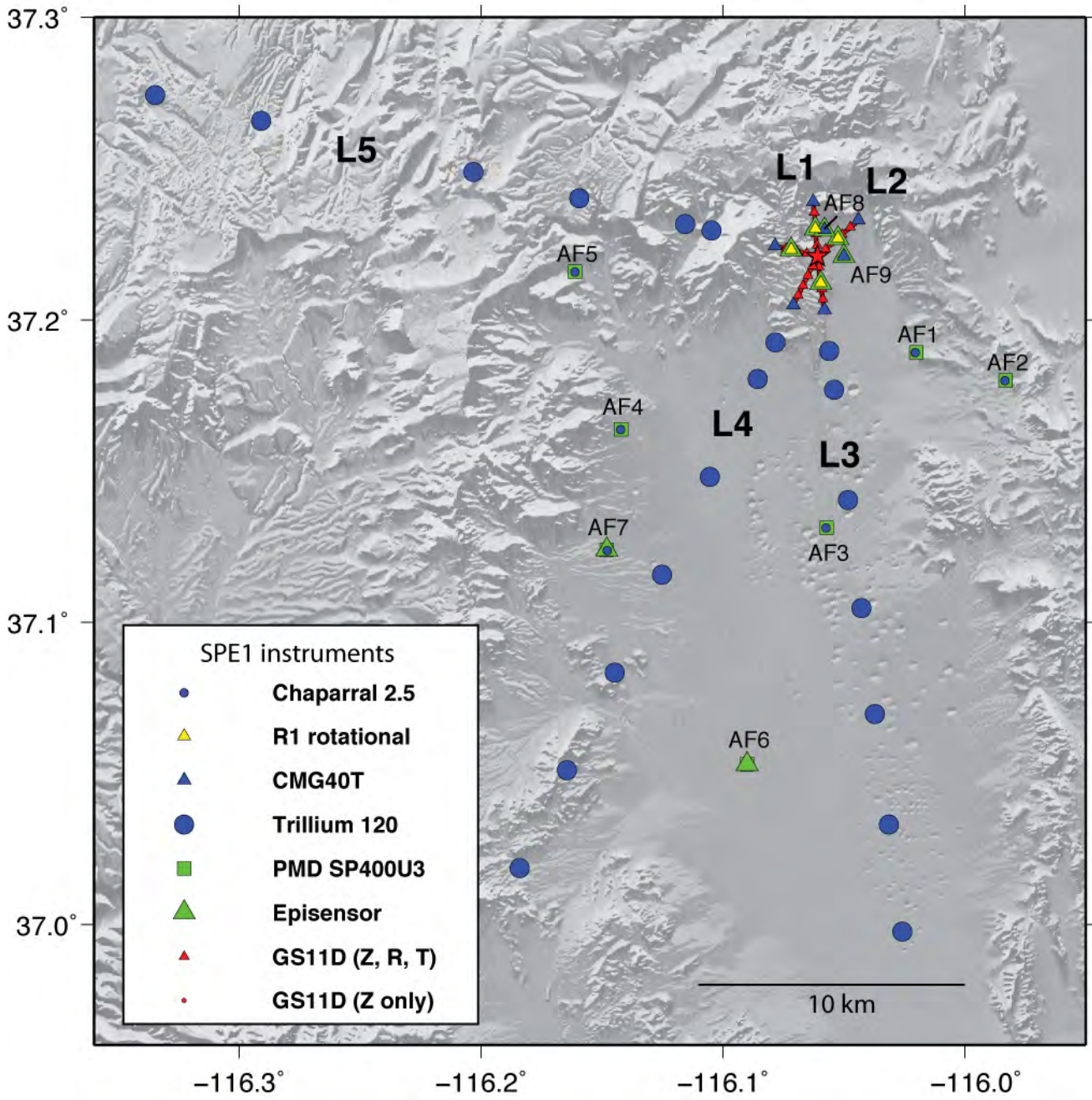


Figure 7
Location Map of Far-Field Instrumentation Layout

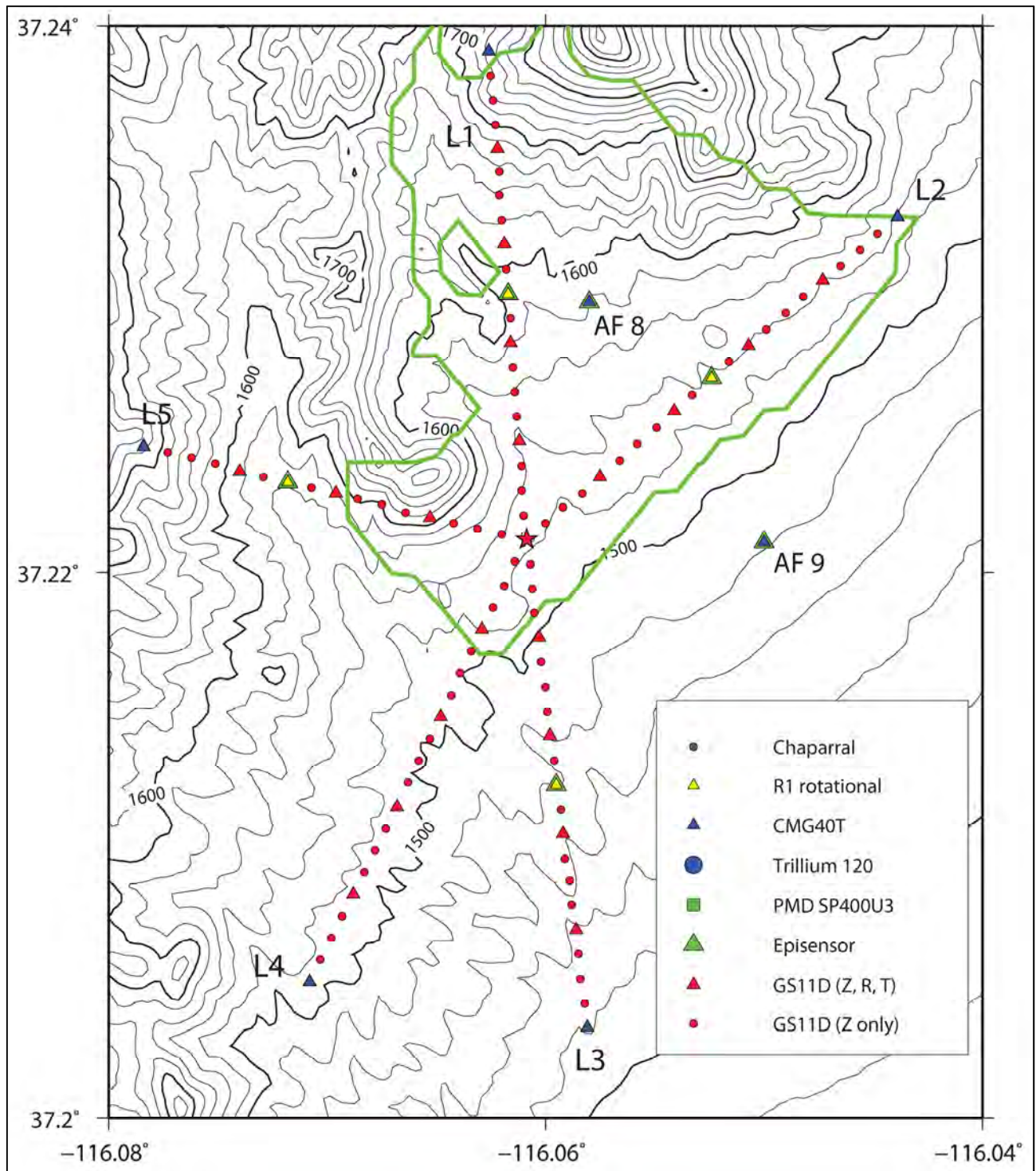


Figure 8
Map Showing Locations of Geophones Placed within Approximately 2 Kilometers of the
SPE-1 Shot-point

(Nominal distance between instruments is 100 meters. The green line is the approximate outline of the granite body at the surface.)

The final list of installed gages is posted on the project data server as file *SPE1ShotSheet.xlsx*. The file includes gage ranges, as-built depths, and details about the accelerometers used.

2.3.4.2 Infrasound Arrays

Prior to the SPE-1 shot, seven arrays consisting of four Inter-Mountain Labs (IML-ST) infrasound sensors were deployed around SGZ. The data were recorded using Reftek RT-130 digitizers sampling at 500 Hz. Each station telemetered data in real time to the SNL trailer at the command center, located approximately 365 m southeast of SGZ.

The infrasound sensors were installed in a roughly triangular geometry, with one sensor and the digitizer at the center and the other three sensors arranged azimuthally ($\sim 120^\circ$ increments) around the center element at a distance of about 30 m. Attached to each sensor were four sections of porous hose about 15 m long for wind noise reduction. The IML-ST sensors have a nominal sensitivity of 0.20 volts per pascal and a flat response from 30 Hz down to where the roll-off begins around 2 Hz (Hart, 2007). Four arrays were installed azimuthally around the test pad approximately 0.25 km from SGZ, and at different elevations due to topography constraints. The remaining three arrays were located at 1, 2, and 5 km respectively linearly south-southeast of SGZ (Figure 9). See Jones et al. (2012) for additional information.

3 Data Collection and Corrections

3.1 Near Field

3.1.1 Data Collection

The data package for SPE-1 includes the raw acceleration-time pairs recorded for all accelerometers. These data are in the form of time–acceleration pairs. The files are in comma separated variables (csv) format.

3.1.2 Data Corrections

Several standard and non-standard corrections were performed on the near-field data sets.

3.1.2.1 Corrections for Gage Position

The SPE-1 test included an array of accelerometers (see Section 2.3.3) positioned near the source, intended to provide measurements of the strong ground motion, or “near field,” regime. Some anomalous records were found during reviews of the near-field data, which are suspected of having been caused by rotation of the gages during installation in the boreholes. This is believed to have occurred in part because the deviation of the boreholes caused sections of the pipe on which the gage packages were inserted to partially “unscrew” during insertion, thus changing the planned orientation of the gages relative to the sources.

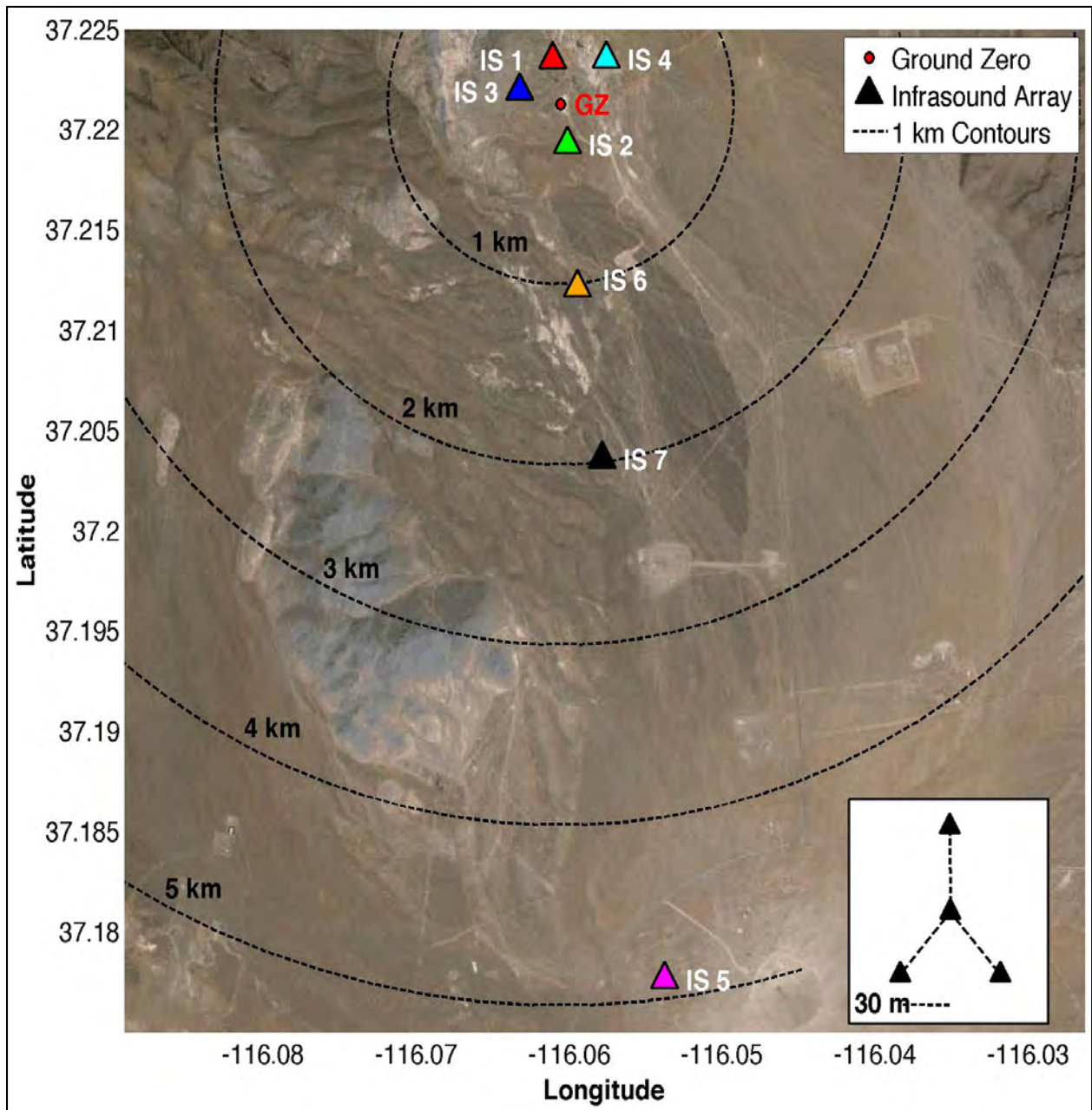


Figure 9
Map Showing the Seven Infrasound Array Locations (Triangles) around
Surface Ground Zero (red)
 Dashed lines are 1 km contours from SGZ. Inset shows an example of the sensor geometry at each array

Scientists at LANL and Applied Research Associates, a DTRA contractor, performed extensive analyses of the suspect data records and found that plots of uncorrected data (i.e., assuming that labeled components were pointed in the desired direction) are inconsistent with the shock environment expected from an explosive source. Further, the data histories exhibit considerable inconsistency between measurement locations, and the peak amplitudes of these data exhibit significant scatter.

A correction was performed by estimating the degree of rotation for each canister, and then correcting the gage data to reflect the rotation. The resulting set of histories provides a self-consistent data set, and the peak amplitudes demonstrated considerably less scatter.

Those corrections were performed as described in detail in Steedman (2013) and summarized here (see also Appendix 6). The acceleration data were reviewed on a timestep-by-timestep basis. The radial and transverse records were resolved using trigonometric calculations, iterating on possible rotation angle, enabling the determination of the angle that provided the maximum outward radial motion for each location. The final reported radial and transverse records were altered to reflect this geometric correction.

However, the suspected rotation of the gages cannot be proven, so this data release includes three sets of data histories representing each of three steps of data correction. The steps are as follows, in successive order:

- Correction for gage package rotation
- Correction for pre-event zero-shift
- Correction for zero-shift that occurs during an explosion

The first of these is a special case that was determined to be needed after a thorough review of data from SPE-1. The other two corrections are standard requirements for acceleration records, and were performed after this first correction was applied.

3.1.2.2 Baseline Shift Corrections

Appendices 5 and 6 discuss the baseline shift corrections that were made to the accelerometers nominally located at the 10-m and 20-m ranges from SGZ prior to analysis. These corrections were made in two stages:

- Correction for pre-arrival baseline shift
- Correction for post-arrival baseline shift

3.2 Far Field

Data were rapidly collected and provided by portable hard drive. Following collection, the data were sent to NSL for reformatting and construction of metadata. In parallel, data were reformatted into Seismic Analysis Code (SAC) format at LLNL. After completion of the data formatting at NSL and construction of metadata, data including responses, were loaded into the database at LLNL.

An important note is that the signal polarity of the GS11D uses the Society of Exploration Geophysics standard: a downward ground motion yields a positive signal. The other instruments have the opposite polarity, i.e., upward ground motion yields a positive signal. For the shot itself, gains were set to unity beforehand.

Data features:

- Difference in polarity between geophones and other instruments
- Data spikes (most obvious on data prior to shot); these were most likely due to issues with the solar panels although thunderstorms and lightning produce similar signals
- Possible cross-talk causing low amplitude signals on dead channels

Initial review of the data revealed that the shot data were mostly good, although some problems occurred with bad channels and incorrect station locations (likely due to cable mix-ups). Initially, the data were checked for instrumentation and metadata problems. Seven sensors appeared to malfunction based on data appearance and amplitude. Although not visible on the shot itself, spikes appear periodically in the data and may be related to the solar panel power setup, although this has not been confirmed. A review of the RefTek logs using *clockview* indicated no significant problems with the data for move-out consistency and timing (Mellors et al., 2011).

4 Post-Experiment Procedures

4.1 Aggregation, Merging, and Archiving of SPE-1 Data

Post-experiment aggregation, merging, archiving, and distribution of SPE-1 data were conducted at UNR by the technical members of the NSL. The process employed the Antelope data processing software system, version 4.11, from Boulder Real Time Technologies (Boulder, Colorado); the data processing suite from the Program for Array Seismic Studies of the Continental Lithosphere (PASSCAL); the CSS 3.0 database format; and the Ubuntu-Linux-based servers at NSL's UNR data center.

4.1.1 Data Aggregation

Data aggregation is the phase of acquiring raw metadata and time series data from project participants, reviewing the submissions, and conducting initial format conversions to standardize the media.

4.1.1.1 Metadata

Metadata were compiled prior to the SPE-1 test and refined during the merging and archival process. For each sensor, NSL asked SPE-1 participants to submit the following items:

- Sensor make/model/type
- Sensor sensitivity factor
- Sensor serial number
- Sensor lat/long, decimal degrees
- Sensor frequency response file
- Sensor depth
- Sensor orientation
- Sensor on-time, off-time
- Sensor
- Data logger make/model
- Data logger serial number
- Data logger response file
- Data logger bit weight
- Data logger channel number
- Channel gain
- Channel sample rate
- Site name
- Site description

These initial metadata were submitted to NSL by SPE investigators through electronic transfer of spreadsheets, figures, and scanned drawings, and were then made available to all participants via the SPE data servers' document archive.

4.1.1.2 Far-Field Waveform Aggregation Procedure

Far-field waveform data, recorded on RefTek RT130 data loggers on removable Secure Digital flash disks, were recovered by field technicians following the SPE-1 test. The native RefTek-formatted data were transferred to standard magnetic hard disk drives (HDDs), and the HDDs were delivered to the NSL Reno data center. Native-format data were duplicated to a redundant disk array, on a dedicated server, and converted to the RefTek “raw” format using PASSCAL’s *rt130cut* conversion program. The “raw” output comprised one raw file per data logger per day. The “raw” formatted files were then converted to miniSEED format, using PASSCAL’s *ref2mseed* program. The output from this conversion process was (1) one miniSEED file per data logger per hour, and (2) one log file per data logger per hour. The log files include recording parameters and state-of-health information for the recording period. All logs and raw- and miniSEED-formatted files were then mirrored to a second disk array on a second dedicated server for data security and for distribution to project investigators for review.

4.1.1.3 Near-Field Waveform Data Aggregation Procedure

Near-field waveform data recorded on high-sample-rate multi-channel digitizers were recovered by project principal investigators and submitted to NSL by electronic file transfer. The data formats included (1) SAC, (2) four-byte integer, and (3) non-standard ASCII formats with accompanying scripts and other supporting metadata. For data received in SAC format, there was no required initial conversion procedure. Other formats required varying amounts of effort to convert to a common format.

4.1.2 Merging of Data Sets

Data merging is the phase of generating a valid CSS 3.0 metadata volume and modifying waveform file headers so that they will synchronize with the CSS 3.0 metadata format.

4.1.2.1 Metadata Merging

Upon receipt of metadata submissions, NSL staff distilled and standardized the information into ASCII files, one per station, in an open format that provides the input to Antelope’s *dbbuild* program. The *dbbuild* format tracks station information changes through time (i.e., station histories), and allows for (1) rapid regeneration of an entire CSS 3.0 database as corrections and additions are required, (2) cross-institution database maintainability, (3) version control and revision history, and (4) a distributable and readable station record that can be useful even without proprietary tools.

4.1.2.1.1 Station Names and Descriptions

Upon submission, most metadata contained station descriptions and names that were meaningful only to the internal processes of the submitting institution. For the purpose of creating a single coherent volume, NSL technical staff created five-character station names that are compliant with the Standard for the Exchange of Earthquake Data (SEED). Where possible, the initial descriptions were preserved in the CSS 3.0 site descriptions to ensure new station names would be easily recognized by the various investigators. The file headers for the far-field stations (submitted as part

of NSL's "SN" network) were changed to remove dashes (hyphens), which were replaced by zeroes to make them SEED compatible (see Appendix 4).

4.1.2.1.2 Channel Codes

NSL staff created SEED-compliant channel codes describing the sample rate (band), instrument type, and orientation of each data channel. However, a collective decision was made by NSL and project investigators to leave the band code unchanged, even though per-instrument sample rates fluctuated from 100, to 500, to 250, to 200 samples per second. This was to avoid generating confusion for the large party of investigators who were not yet familiar with the CSS 3.0 database, which is sometimes terse and detailed and can become lengthy when many configuration changes are made across a large array during the course of recording. In addition, it was widely held as important that channel codes be tied to certain sensor types to facilitate rapid association of a channel's code with the sensor's location relative to the source.

4.1.2.1.3 Precision of Sensor Location

Sensor locations were submitted to NSL in State Plane Coordinates (SPC, feet) and geographic coordinates (decimal degrees). The submitted geographic coordinate submissions were merged directly into the CSS 3.0 metadata where station lat/long values were required. The SPC station locations were used to calculate northing and easting offsets in feet from the location of the SPE-1 source (station SP-01, northing 900077.22, easting 676640.6), and these offsets were then converted to meters using the conversion factor $1 \text{ m} = 3.28084 \text{ ft}$.

4.1.2.1.4 Precision of Sensor Orientation

For the most part, measured sensor orientations were not submitted to NSL, with the exception of the vertical angles (in the radial direction) of the near-field borehole accelerometers. The remainder were submitted as orientation codes (N=North, E=East, Z=Vertical, R=Radial, T=Tangential, L=Lateral) and NSL calculated the azimuths of the sensor axes from the geographic coordinates. All azimuthal calculations were based on the assumption that the particular axis of the sensor was correctly aligned, e.g., that a radial orientation was indeed radial, and that the geographic coordinates are accurate to $<0.3 \text{ m}$. The estimated error on horizontal orientation is <5 degrees.

4.1.2.1.5 Sensor Sensitivity Factors

Measured sensitivity factors were submitted for the near-field borehole accelerometers (stations BH-, DT-, and SL-), and these were merged in to the CSS 3.0 metadata. For the remaining sensors, CSS 3.0 metadata were constructed using nominal sensitivity values provided in manufacturers' information sheets. Accelerometer sensitivities vary by location to optimize response with respect to the estimated wavefield amplitudes. Sensitivities are measured, not nominal, as each DT-* sensor was tested at DTRA prior to deployment. A numerical (e.g., pole-and-zero) frequency response is not available. Frequency response is expected to be essentially flat for frequencies of interest (Winningham, 2011) and represented as constant in the metadata. The calibration factor for DT-* includes pre-amplifier gain and digitizer constant as well as sensitivity. SL-* sensor calibration includes a cable attenuation factor as well.

4.1.2.1.6 *Gains*

For far-field RT130 seismic data, channel gains were recovered from the logs generated from the raw RefTek to miniSEED data reduction process described above. For other instrumentation time series, particularly near-field high-sample-rate accelerometer gages, gain values were reported by the principal investigator, reviewed, and confirmed prior to integration with either the CSS 3.0 database or in another archive format relevant to the data set.

4.1.2.2 *Merging Waveform Data*

The procedure for merging waveforms included correcting waveform file headers to reflect the appropriate network-station-channel-location (*net_sta_chan_loc*) codes, and then using the Antelope *miniseed2db* or *sac2db* programs to generate a CSS 3.0 “wfdisc” table. The “wfdisc” table provides the mechanism to associate the time series data with the metadata set that describe the waveforms’ response, sensor parameters, etc.

For miniSEED files, header modification was done using the PASSCAL *fixhdr* program. By default, the station and channel names in miniSEED file headers are set to the data logger serial number and stream codes. The data logger and channel codes are then mapped to SEED *net/sta/chan/loc*. The *net_sta_chan_loc* code maps were derived from the site metadata for each data logger configuration.

For SAC files, the header modifications were done using the SAC analysis software, distributed through IRIS.

4.1.3 **Data Archiving**

Archiving is the phase of presenting final data products. It includes completion of quality control procedures and generation of final product formats.

4.1.3.1 *Metadata Formats*

4.1.3.1.1 *CSS 3.0*

The CSS 3.0 metadata format is an industry/community standard and is the format supported by the Antelope system. It is a readable and open database system that allows for schema extensions and therefore is flexible, scalable, and adaptable to non-standard sensor array configurations.

4.1.3.1.2 *Dataless SEED*

The dataless SEED format is an industry/community standard for metadata that includes station histories as well as sensor and data logger response information. It is distributed as a single file, and can be read and imported by a wide variety of programs and applications. The volume distributed by NSL was generated from CSS 3.0 metadata using the Antelope application *db2sd*.

4.1.3.1.3 *Dbbuild*

The *dbbuild* format is an ASCII text-based format that documents site parameters throughout all epochs, or periods of distinct recording configurations. The *dbbuild*-based metadata comprise one text file per station, and while the files by themselves do not include sensor frequency response or data logger response, they do include sensor sensitivity factors. As input to the Antelope *dbbuild*

program, which builds CSS 3.0 metadata (and in turn is converted to dataless SEED), the *dbbuild-format* files are the fundamental metadata records maintained by NSL for all SPE stations.

4.1.3.2 Time Series Formats

There are many time-series data formats, but for simplicity and for reusability of conversion and processing scripts, the technical staff at NSL resolved to create an archive based on either miniSEED or SAC formats. MiniSEED is the preferred format for data submissions to IRIS, and also the standard format for most Antelope-based programs and tools. SAC is the most widely known and used time-series format, and in some cases, such as with very high-sample-rate data (e.g., one million samples per second), it has capabilities that miniSEED does not.

4.1.3.3 Quality Control Measures

While the quality control of time-series data is left to SPE investigators (the near-field and far-field data committees), NSL is charged with creating a coherent database that is up to date and accurate with respect to the data submissions. As such, there are four quality control measures used to verify the data products for SPE-1.

4.1.3.3.1 Manual Inspection of dbbuild-Format Files

All metadata submissions are converted initially to the *dbbuild-format*. These files are reviewed for completeness and then checked in to the Concurrent Versioning System revision control system. The use of revision control allows NSL to track completeness of array-wide edits, and is important for tracking metadata errors and corrections.

4.1.3.3.2 Output Warnings and Errors from dbbuild Program

The *dbbuild-format* files are used by the *dbbuild* program to generate the CSS 3.0 metadata. All runs of *dbbuild* are conducted with the use of verbose warnings, the standard output is captured in a log, and the log is reviewed after the run completes. This process allows NSL to find and fix inconsistencies, incomplete entries, and mistakes in the *dbbuild-format* metadata that are not caught during manual review.

4.1.3.3.3 Antelope dbverify Program

After generating a coherent CSS 3.0 metadata set that passes the first two levels of quality control, the data are examined for any additional problems using the Antelope *dbverify* program. This program performs consistency checks between database tables and is largely a tool for checking the validity of database schema and formats, rather than for finding omissions or typographic mistakes.

4.1.3.3.4 Output from dbjoin and dbfixids

The final step in each iterative generation of a CSS 3.0 metadata set is to synchronize the *wfdisc* table with the new channel identifiers, waveform identifiers, channel names, and calibration values that often change as metadata are refined and improved. This process not only corrects out-of-sync values in the *wfdisc* tables, but also warns when there are entries in the *wfdisc* table that do not join with the CSS 3.0 metadata. This reveals the case where waveforms have been submitted, but no metadata exist for the particular station. This situation can occur when new stations are added, or when data loggers are changed in the field without the updated information being submitted.

Otherwise it can point up a case where NSL has missed a submission. This measure prompts staff to re-examine emails, contact field technicians, etc. to sort out why metadata are missing and contributes greatly to the completeness of the SPE-1 archive.

5 Summary

This report coincides with the official release of near- and far-field seismic station, gage, and diagnostic data for SPE-1. It describes the location of data and supporting documents on the SPE data server. The report includes a description of the experiment, the types of data and instruments, corrections made to the accelerometer data, and post-experiment data processing. This data release includes separate sets of these data, including the raw data as well as the data reflecting the application of the corrections.

6 Acknowledgements

The Source Physics Experiment (SPE) would not have been possible without the support of many people from several organizations. The authors wish to express their gratitude to the U.S. Department of Energy, National Nuclear Security Administration, Defense Nuclear Nonproliferation Research and Development (DNN R&D) and the SPE working group, a multi-institutional and interdisciplinary group of scientists and engineers. Deepest appreciation is given to Robert White and Ryan Emmitt (NSTec) for their tireless work on the seismic array, and to the Nevada Seismological Laboratory at UNR for their support of the seismic network and for data aggregation. Thanks to U.S. Geological Survey, IRIS, Program for Array Seismic Studies of the Continental Lithosphere (PASSCAL) Instrument Center, Lawrence Berkeley National Laboratory, and Dr. Roger Waxler (University of Mississippi) for instrumentation partnership. This work was done by NSTec under Contract No. DE-AC52-06NA25946.

7 References

- Broome, S. T., and T. Pfeifle, 2011. Written communication prepared for the U.S. Department of Energy, National Security Administration Nevada Site Office. Subject: "Phase 1 Mechanical Testing Results on Core from Borehole U-15n, Nevada National Security Site, in Support of NCNS Source Physics Experiment." Sandia National Laboratories Report, June 8, 2011.
- Ford, S., and W. R. Walter, 2013. "An Explosion Model Comparison with Insights from the Source Physics Experiments," *Bull. Seism. Soc. Am.*, Vol. 103, pp. 2937–2945, doi:10.1785/0120130035.
- Hart, D. M., 2007. *Evaluation of Inter-Mountain Labs Infrasound Sensors July 2007*. Sandia National Laboratories Technical Report, SAND2007-7020. Albuquerque, NM.
- Jones, K. R., R. W. Whitaker, and S. J. Arrowsmith, 2012. "Infrasound Observations from the Source Physics Experiment (Tests 1 and 2) at the Nevada National Security Site." In:

Proceedings of the 2012 Monitoring Research Review: Ground-Based Nuclear Explosion Monitoring Technologies, Volume II. Albuquerque, NM.

- Mellors, R., P. Harben, S. Ford, J. Wagoner, B. Walter, A. Rodgers, T. Hauk, S. Ruppert, S. Myers, E. Matzel, D. Dodge, M. Pasyanos, R. Gok, N. Simmons, A. Petersson, B. Sjogreen, and J. P. Lewis, 2011. "SPE 1 Data Quicklook Report." LLNL-TR-485228. Livermore, CA.
- Orkild, P. P., D. R. Townsend, M. J. Baldwin, D. L. Healey, G. D. Bath, C. E. Jahren, and J. G. Rosenbaum, 1983. *Geologic and Geophysical Investigations of Climax Stock Intrusive, Nevada*. Open-File Report 83-377. U. S. Geological Survey, Denver, CO.
- Pitarka, A., R. J. Mellors, A. J. Rodgers, S. R. Ford, P. E. Harben, J. L. Wagoner, W. R. Walter, M. E. Pasyanos, A. Petersson, O. Y. Vorobiev, H. Xu, S. D. Ruppert, S. C. Myers, E. M. Matzel, and D. A. Dodge, 2012. "Analysis and Simulation of Far-Field Seismic Data from the Source Physics Experiment." In: *Proceedings of the 2012 Monitoring Research Review: Ground-Based Nuclear Explosion Monitoring Technologies, Volume II.* Albuquerque, NM.
- Rougier, E., and D. Steedman, 2013. *SPE-1 Baseline Shift Corrections*. Los Alamos National Laboratory Report LA-UR-13-23956. Los Alamos, NM.
- Snelson, C. M., V. D. Chipman, R. L. White, R. F. Emmitt, M. J. Townsend, D. L. Barker, and P. Lee, 2012. "An Overview of the Source Physics Experiment at the Nevada National Security Site." In: *Proceedings of the 2012 Monitoring Research Review: Ground-Based Nuclear Explosion Monitoring Technologies, Volume I.* Albuquerque, NM.
- Snelson, C. M., R. Mellors, H. J. Patton, A. J. Sussman, M. J. Townsend, and W. R. Walter, 2013, *Source Physics Experiments to Validate a New Paradigm for Nuclear Test Monitoring*, Eos Trans., American Geophysical Union, Vol. 94, No. 27, pp. 237–239.
- Steedman, D. W., 2013. *Review of Data from Shock Physics Experiments SPE-1, SPE-2, and SPE-3: Data Corrections and Phenomenology Analysis*. Los Alamos National Laboratory Report LA-UR-13-22561. Los Alamos, NM.
- Townsend, M., L. Prothro, and C. Obi, 2012. *Geology of the Source Physics Experiment Site, Climax Stock, Nevada National Security Site*. DOE/NV/25946--1448. Prepared by National Security Technologies, LLC, Las Vegas, NV.
- Winningham, K, Defense Threat Reduction Agency, 2011. Personal communication to K. Smith, University of Nevada, Reno Seismological Laboratory, regarding frequency response of borehole sensors.

List of Appendices

1. Source Hole and Instrument Hole Data
2. Instrument Metadata for SPE-1
3. Selected Metadata for SPE-1 Borehole Sensors
4. Selected Metadata for SPE-1 Surface Stations
5. *SPE-1 Baseline Shift Corrections*, LA-UR-13-23956, prepared by E. Rougier and D. Steedman, Los Alamos National Laboratory
6. *Review of Data from Source Physics Experiment-1: Data Corrections* (condensed version of Los Alamos National Laboratory Report LA-UR-22561 [2013] prepared by D. Steedman)

Appendix 1
Source Hole and
Instrument Hole Data

Appendix 1
Construction Data for Holes Drilled at the U-15n Site
(As-built coordinates and elevations as of December 14, 2011)

Hole Name	State Planar Coordinates at Collar ^a		UTM Coordinates at Collar ^b		Well Coordinates at Collar ^c		Ground Elevation ^d	Conductor Hole	Conductor Casing	Drilled Depth
	Northing (feet)	Easting (feet)	Northing (meters)	Easting (meters)	Latitude	Longitude	feet	Depth (feet)	Depth (feet)	(feet)
U-15n Source Hole	900,077.28	676,640.62	4,119,823.7	583,318.7	37.221195	116.060867	5,001.82	7.5 ^e	7.0 ^g	199
U-15n#1	900,107.01	676,655.17	4,119,832.8	583,323.1	37.221267	116.060816	5,002.00	7 ^f	6.5 ^h	190 ⁱ
U-15n#2	900,075.27	676,608.54	4,119,823.1	583,308.9	37.221190	116.060977	5,002.16	10 ^f	9.5 ^h	190 ⁱ
U-15n#3	900,050.67	676,659.48	4,119,815.6	583,324.5	37.221121	116.060803	5,001.66	10 ^f	9.5 ^h	190 ⁱ
U-15n#4	900,018.48	676,612.53	4,119,805.8	583,310.2	37.221034	116.060965	5,001.59	10 ^f	9.5 ^h	192 ⁱ
U-15n#5	900,082.71	676,706.51	4,119,825.5	583,338.8	37.221208	116.060641	5,001.29	10 ^f	9.5 ^h	192 ⁱ
U-15n#6	900,131.75	676,603.86	4,119,840.3	583,307.4	37.221345	116.060992	5,005.07	7 ^f	6.5 ^h	190 ⁱ

- a. Central Nevada State Planar coordinates, in feet, NAD 27
- b. Universal Transverse Mercator, zone 11, in meters, NAD 83
- c. Lat/Long presented as decimal degrees
- d. National Geodetic Vertical Datum, 1929
- e. 48-inch hole
- f. 12¼-inch hole
- g. 42-inch steel casing
- h. 10-inch steel casing
- i. 8-inch hole

Appendix 2

Instrument Metadata for SPE-1

**Appendix 2
Instrument Metadata for SPE-1**

Instrument ID	Instrument Name	Instrument Code	Frequency Band	Sample Rate (samples/second)	Directory	Data File	Response Type
3	Geospace GS-11D 380ohm/Reftek 130 Datalogger	gs11d	High frequency	500	response	gs11d+rt130@500	Velocity
13	Episensor 200 Hz 1.25 Volt per g/Reftek 130 Datalo	epi_1.	Broad-band	500	response	epi_1.25_vpg+rt130@500	Acceleration
14	Eentec R1 Rotational Seismometer/Reftek 130 Datalo	eentec	Broad-band	500	response	eentec_r1+rt130@500	Velocity
15	Episensor 200 Hz 1.25 Volt per g/Reftek 130 Datalo	epi_1.	Broad-band	250	response	epi_1.25_vpg+rt130@250	Acceleration
18	Guralp CMG40T_30sec/Reftek 130 Datalogger	cmg40t	Broad-band	500	response	cmg40t_30sec+rt130@500	Velocity
19	Guralp CMG40T_30sec/Reftek 130 Datalogger	cmg40t	Broad-band	250	response	cmg40t_30sec+rt130@250	Velocity
23	Nanometrics Trillium 120 Compact/Reftek 130 Datalo	trilli	Broad-band	500	response	trillium_120c+rt130@500	Velocity
24	Nanometrics Trillium 120 Compact/Reftek 130 Datalo	trilli	Broad-band	500	response	trillium_120c+rt130@500	Velocity
25	Nanometrics Trillium 120 Compact/Reftek 130 Datalo	trilli	Broad-band	100	response	trillium_120c+rt130@100	Velocity
32	Chapparral 2.5 microphone/Reftek 130 Datalogger	chapar	Long-period	250	response	chapparral_25+rt130@250	Infrasound
33	PMD SP400U3/Reftek 130 Datalogger	SP400U	Broad-band	250	response	SP400U3+rt130@250	Velocity
36	Episensor 200 Hz 1.25 Volt per g/Reftek 130 Datalo	epi_1.	Broad-band	250	response	epi_1.25_vpg+rt130@250	Acceleration
37	EGE-73A Accelerometer 5000g/DTRA Datalogger	ege73a	Broad-band	1000000	response	ege73a+dtra_dl@1000000	Acceleration
38	EGE-73A Accelerometer 5000g/DTRA Datalogger	ege73a	Broad-band	500000	response	ege73a+dtra_dl@500000	Acceleration
39	7264B Accelerometer 2000g/DTRA Datalogger	e7264b	Broad-band	1000000	response	e7264b+dtra_dl@1000000	Acceleration
40	7264B Accelerometer 2000g/DTRA Datalogger	e7264b	Broad-band	500000	response	e7264b+dtra_dl@500000	Acceleration
41	7264C Accelerometer 500g/DTRA Datalogger	e7264c	Broad-band	1000000	response	e7264c+dtra_dl@1000000	Acceleration
42	7264C Accelerometer 500g/DTRA Datalogger	e7264c	Broad-band	500000	response	e7264c+dtra_dl@500000	Acceleration
46	EGCS-D0-50g Accelerometer/DTRA Datalogger	egcsd0	Broad-band	500000	response	egcsd0_50+dtra_dl@500000	Acceleration
47	EGCS-D0-100g Accel/DTRA Datalogger	egcsd0	Broad-band	1000000	response	egcsd0_100+dtra_dl@1000000	Acceleration
48	EGCS-D0-100g Accel/DTRA Datalogger	egcsd0	Broad-band	500000	response	egcsd0_100+dtra_dl@500000	Acceleration
49	EGCS-D0-50g Accelerometer/DTRA Datalogger	egcsd0	Broad-band	1000000	response	egcsd0_50+dtra_dl@1000000	Acceleration
50	Endevco 7264B-500/SNL Datalogger	endevc	Broad-band	4000	response	endevco_5c+snl_dl@4000	Acceleration
52	IML ST Infrasound/Reftek 130 Datalogger	iml_st	Long-period	500	response	iml_st+rt130@500	Infrasound

Appendix 3

Selected Metadata for SPE-1 Borehole Sensors

Appendix 3
Selected Metadata for SPE-1 Borehole Sensors

SPE Borehole Station	Channel	Instrument ID ^a	edepth ^b km	Northing	Easting	Elevation	Latitude	Longitude	Elevation
				SPC NAD27 ft		NGVD29 ft	GEO NAD83 dec.deg		NAVD88 m
				NSTec Survey & Colog Deviation ^c			USACE Corpscon6 Conversion ^d		
BH-01	FNR_1	37	0.0549	900,103.3	676,651.3	4,822.47	37.22127	116.06083	1470.90
	GNR_1	38							
	FNT_1	39							
	GNT_1	40							
BH-01	FNT_2	39	0.0457	900,102.6	676,650.8	4,852.47	37.22126	116.06083	1480.04
	GNT_2	40							
BH-01	FNR_3	37	0.0152	900,106.2	676,653.8	4,952.47	37.22127	116.06082	1510.52
	GNR_3	38							
	FNT_3	41							
	GNT_3	42							
	FNL_3	41							
	GNL_3	42							
BH-02	FNR_1	37	0.0549	900,076.4	676,614.2	4,822.47	37.22119	116.06096	1470.90
	GNR_1	38							
	FNT_1	39							
	GNT_1	40							
	FNL_1	39							
	GNL_1	40							
BH-02	FNR_2	37	0.0457	900,076.3	676,613.4	4,852.47	37.22119	116.06096	1480.04
	GNR_2	38							
	FNT_2	39							
	GNT_2	40							
	FNL_2	39							
	GNL_2	40							
BH-02	FNR_3	37	0.0152	900,075.8	676,609.5	4,952.47	37.22119	116.06097	1510.52
	GNR_3	38							
	FNT_3	41							
	GNT_3	42							
	FNL_3	41							
	GNL_3	42							
BH-03	FNR_1	37	0.0549	900,051.2	676,661.2	4,822.47	37.22112	116.06080	1470.90
	GNR_1	38							
	FNT_1	39							
	GNT_1	40							
BH-03	FNR_2	37	0.0457	900,051.5	676,660.6	4,852.47	37.22112	116.06080	1480.04
	GNR_2	38							
	FNT_2	39							
	GNT_2	40							
	FNL_2	39							
	GNL_2	40							
BH-03	FNR_3	37	0.0152	900,051.1	676,659.5	4,952.47	37.22112	116.06080	1510.52
	GNR_3	38							
	FNT_3	41							
	GNT_3	42							
	FNL_3	41							
	GNL_3	42							
BH-04	FNR_1	39	0.0549	900,015.0	676,612.6	4,822.47	37.22102	116.06096	1470.90
	GNR_1	40							
	FNT_1	37							
	GNT_1	38							
	FNL_1	37							
	GNL_1	38							
BH-04	FNR_2	39	0.0457	900,015.8	676,612.8	4,852.47	37.22103	116.06096	1480.04
	GNR_2	40							
	FNT_2	37							
	GNT_2	38							
	FNL_2	37							
	GNL_2	38							
BH-04	FNR_3	41	0.0152	900,018.1	676,612.7	4,952.47	37.22103	116.06096	1510.52
	GNR_3	42							
	FNT_3	37							
	GNT_3	38							
	FNL_3	37							
	GNL_3	38							

Appendix 3
Selected Metadata for SPE-1 Borehole Sensors

SPE Borehole Station	Channel	Instrument ID ^a	edepth ^b km	Northing	Easting	Elevation	Latitude	Longitude	Elevation
				SPC NAD27 ft		NGVD29 ft	GEO NAD83 dec.deg		NAVD88 m
				NSTec Survey & Colog Deviation ^c			USACE Corpscon6 Conversion ^d		
BH-05	FNR_2	39	0.0457	900,083.6	676,706.5	4,852.47	37.22121	116.06064	1480.04
	GNR_2	40							
	FNT_2	39							
	GNT_2	40							
	FNL_2	39							
	GNL_2	40							
BH-05	FNR_1	41	0.0152	900,083.1	676,706.6	4,952.47	37.22121	116.06064	1510.52
	GNR_1	42							
	FNT_1	37							
	GNT_1	38							
	FNL_1	37							
	GNL_1	38							
BH-06	FNR_1	39	0.0549	900,131.2	676,604.9	4,822.47	37.22134	116.06099	1470.90
	GNR_1	40							
	FNT_1	37							
	GNT_1	38							
	FNL_1	37							
	GNL_1	38							
BH-06	FNR_2	39	0.0457	900,131.4	676,604.7	4,852.47	37.22134	116.06099	1480.04
	GNR_2	40							
	FNT_2	37							
	GNT_2	38							
	FNL_2	37							
	GNL_2	38							
BH-06	FNR_3	37	0.0152	900,131.7	676,604.0	4,952.47	37.22134	116.06099	1510.52
	GNR_3	38							
	FNT_3	37							
	GNT_3	38							
	FNL_3	37							
	GNL_3	38							

NOTES

- a. See Appendix 2 for key to instruments.
- b. Depth in kilometers at which the instrument is positioned, relative to the ground surface elevation at the borehole collar.
- c. State Plane Coordinates at sensor location based on borehole collar location, as surveyed by NSTec, corrected for borehole deviation along borehole path, as measured by IDS Colog Group .
- d. Conversion of NSTec State Plane coordinates to latitude/longitude using the USACE "Corpscon6" application.

ABBREVIATIONS

SPC	State Plane Coordinate System, Zone 2702 Nevada Central
NAD27	North American Datum 1927
ft	U.S. Survey Feet
NGVD29	National Geodetic Vertical Datum 1929
NSTec	National Security Technologies, Inc.
GEO	Geographical Coordinate System
NAD83	North American Datum 1983
NAVD88	North American Vertical Datum 1988
m	Meters
USACE	U.S. Army Corps of Engineers

Appendix 4

Selected Metadata for SPE-1 Surface Stations

(Includes a list of known poor data channels
on far-field [>100 m] data)

Appendix 4
Selected Metadata for SPE-1 Surface Stations

Station Name	Station Header ID ^a	Instrument ID ^b	Estimated Latitude ^c (degrees)	Estimated Longitude ^d (degrees)	Elevation (km amsl)	Station Full Name
SP-01	SP-01		37.2212	-116.0609	1.5246	NNSS-SPE Shot Point 1
L1-01	L1001	3	37.2221	-116.061	1.529	NNSS-SPE Line 1 site 01
L1-02	L1002	3	37.223	-116.0611	1.537	NNSS-SPE Line 1 site 02
L1-03	L1003	3	37.2239	-116.0611	1.54	NNSS-SPE Line 1 site 03
L1-04	L1004	3	37.2248	-116.0612	1.537	NNSS-SPE Line 1 site 04
L1-05	L1005	3	37.2257	-116.0613	1.55	NNSS-SPE Line 1 site 05
L1-06	L1006	3	37.2266	-116.0614	1.558	NNSS-SPE Line 1 site 06
L1-07	L1007	3	37.2275	-116.0615	1.559	NNSS-SPE Line 1 site 07
L1-08	L1008	3	37.2284	-116.0616	1.572	NNSS-SPE Line 1 site 08
L1-09	L1009	3	37.2293	-116.0616	1.589	NNSS-SPE Line 1 site 09
L1-10	L1010	3, 13, 14	37.2302	-116.0617	1.585	NNSS-SPE Line 1 site 10
L1-11	L1011	3	37.2311	-116.0618	1.597	NNSS-SPE Line 1 site 11
L1-12	L1012	3	37.232	-116.0619	1.604	NNSS-SPE Line 1 site 12
L1-13	L1013	3	37.2329	-116.062	1.616	NNSS-SPE Line 1 site 13
L1-14	L1014	3	37.2338	-116.0621	1.633	NNSS-SPE Line 1 site 14
L1-15	L1015	3	37.2347	-116.0621	1.656	NNSS-SPE Line 1 site 15
L1-16	L1016	3	37.2355	-116.0622	1.674	NNSS-SPE Line 1 site 16
L1-17	L1017	3	37.2364	-116.0623	1.706	NNSS-SPE Line 1 site 17
L1-18	L1018	3	37.2373	-116.0624	1.739	NNSS-SPE Line 1 site 18
L1-19	L1019	3	37.2382	-116.0625	1.738	NNSS-SPE Line 1 site 19
L1-20	L1020	18	37.2391	-116.0626	1.752	NNSS-SPE Line 1 site 20
L2-01	L2001	3	37.2218	-116.06	1.52	NNSS-SPE Line 2 site 01
L2-02	L2002	3	37.2224	-116.0592	1.515	NNSS-SPE Line 2 site 02
L2-03	L2003	3	37.2229	-116.0583	1.528	NNSS-SPE Line 2 site 03
L2-04	L2004	3	37.2235	-116.0575	1.528	NNSS-SPE Line 2 site 04
L2-05	L2005	3	37.2241	-116.0566	1.532	NNSS-SPE Line 2 site 05
L2-06	L2006	3	37.2247	-116.0558	1.531	NNSS-SPE Line 2 site 06
L2-07	L2007	3	37.2253	-116.0549	1.53	NNSS-SPE Line 2 site 07
L2-08	L2008	3	37.2259	-116.0541	1.53	NNSS-SPE Line 2 site 08
L2-09	L2009	3	37.2265	-116.0533	1.537	NNSS-SPE Line 2 site 09
L2-10	L2010	3, 13, 14	37.2271	-116.0524	1.531	NNSS-SPE Line 2 site 10
L2-11	L2011	3	37.2277	-116.0516	1.537	NNSS-SPE Line 2 site 11
L2-12	L2012	3	37.2283	-116.0507	1.537	NNSS-SPE Line 2 site 12
L2-13	L2013	3	37.2289	-116.0499	1.536	NNSS-SPE Line 2 site 13
L2-14	L2014	3	37.2295	-116.049	1.541	NNSS-SPE Line 2 site 14
L2-15	L2015	3	37.2301	-116.0482	1.543	NNSS-SPE Line 2 site 15
L2-16	L2016	3	37.2307	-116.0473	1.536	NNSS-SPE Line 2 site 16
L2-17	L2017	3	37.2312	-116.0465	1.549	NNSS-SPE Line 2 site 17
L2-18	L2018	3	37.2318	-116.0456	1.548	NNSS-SPE Line 2 site 18
L2-19	L2019	3	37.2324	-116.0448	1.552	NNSS-SPE Line 2 site 19
L2-20	L2020	18	37.233	-116.0439	1.533	NNSS-SPE Line 2 site 20
L3-01	L3001	3	37.2203	-116.0607	1.516	NNSS-SPE Line 3 site 01
L3-02	L3002	3	37.2194	-116.0606	1.512	NNSS-SPE Line 3 site 02
L3-03	L3003	3	37.2185	-116.0605	1.512	NNSS-SPE Line 3 site 03
L3-04	L3004	3	37.2176	-116.0603	1.496	NNSS-SPE Line 3 site 04
L3-05	L3005	3	37.2167	-116.0602	1.496	NNSS-SPE Line 3 site 05
L3-06	L3006	3	37.2158	-116.06	1.494	NNSS-SPE Line 3 site 06
L3-07	L3007	3	37.2149	-116.0599	1.487	NNSS-SPE Line 3 site 07
L3-08	L3008	3	37.214	-116.0598	1.484	NNSS-SPE Line 3 site 08
L3-09	L3009	3	37.2131	-116.0596	1.469	NNSS-SPE Line 3 site 09
L3-10	L3010	3, 13, 14	37.2122	-116.0595	1.481	NNSS-SPE Line 3 site 10
L3-11	L3011	3	37.2113	-116.0593	1.475	NNSS-SPE Line 3 site 11
L3-12	L3012	3	37.2104	-116.0592	1.464	NNSS-SPE Line 3 site 12
L3-13	L3013	3	37.2095	-116.0591	1.459	NNSS-SPE Line 3 site 13
L3-14	L3014	3	37.2087	-116.0589	1.463	NNSS-SPE Line 3 site 14
L3-15	L3015	3	37.2078	-116.0588	1.453	NNSS-SPE Line 3 site 15
L3-16	L3016	3	37.2069	-116.0586	1.437	NNSS-SPE Line 3 site 16
L3-17	L3017	3	37.206	-116.0585	1.431	NNSS-SPE Line 3 site 17
L3-18	L3018	3	37.2051	-116.0584	1.434	NNSS-SPE Line 3 site 18
L3-19	L3019	3	37.2042	-116.0582	1.428	NNSS-SPE Line 3 site 19

Appendix 4
Selected Metadata for SPE-1 Surface Stations

Station Name	Station Header ID ^a	Instrument ID ^b	Estimated Latitude ^c (degrees)	Estimated Longitude ^d (degrees)	Elevation (km amsl)	Station Full Name
L3-20	L3020	18	37.2033	-116.0581	1.423	NNSS-SPE Line 3 site 20
L3-23	L3023	24, 25	37.1899	-116.056	1.345	NNSS-SPE Line 3 site 23
L3-26	L3026	25	37.177	-116.0539	1.31	NNSS-SPE Line 3 site 26
L3-28	L3028	25	37.1407	-116.0482	1.285	NNSS-SPE Line 3 site 28
L3-30	L3030	23, 24, 25	37.1049	-116.0426	1.274	NNSS-SPE Line 3 site 30
L3-32	L3032	24, 25	37.0697	-116.037	1.236	NNSS-SPE Line 3 site 32
L3-34	L3034	24, 25	37.033	-116.0314	1.218	NNSS-SPE Line 3 site 34
L3-36	L3036	24, 25	36.9976	-116.0258	1.204	NNSS-SPE Line 3 site 36
L4-01	L4001	3	37.2204	-116.0614	1.523	NNSS-SPE Line 4 site 01
L4-02	L4002	3	37.2195	-116.0619	1.521	NNSS-SPE Line 4 site 02
L4-03	L4003	3	37.2187	-116.0624	1.532	NNSS-SPE Line 4 site 03
L4-04	L4004	3	37.2179	-116.0629	1.523	NNSS-SPE Line 4 site 04
L4-05	L4005	3	37.2171	-116.0634	1.502	NNSS-SPE Line 4 site 05
L4-06	L4006	3	37.2163	-116.0639	1.499	NNSS-SPE Line 4 site 06
L4-07	L4007	3	37.2155	-116.0643	1.513	NNSS-SPE Line 4 site 07
L4-08	L4008	3	37.2147	-116.0648	1.505	NNSS-SPE Line 4 site 08
L4-09	L4009	3	37.2139	-116.0653	1.507	NNSS-SPE Line 4 site 09
L4-10	L4010	3	37.2131	-116.0658	1.504	NNSS-SPE Line 4 site 10
L4-11	L4011	3	37.2123	-116.0663	1.508	NNSS-SPE Line 4 site 11
L4-12	L4012	3	37.2114	-116.0668	1.511	NNSS-SPE Line 4 site 12
L4-13	L4013	3	37.2106	-116.0673	1.512	NNSS-SPE Line 4 site 13
L4-14	L4014	3	37.2098	-116.0678	1.511	NNSS-SPE Line 4 site 14
L4-15	L4015	3	37.209	-116.0683	1.514	NNSS-SPE Line 4 site 15
L4-16	L4016	3	37.2082	-116.0688	1.514	NNSS-SPE Line 4 site 16
L4-17	L4017	3	37.2074	-116.0693	1.512	NNSS-SPE Line 4 site 17
L4-18	L4018	3	37.2066	-116.0698	1.508	NNSS-SPE Line 4 site 18
L4-19	L4019	3	37.2058	-116.0703	1.513	NNSS-SPE Line 4 site 19
L4-20	L4020	18	37.205	-116.0708	1.507	NNSS-SPE Line 4 site 20
L4-23	L4023	24, 25	37.1928	-116.0782	1.44	NNSS-SPE Line 4 site 23
L4-26	L4026	24, 25	37.1807	-116.0856	1.38	NNSS-SPE Line 4 site 26
L4-28	L4028	24, 25	37.1483	-116.1053	1.355	NNSS-SPE Line 4 site 28
L4-30	L4030	24, 25	37.1159	-116.125	1.378	NNSS-SPE Line 4 site 30
L4-32	L4032	24, 25	37.0835	-116.1447	1.421	NNSS-SPE Line 4 site 32
L4-34	L4034	24, 25	37.051	-116.1644	1.568	NNSS-SPE Line 4 site 34
L4-36	L4036	24, 25	37.0186	-116.1841	1.527	NNSS-SPE Line 4 site 36
L5-01	L5001	3	37.2214	-116.062	1.539	NNSS-SPE Line 5 site 01
L5-02	L5002	3	37.2216	-116.0631	1.556	NNSS-SPE Line 5 site 02
L5-03	L5003	3	37.2218	-116.0642	1.577	NNSS-SPE Line 5 site 03
L5-04	L5004	3	37.222	-116.0653	1.622	NNSS-SPE Line 5 site 04
L5-05	L5005	3	37.2222	-116.0664	1.641	NNSS-SPE Line 5 site 05
L5-06	L5006	3	37.2225	-116.0675	1.619	NNSS-SPE Line 5 site 06
L5-07	L5007	3	37.2227	-116.0686	1.612	NNSS-SPE Line 5 site 07
L5-08	L5008	3	37.2229	-116.0696	1.589	NNSS-SPE Line 5 site 08
L5-09	L5009	3	37.2231	-116.0707	1.579	NNSS-SPE Line 5 site 09
L5-10	L5010	3, 13, 14	37.2233	-116.0718	1.568	NNSS-SPE Line 5 site 10
L5-11	L5011	3	37.2235	-116.0729	1.566	NNSS-SPE Line 5 site 11
L5-12	L5012	3	37.2237	-116.074	1.586	NNSS-SPE Line 5 site 12
L5-13	L5013	3	37.224	-116.0751	1.612	NNSS-SPE Line 5 site 13
L5-14	L5014	3	37.2242	-116.0762	1.642	NNSS-SPE Line 5 site 14
L5-15	L5015	3	37.2244	-116.0773	1.678	NNSS-SPE Line 5 site 15
L5-16	L5016	18	37.2246	-116.0784	1.725	NNSS-SPE Line 5 site 16
L5-24	L5024	24, 25	37.2297	-116.1047	1.767	NNSS-SPE Line 5 site 24
L5-26	L5026	24, 25	37.2319	-116.1156	1.808	NNSS-SPE Line 5 site 26
L5-28	L5028	24, 25	37.2404	-116.1594	1.911	NNSS-SPE Line 5 site 28
L5-30	L5030	24, 25	37.249	-116.2032	2.074	NNSS-SPE Line 5 site 30
L5-34	L5034	24, 25	37.266	-116.2909	2.077	NNSS-SPE Line 5 site 34
L5-36	L5036	24, 25	37.2745	-116.3347	2.1	NNSS-SPE Line 5 site 36
AF-01	AF001	32, 33	37.216	-116.1611	1.6371	NNSS-SPE AFTAC site 01
AF-02	AF002	32, 33	37.164	-116.1423	1.4941	NNSS-SPE AFTAC site 02
AF-03	AF003	32, 33	37.1313	-116.0573	1.2618	NNSS-SPE AFTAC site 03

Appendix 4
Selected Metadata for SPE-1 Surface Stations

Station Name	Station Header ID ^a	Instrument ID ^b	Estimated Latitude ^c (degrees)	Estimated Longitude ^d (degrees)	Elevation (km amsl)	Station Full Name
AF-04	AF004	32, 33	37.1801	-115.9834	1.437	NNSS-SPE AFTAC site 04
AF-05	AF005	32, 33	37.1894	-116.0204	1.3372	NNSS-SPE AFTAC site 05
AF-06	AF006	36	37.0531	-116.0903	1.2484	NNSS-SPE AFTAC site 06
AF-07	AF007	32, 33	37.1239	-116.1478	1.4521	NNSS-SPE AFTAC site 07
AF-08	AF008	15, 19	37.2211	-116.0496	1.4539	NNSS-SPE AFTAC site 08
AF-09	AF009	15, 19	37.2299	-116.0577	1.549	NNSS-SPE AFTAC site 09
BH-01	BH-01	Note d	37.2213	-116.0608	1.5248	NNSS-SPE DTRA Borehole 01
BH-02	BH-02	Note d	37.2212	-116.061	1.5249	NNSS-SPE DTRA Borehole 02
BH-03	BH-03	Note d	37.2211	-116.0608	1.5247	NNSS-SPE DTRA Borehole 03
BH-04	BH-04	Note d	37.221	-116.061	1.5247	NNSS-SPE DTRA Borehole 04
BH-05	BH-05	Note d	37.2212	-116.0606	1.5246	NNSS-SPE DTRA Borehole 05
BH-06	BH-06	Note d	37.2214	-116.061	1.5257	NNSS-SPE DTRA Borehole 06
DT-07	DT-07	47, 48	37.2212	-116.0609	1.5247	NNSS-SPE DTRA Surface sp1 0m
DT-08	DT-08	47, 48	37.2211	-116.0609	1.5247	NNSS-SPE DTRA Surface sp1 10m
DT-09	DT-09	47, 48	37.221	-116.061	1.5246	NNSS-SPE DTRA Surface sp1 20m
DT-10	DT-10	47, 48	37.221	-116.061	1.5246	NNSS-SPE DTRA Surface sp1 30m
DT-11	DT-11	46, 49	37.2209	-116.0611	1.5225	NNSS-SPE DTRA Surface sp1 40m
DT-12	DT-12	46, 49	37.2208	-116.0611	1.5223	NNSS-SPE DTRA Surface sp1 50m
SL-01	SL-01	50	37.2212	-116.0609	1.5247	NNSS-SPE Sandia NL surface 01 sp1
SL-02	SL-02	50	37.2211	-116.0609	1.5246	NNSS-SPE Sandia NL surface 02 sp1
SL-03	SL-03	50	37.221	-116.061	1.5246	NNSS-SPE Sandia NL surface 03 sp1
SL-04	SL-04	50	37.221	-116.061	1.5245	NNSS-SPE Sandia NL surface 04 sp1
SL-05	SL-05	50	37.2209	-116.0611	1.5224	NNSS-SPE Sandia NL surface 05 sp1
SL-06	SL-06	50	37.2208	-116.0611	1.5222	NNSS-SPE Sandia NL surface 06 sp1
IS11	IS11	52	37.2235	-116.0614	1.5451	NNSS-SPE Sandia Inf 250 m N
IS12	IS12	52	37.2234	-116.0611	1.5419	NNSS-SPE Sandia Inf 233 m N
IS13	IS13	52	37.2232	-116.0609	1.5385	NNSS-SPE Sandia Inf 208 m N
IS14	IS14	52	37.2232	-116.0614	1.5451	NNSS-SPE Sandia Inf 218 m N
IS21	IS21	52	37.2193	-116.0604	1.5138	NNSS-SPE Sandia Inf 226 m S
IS22	IS22	52	37.219	-116.0605	1.5163	NNSS-SPE Sandia Inf 251 m S
IS23	IS23	52	37.2189	-116.0603	1.512	NNSS-SPE Sandia Inf 271 m S
IS24	IS24	52	37.2188	-116.0608	1.5182	NNSS-SPE Sandia Inf 270 m S
IS31	IS31	52	37.2219	-116.0635	1.5704	NNSS-SPE Sandia Inf 249 m W
IS32	IS32	52	37.2217	-116.0636	1.5659	NNSS-SPE Sandia Inf 251 m W
IS33	IS33	52	37.2215	-116.0634	1.5597	NNSS-SPE Sandia Inf 229 m W
IS34	IS34	52	37.2215	-116.0638	1.5627	NNSS-SPE Sandia Inf 261 m W
IS41	IS41	52	37.2235	-116.0579	1.5325	NNSS-SPE Sandia Inf 363 m E
IS42	IS42	52	37.2233	-116.058	1.5315	NNSS-SPE Sandia Inf 339 m E
IS43	IS43	52	37.2232	-116.0576	1.5301	NNSS-SPE Sandia Inf 353 m E
IS44	IS44	52	37.2233	-116.0582	1.5301	NNSS-SPE Sandia Inf 320 m E
IS51	IS51	52	37.1776	-116.0541	1.3107	NNSS-SPE Sandia Inf 5 Km S
IS52	IS52	52	37.1773	-116.0542	1.3107	NNSS-SPE Sandia Inf 5 Km S
IS53	IS53	52	37.1771	-116.054	1.3107	NNSS-SPE Sandia Inf 5 Km S
IS54	IS54	52	37.1773	-116.0545	1.3106	NNSS-SPE Sandia Inf 5 Km S
IS61	IS61	52	37.2125	-116.0595	1.4833	NNSS-SPE Sandia Inf 1 Km S
IS62	IS62	52	37.2122	-116.0594	1.4826	NNSS-SPE Sandia Inf 1 Km S
IS63	IS63	52	37.2123	-116.0591	1.4809	NNSS-SPE Sandia Inf 1 Km S
IS64	IS64	52	37.2121	-116.0598	1.4821	NNSS-SPE Sandia Inf 1 Km S
IS71	IS71	52	37.2035	-116.0581	1.4267	NNSS-SPE Sandia Inf 2 Km S
IS72	IS72	52	37.2033	-116.0581	1.4253	NNSS-SPE Sandia Inf 2 Km S
IS73	IS73	52	37.2033	-116.0578	1.4201	NNSS-SPE Sandia Inf 2 Km S
IS74	IS74	52	37.2033	-116.0583	1.4261	NNSS-SPE Sandia Inf 2 Km S

NOTES:

- a. Headers of far-field stations changed to remove hyphens and replace with zeroes. Near-field headers retain the dash, as they are being submitted as an assembled data set with it's own meta-data volume in CSS3.0
- b. See Appendix 2 for key to instruments
- c. Locations north of the equator have positive latitudes
- d. Locations east of the Greenwich Meridian have positive longitudes
- e. Collar location of instrument borehole. See Appendix 3 for borehole instrument metadata.

km = kilometers

amsl = above mean sea level

See following table with list of known poor data channels identified along the five surface geophone lines.

Appendix 4

List of Known Poor Data Channels on Source Physics Experiment Far Field (>100 m) Geophone Lines

Channel	Potential Issue
Line 1	
L1-10.CN(ZT)	Polarity reversal?
L1-16.CLZ	No signal
L1-17.CLZ	No signal
Line 2	
L2-02.CLZ	Low amplitude; crosstalk?
L2-10.DJR	No signal
L2-17.CLZ	No signal
L2-18.CLZ	No signal
L2-19.CLZ	No signal
Line 3	
L3-01.CLZ	Low amplitude
L3-10.DJ(ZRT)	No signal
L3-30.CHE	No signal
L3-34.CHN	No signal
L3-36.CH(ZNE)	No signal
Line 4	
L4-06.CLZ	Low amplitude
L4-19.CLZ	Noise
L4-32.CH(NE)	Low amplitude
L4-34.CH(ZNE)	Monochromatic noise
Line 5	
L5-05.CLZ	Low amplitude; crosstalk?
L5-08.CLT	High amplitude?
L5-11.CLZ	High amplitude?
L5-26.CHN	No signal
L5-36.CH(ZNE)	No signal

Appendix 5

SPE-1 Baseline Shift Corrections **LA-UR-13-23956**

Prepared by E. Rougier and D. Steedman
Los Alamos National Laboratory

LA-UR-13-23956

Approved for public release; distribution is unlimited.

Title: SPE-1 BASELINE SHIFT CORRECTIONS

Author(s): Rougier, Esteban
Steedman, David W.

Intended for: Report

Issued: 2013-05-30 (Draft)



Disclaimer:

Los Alamos National Laboratory, an affirmative action/equal opportunity employer, is operated by the Los Alamos National Security, LLC for the National Nuclear Security Administration of the U.S. Department of Energy under contract DE-AC52-06NA25396. By approving this article, the publisher recognizes that the U.S. Government retains nonexclusive, royalty-free license to publish or reproduce the published form of this contribution, or to allow others to do so, for U.S. Government purposes. Los Alamos National Laboratory requests that the publisher identify this article as work performed under the auspices of the U.S. Department of Energy. Los Alamos National Laboratory strongly supports academic freedom and a researcher's right to publish; as an institution, however, the Laboratory does not endorse the viewpoint of a publication or guarantee its technical correctness.

SPE-1 BASELINE SHIFT CORRECTIONS

E. Rougier and D. W. Steedman
Geophysics Group, Los Alamos National Laboratory

Acknowledgements

The Source Physics Experiments (SPE) would not have been possible without the support of many people from several organizations. The author (s) wish to express their gratitude to the SPE working group, a multi-institutional and interdisciplinary group of scientists and engineers from National Security Technologies (NSTec), Lawrence Livermore National Laboratory (LLNL), Los Alamos National Laboratory (LANL), Sandia National Laboratories (SNL), the Defense Threat Reduction Agency (DTRA), and the Air Force Technical Applications Center (AFTAC). Deepest appreciation to Mrs. Bob White and Ryan Emmitt (NSTec) for their tireless support on the seismic array and to the University of Nevada, Reno (UNR) for their support with the seismic network and data aggregation. Thanks to U.S. Geological Survey (USGS), the Incorporated Research Institutions for Seismology (IRIS) Program for Array Seismic Studies of the Continental Lithosphere (PASSCAL) Instrument Center, Lawrence Berkeley National Laboratory (LBNL), and Dr. Roger Waxler (University of Mississippi) for instrumentation partnership. The author(s) also wish to thank the National Nuclear Security Administration, Defense Nuclear Nonproliferation Research and Development (DNN R&D) for their sponsorship of the National Center for Nuclear Security (NCNS) and its Source Physics Experiment (SPE) working group. This work was sponsored by the NNSA under award number DE-AC52-06NA25946.

Disclaimer

The baseline shift corrections presented in this report have been made following a set of practices considered by the authors to be appropriate. This report is intended to document those corrections which were made to support subsequent analyses by the authors.

1. BASELINE SHIFT CORRECTION PROCESS

The acceleration data obtained from the free-field accelerometers nominally located at the 10-m and 20-m range from ground zero (GZ) require baseline shift correction prior to analysis (*e.g.*, comparison with hydrodynamic calculation results, seismic-related analysis, *etc.*).

We used as our starting point the accelerometer data that were corrected in the manner of References 1 and 2 for gauge rotations that were described by Reference 3. These records are referred to herein as a^{orig} .

The baseline shift corrections presented in this work were made in two main stages:

- Correction for pre-arrival baseline shift.
- Correction for post-arrival baseline shift.

1.1. Correction for pre-arrival baseline shift

A typical accelerometer record will display a DC shift caused by electronic drift in the measurement and recording system. This appears as a constant offset from the expected pre-shock 0. acceleration. The cumulative offset during integration for velocity renders the data useless and must be corrected to achieve accurate portrayal of the velocity positive phase. To compensate, the pre-arrival baseline

shift acceleration was computed from the data and then subtracted from all points in the record. For each of the components of the acceleration the correction was made as shown in equation (1).

$$a^{pre} = a^{orig} + a^{c-pre} \quad (1)$$

where a^{c-pre} is the pre-arrival acceleration baseline shift correction and a^{pre} is the acceleration record corrected by this pre-arrival shift.

1.2. Correction for post-arrival baseline shift

A second shift occurs in many accelerometer records as the explosive wave shocks the instruments. This phenomenon has little noticeable effect on the outward phase velocity (either peak or duration) and is often neglected. However, some analysis (e.g., Ref. 4) is based on displacement records and this analysis is greatly facilitated by accomplishing a second correction for this post-shock shift. This second correction was made in the velocity domain. In other words, the acceleration data were integrated with respect to time in order to obtain the velocity waveforms. The time interval considered in this analysis goes from 0.0s (shot time) to 0.1s. Each component of the velocity waveforms was corrected so that the waveform reaches a condition as close as possible to steady state; i.e., zero velocity as shown in Figure 1. The correction on the acceleration was derived from the correction on the velocity by performing a simple derivation. The final acceleration records for each component were obtained by adding the post-arrival correction on the acceleration to the pre-arrival corrected acceleration, as shown in equation (2).

$$a^{final} = a^{pre} + a^{c-post} \quad (2)$$

where a^{final} is the final (corrected) acceleration record, a^{pre} is obtained from equation (1) and a^{c-post} is the post-arrival acceleration baseline shift.

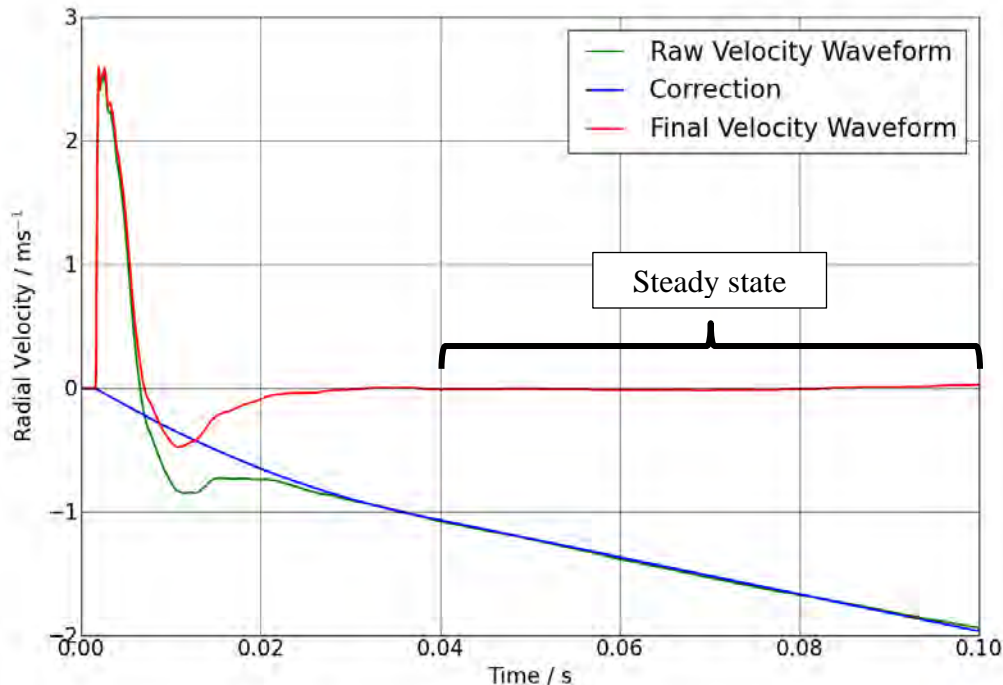


Figure 1. Example of velocity correction.

2. FIGURES

In this section we present the velocity and displacement waveforms for the three components of the corrected data. The affected data records are listed in the following table.

Depth	Component	Borehole #					
		1	2	3	4	5	6
1 (180 ft)	R	✓	✓		✓		✓
	T	✓	✓		✓		✓
	L		✓		✓		✓
2 (150 ft)	R		✓	✓	✓		✓
	T		✓	✓	✓		✓
	L		✓	✓	✓		✓
3 (50 ft)	R	✓	✓	✓	✓	✓	✓
	T	✓	✓	✓	✓	✓	✓
	L	✓	✓	✓	✓	✓	✓

2.1. Records corrected for pre-arrival baseline shift

The key to the legend in the graphs presented in this section is the following:

- v^{orig} represents the velocity waveform obtained by integrating the accelerometer data that were corrected in the manner of References 1 and 2 to for gauge rotations that were described by Reference 3.
- v^{c-pre} represents the pre-arrival baseline shift acceleration correction in the velocity space.
- v^{pre} represents the velocity waveforms corrected for the pre-arrival baseline shift.

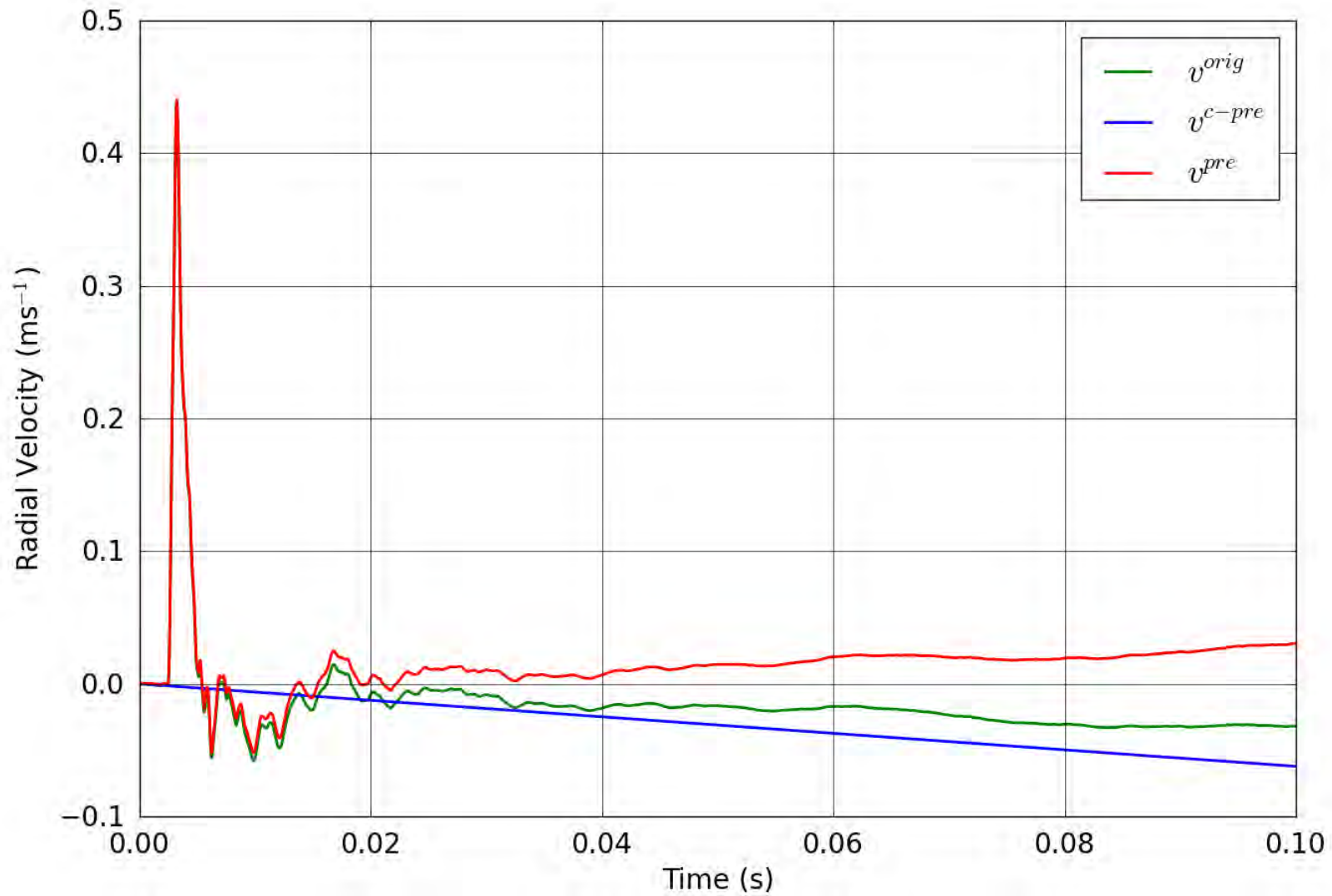


Figure 2. SPE-1 Gauge 1-1-R – Pre-shot baseline correction of the radial velocity.

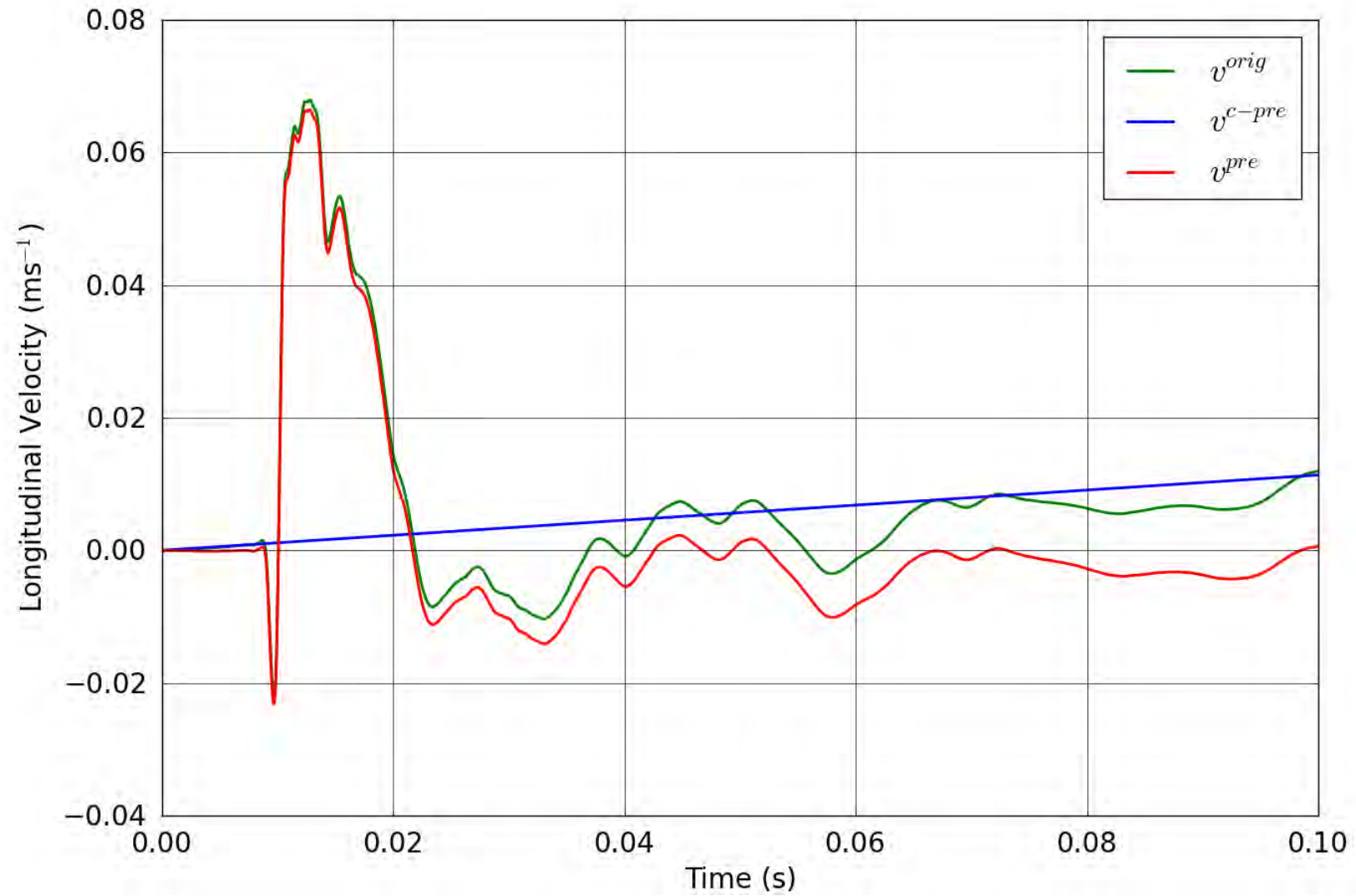


Figure 3. SPE-1 Gauge 1-3-L – Pre-shot baseline correction of the longitudinal velocity.

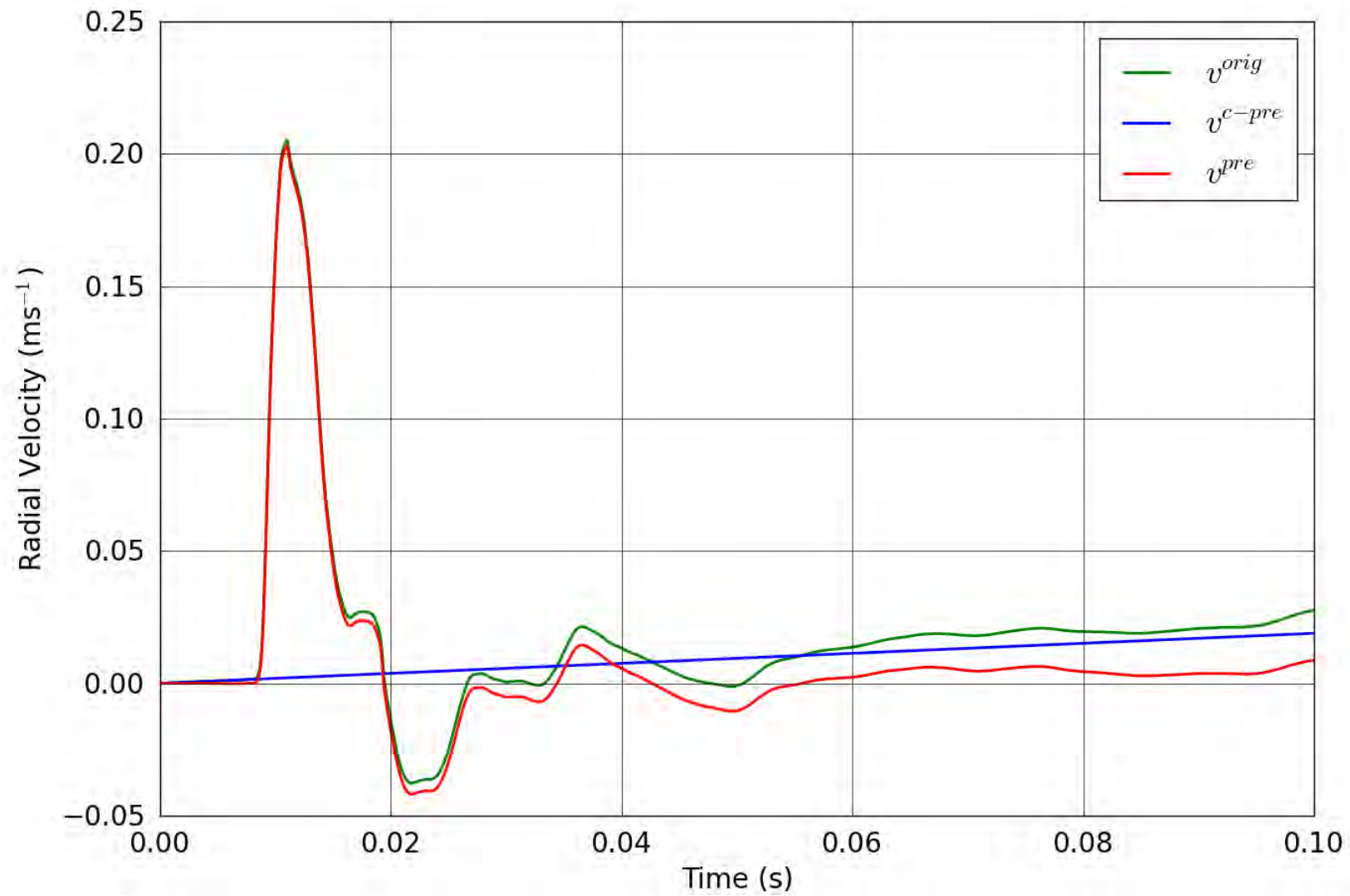


Figure 4. SPE-1 Gauge 1-3-R – Pre-shot baseline correction of the radial velocity.

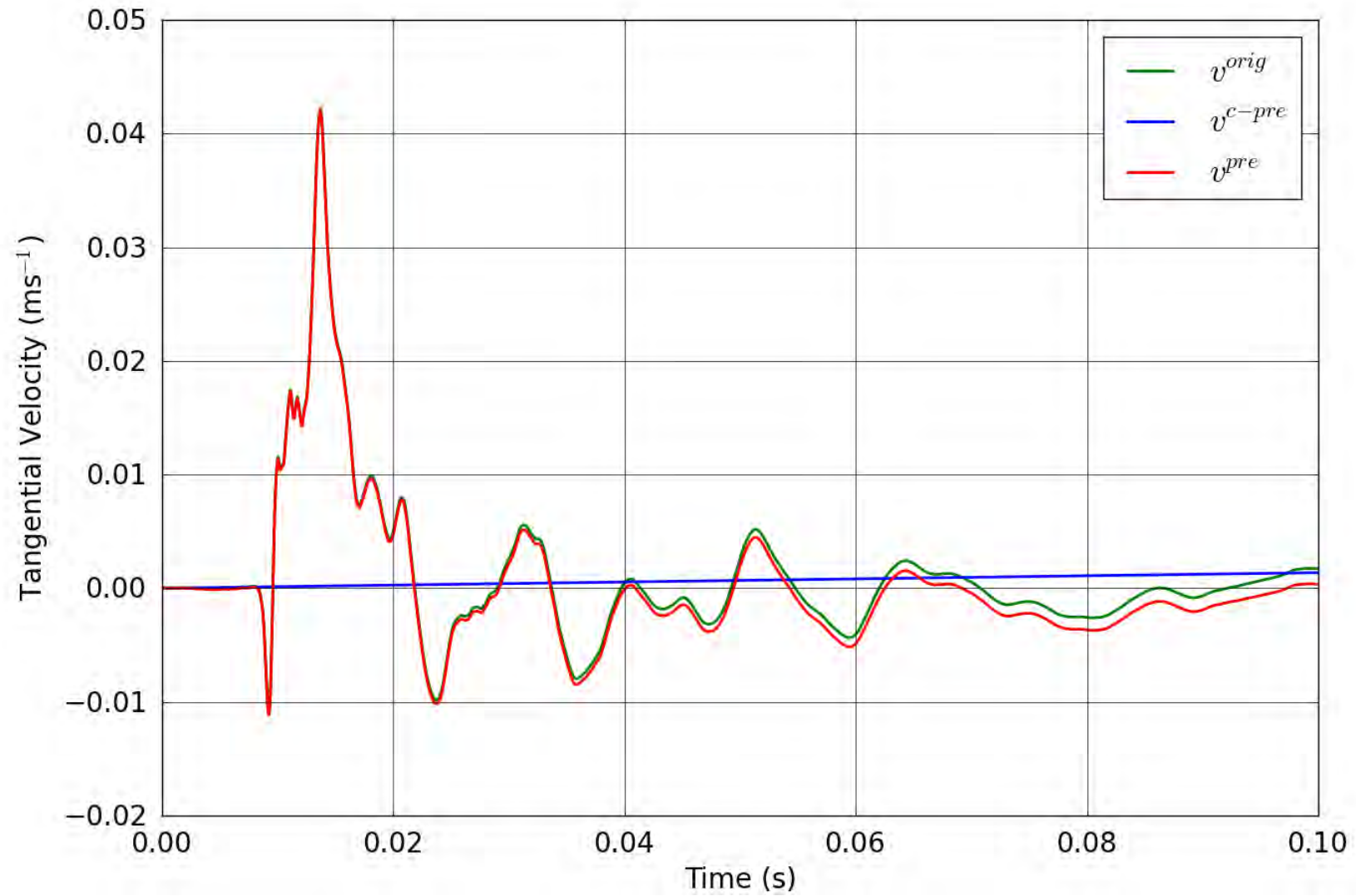


Figure 5. SPE-1 Gauge 1-3-T – Pre-shot baseline correction of the tangential velocity.

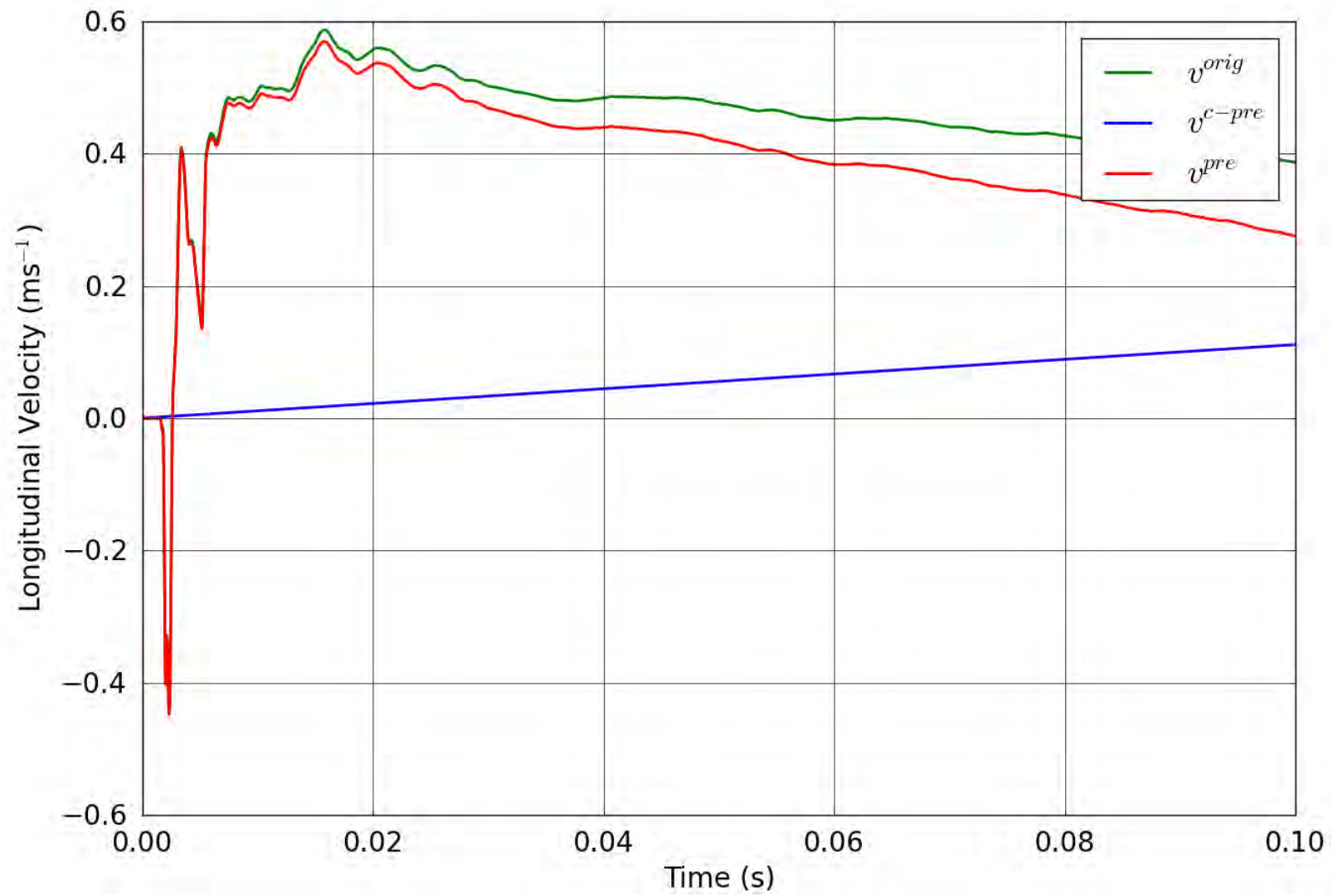


Figure 6. SPE-1 Gauge 2-1-L – Pre-shot baseline correction of the longitudinal velocity.

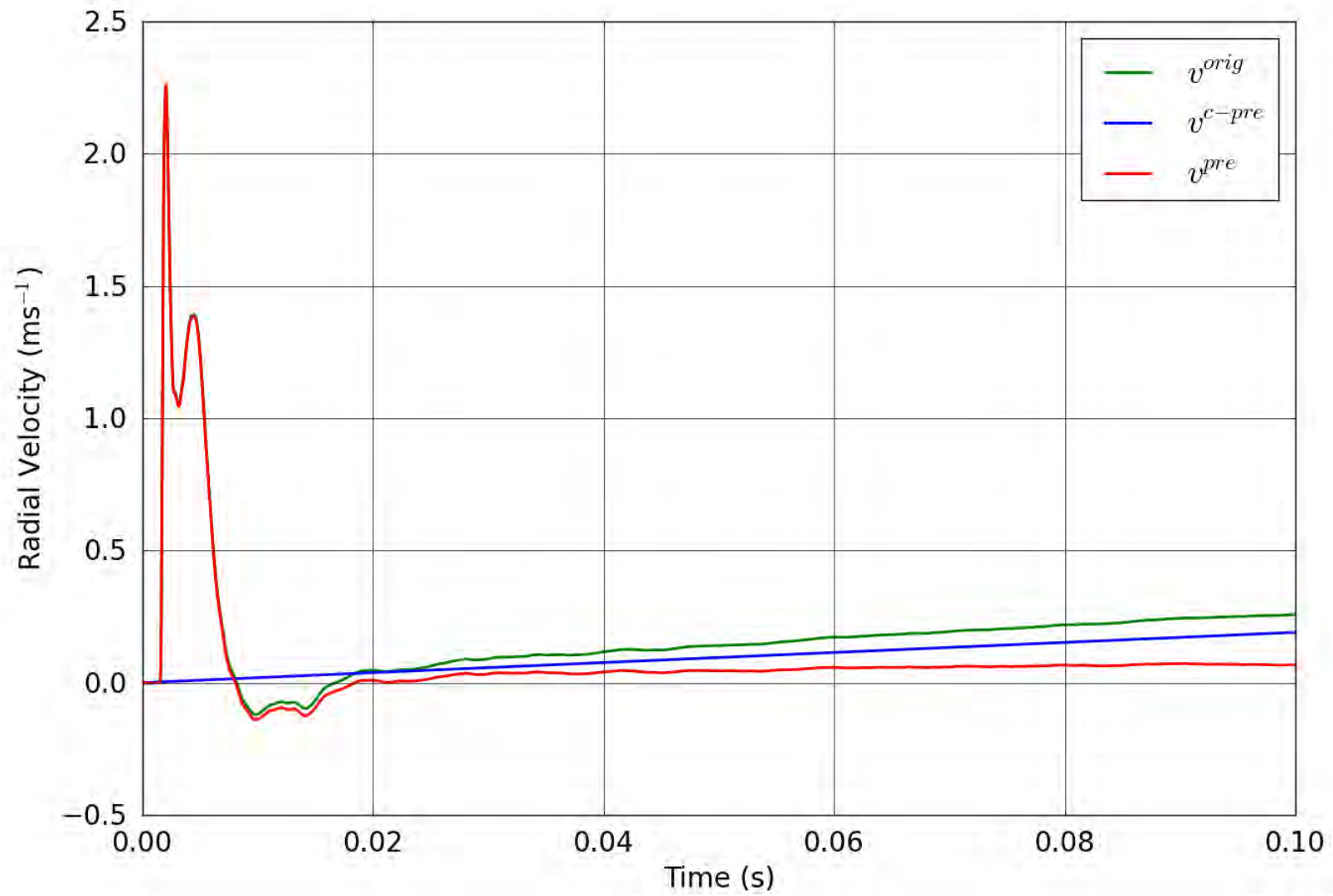


Figure 7. SPE-1 Gauge 2-1-R – Pre-shot baseline correction of the radial velocity.

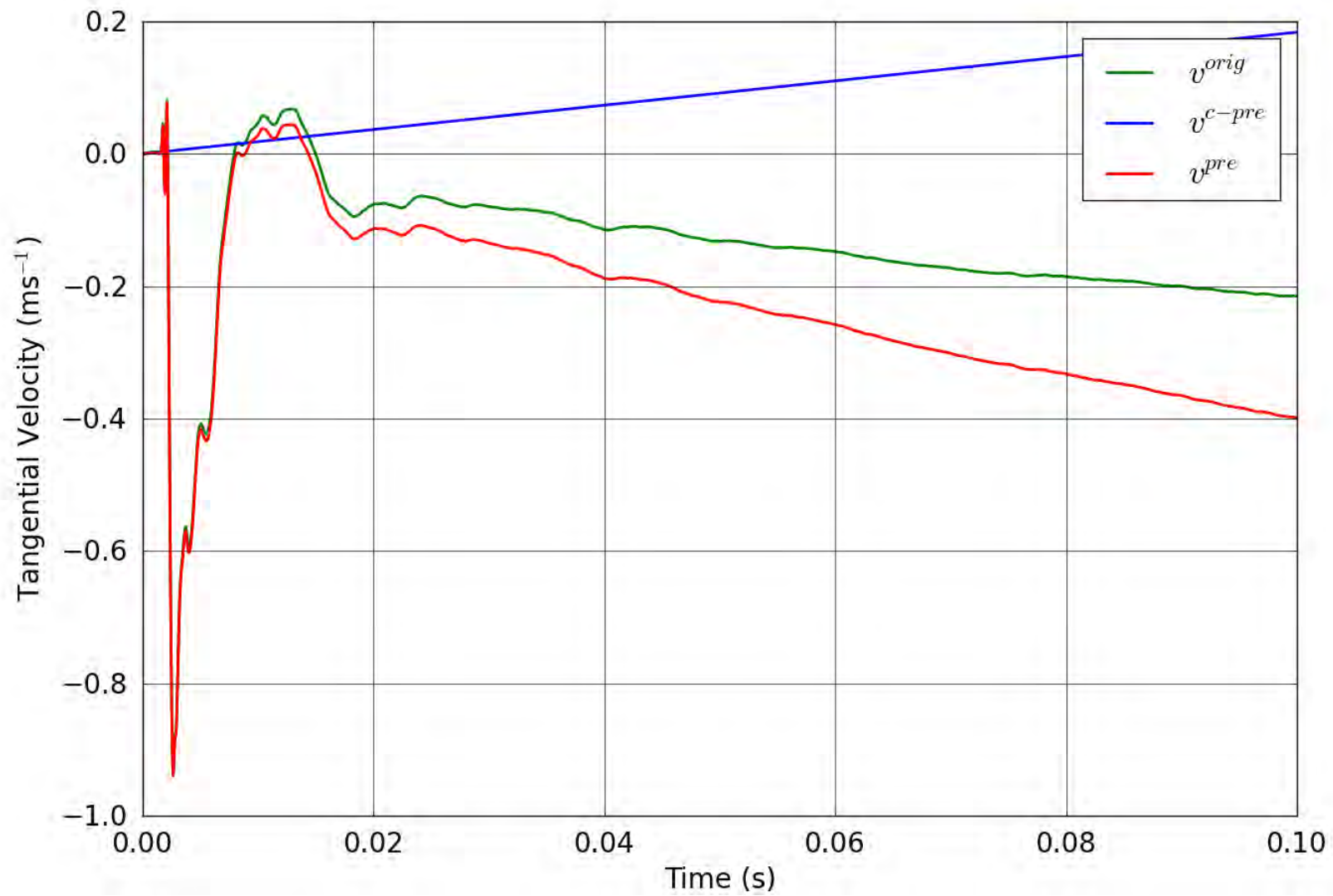


Figure 8. SPE-1 Gauge 2-1-T – Pre-shot baseline correction of the tangential velocity.

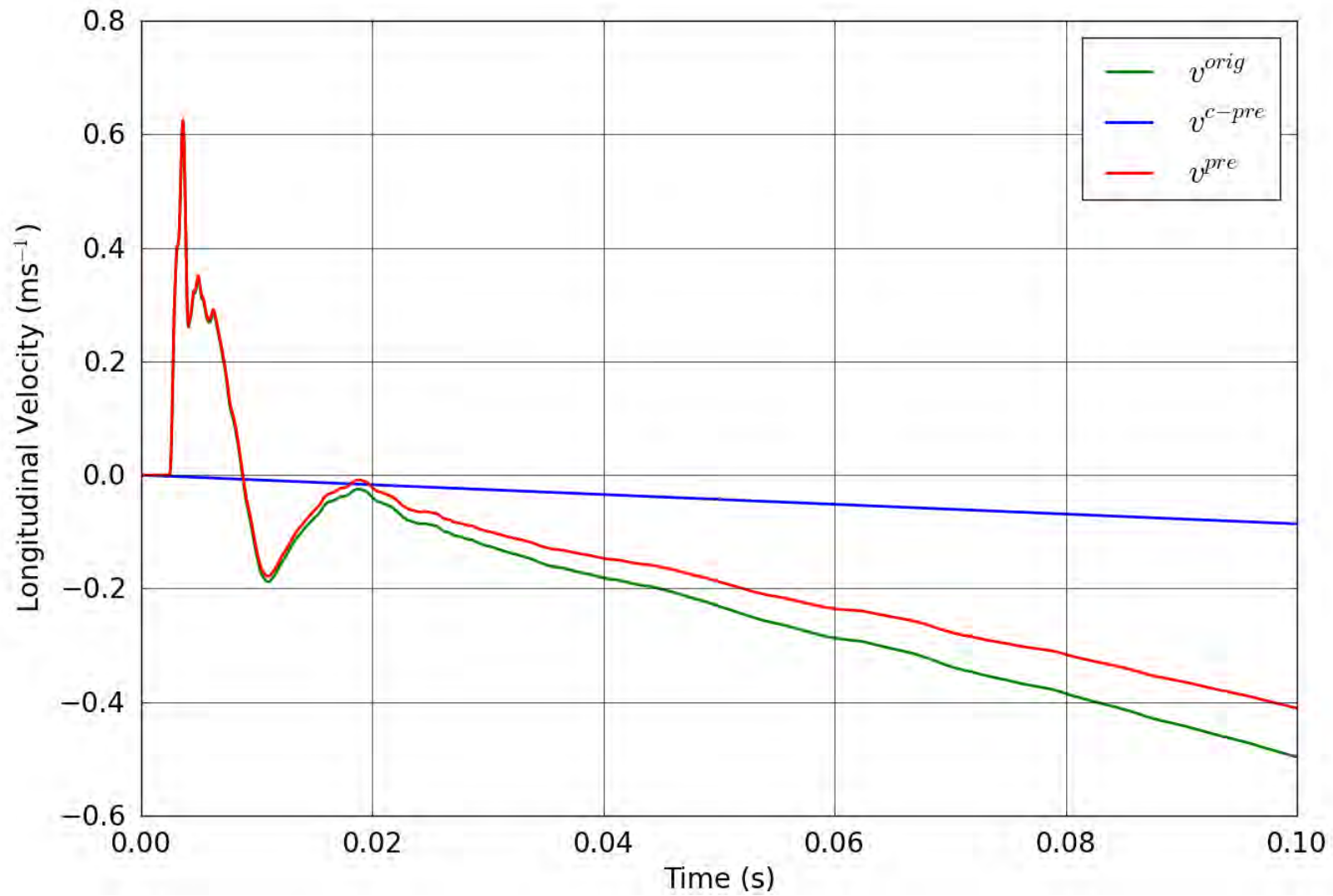


Figure 9. SPE-1 Gauge 2-2-L – Pre-shot baseline correction of the longitudinal velocity.

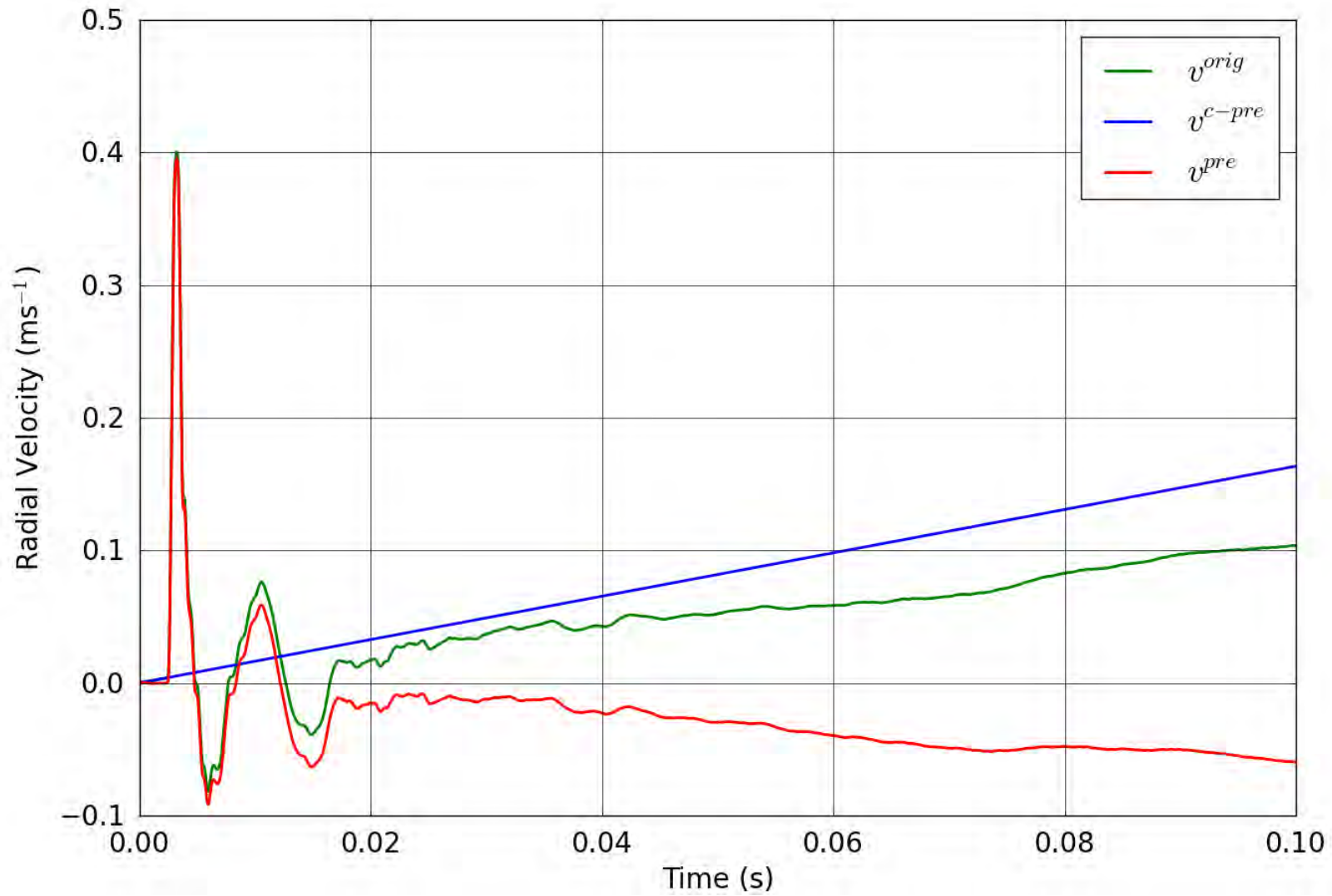


Figure 10. SPE-1 Gauge 2-2-R – Pre-shot baseline correction of the radial velocity.

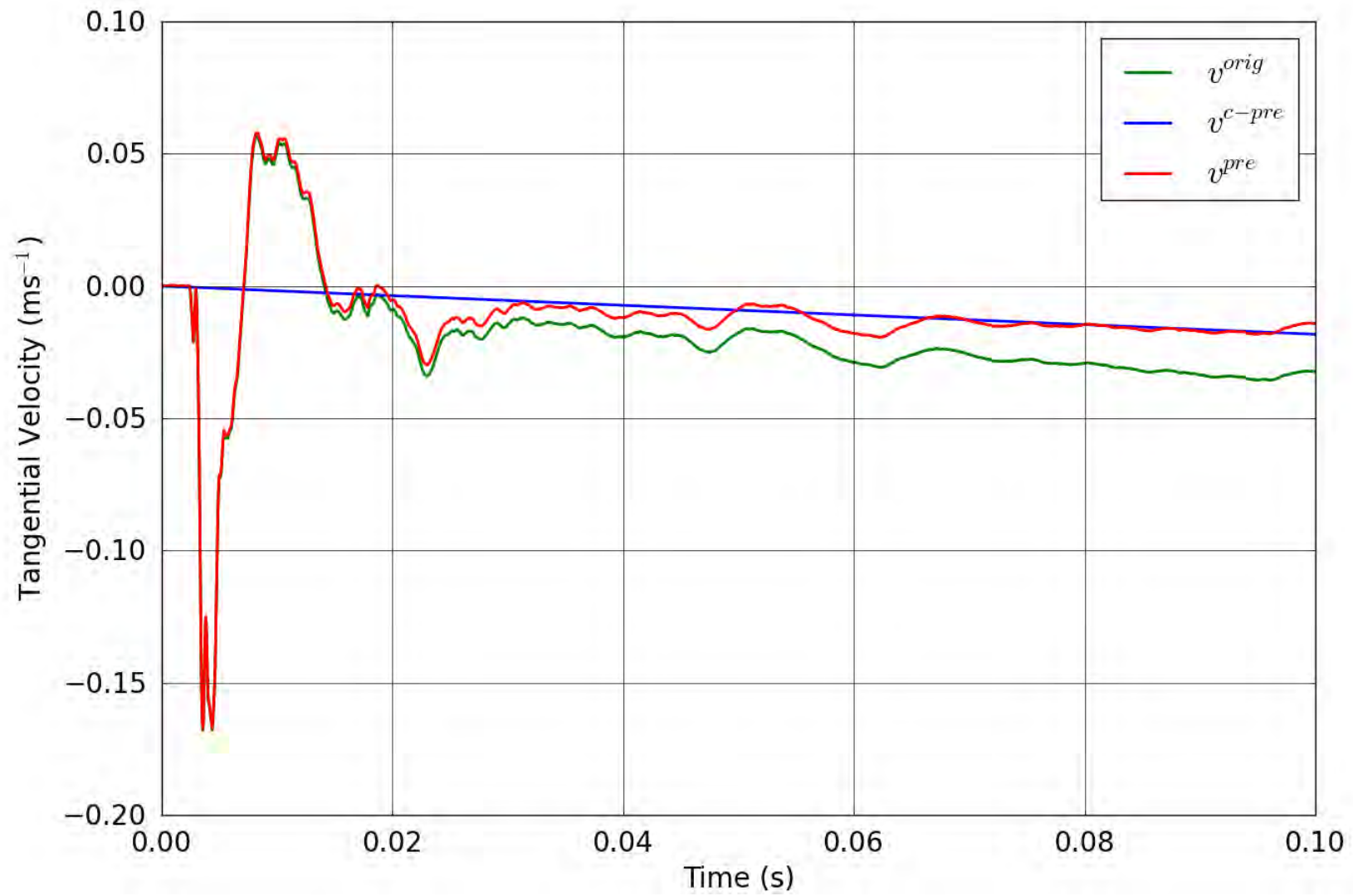


Figure 11. SPE-1 Gauge 2-2-T – Pre-shot baseline correction of the tangential velocity.

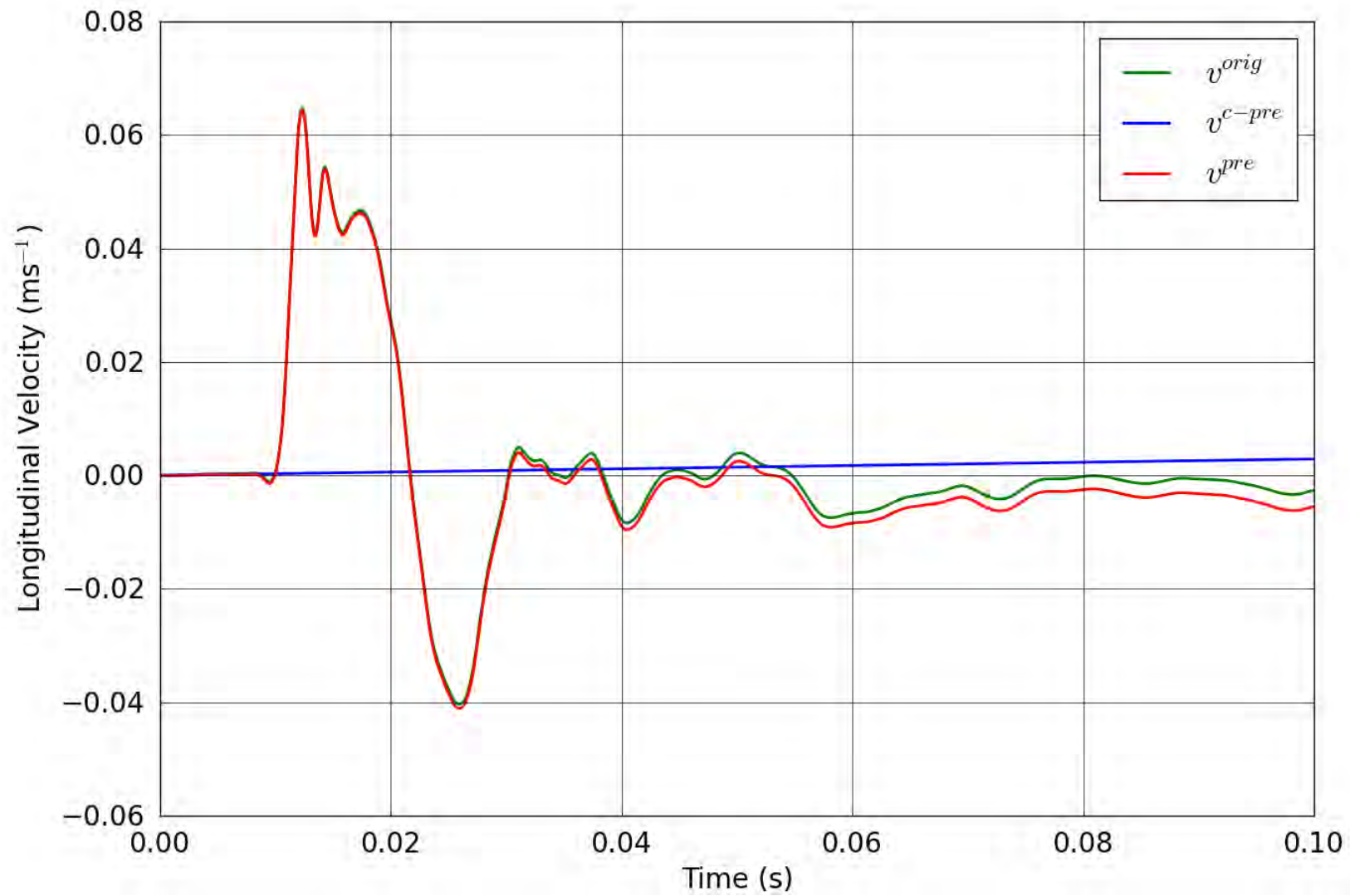


Figure 12. SPE-1 Gauge 2-3-L – Pre-shot baseline correction of the longitudinal velocity.

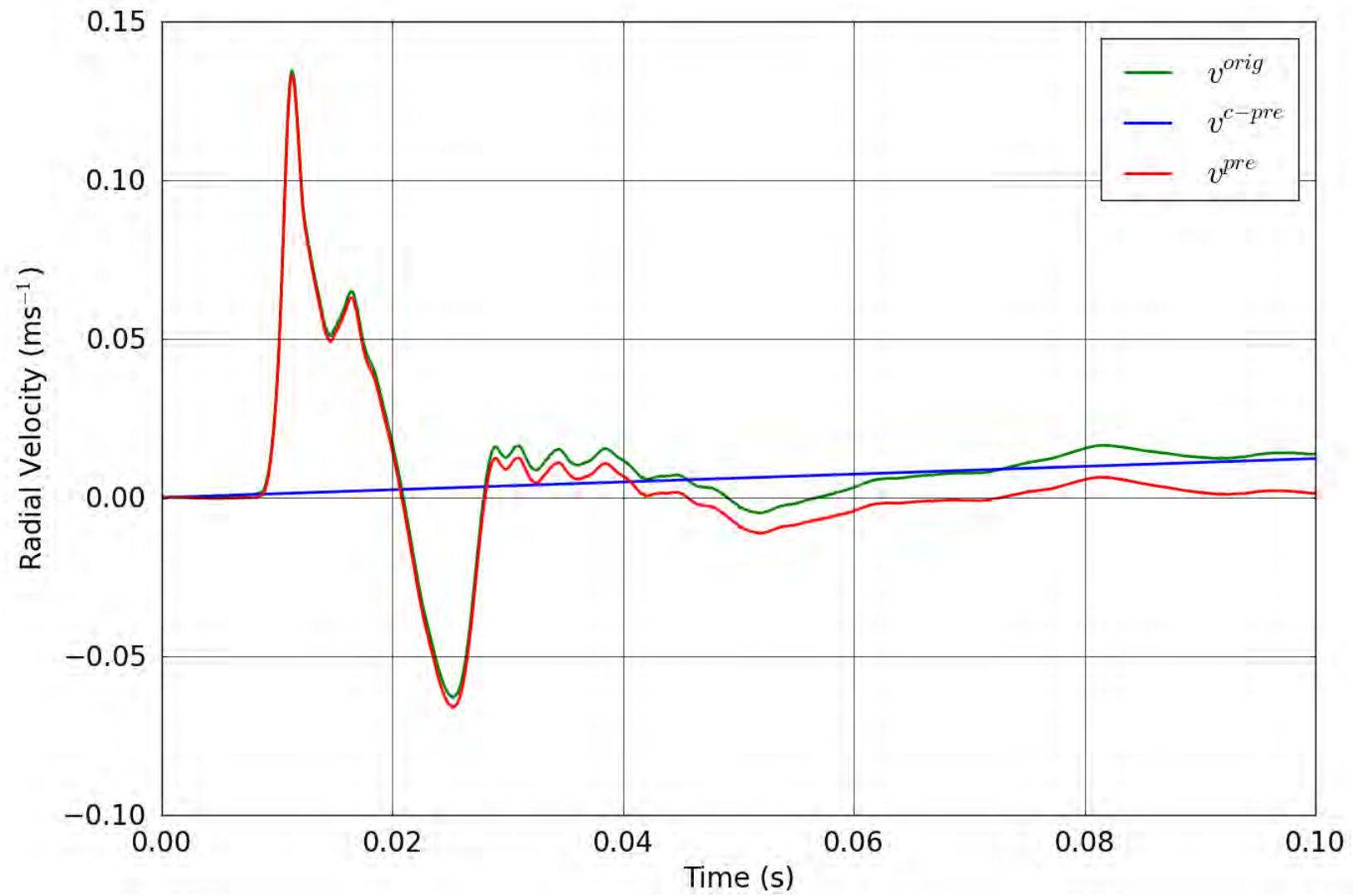


Figure 13. SPE-1 Gauge 2-3-R – Pre-shot baseline correction of the radial velocity.

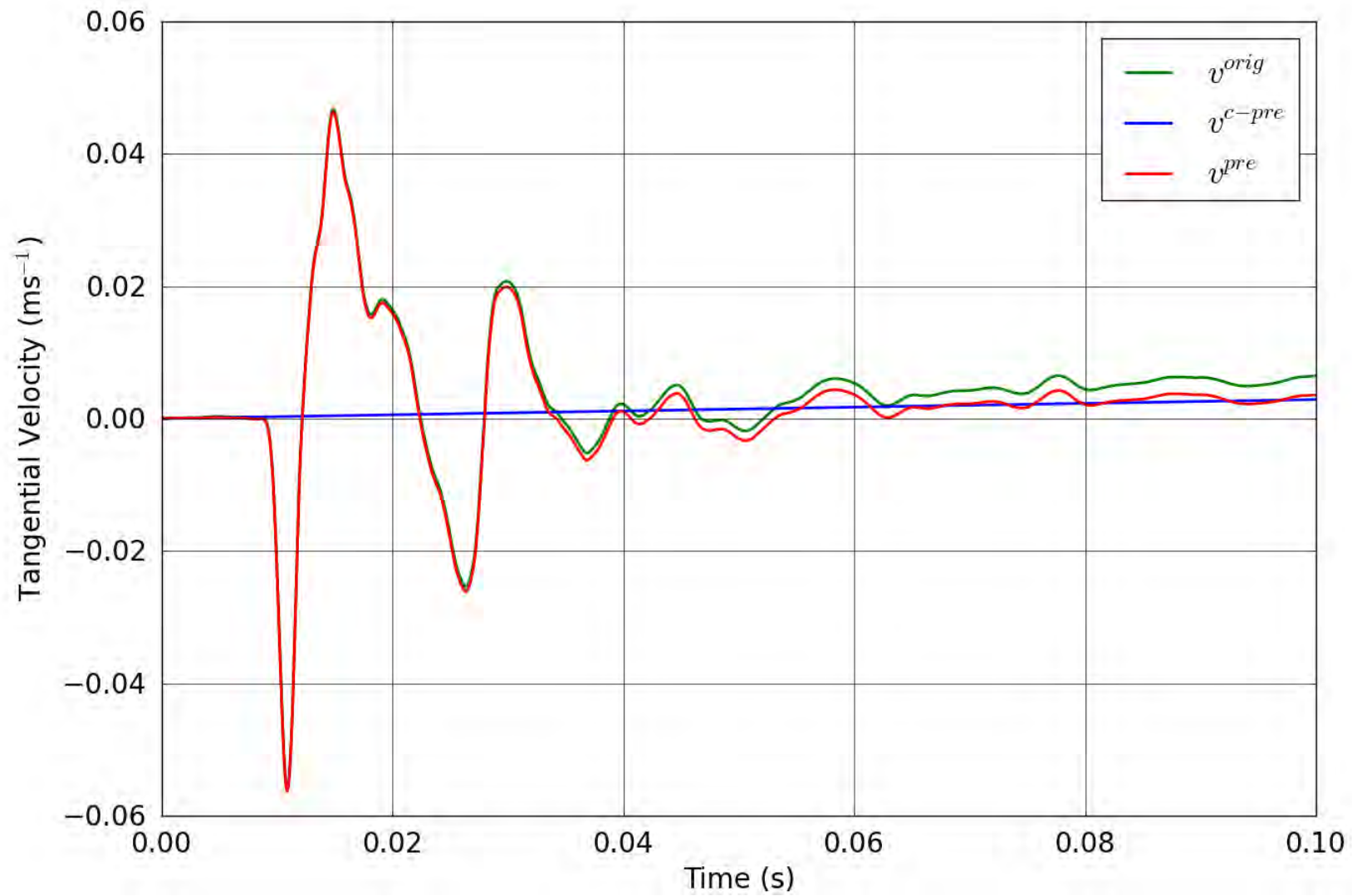


Figure 14. SPE-1 Gauge 2-3-T – Pre-shot baseline correction of the tangential velocity.

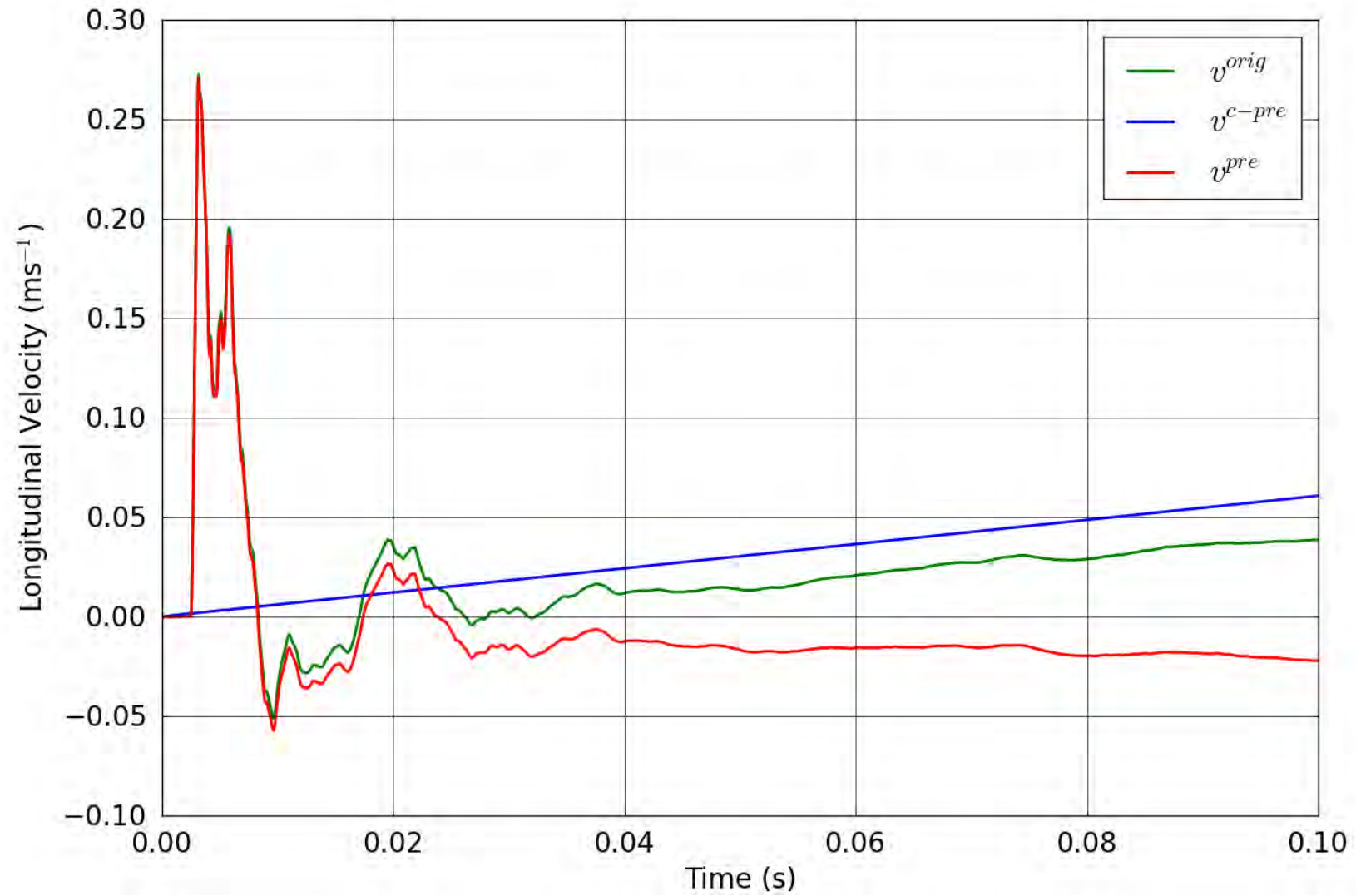


Figure 15. SPE-1 Gauge 3-2-L – Pre-shot baseline correction of the longitudinal velocity.

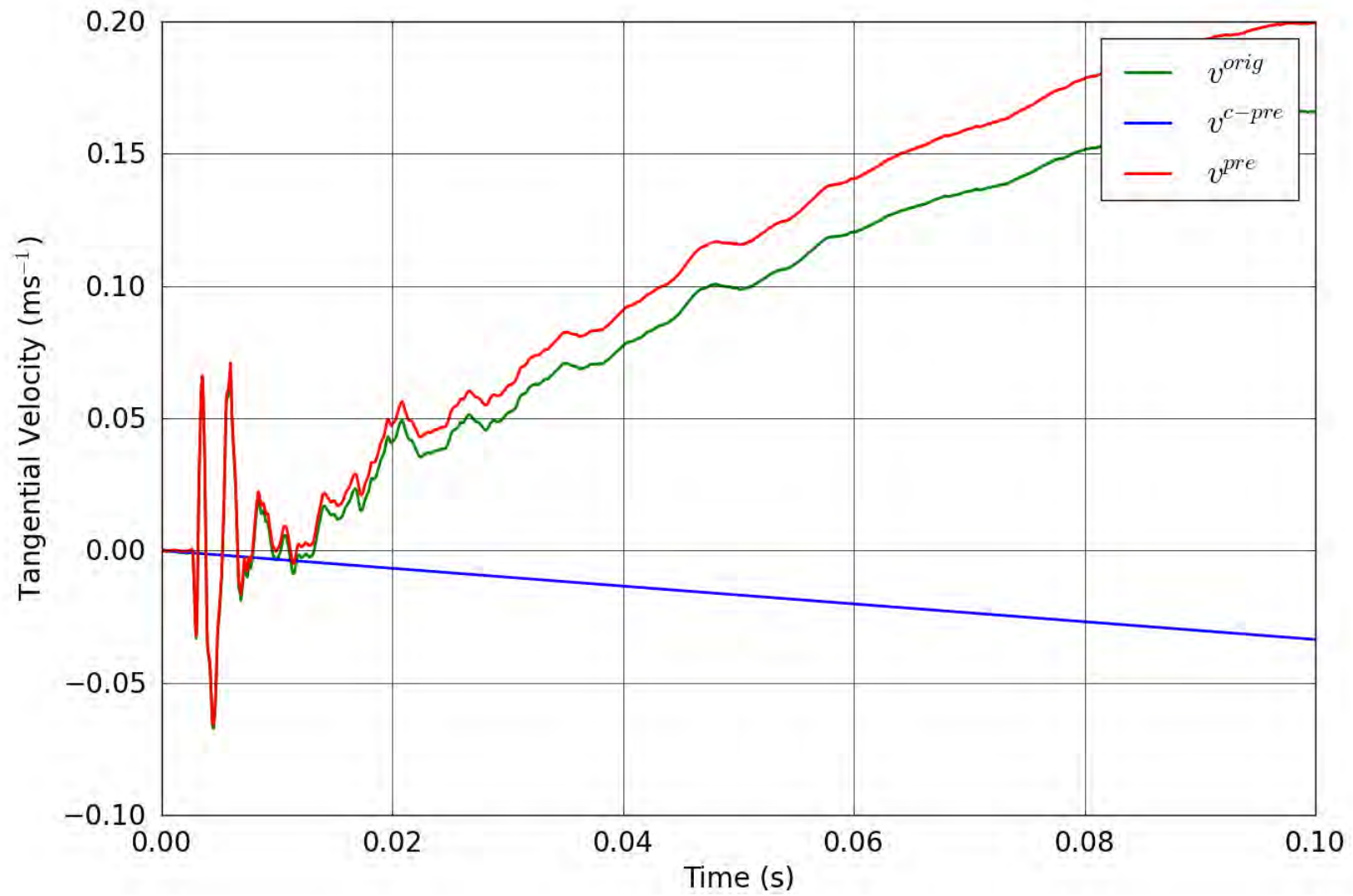


Figure 16. SPE-1 Gauge 3-2-T – Pre-shot baseline correction of the tangential velocity.

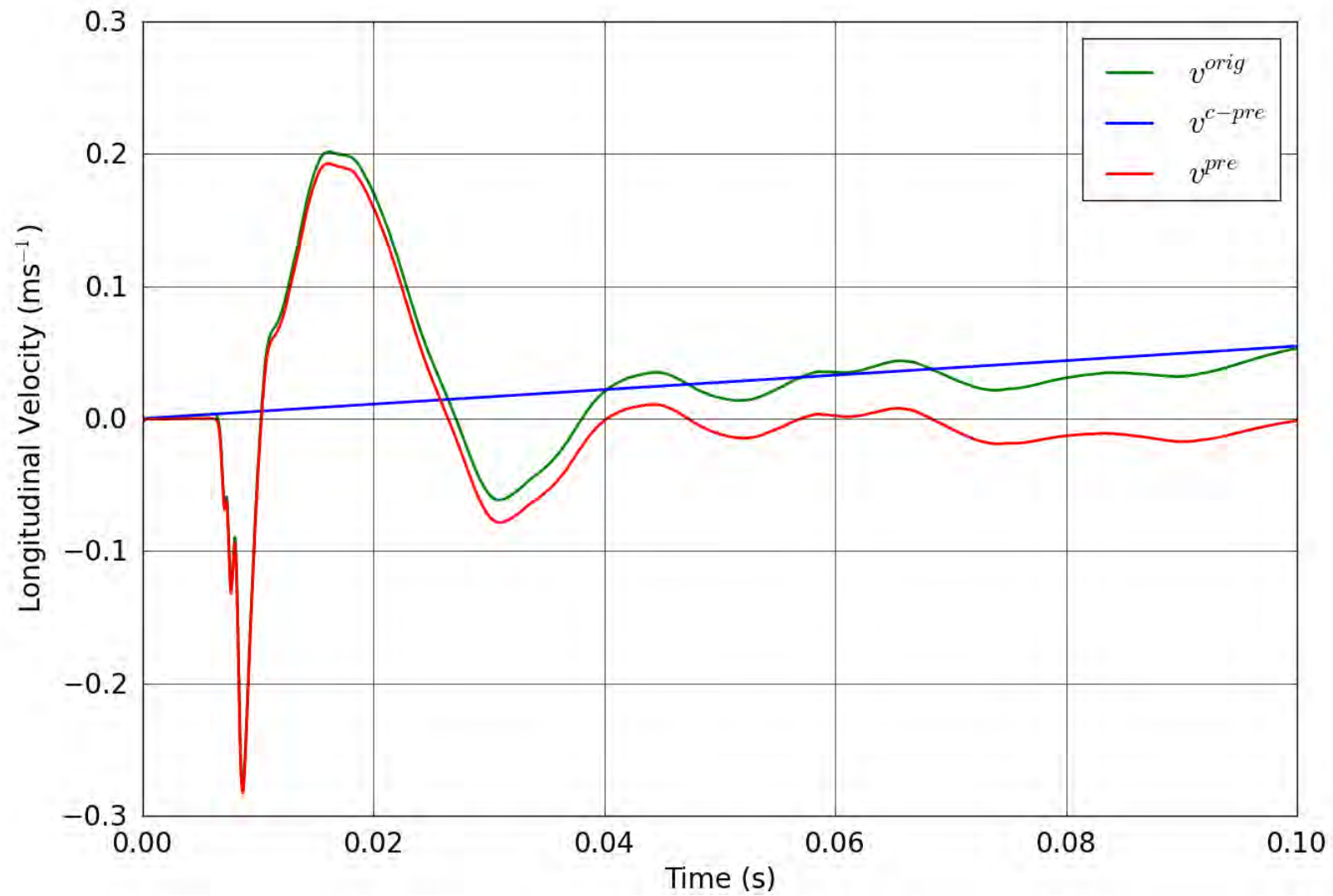


Figure 17. SPE-1 Gauge 3-3-L – Pre-shot baseline correction of the longitudinal velocity.

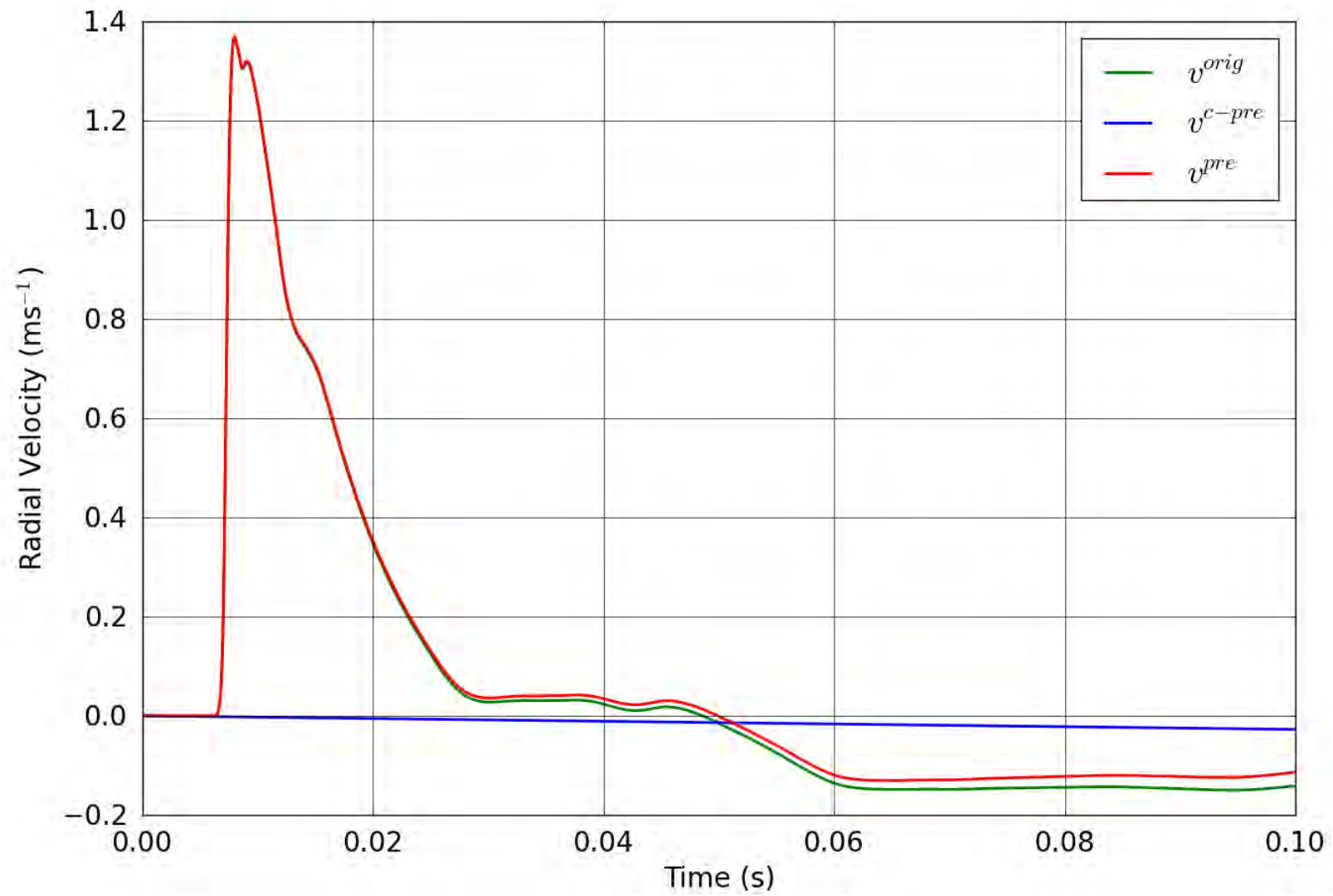


Figure 18. SPE-1 Gauge 3-3-R – Pre-shot baseline correction of the radial velocity.

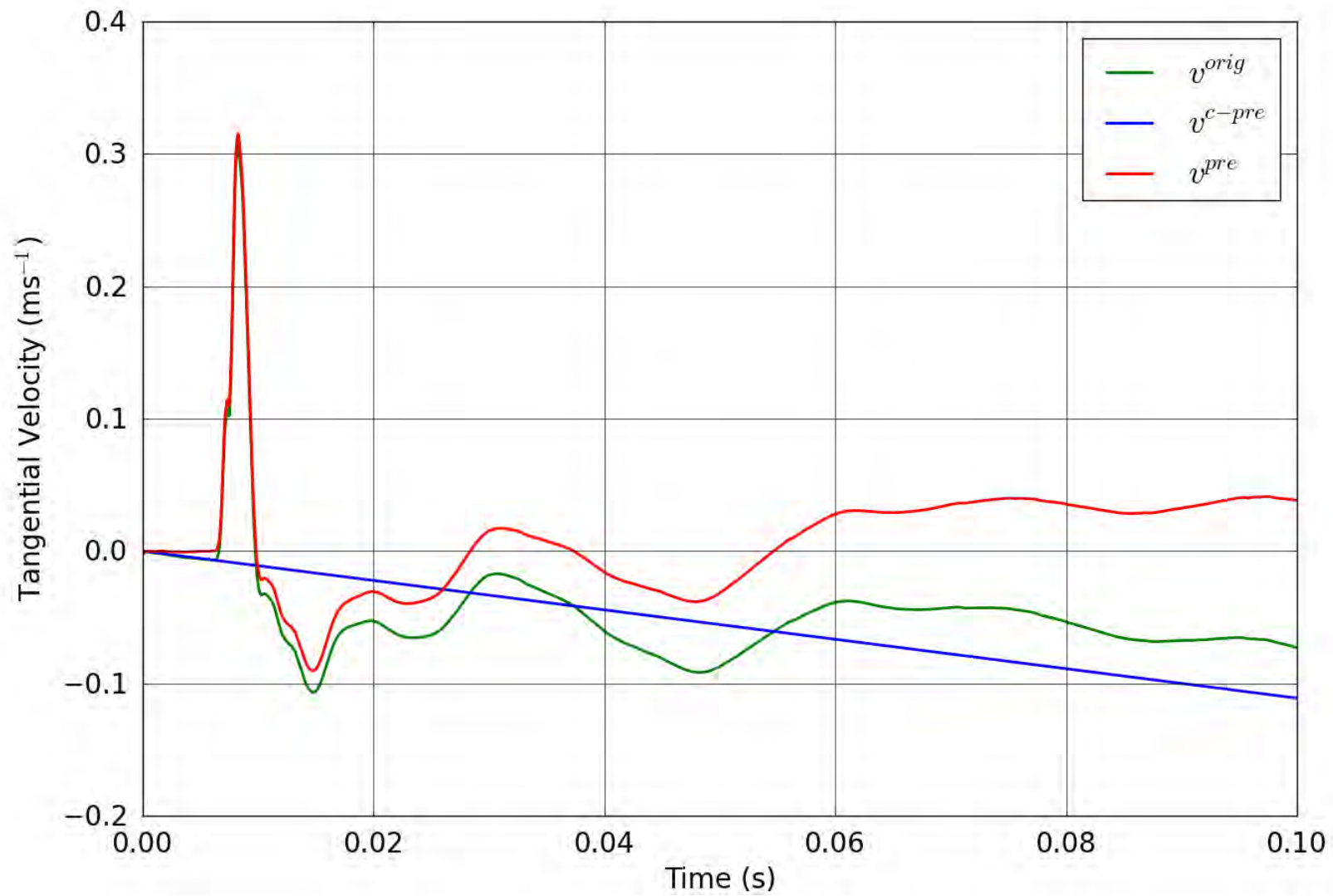


Figure 19. SPE-1 Gauge 3-3-T – Pre-shot baseline correction of the tangential velocity.

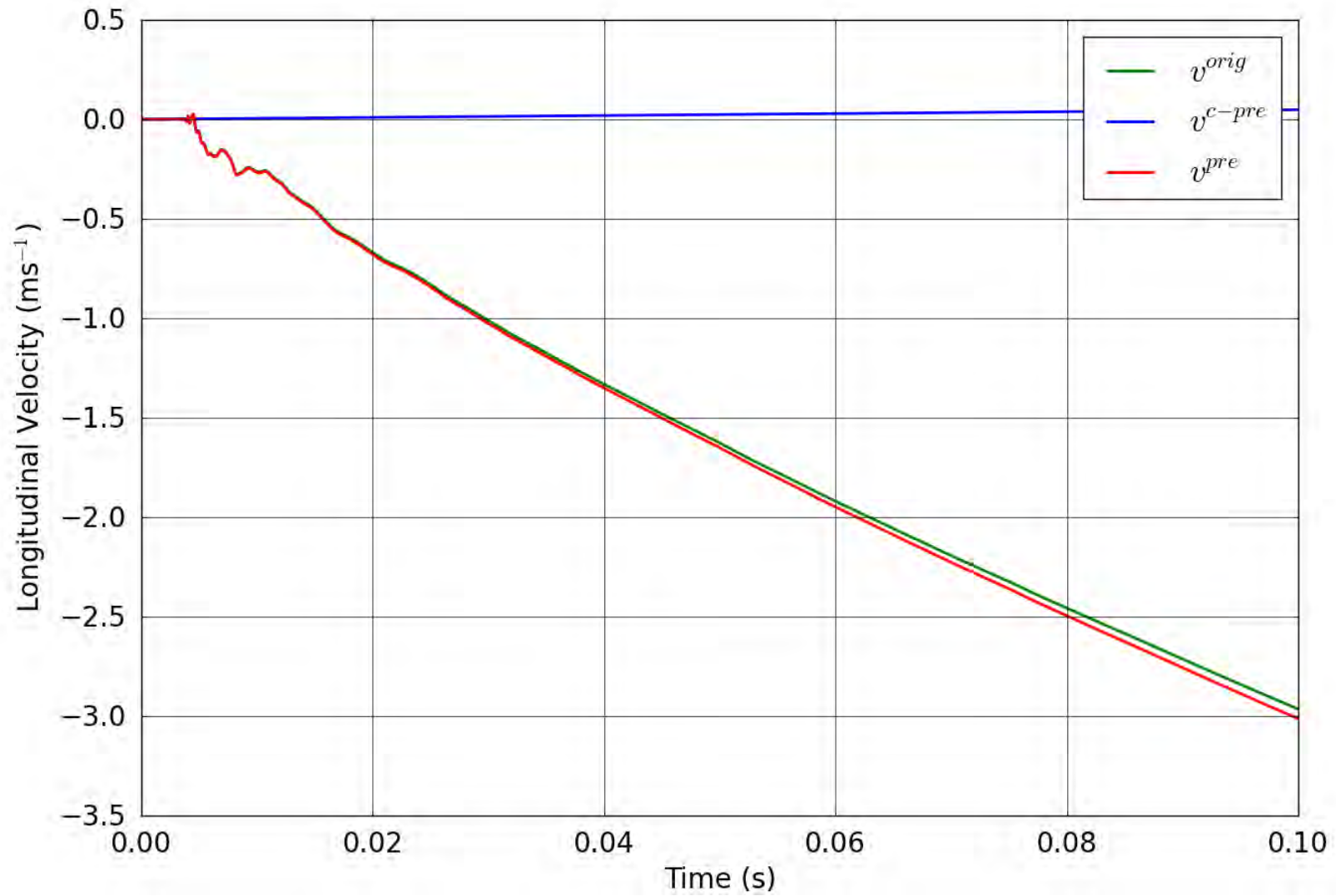


Figure 20. SPE-1 Gauge 4-1-L – Pre-shot baseline correction of the longitudinal velocity.

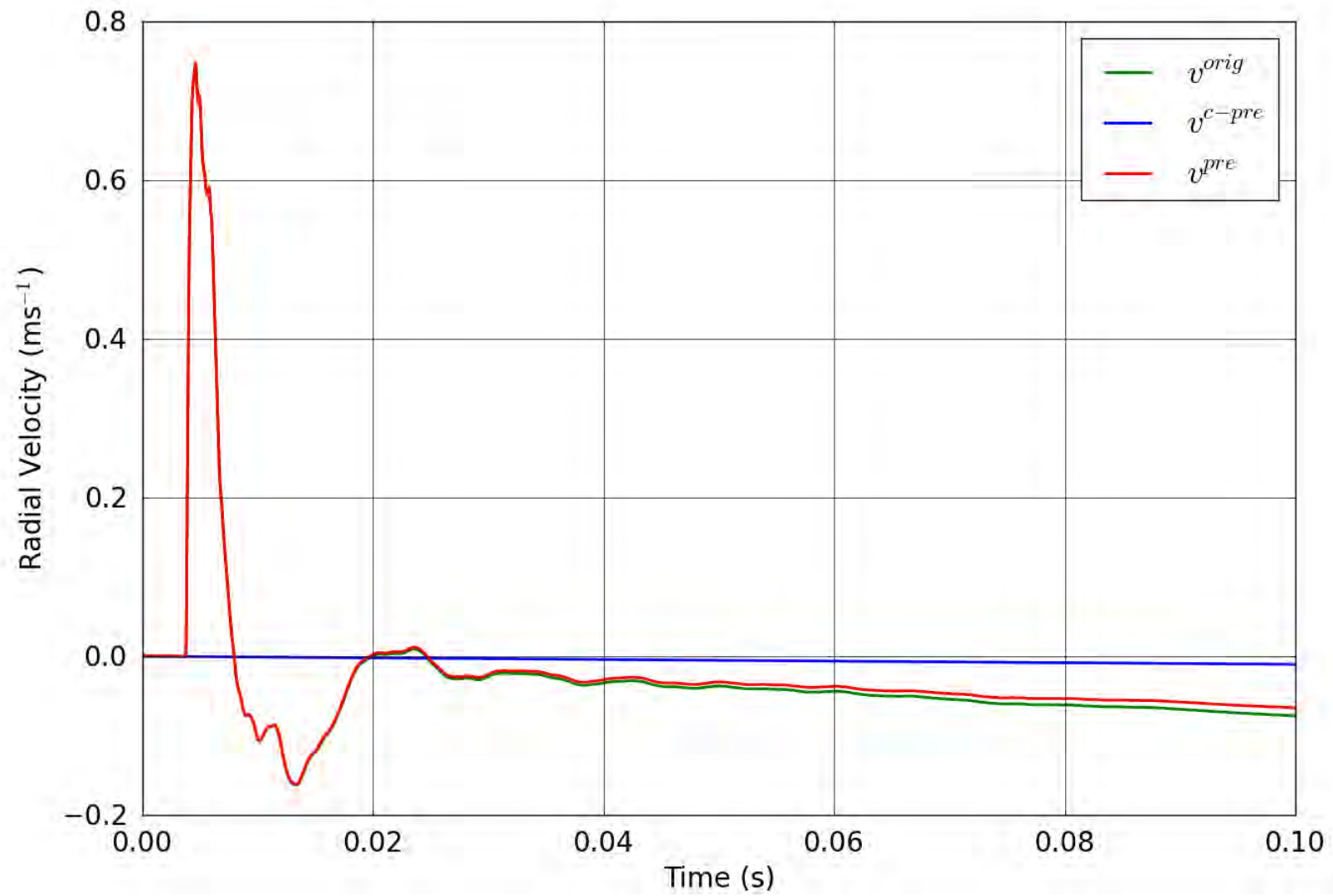


Figure 21. SPE-1 Gauge 4-1-R – Pre-shot baseline correction of the radial velocity.

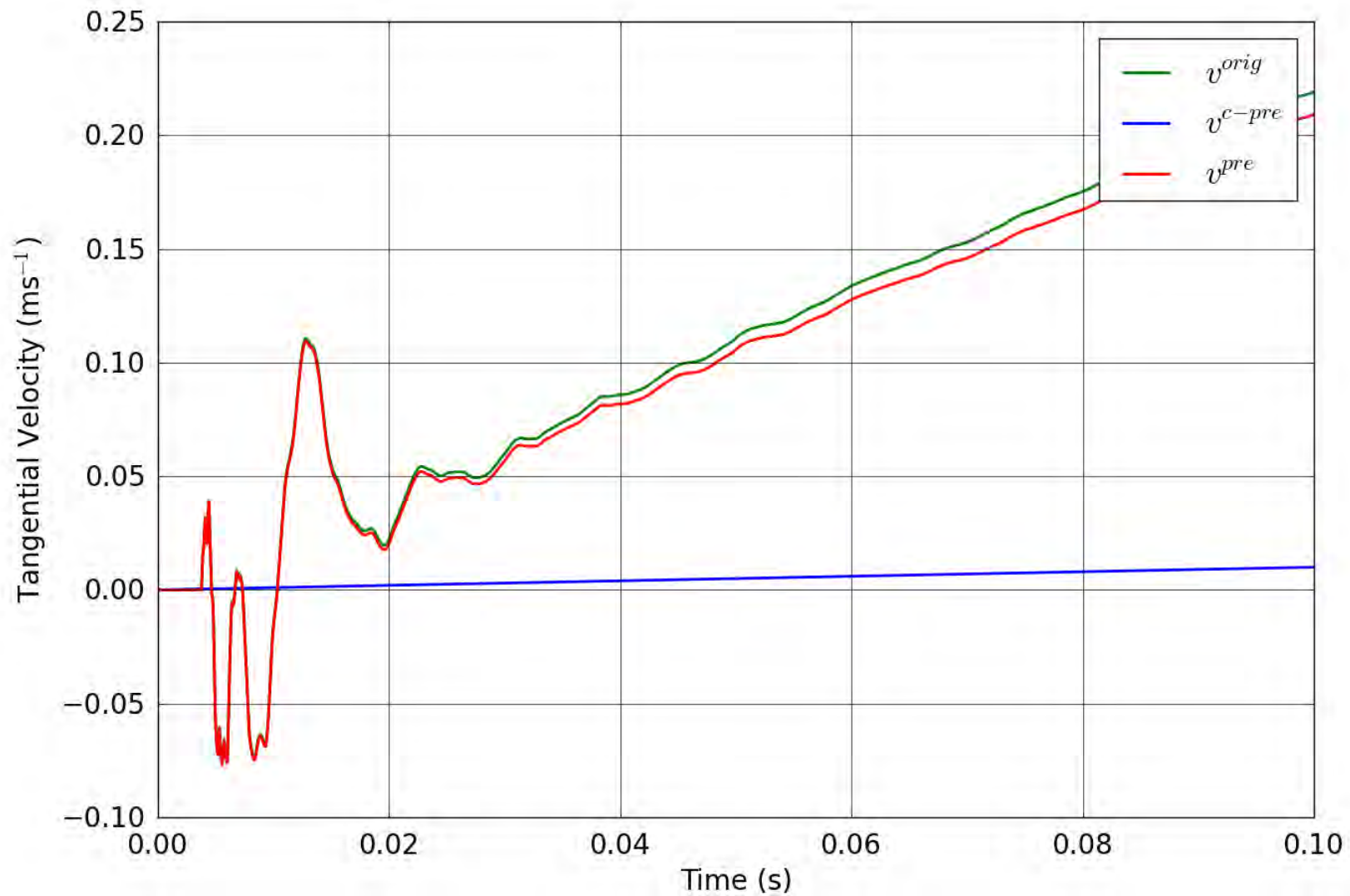


Figure 22. SPE-1 Gauge 4-1-T – Pre-shot baseline correction of the tangential velocity.

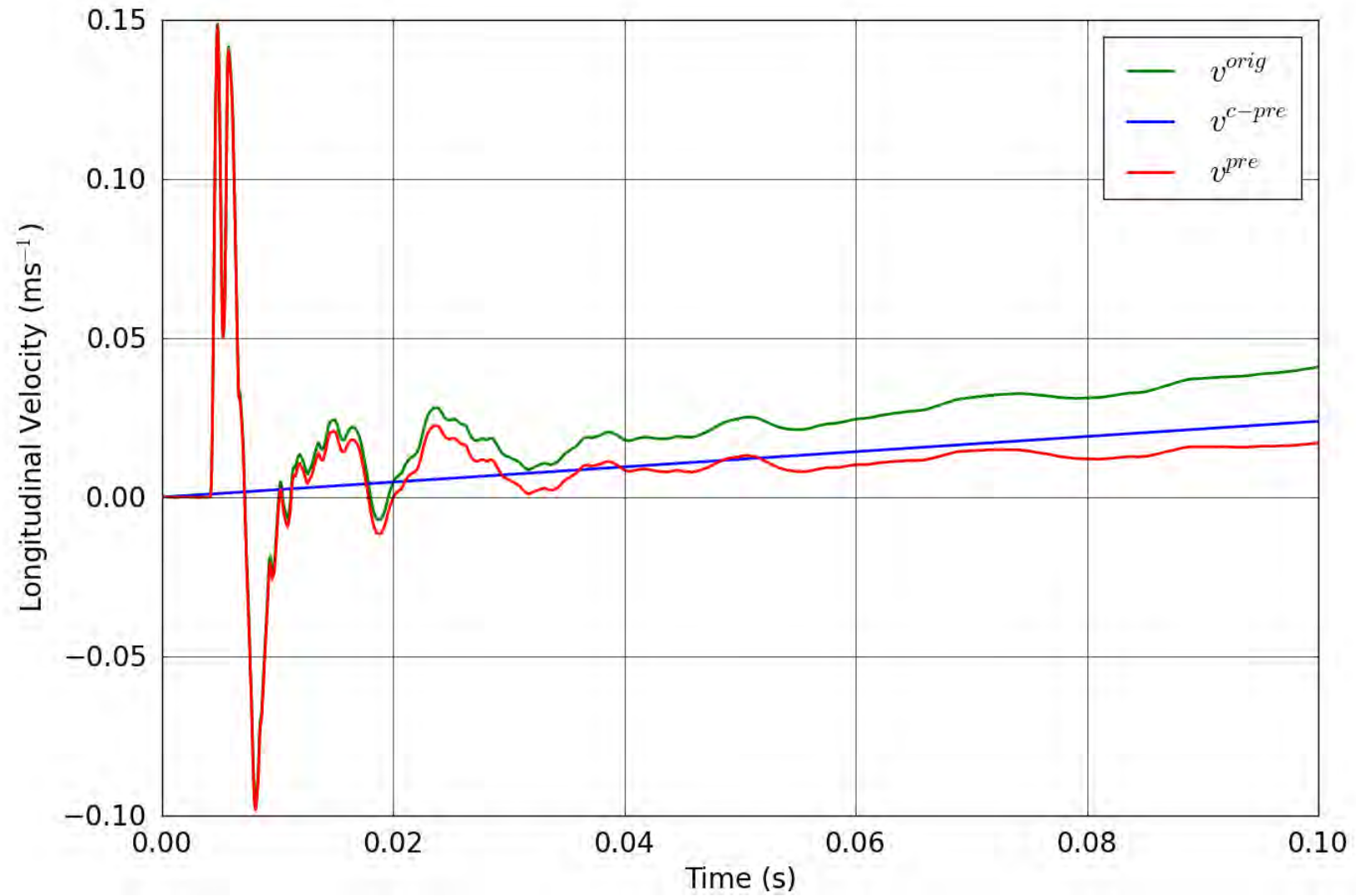


Figure 23. SPE-1 Gauge 4-2-L – Pre-shot baseline correction of the longitudinal velocity.

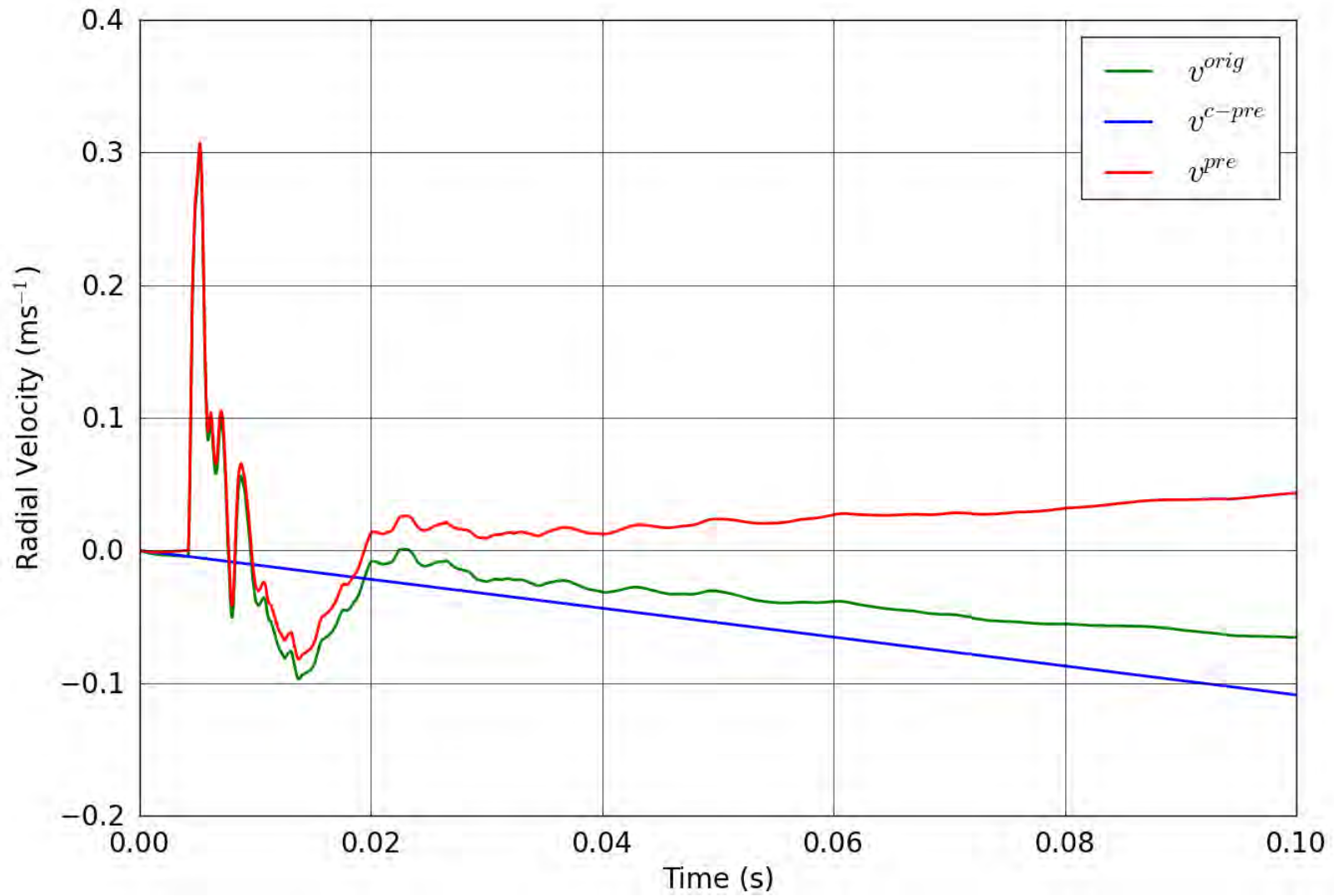


Figure 24. SPE-1 Gauge 4-2-R – Pre-shot baseline correction of the radial velocity.

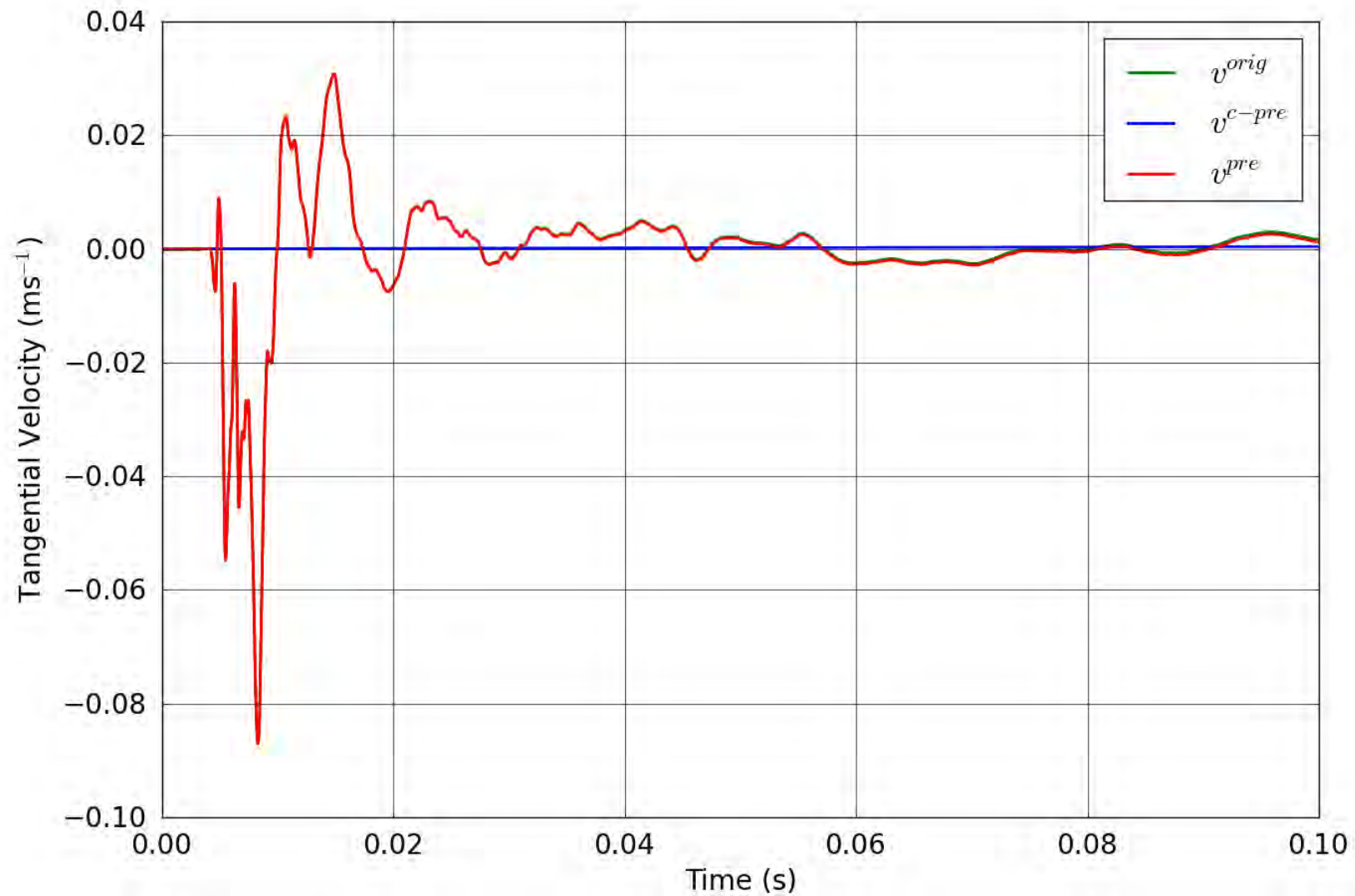


Figure 25. SPE-1 Gauge 4-2-T – Pre-shot baseline correction of the tangential velocity.

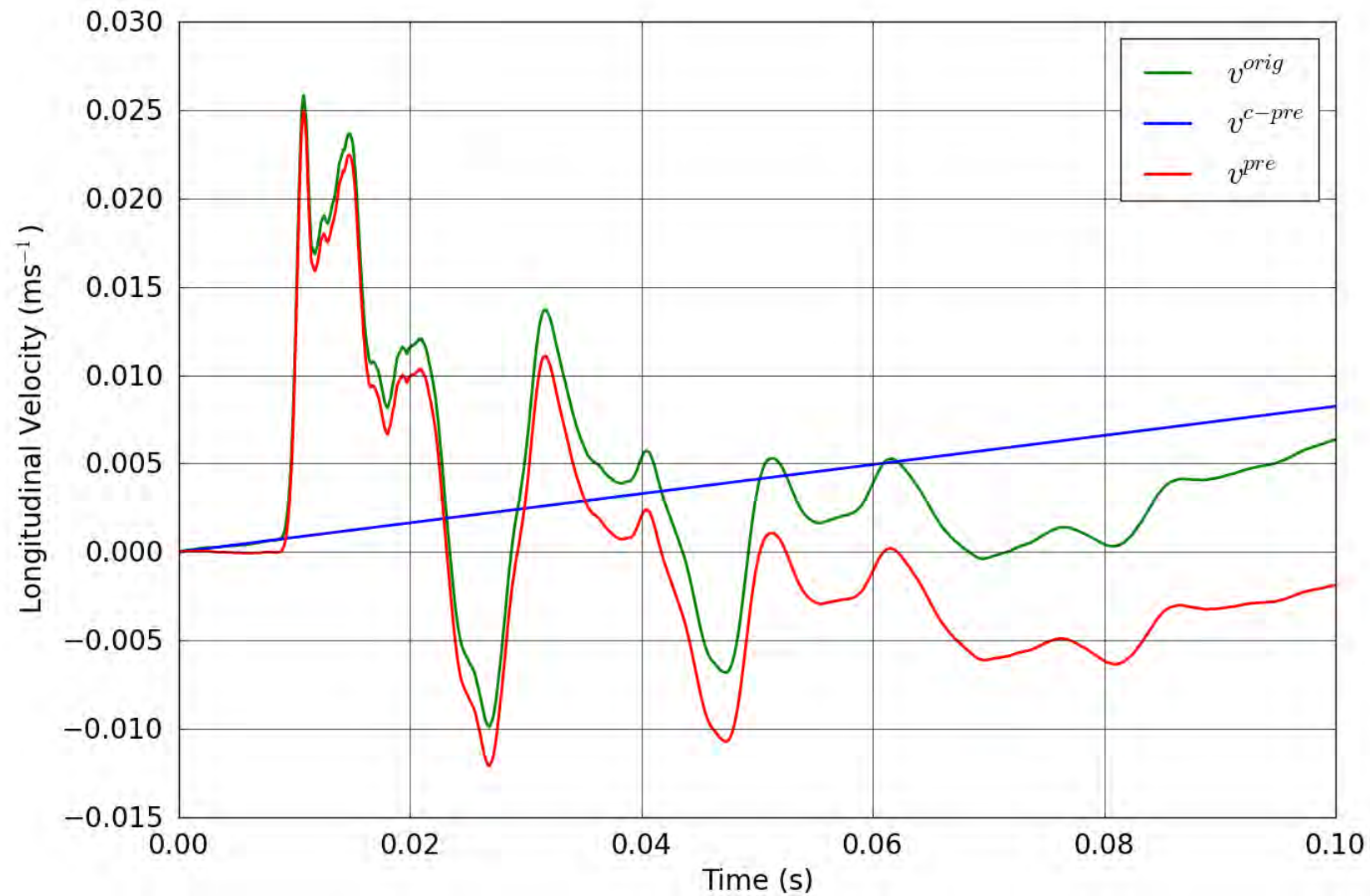


Figure 26. SPE-1 Gauge 4-3-L – Pre-shot baseline correction of the longitudinal velocity.

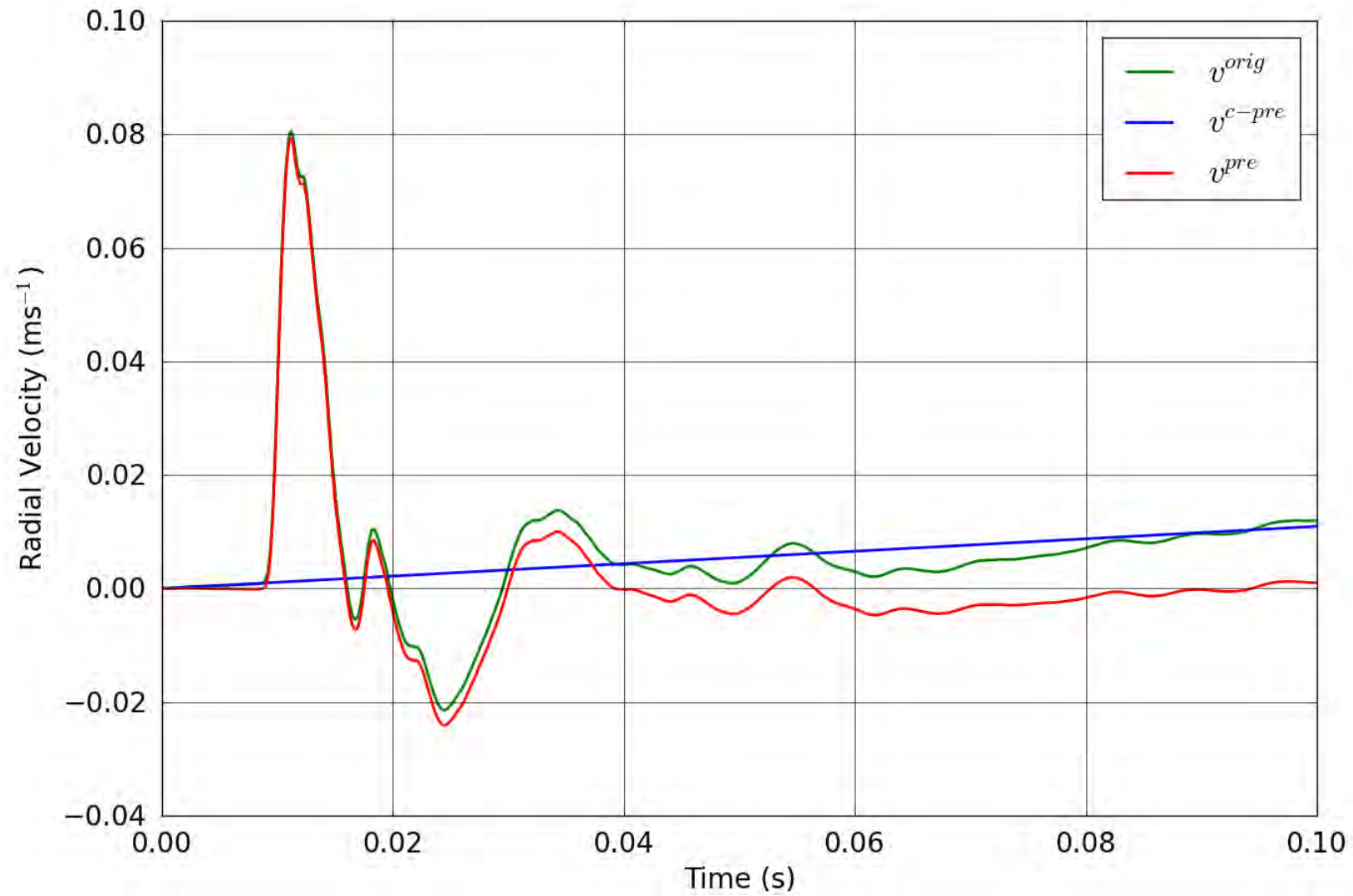


Figure 27. SPE-1 Gauge 4-3-R – Pre-shot baseline correction of the radial velocity.

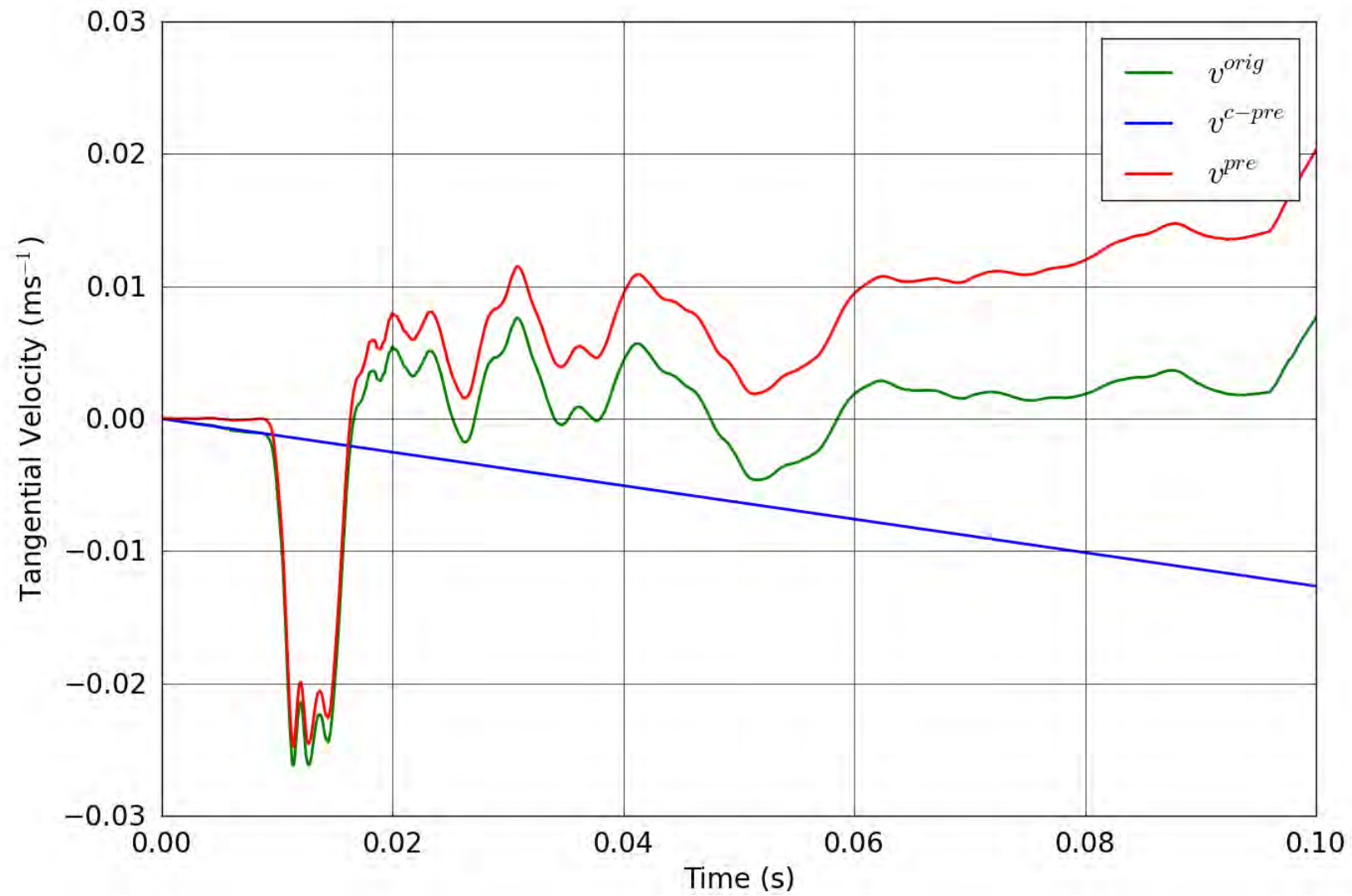


Figure 28. SPE-1 Gauge 4-3-T – Pre-shot baseline correction of the tangential velocity.

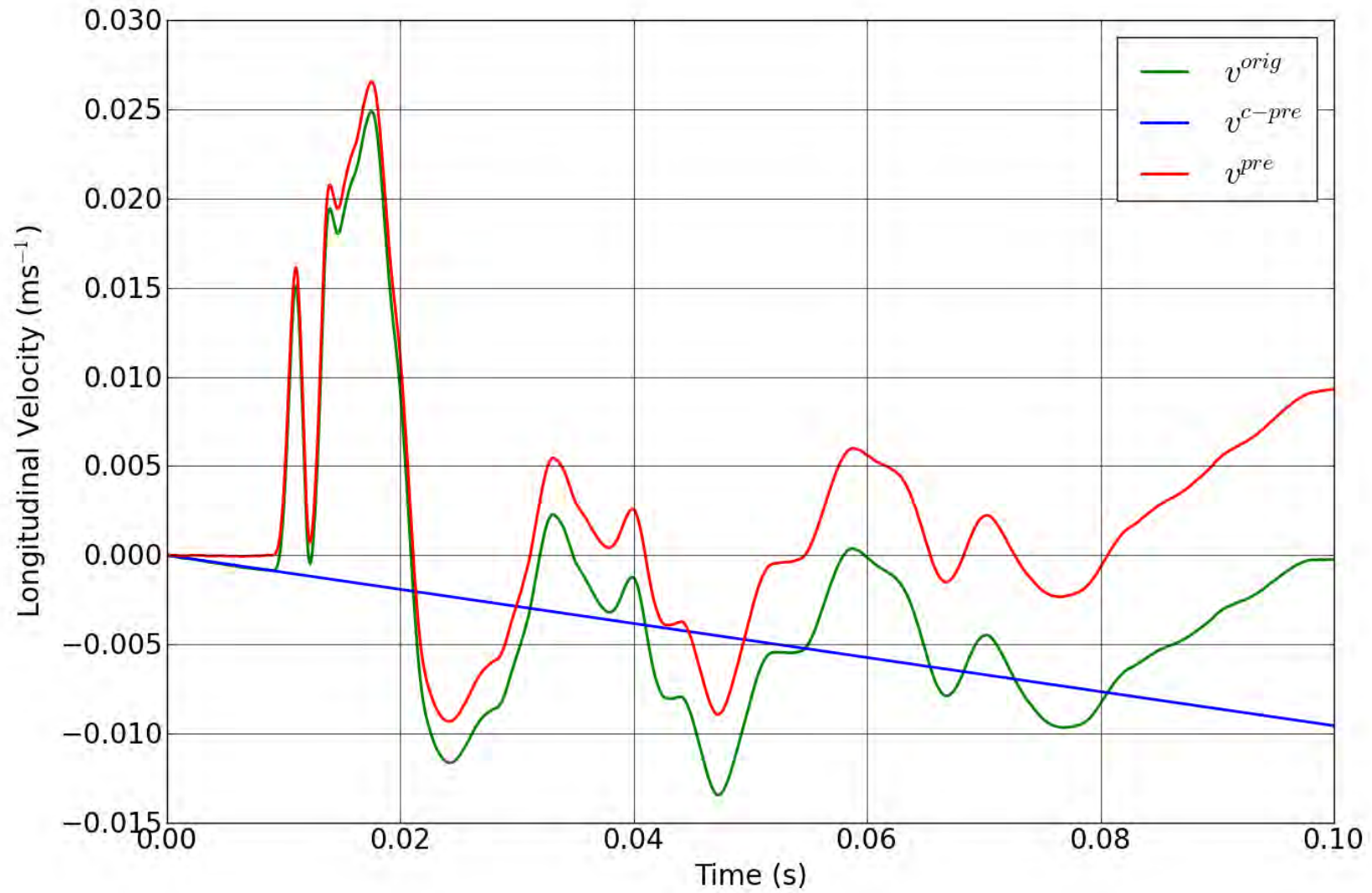


Figure 29. SPE-1 Gauge 5-3-L – Pre-shot baseline correction of the longitudinal velocity.

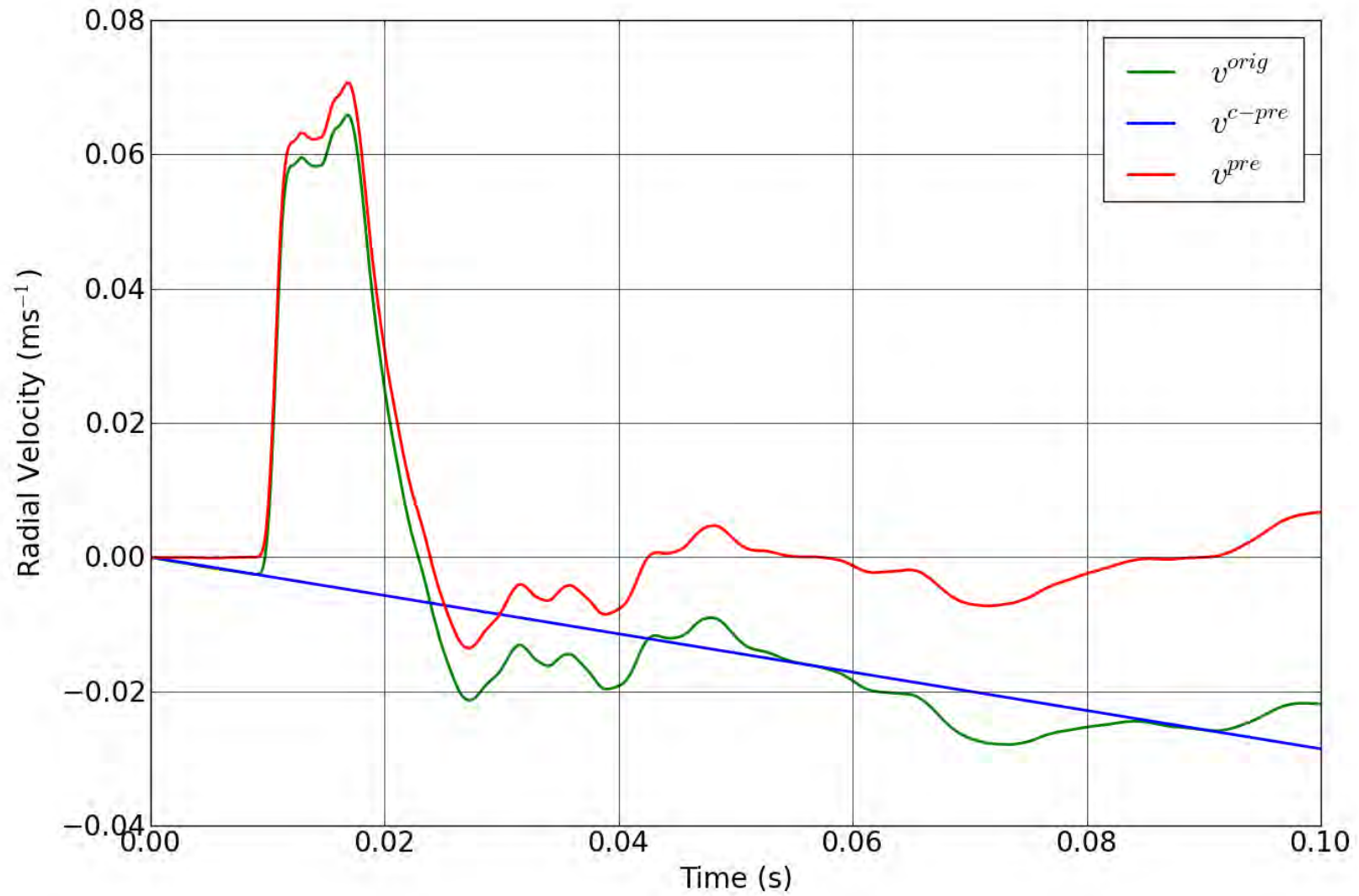


Figure 30. SPE-1 Gauge 5-3-R – Pre-shot baseline correction of the radial velocity.

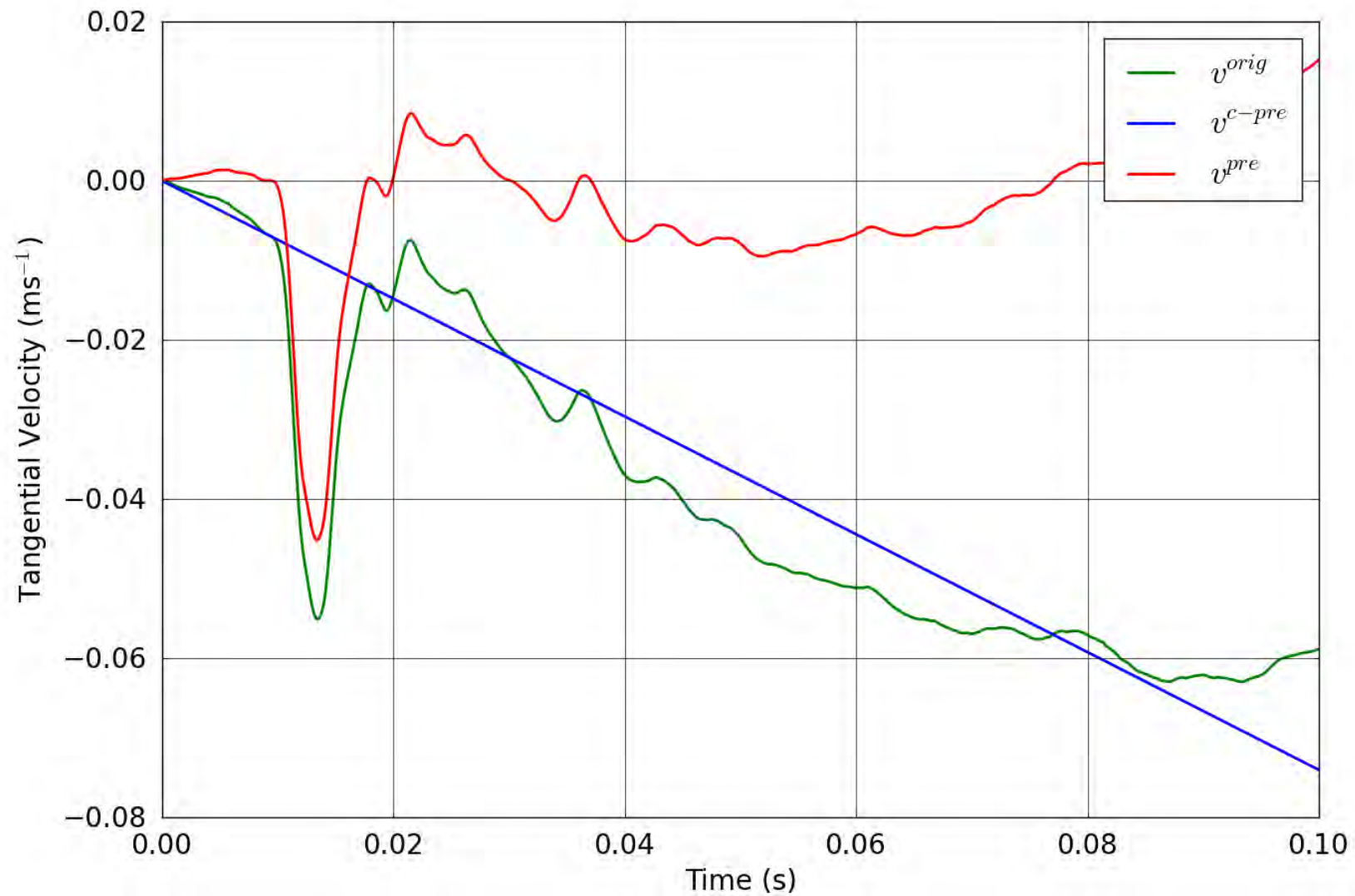


Figure 31. SPE-1 Gauge 5-3-T – Pre-shot baseline correction of the tangential velocity.

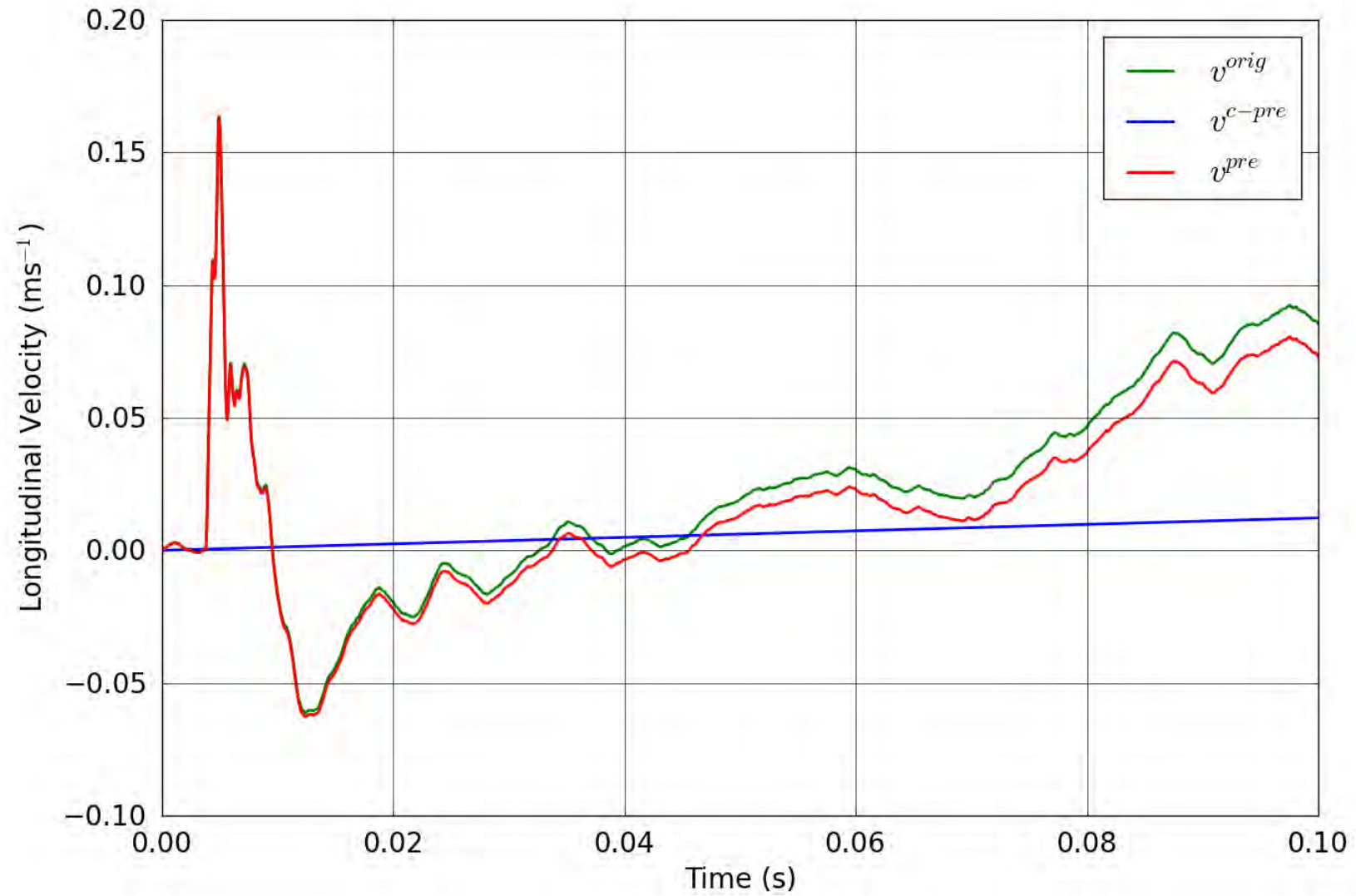


Figure 32. SPE-1 Gauge 6-1-L – Pre-shot baseline correction of the longitudinal velocity.

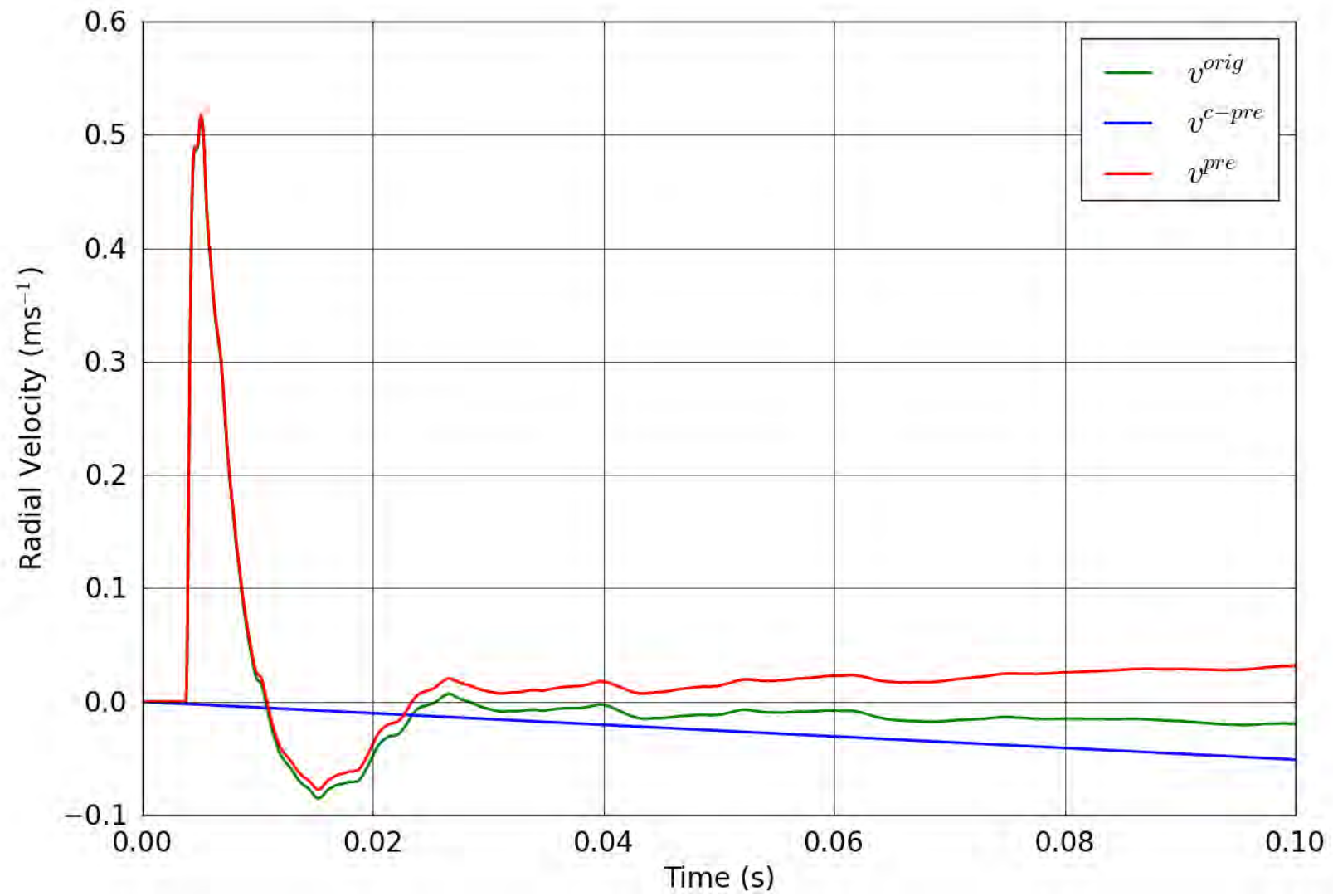


Figure 33. SPE-1 Gauge 6-1-R – Pre-shot baseline correction of the radial velocity.

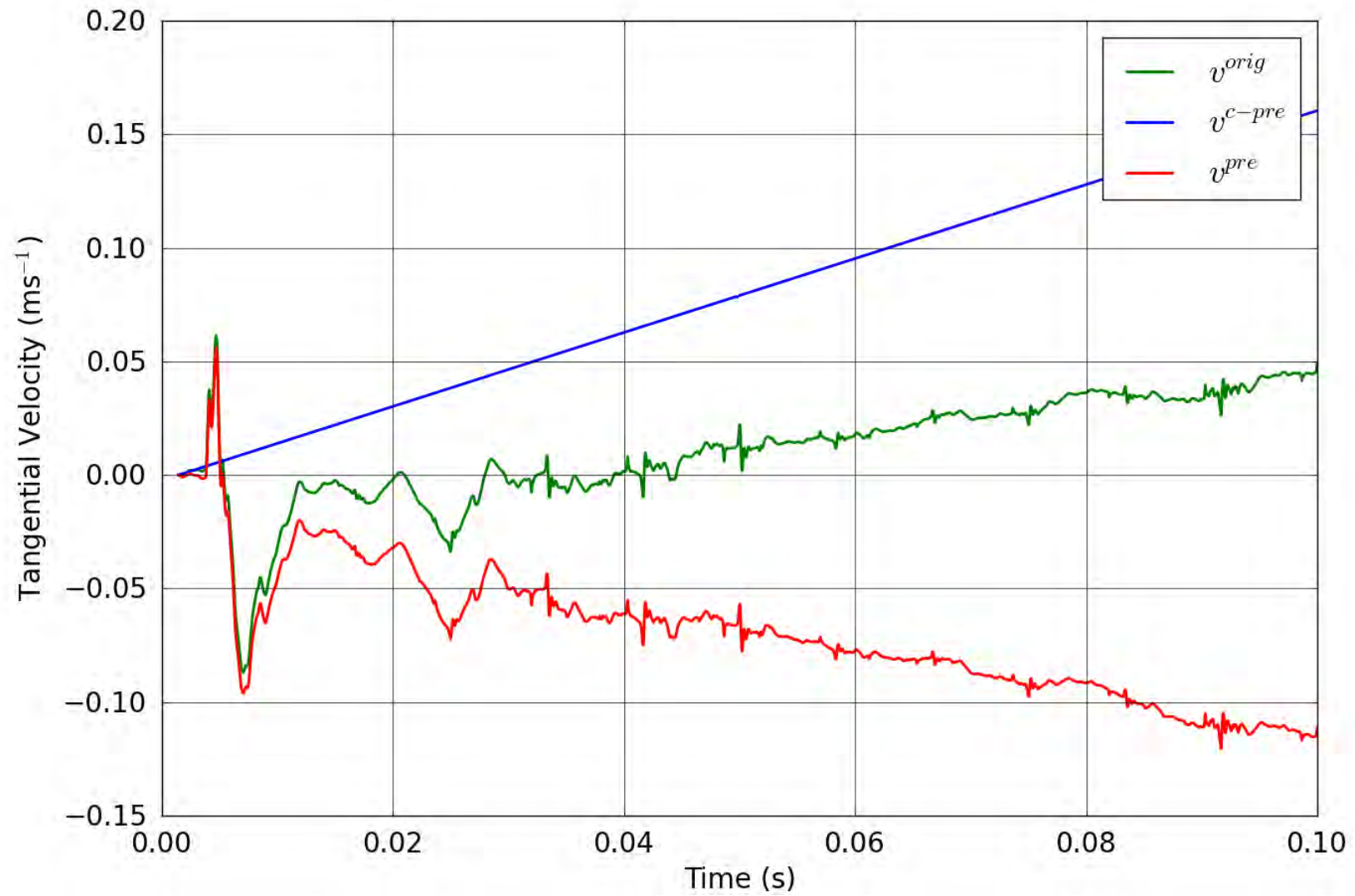


Figure 34. SPE-1 Gauge 6-1-T – Pre-shot baseline correction of the tangential velocity.

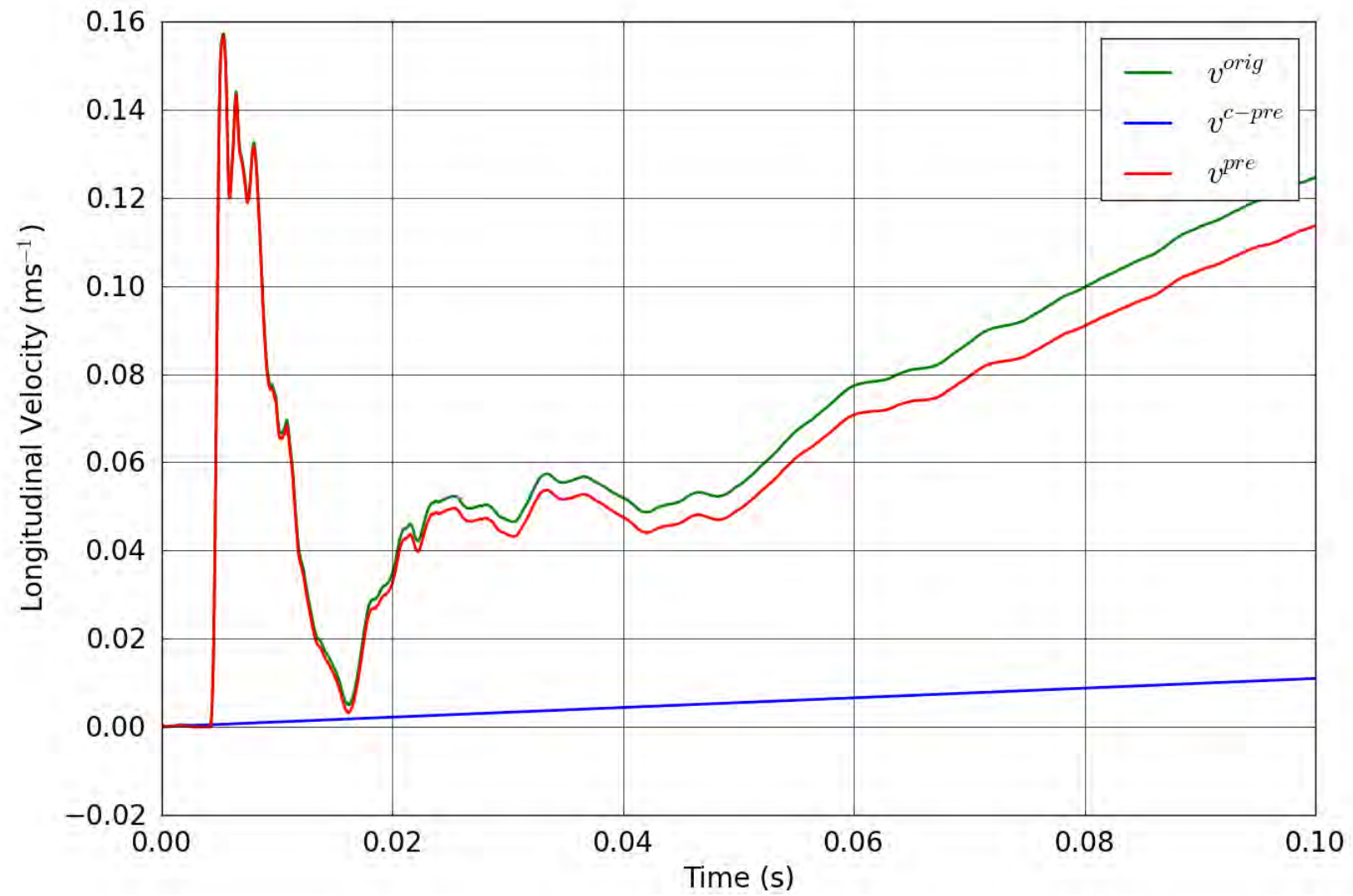


Figure 35. SPE-1 Gauge 6-2-L – Pre-shot baseline correction of the longitudinal velocity.

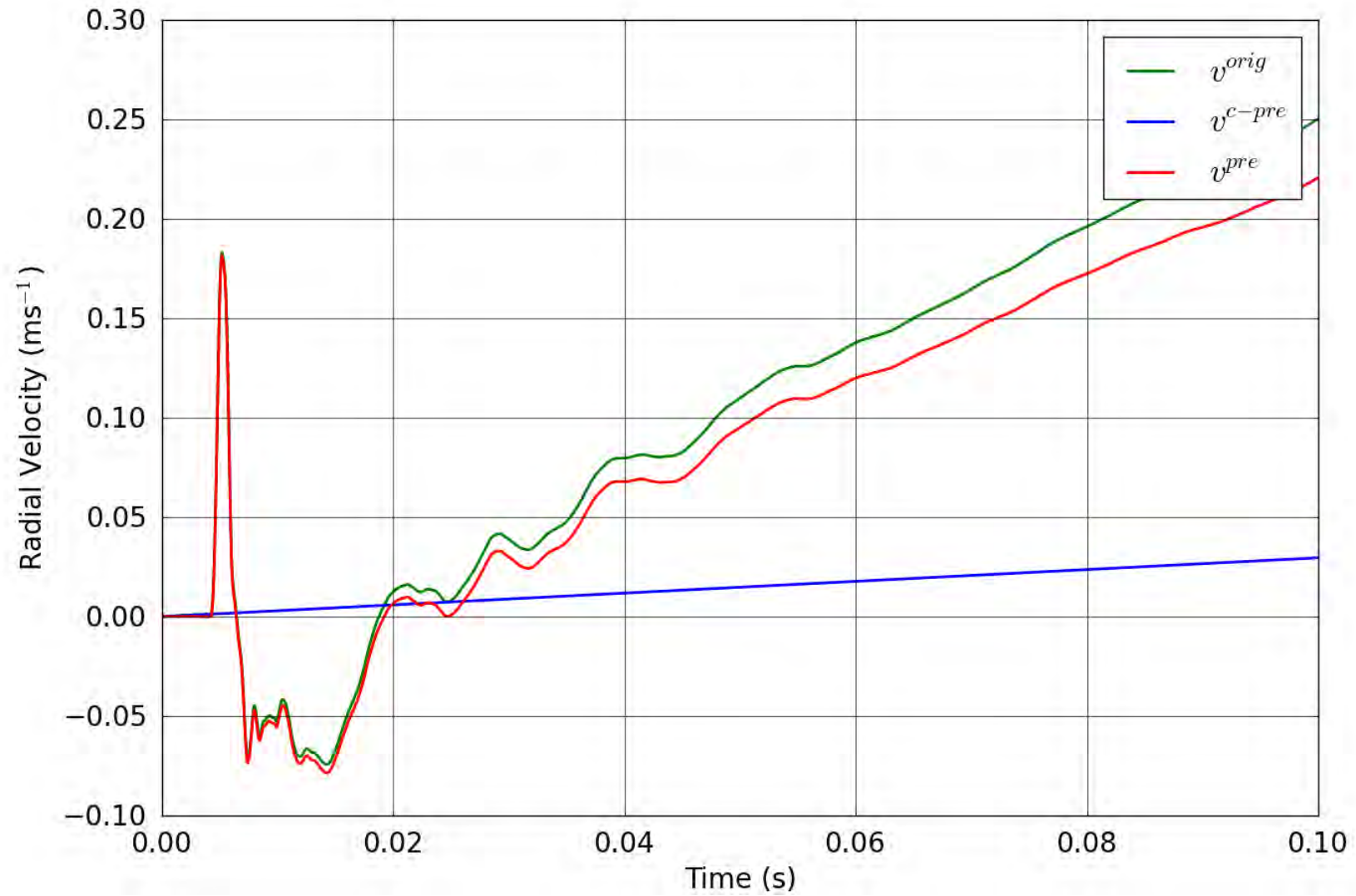


Figure 36. SPE-1 Gauge 6-2-R – Pre-shot baseline correction of the radial velocity.

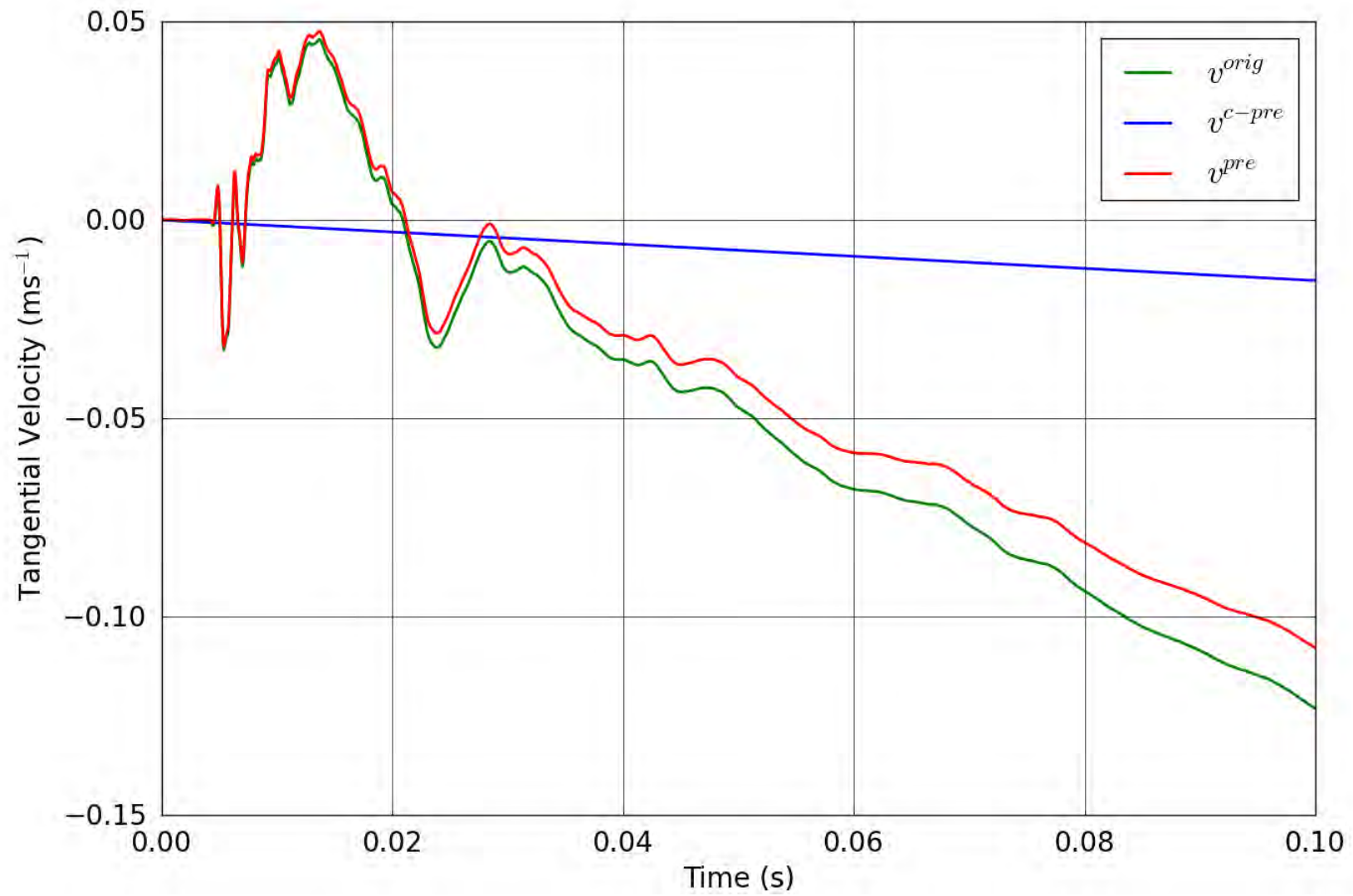


Figure 37. SPE-1 Gauge 6-2-T – Pre-shot baseline correction of the tangential velocity.

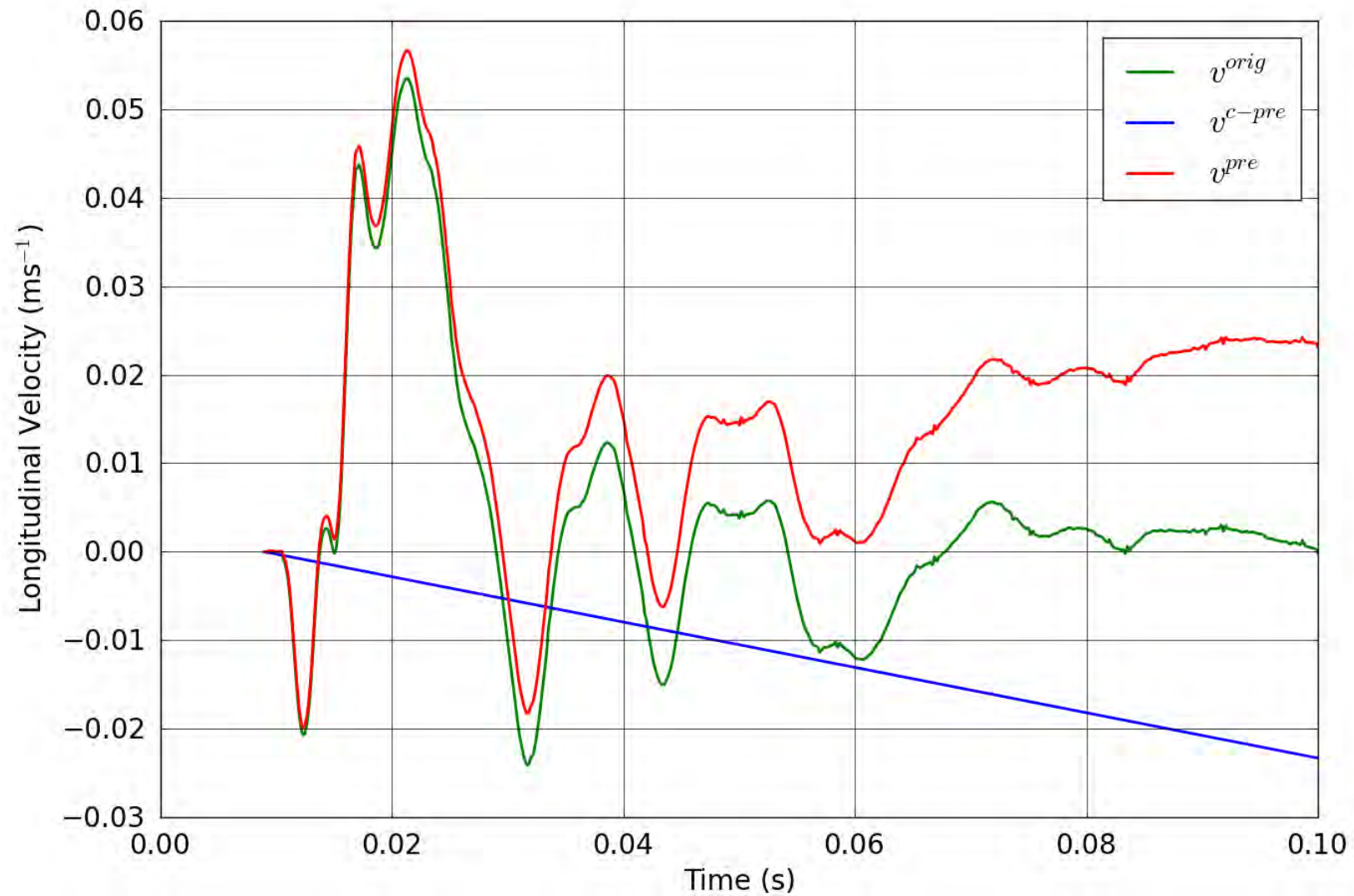


Figure 38. SPE-1 Gauge 6-3-L – Pre-shot baseline correction of the longitudinal velocity.

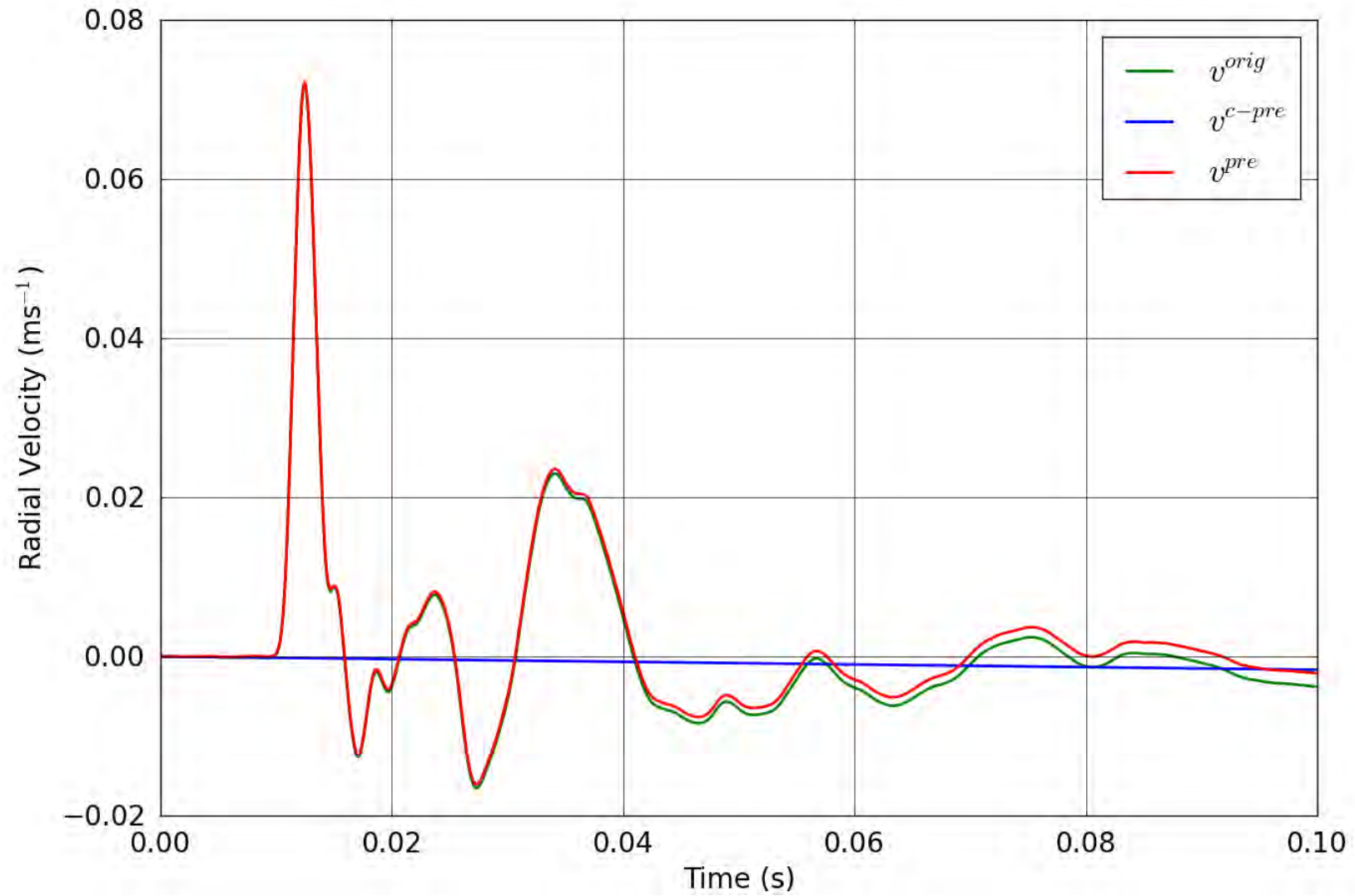


Figure 39. SPE-1 Gauge 6-3-R – Pre-shot baseline correction of the radial velocity.

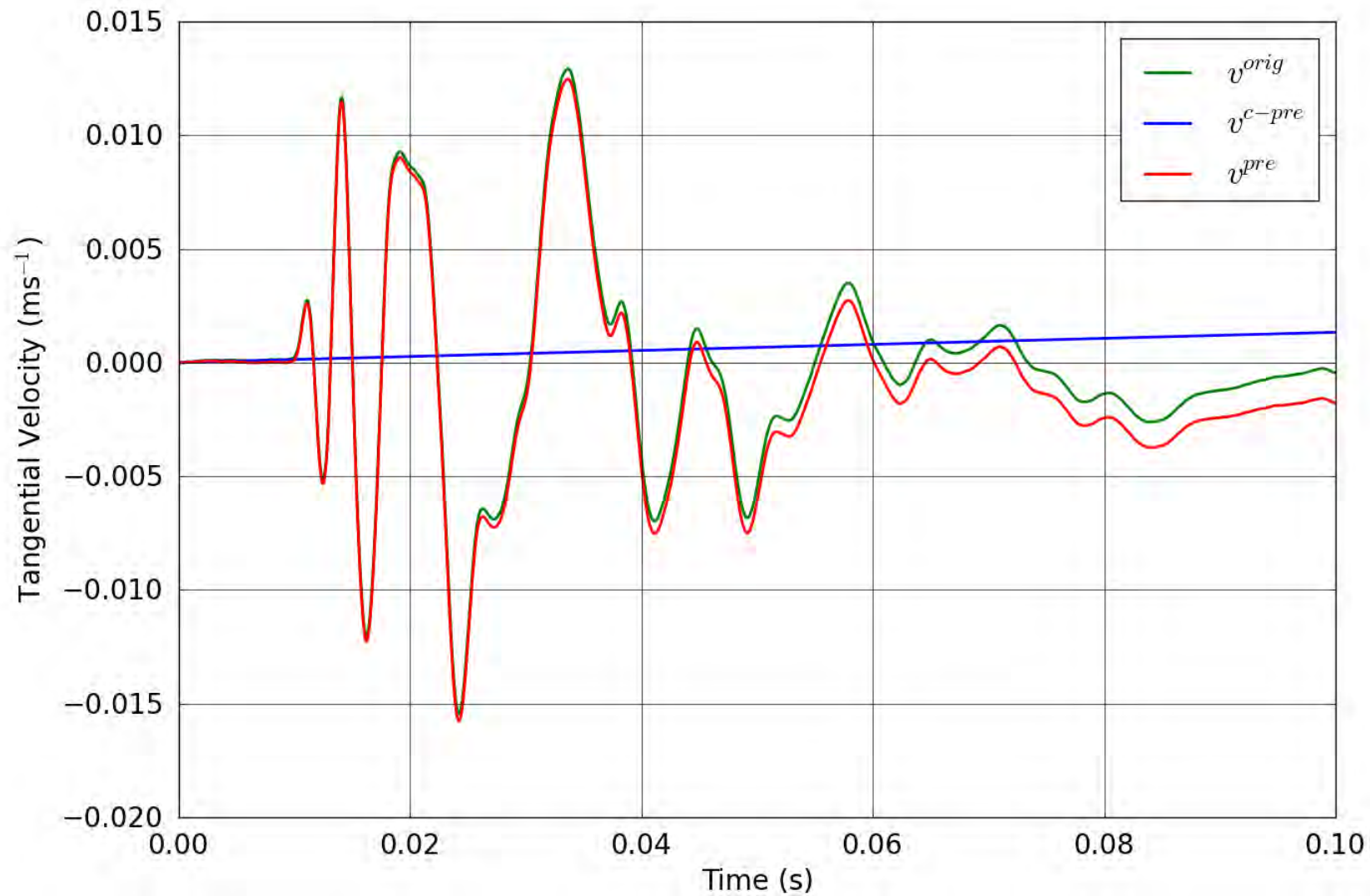


Figure 40. SPE-1 Gauge 6-3-T – Pre-shot baseline correction of the tangential velocity.

2.2. Records corrected for post-arrival baseline shift

The following plots reflect application of both the pre-arrival and the post-arrival baseline shifts. For each record we show the velocity waveform as displayed in Section 1.1 along with a plot of the post-arrival correction and the final velocity waveform. The velocity plot for each gauge is followed by the plot of displacement for this final correction.

The key to the legend in the graphs presented in this section is the following:

- v^{pre} represents the velocity waveforms corrected for the pre-arrival baseline shift.
- v^{c-post} represents the post-arrival baseline shift acceleration correction in the velocity space.
- v^{final} represents the final velocity waveforms corrected for pre- and post-arrival baseline shifts.

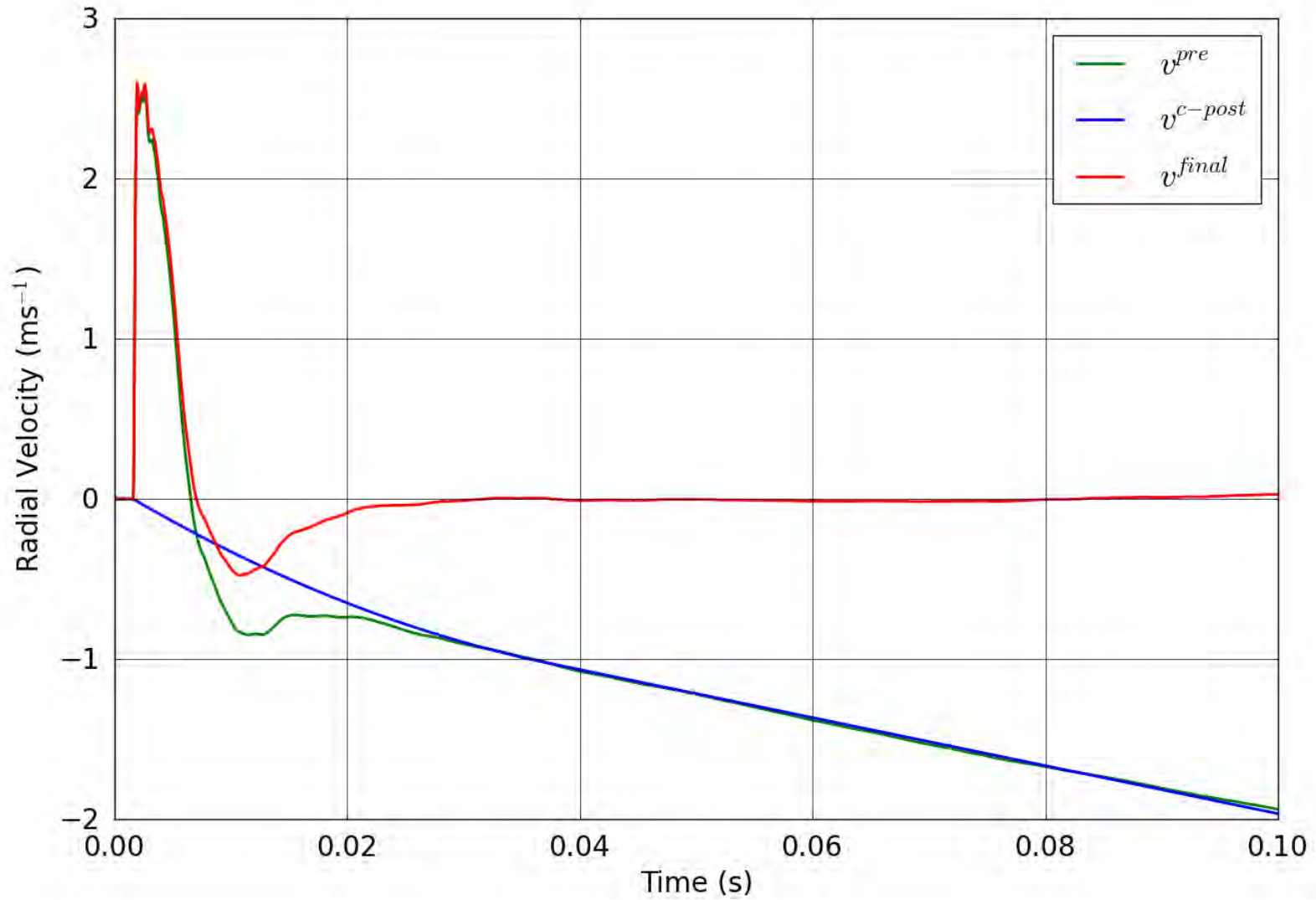


Figure 41. SPE-1 Gauge 1-1-R – Correction of the radial velocity.

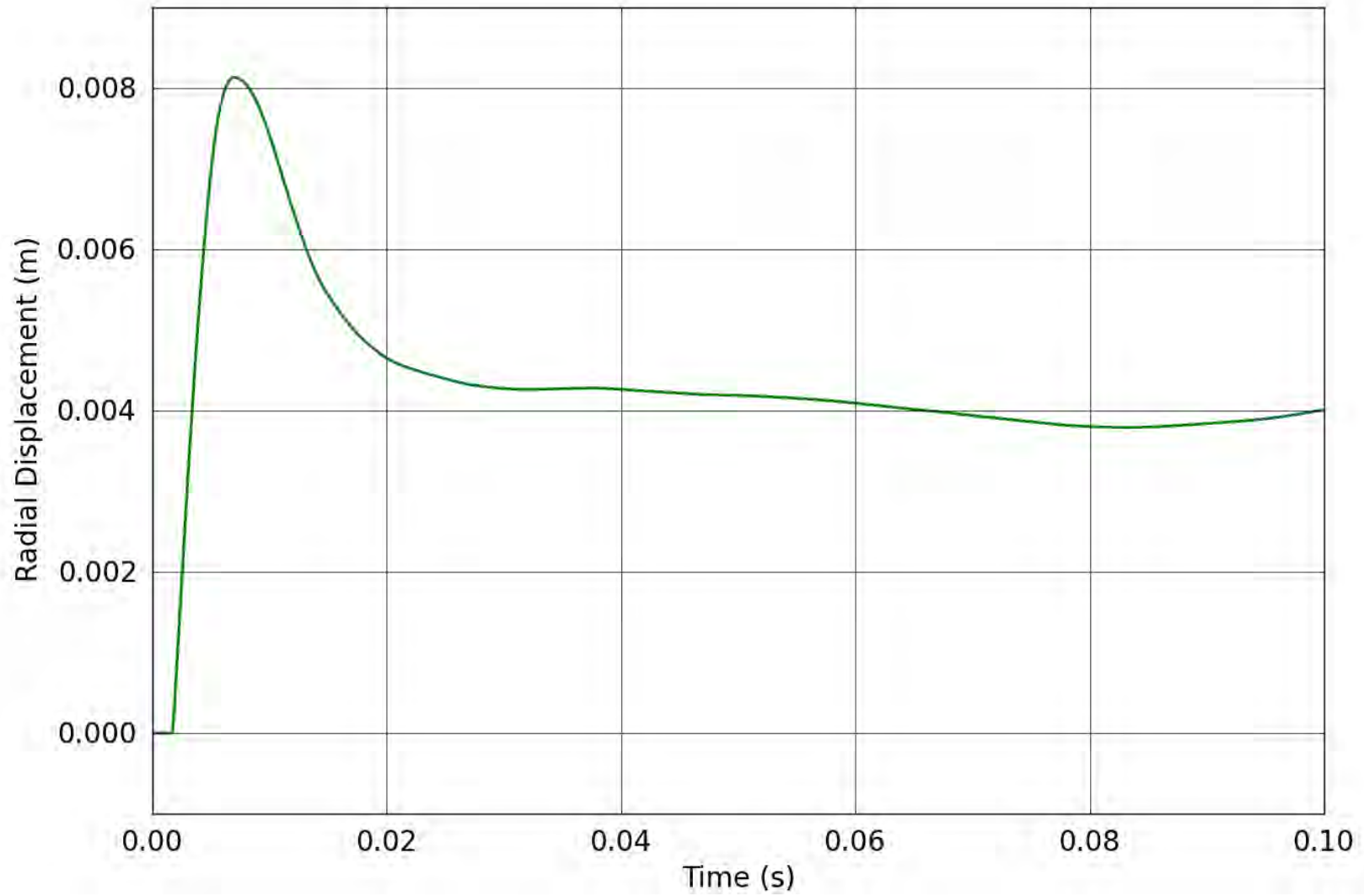


Figure 42. SPE-1 Gauge 1-1-R – Radial displacement obtained from the corrected radial velocity.

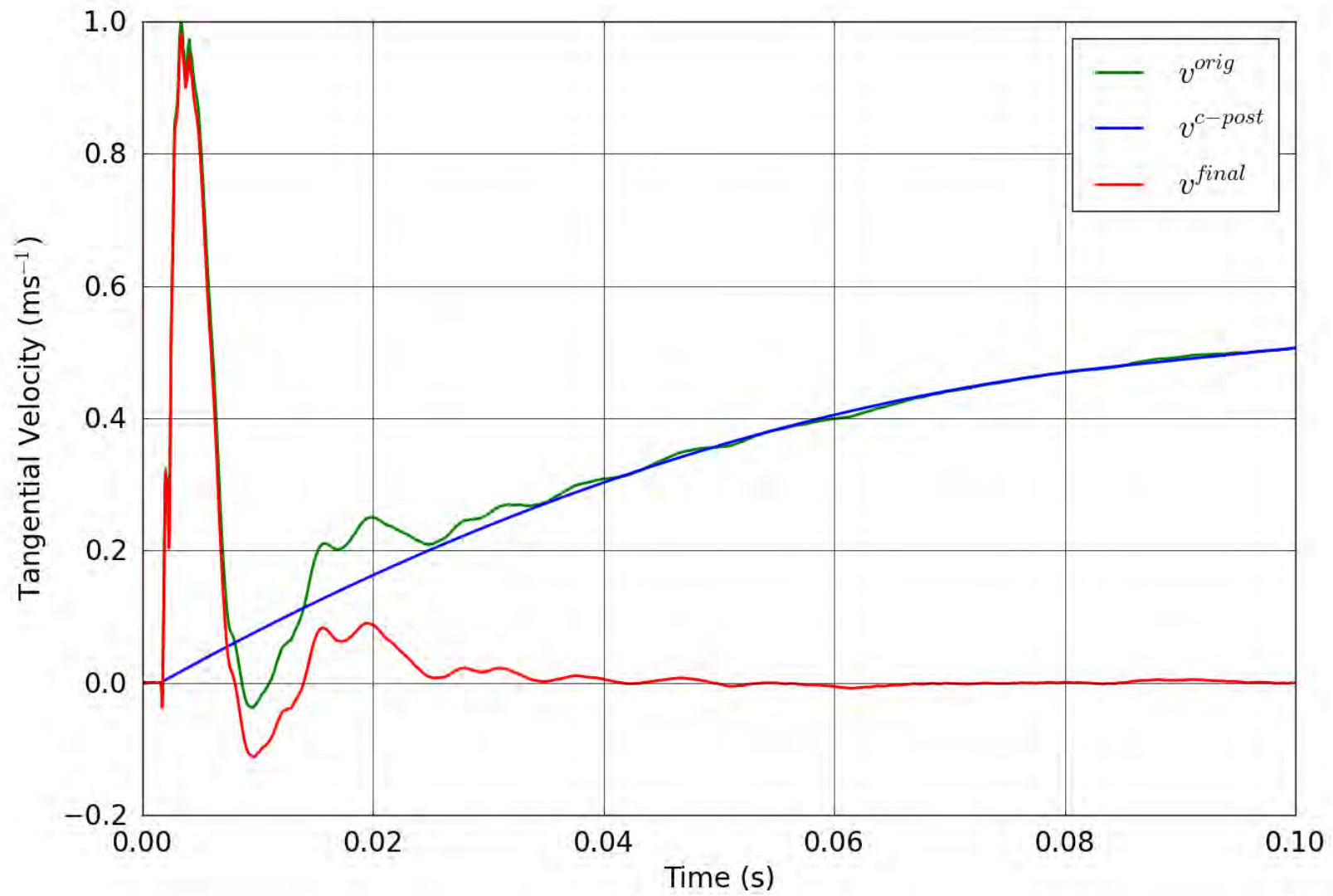


Figure 43. SPE-1 Gauge 1-1-T – Correction of the tangential velocity.

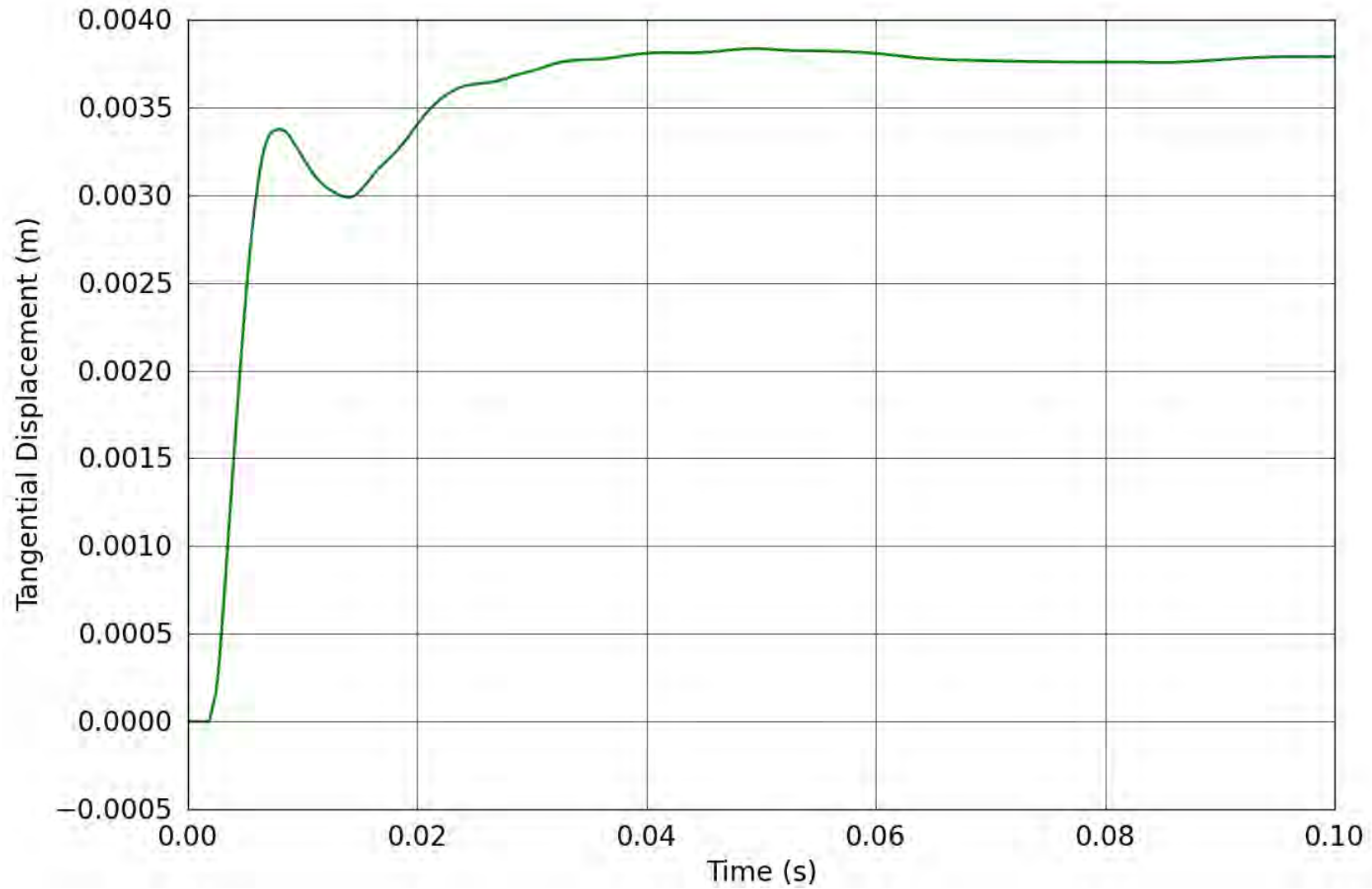


Figure 44. SPE-1 Gauge 1-1-T – Tangential displacement obtained from the corrected tangential velocity.

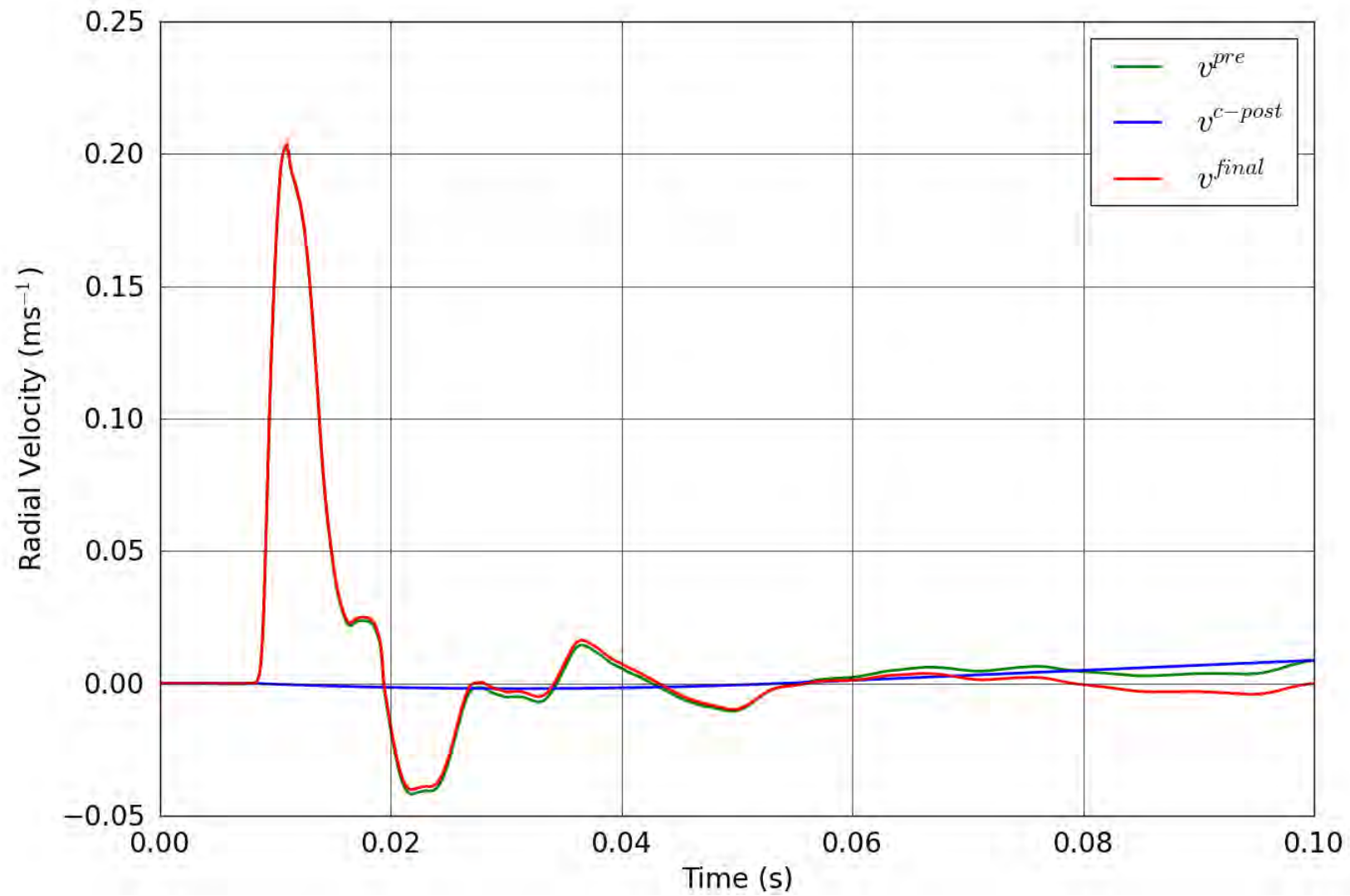


Figure 45. SPE-1 Gauge 1-3-R – Correction of the radial velocity.

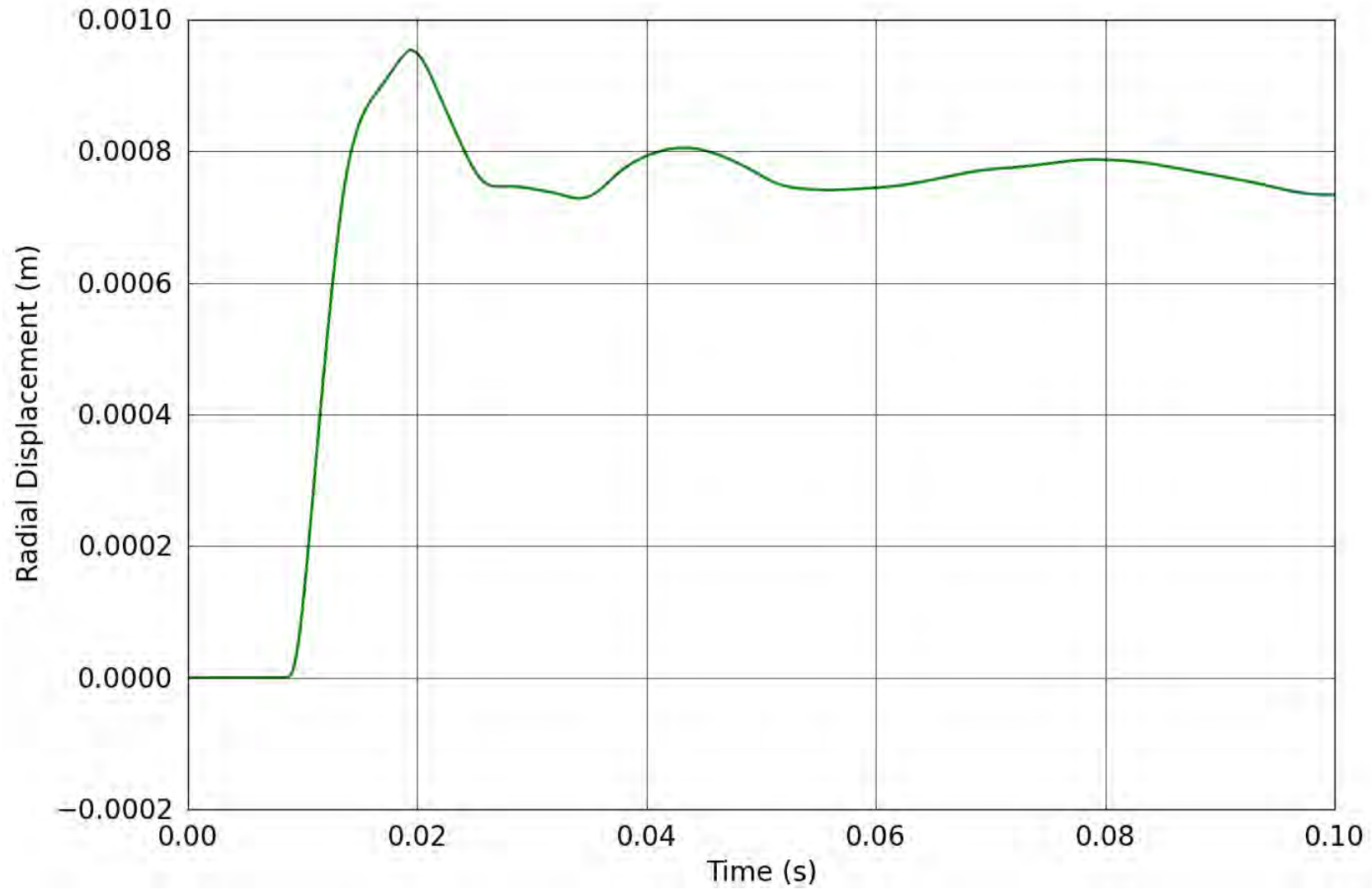


Figure 46. SPE-1 Gauge 1-3-R – Radial displacement obtained from the corrected radial velocity.

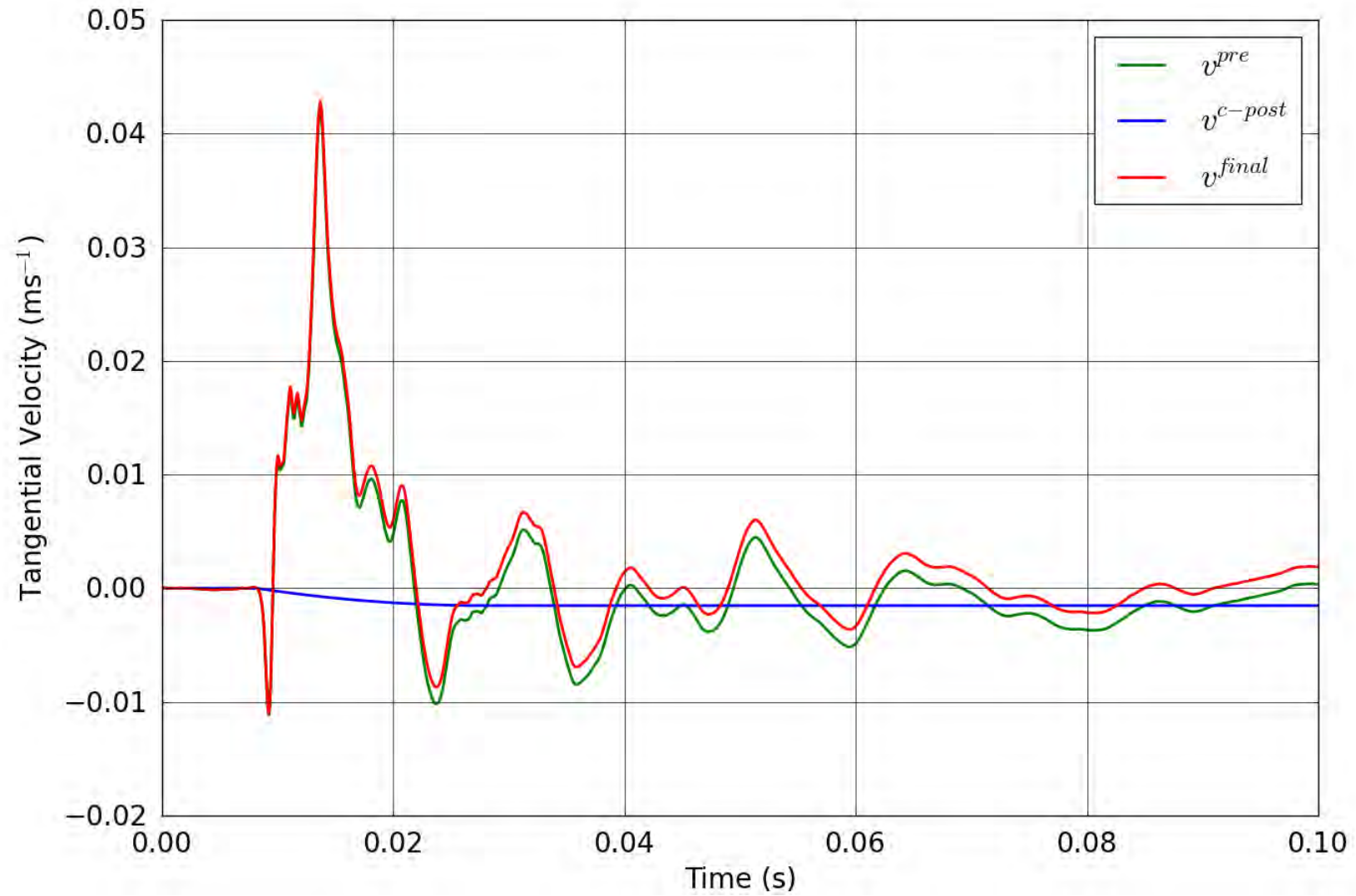


Figure 47. SPE-1 Gauge 1-3-T – Correction of the tangential velocity.

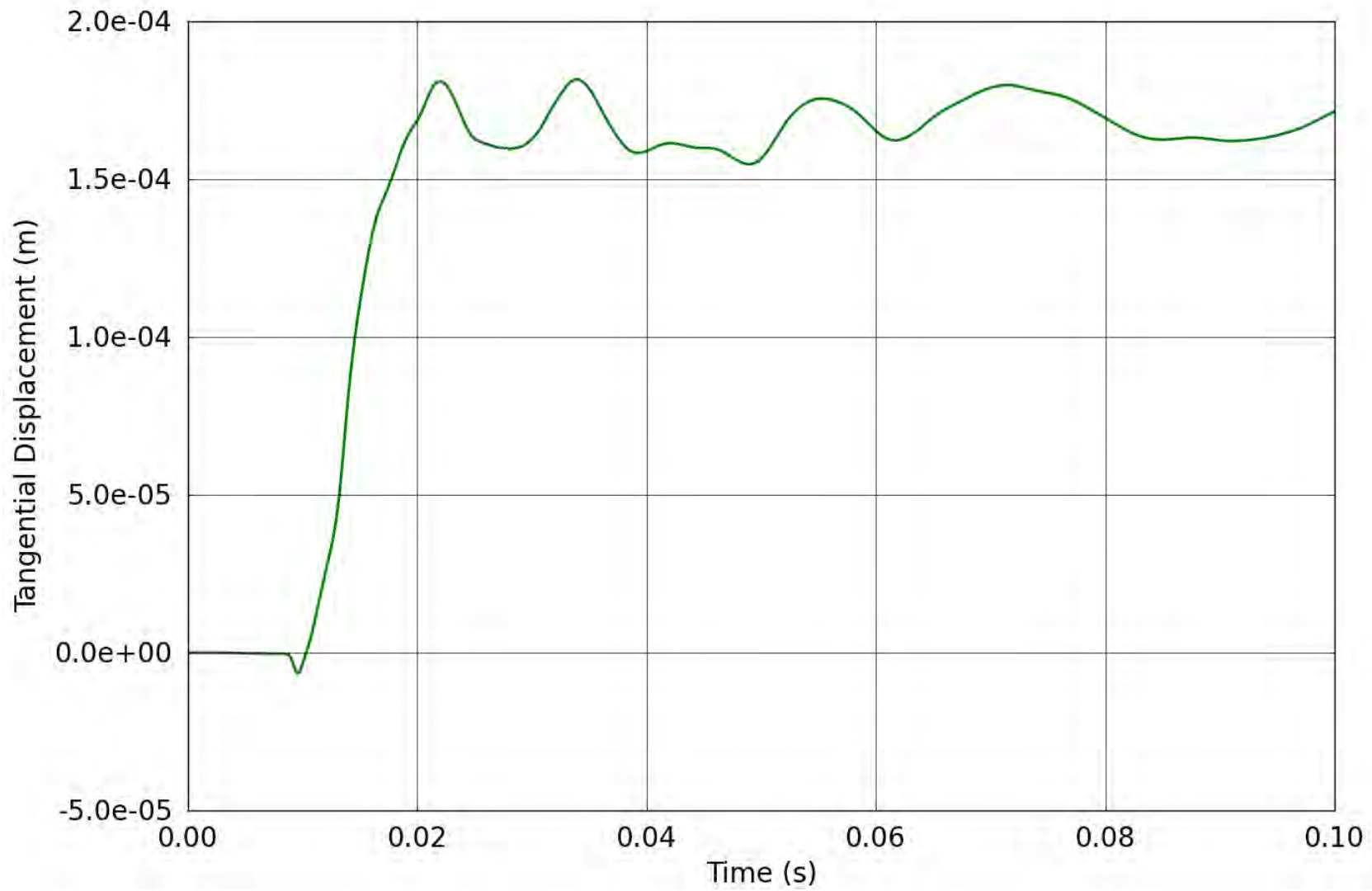


Figure 48. SPE-1 Gauge 1-3-T – Tangential displacement obtained from the corrected tangential velocity.

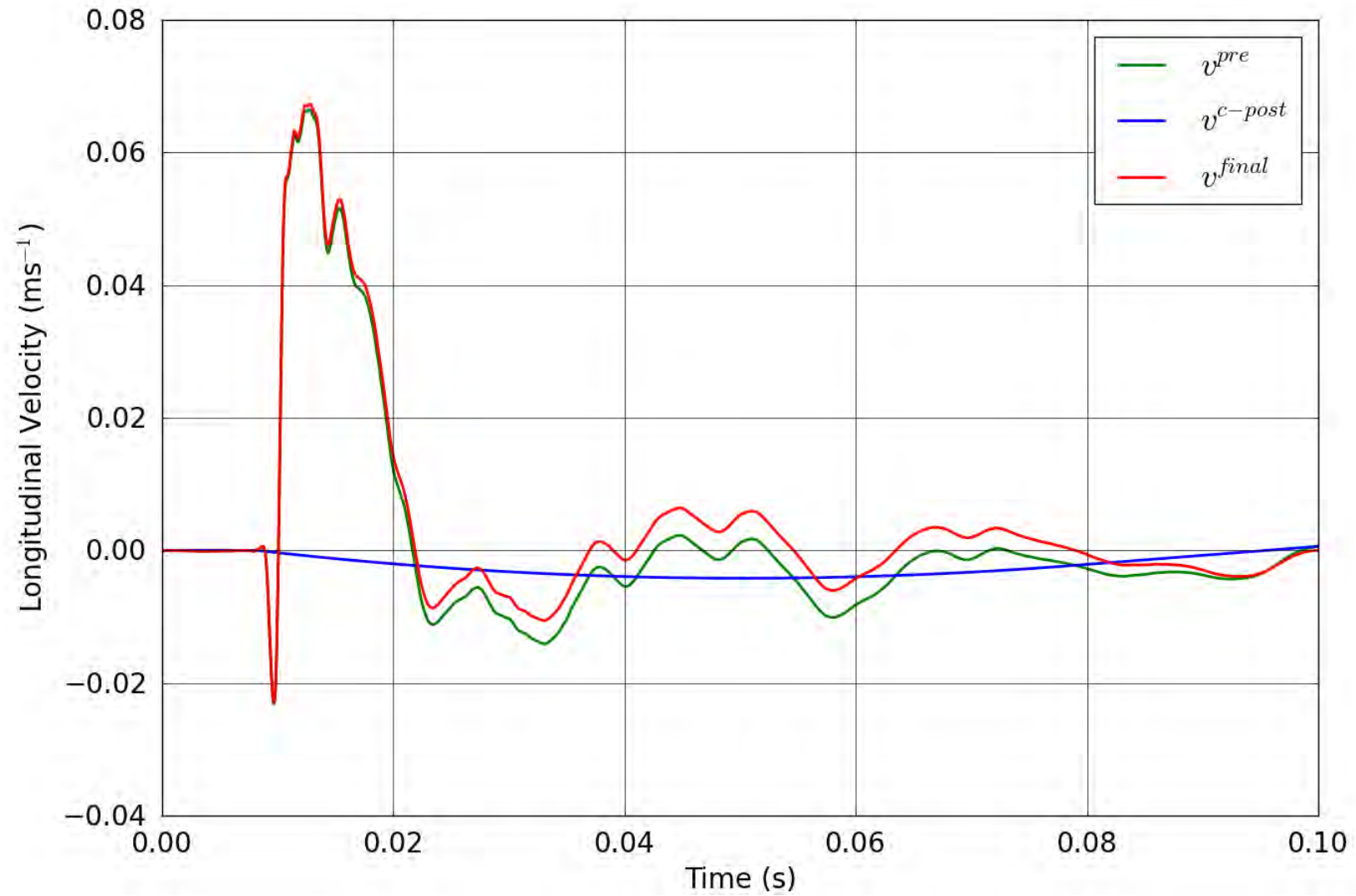


Figure 49. SPE-1 Gauge 1-3-L – Correction of the longitudinal velocity.

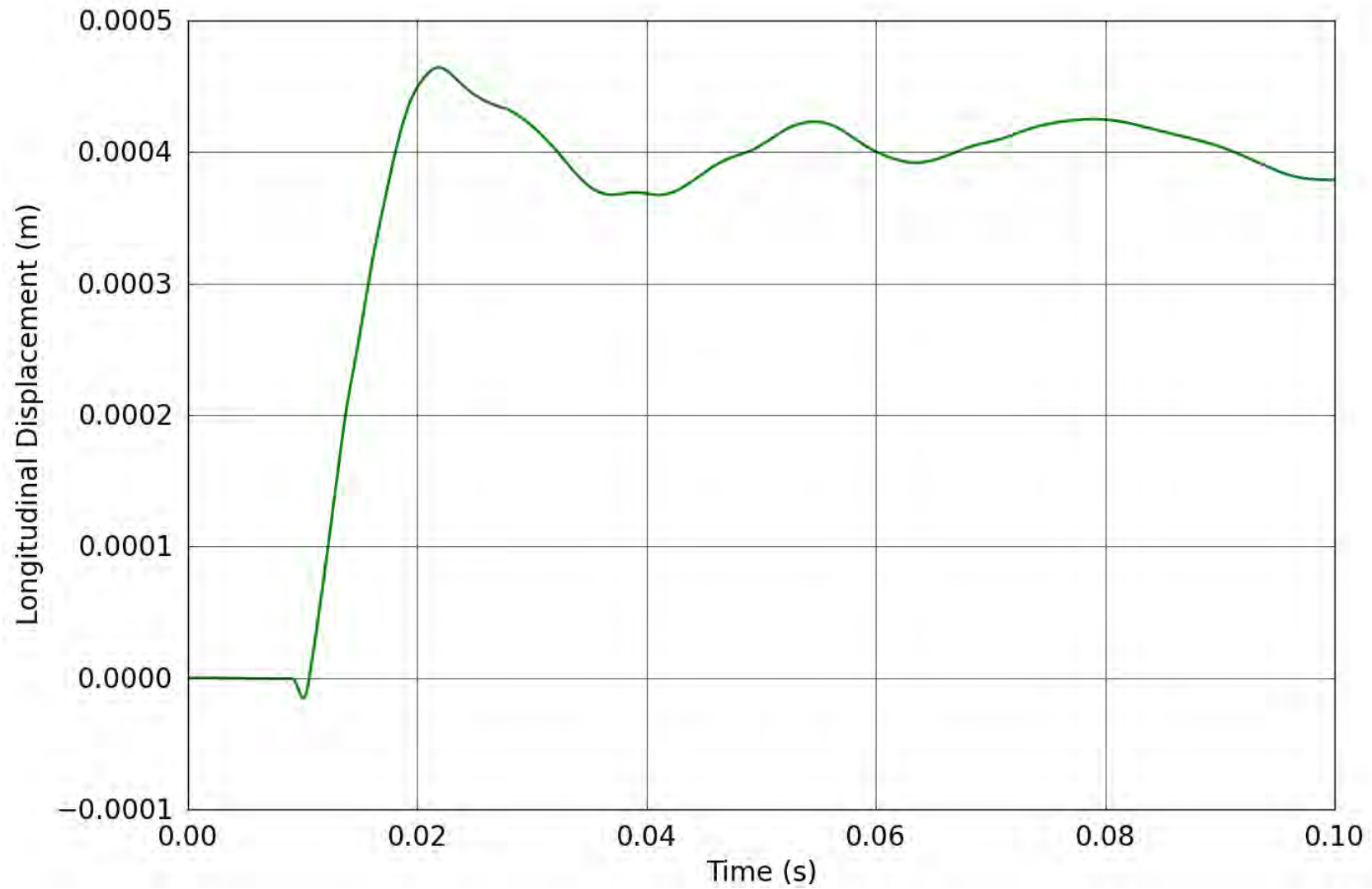


Figure 50. SPE-1 Gauge 1-3-L – Longitudinal displacement obtained from the corrected longitudinal velocity.

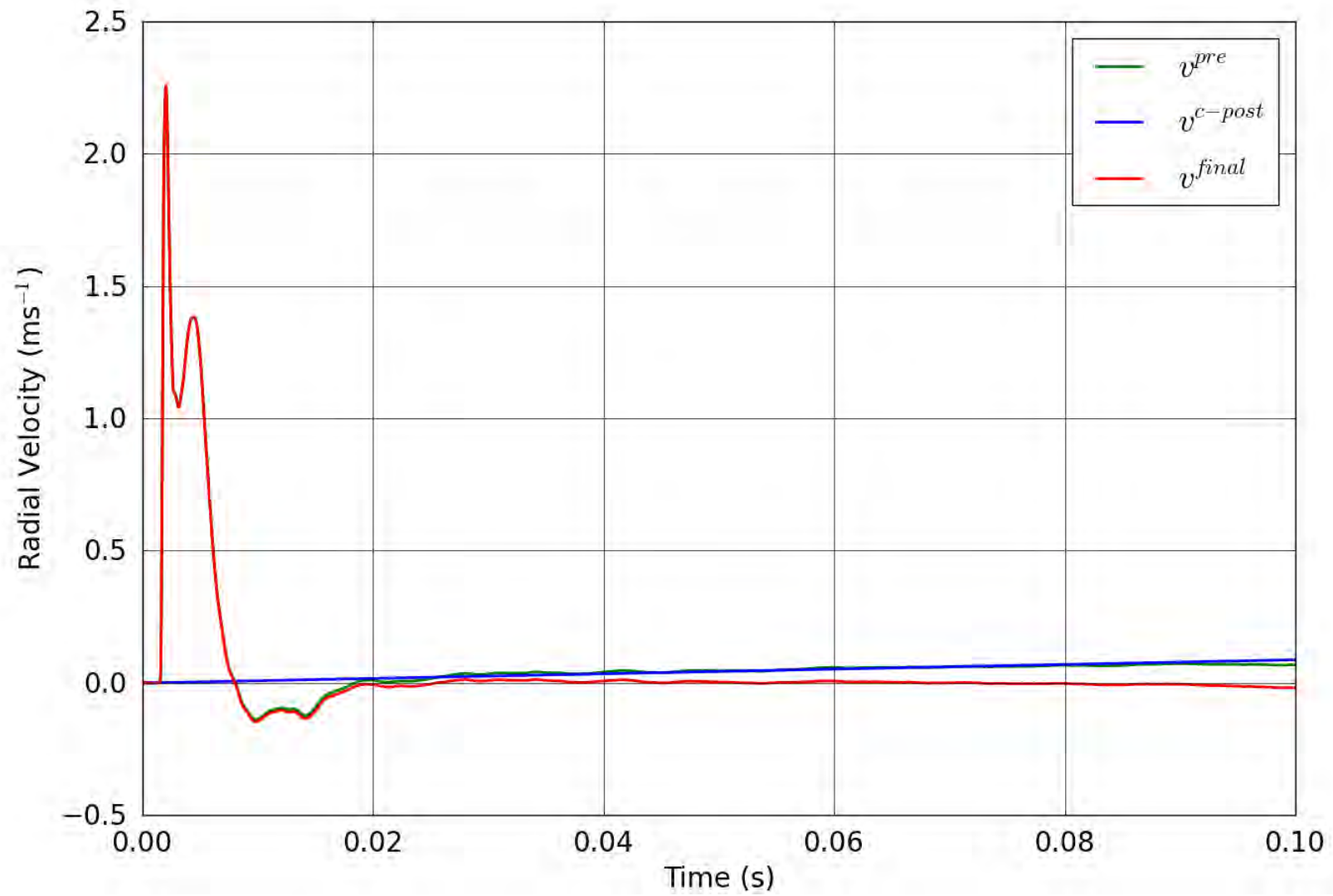


Figure 51. SPE-1 Gauge 2-1-R – Correction of the radial velocity.

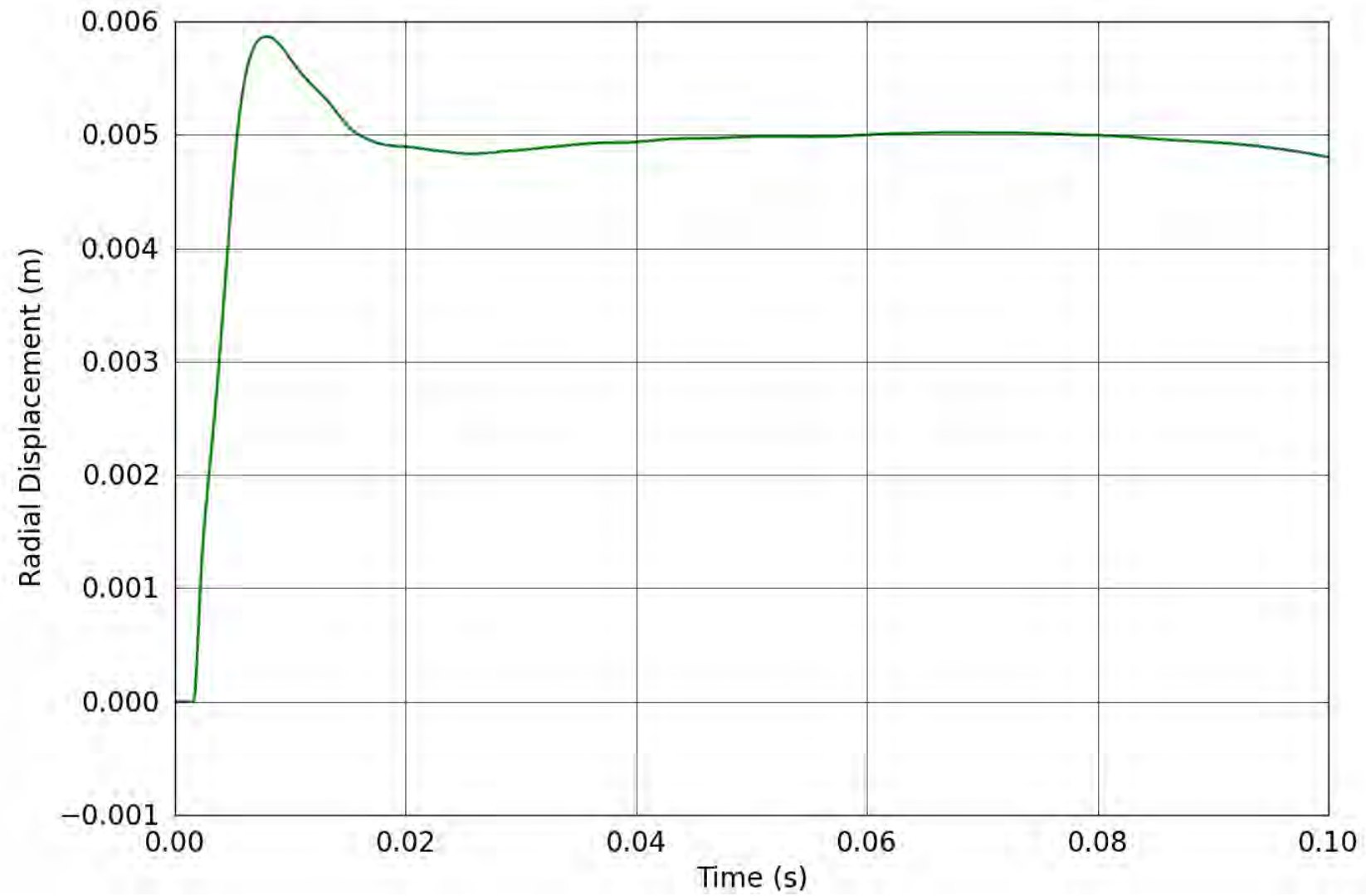


Figure 52. SPE-1 Gauge 2-1-R – Radial displacement obtained from the corrected radial velocity.

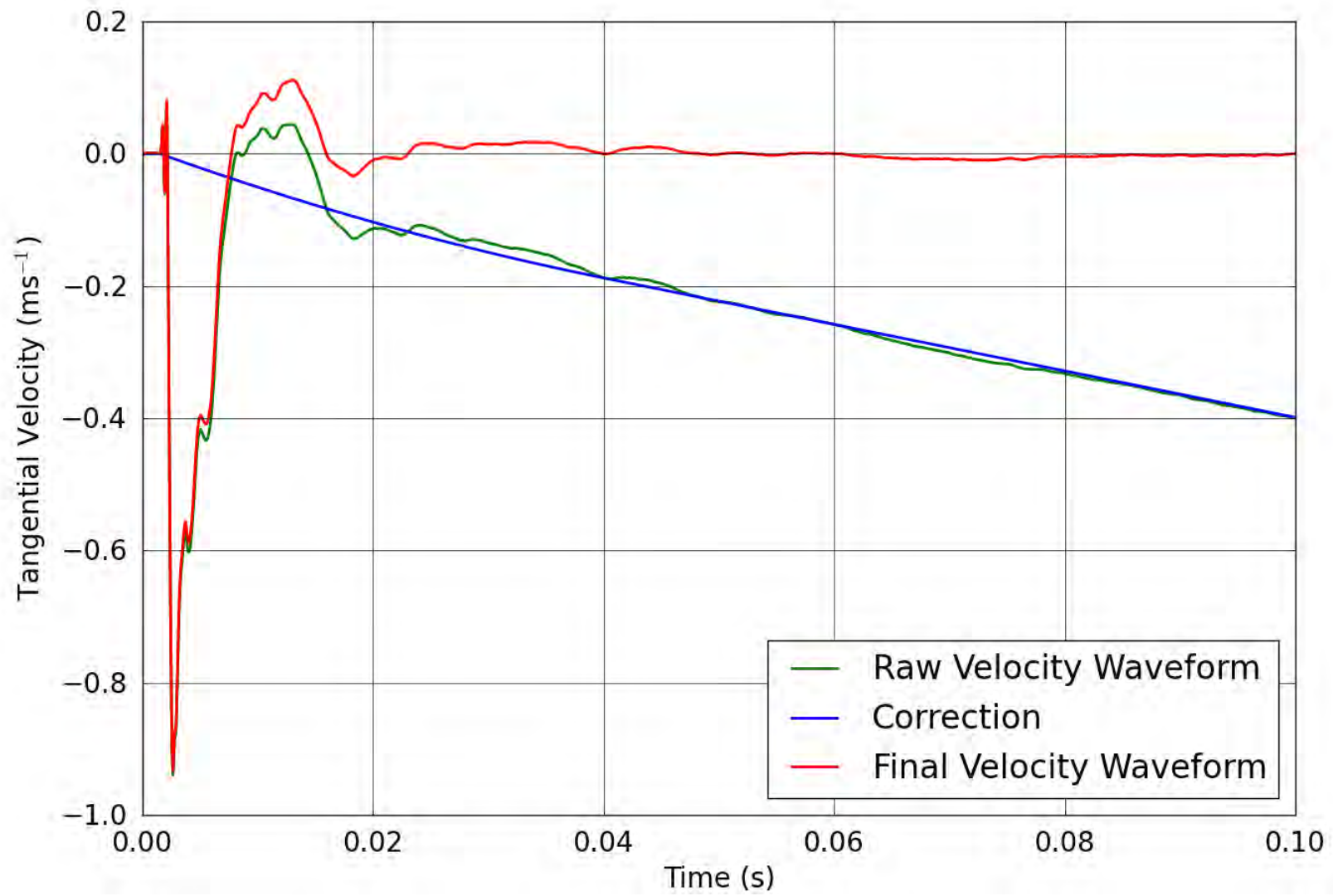


Figure 53. SPE-1 Gauge 2-1-T – Correction of the tangential velocity.

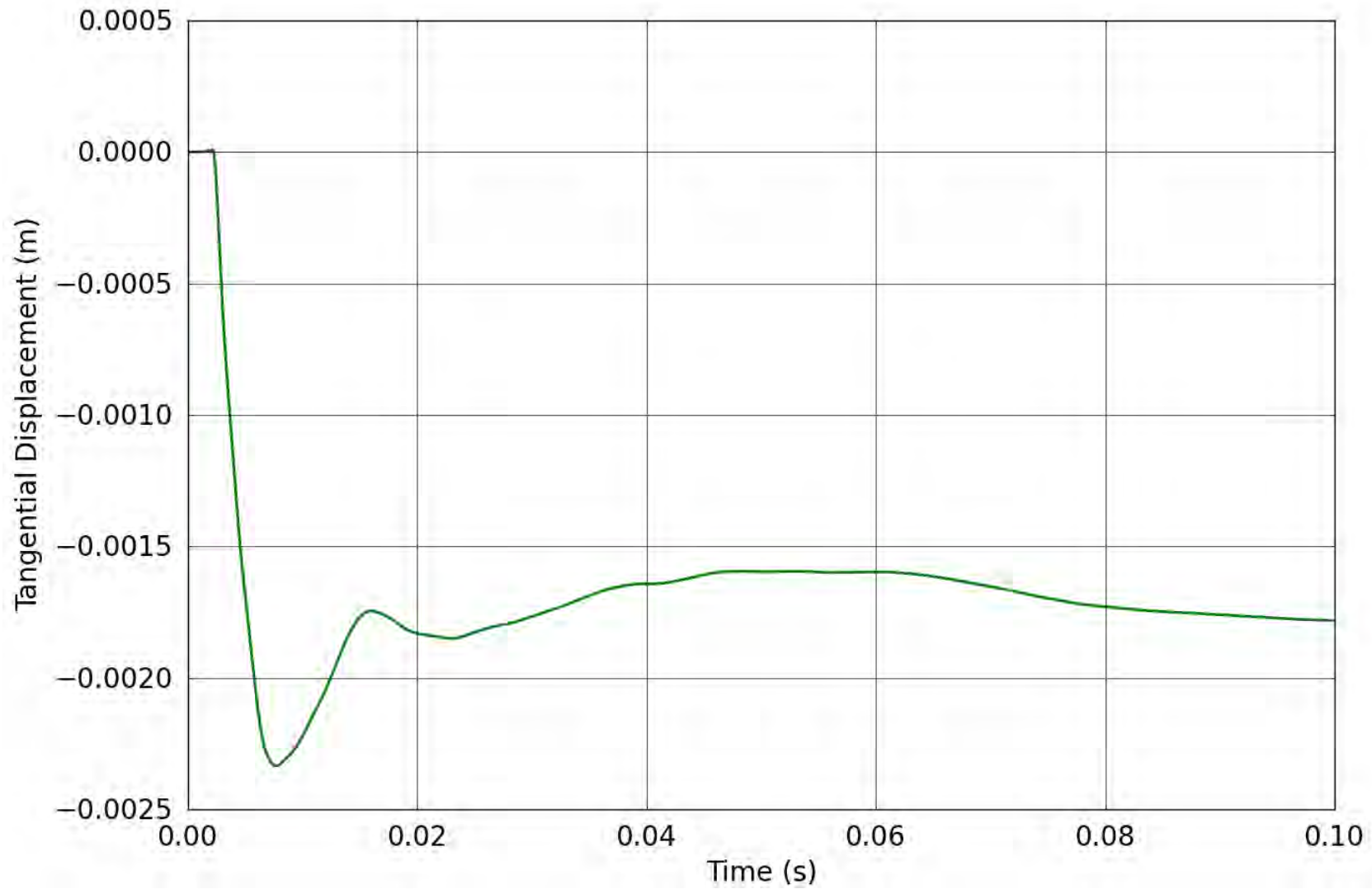


Figure 54. SPE-1 Gauge 2-1-T – Tangential displacement obtained from the corrected tangential velocity.

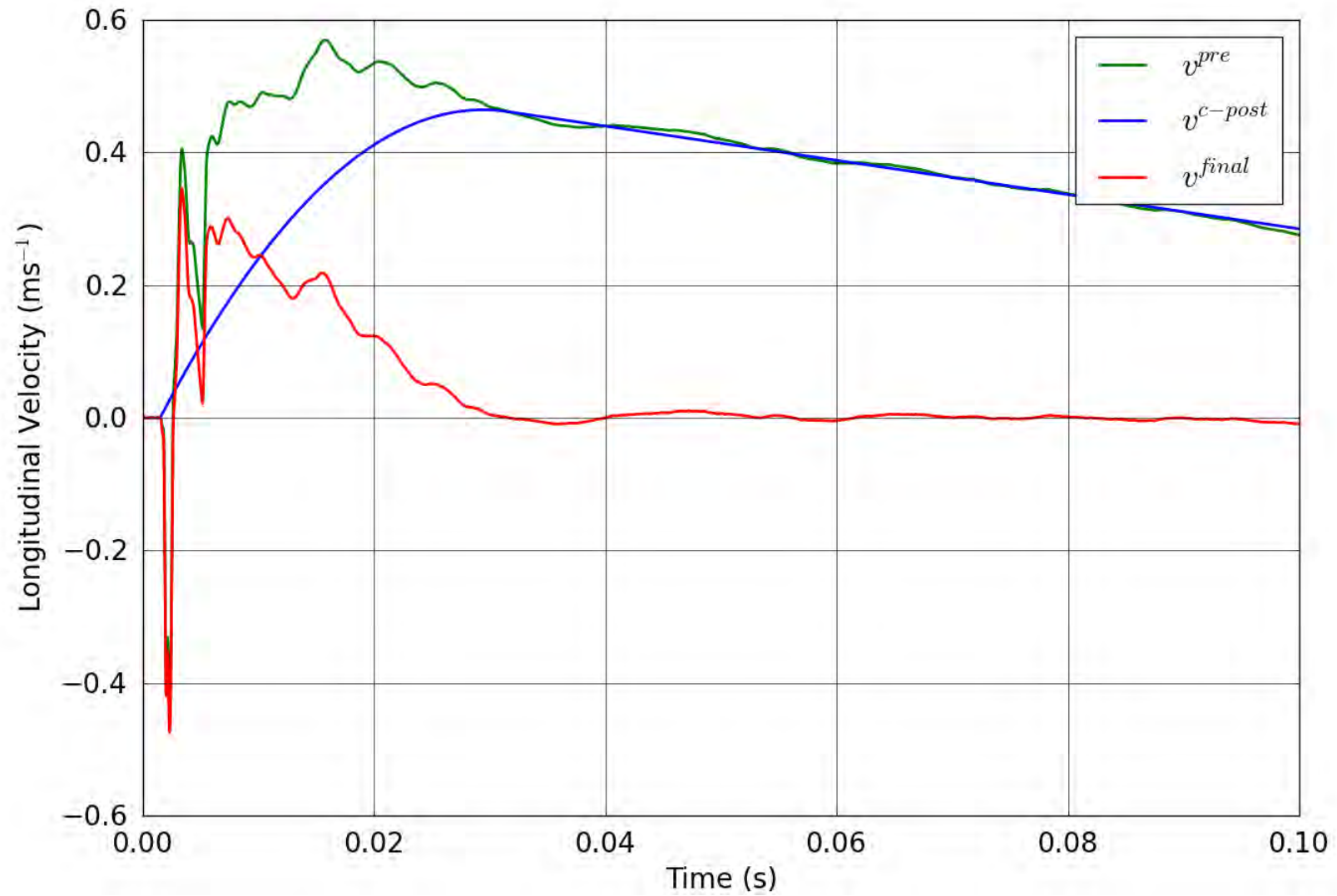


Figure 55. SPE-1 Gauge 2-1-L – Correction of the longitudinal velocity.

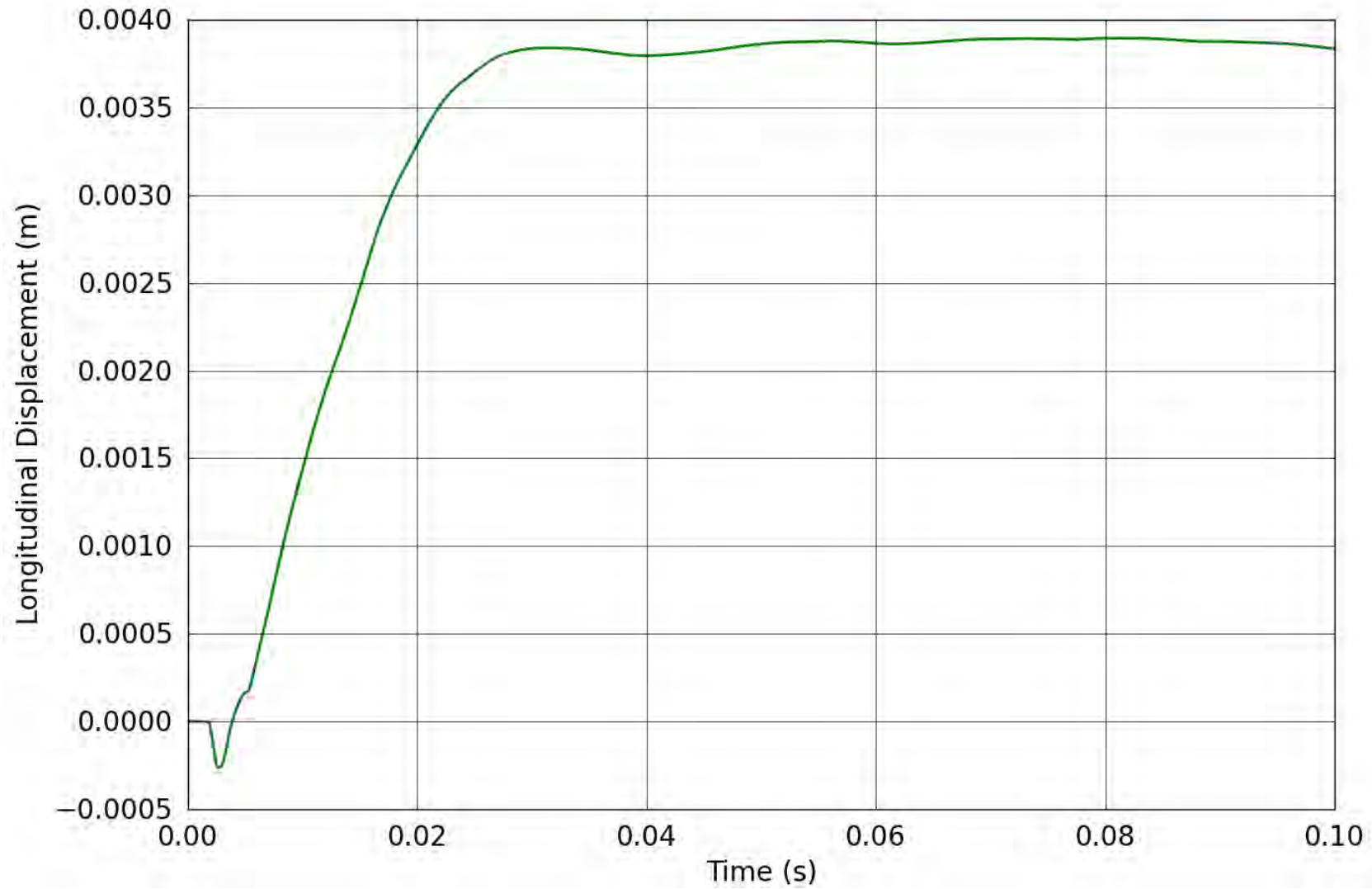


Figure 56. SPE-1 Gauge 2-1-L – Longitudinal displacement obtained from the corrected longitudinal velocity.

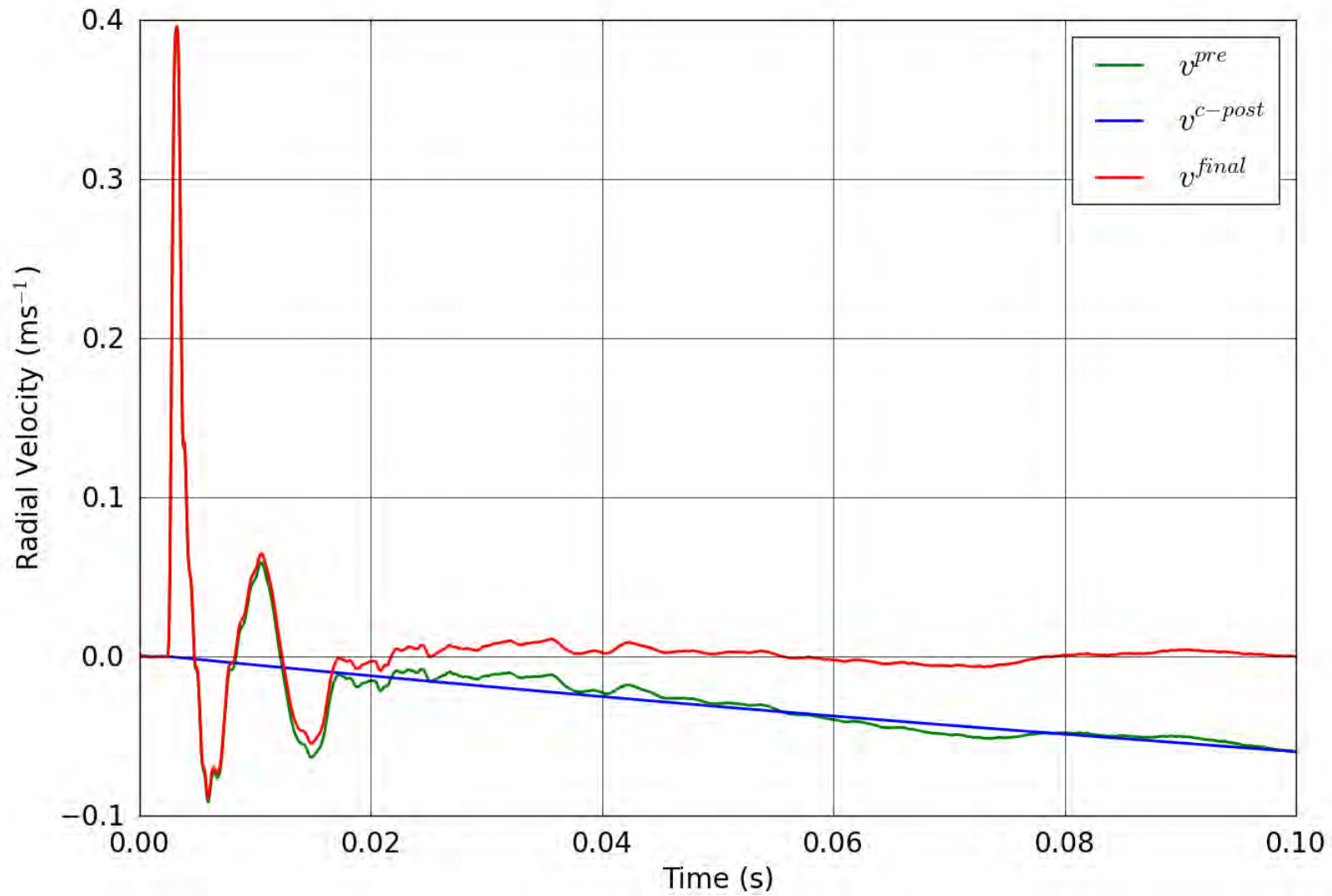


Figure 57. SPE-1 Gauge 2-2-R – Correction of the radial velocity.

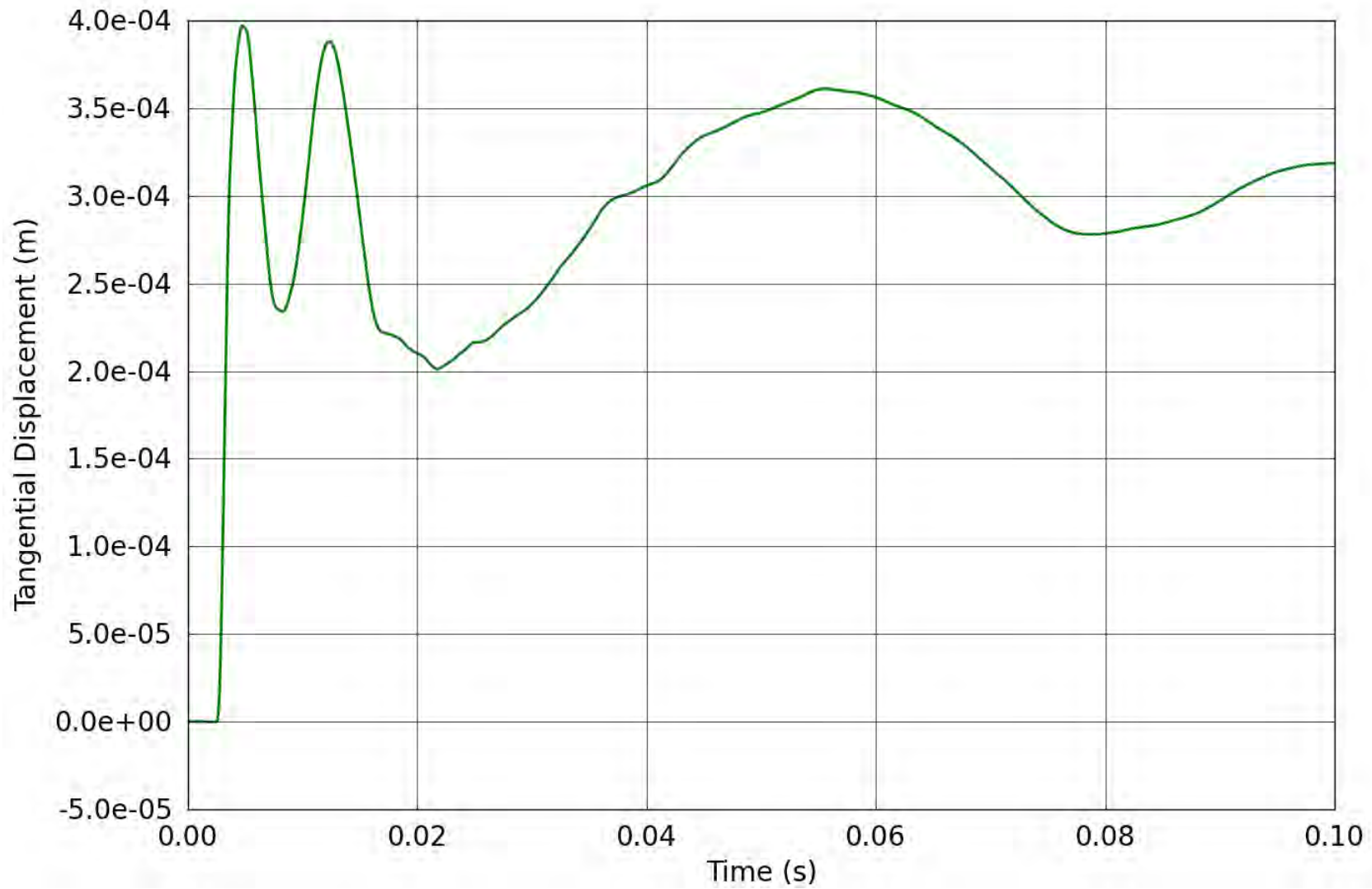


Figure 58. SPE-1 Gauge 2-2-R – Radial displacement obtained from the corrected radial velocity.

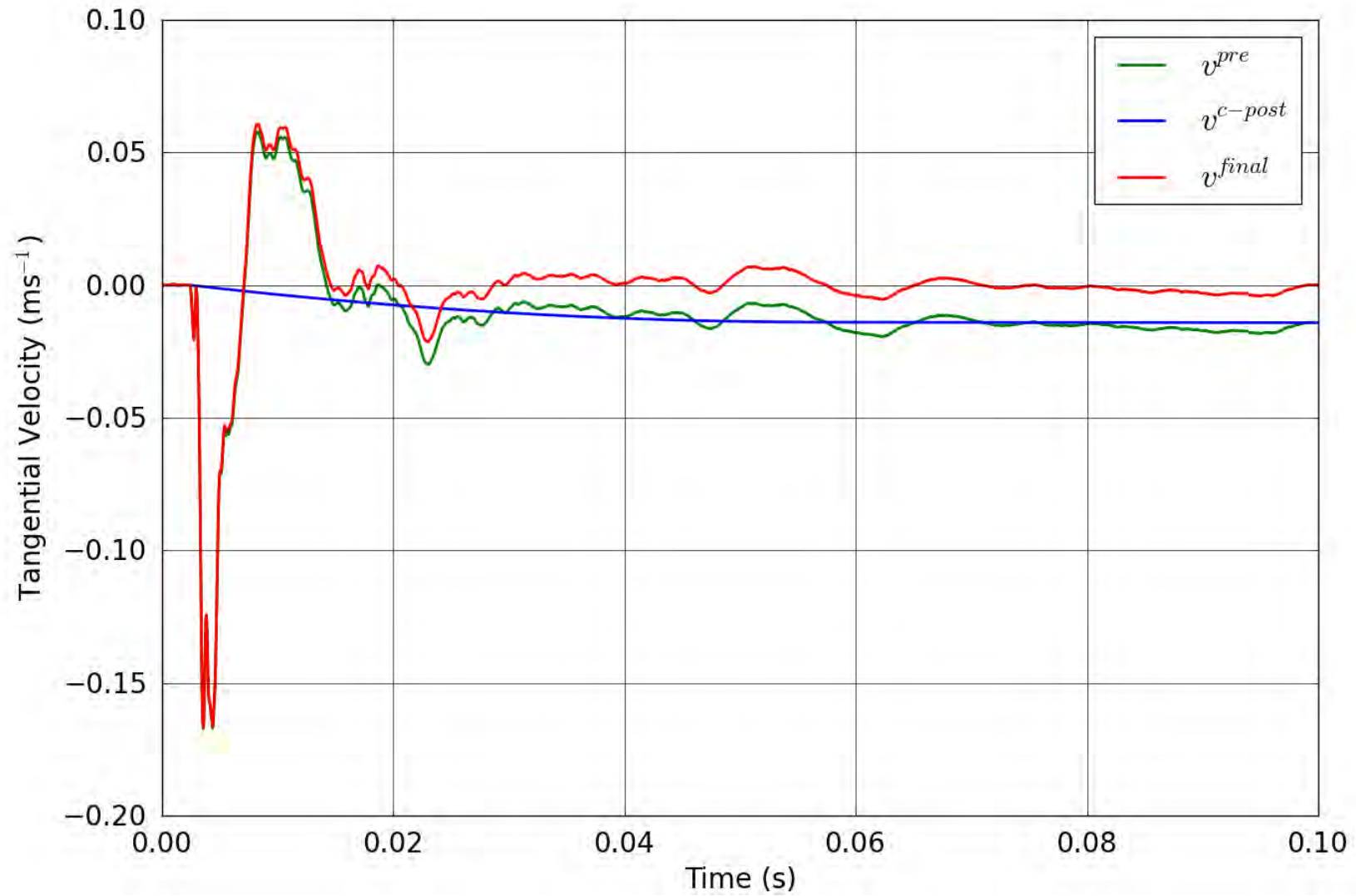


Figure 59. SPE-1 Gauge 2-2-T – Correction of the tangential velocity.

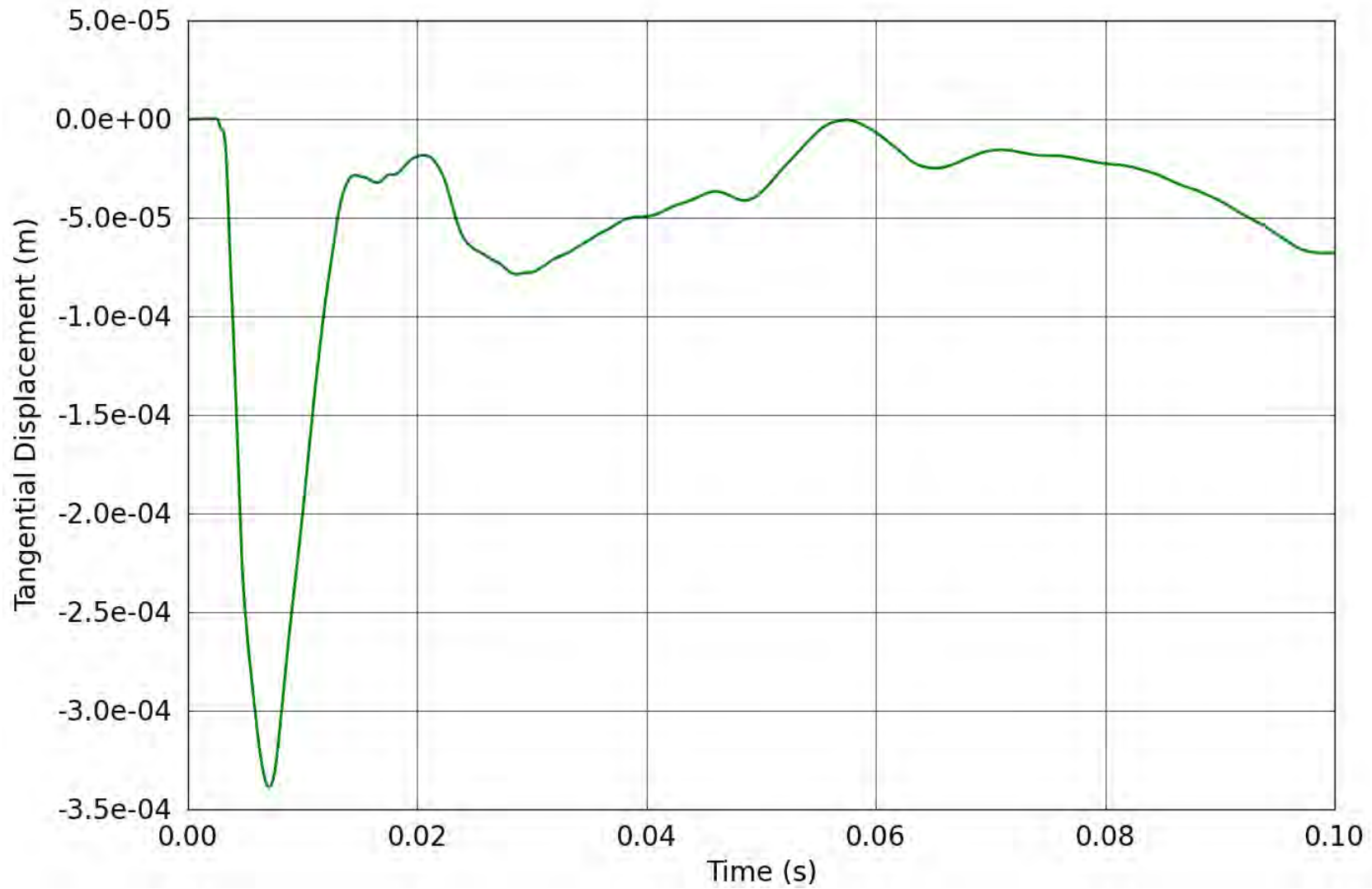


Figure 60. SPE-1 Gauge 2-2-T – Tangential displacement obtained from the corrected tangential velocity.

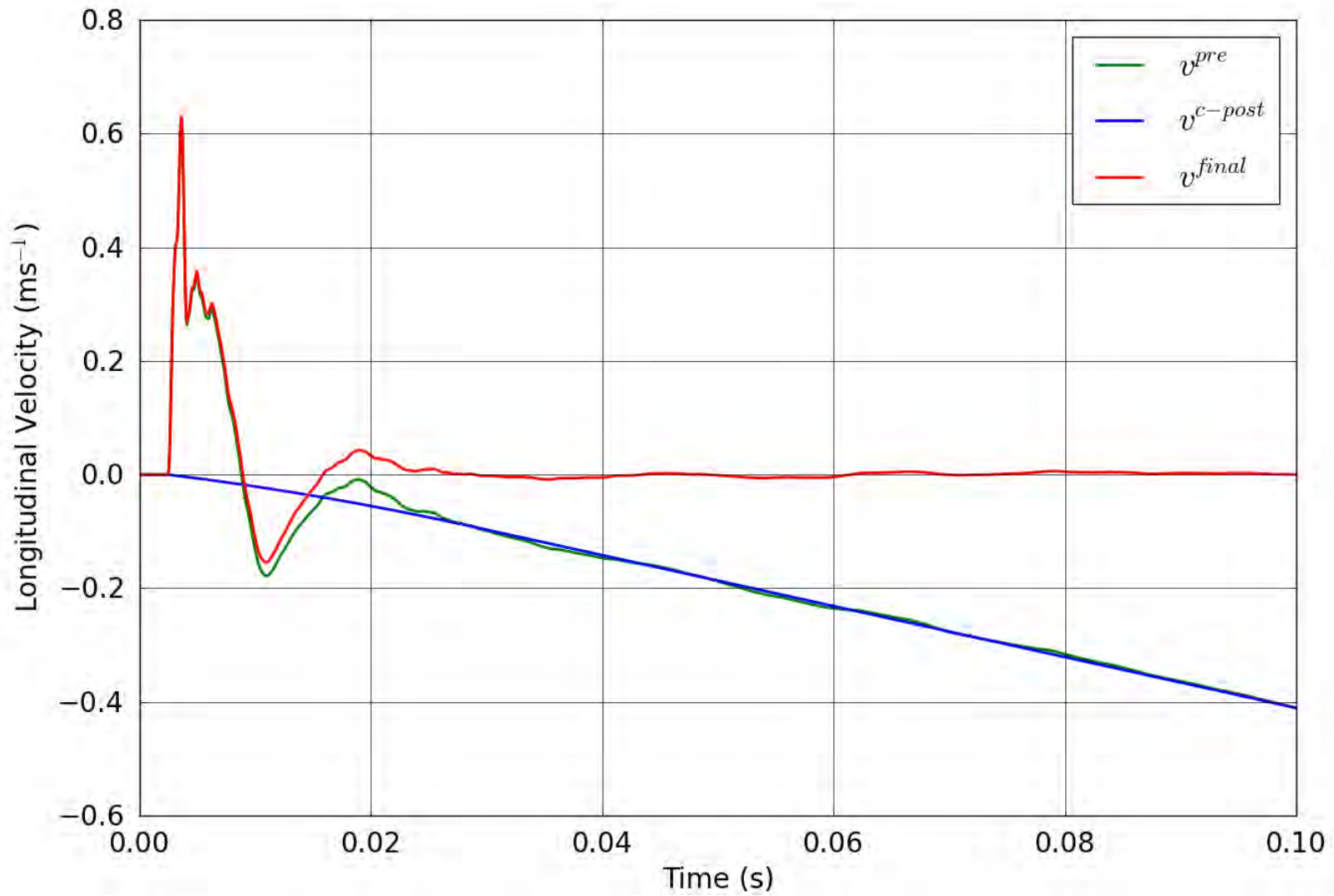


Figure 61. SPE-1 Gauge 2-2-L – Correction of the longitudinal velocity.

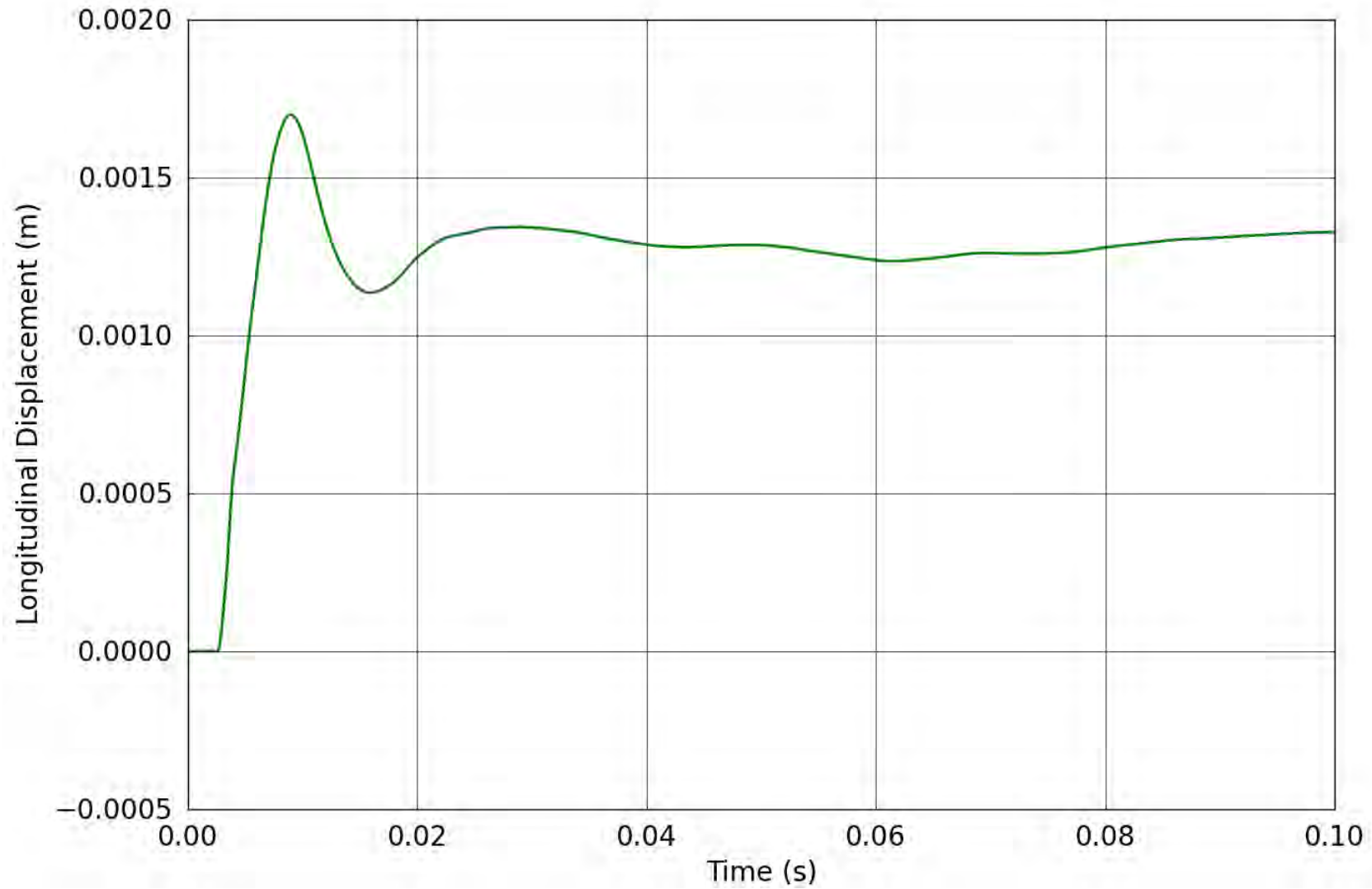


Figure 62. SPE-1 Gauge 2-2-L – Longitudinal displacement obtained from the corrected longitudinal velocity.

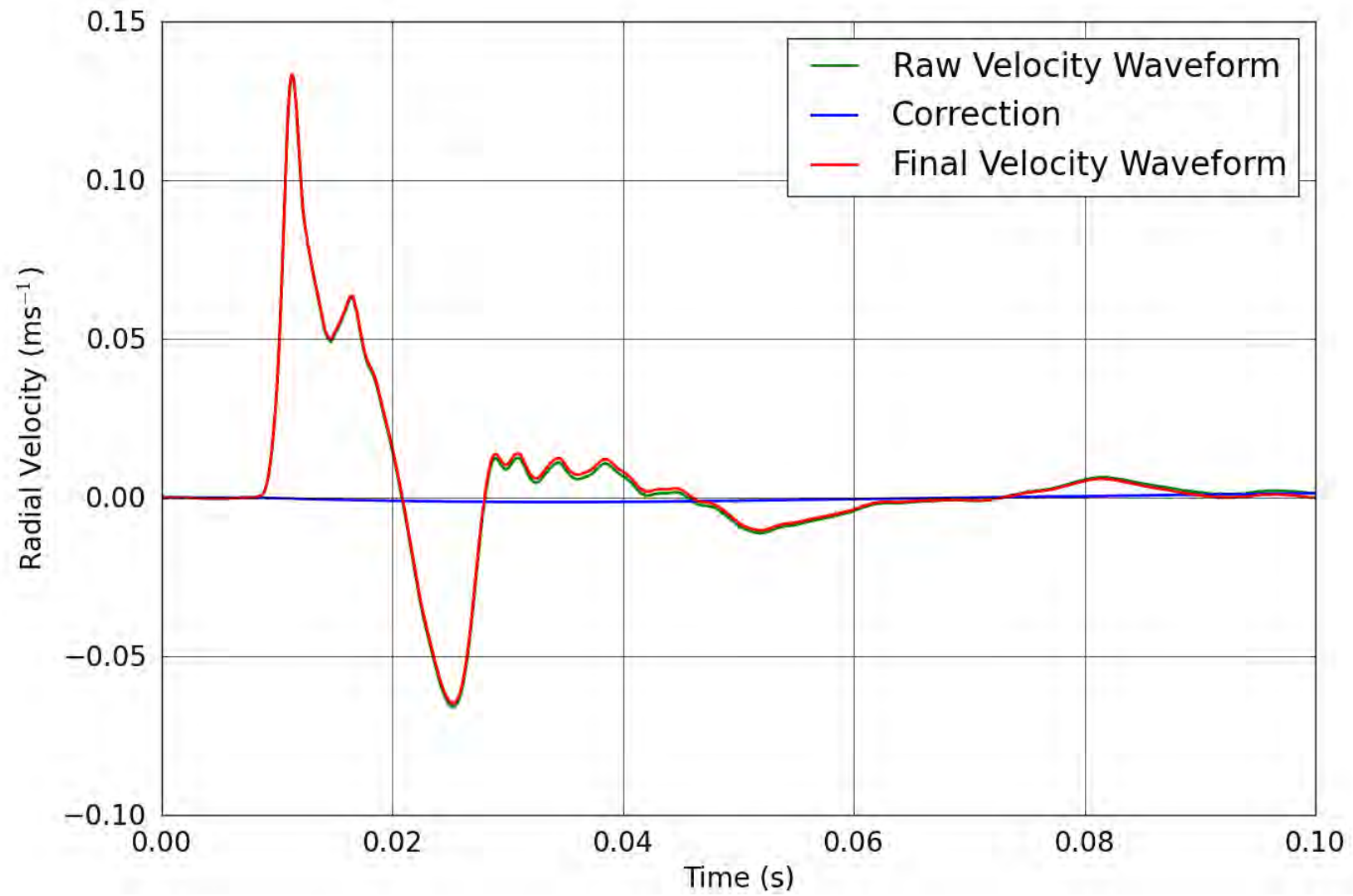


Figure 63. SPE-1 Gauge 2-3-R – Correction of the radial velocity.

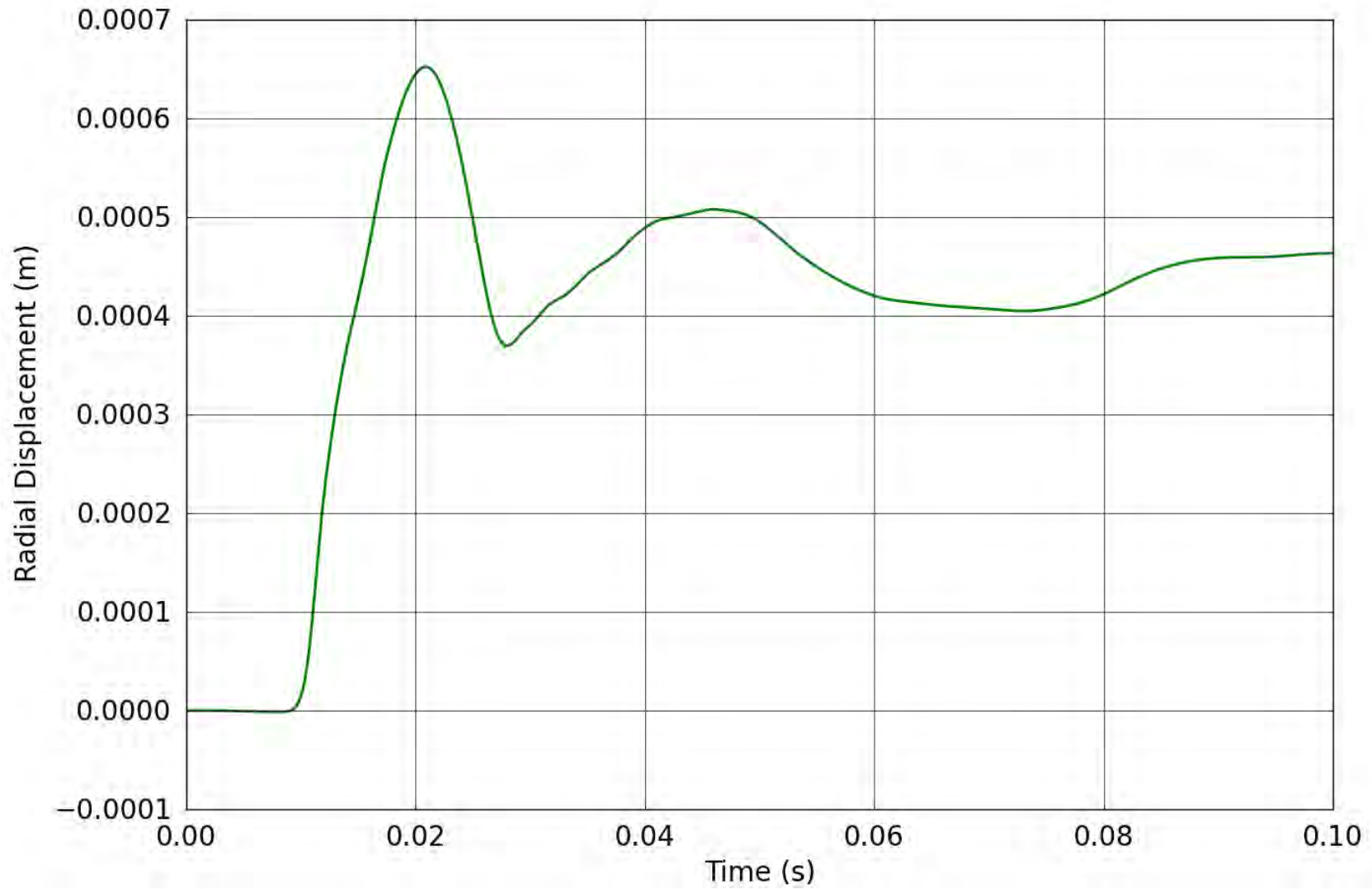


Figure 64. SPE-1 Gauge 2-3-R – Radial displacement obtained from the corrected radial velocity.

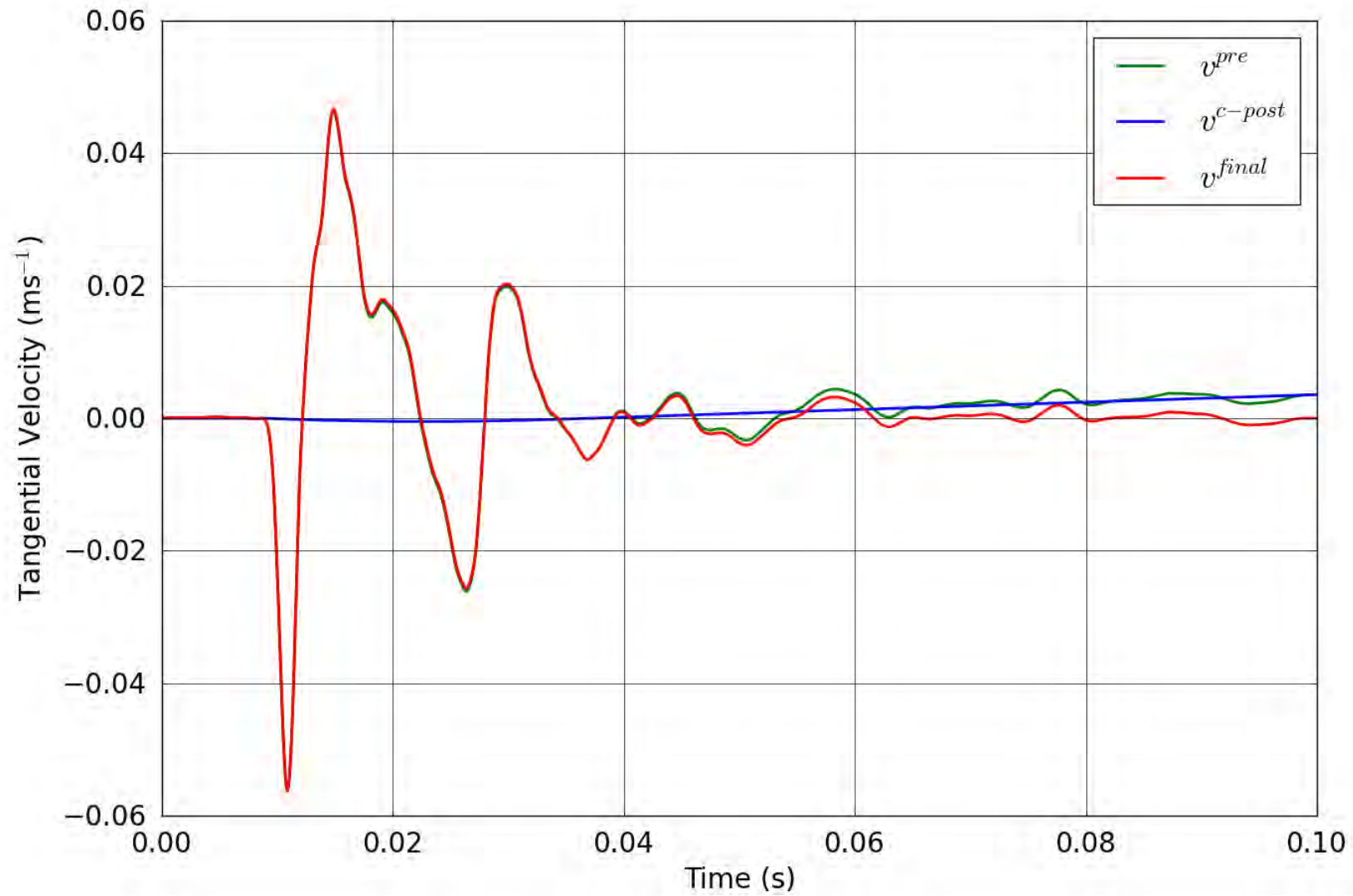


Figure 65. SPE-1 Gauge 2-3-T – Correction of the tangential velocity.

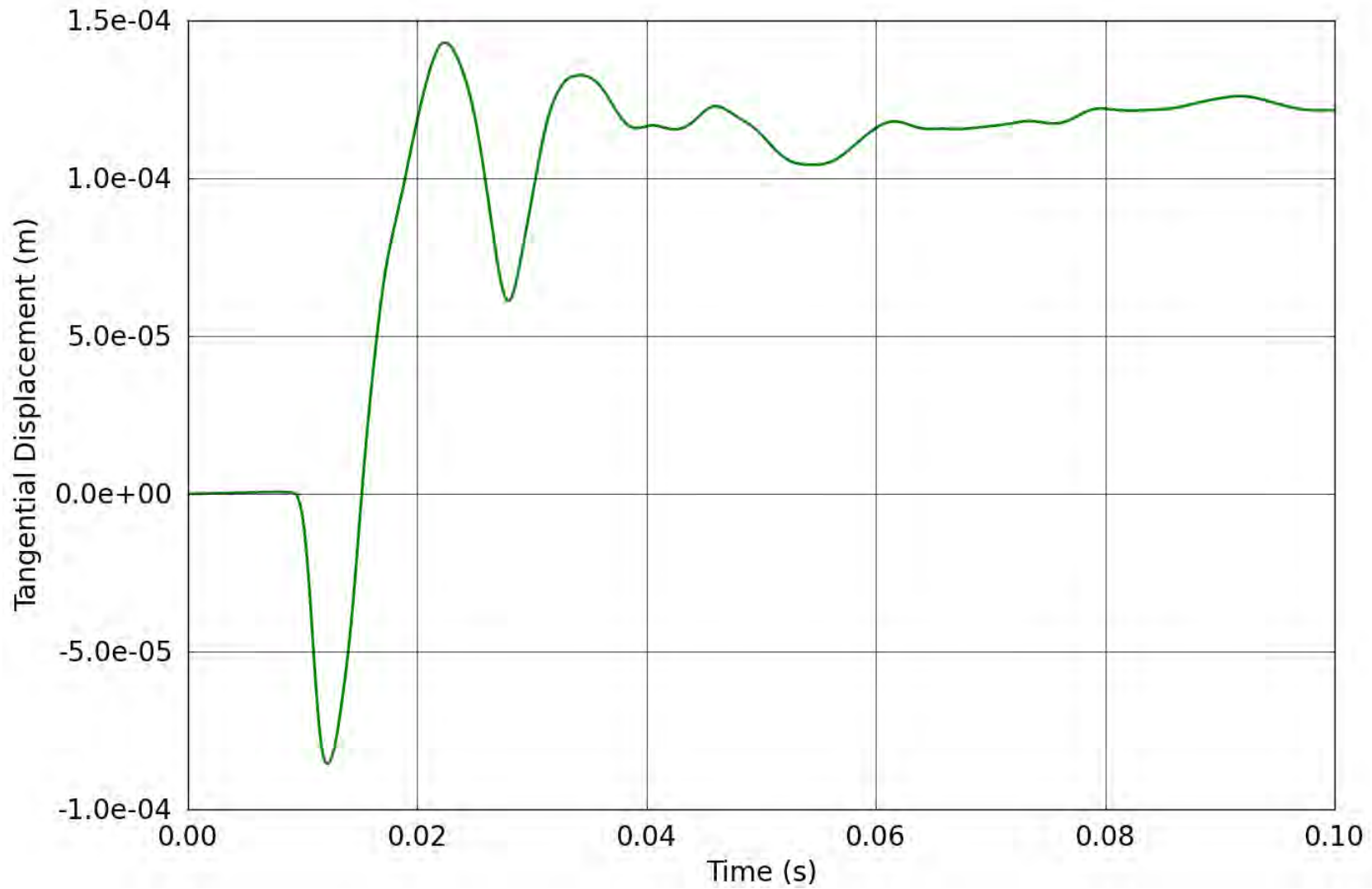


Figure 66. SPE-1 Gauge 2-3-T – Tangential displacement obtained from the corrected tangential velocity.

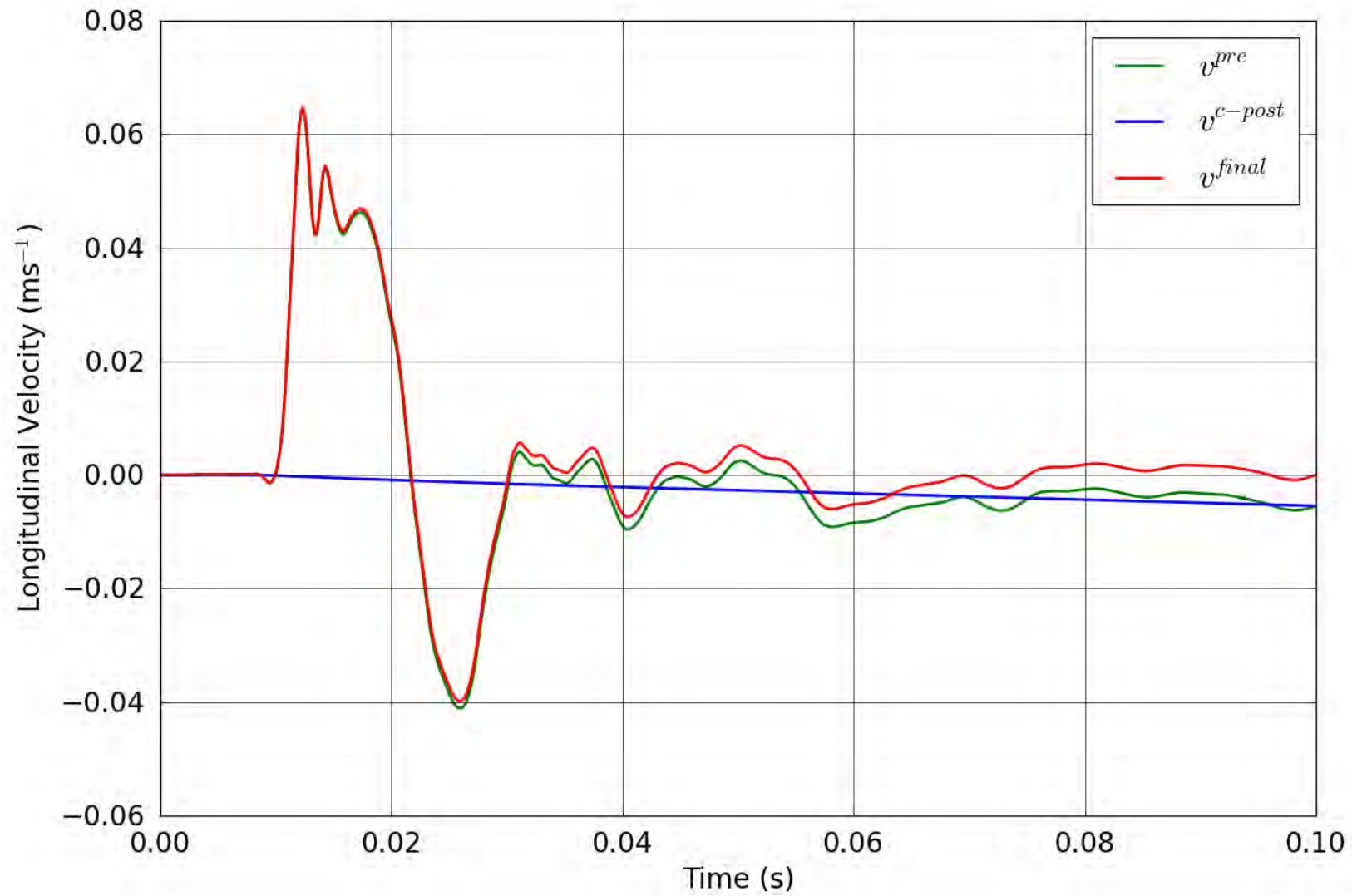


Figure 67. SPE-1 Gauge 2-3-L – Correction of the longitudinal velocity.

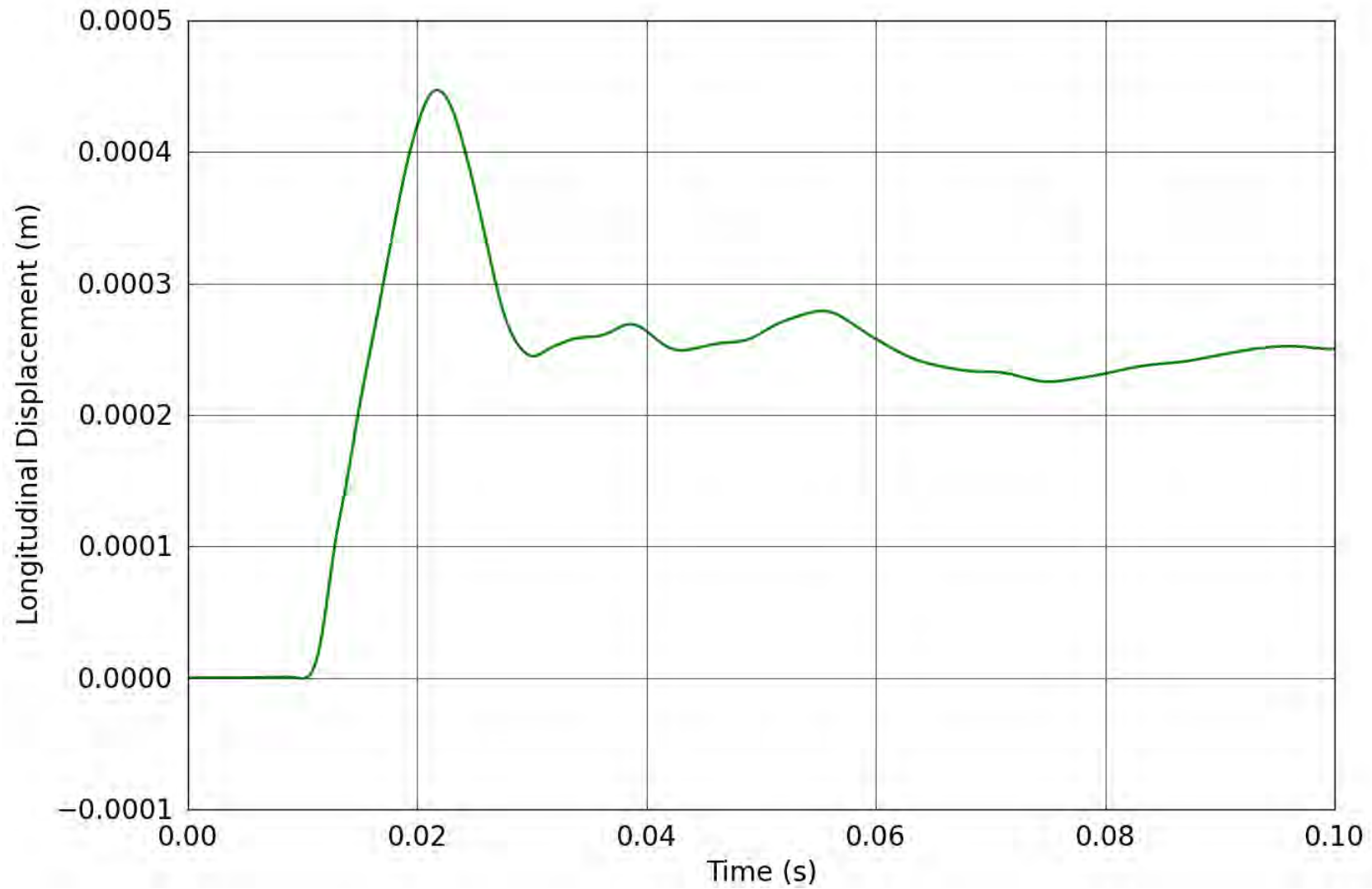


Figure 68. SPE-1 Gauge 2-3-L – Longitudinal displacement obtained from the corrected longitudinal velocity.

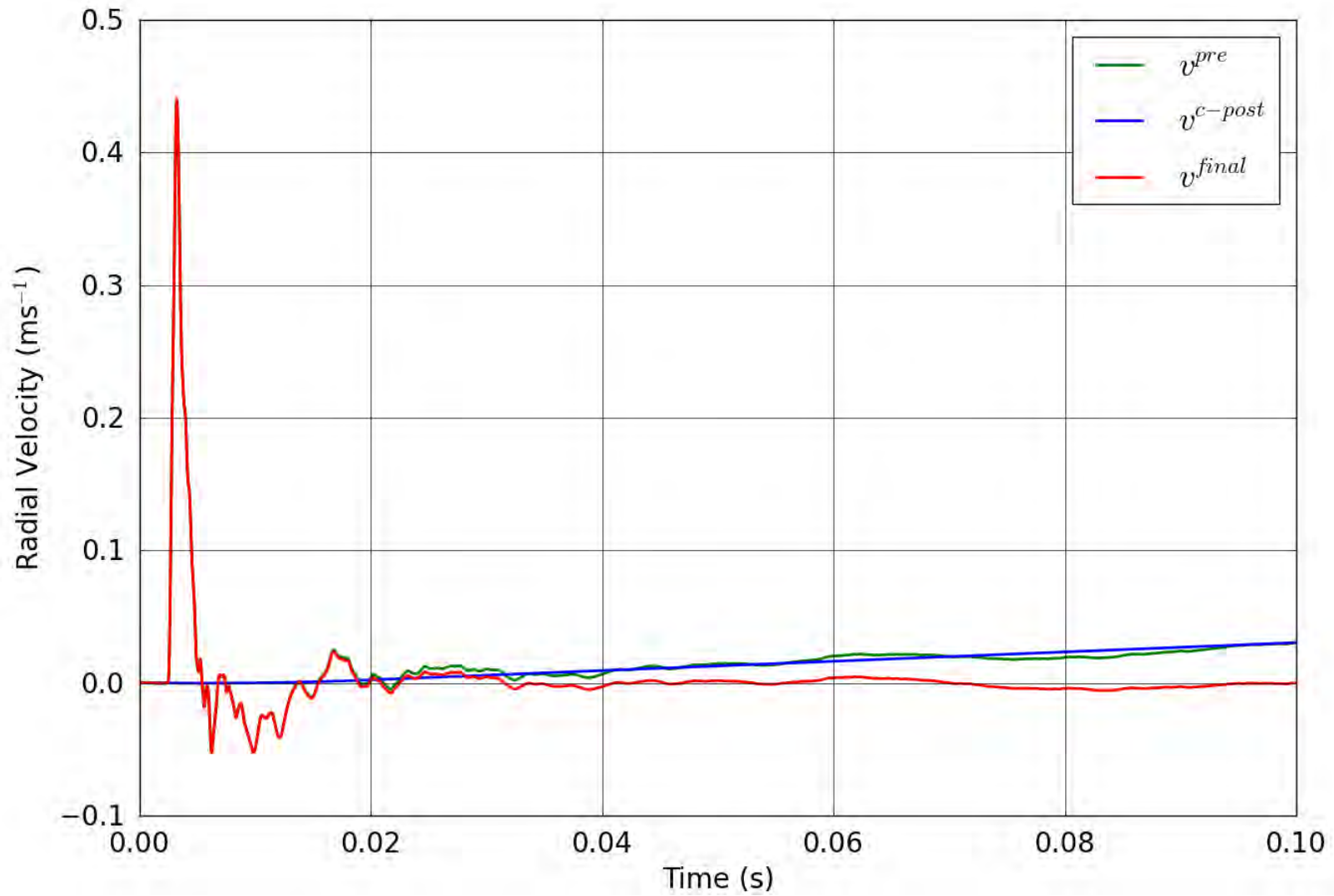


Figure 69. SPE-1 Gauge 3-2-R – Correction of the radial velocity.

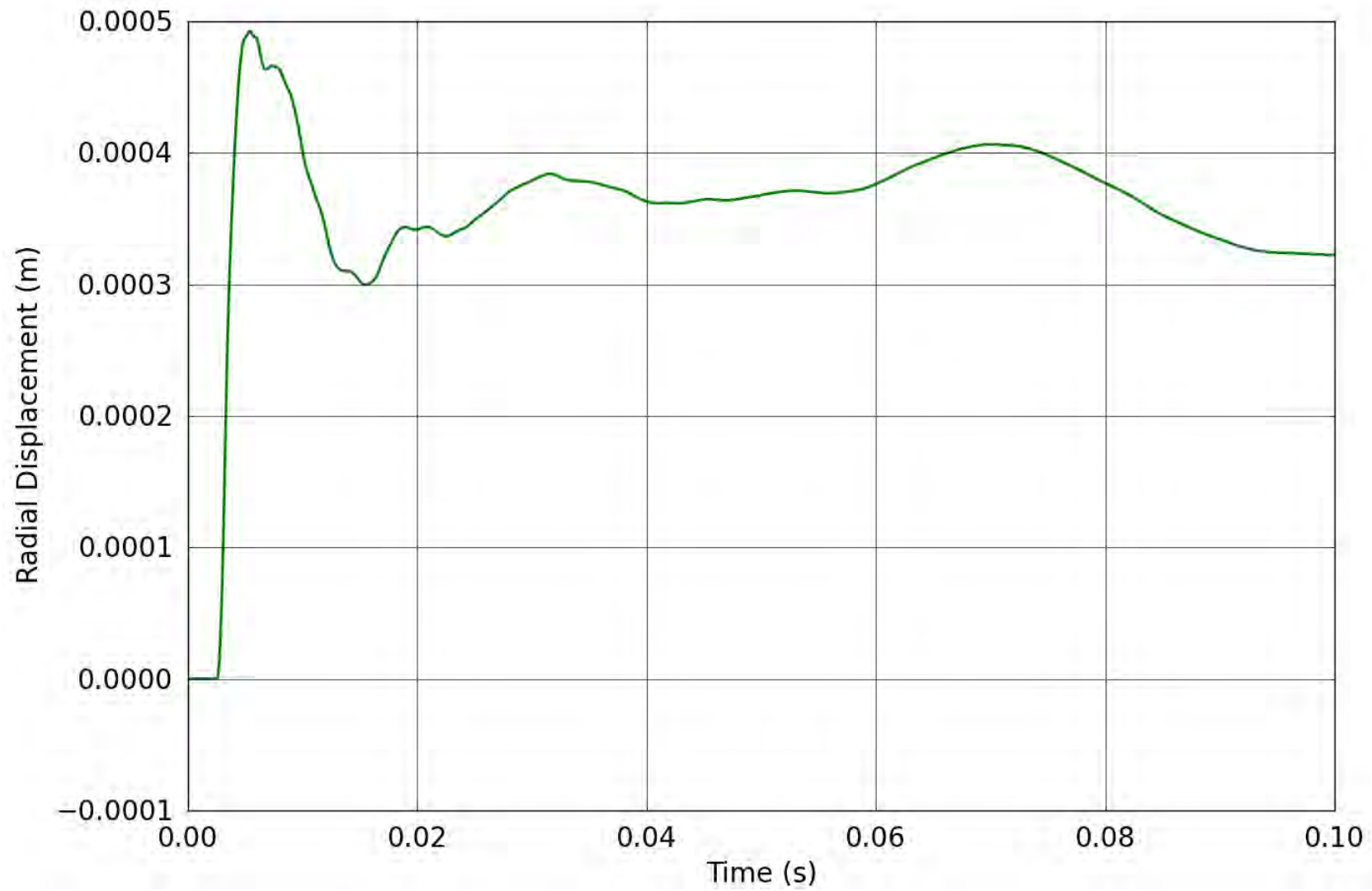


Figure 70. SPE-1 Gauge 3-2-R – Radial displacement obtained from the corrected radial velocity.

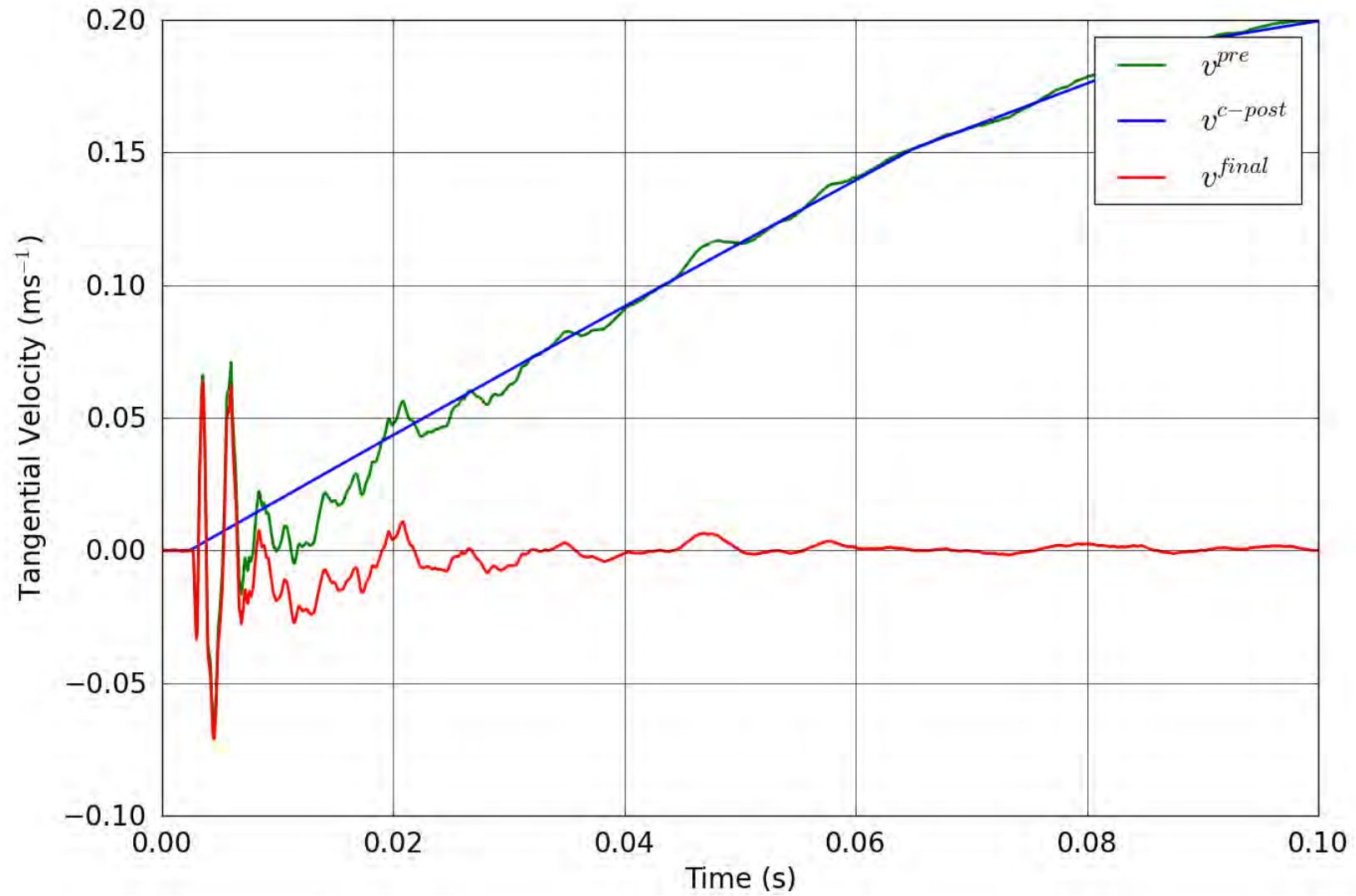


Figure 71. SPE-1 Gauge 3-2-T – Correction of the tangential velocity.

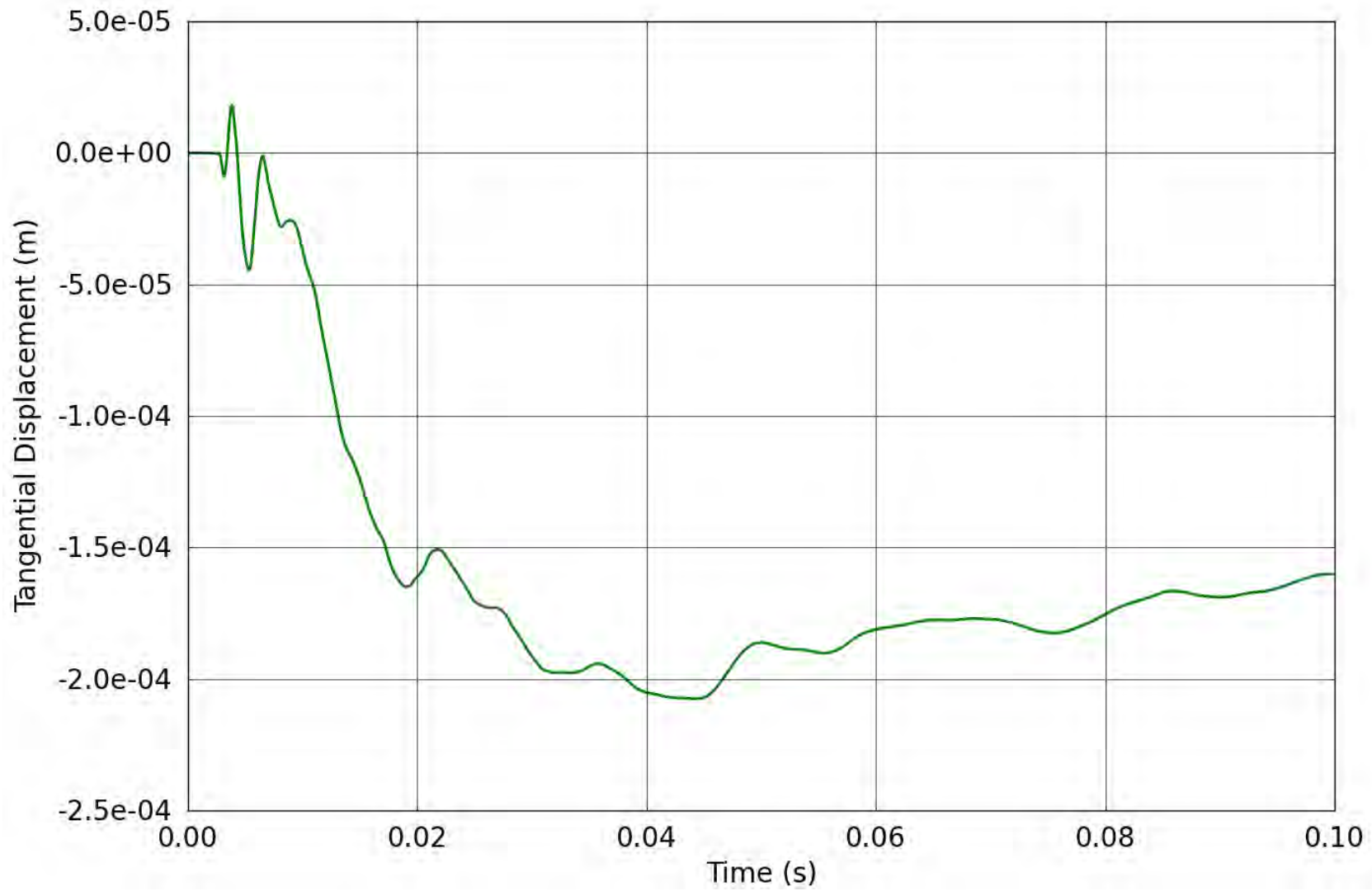


Figure 72. SPE-1 Gauge 3-2-T – Tangential displacement obtained from the corrected tangential velocity.

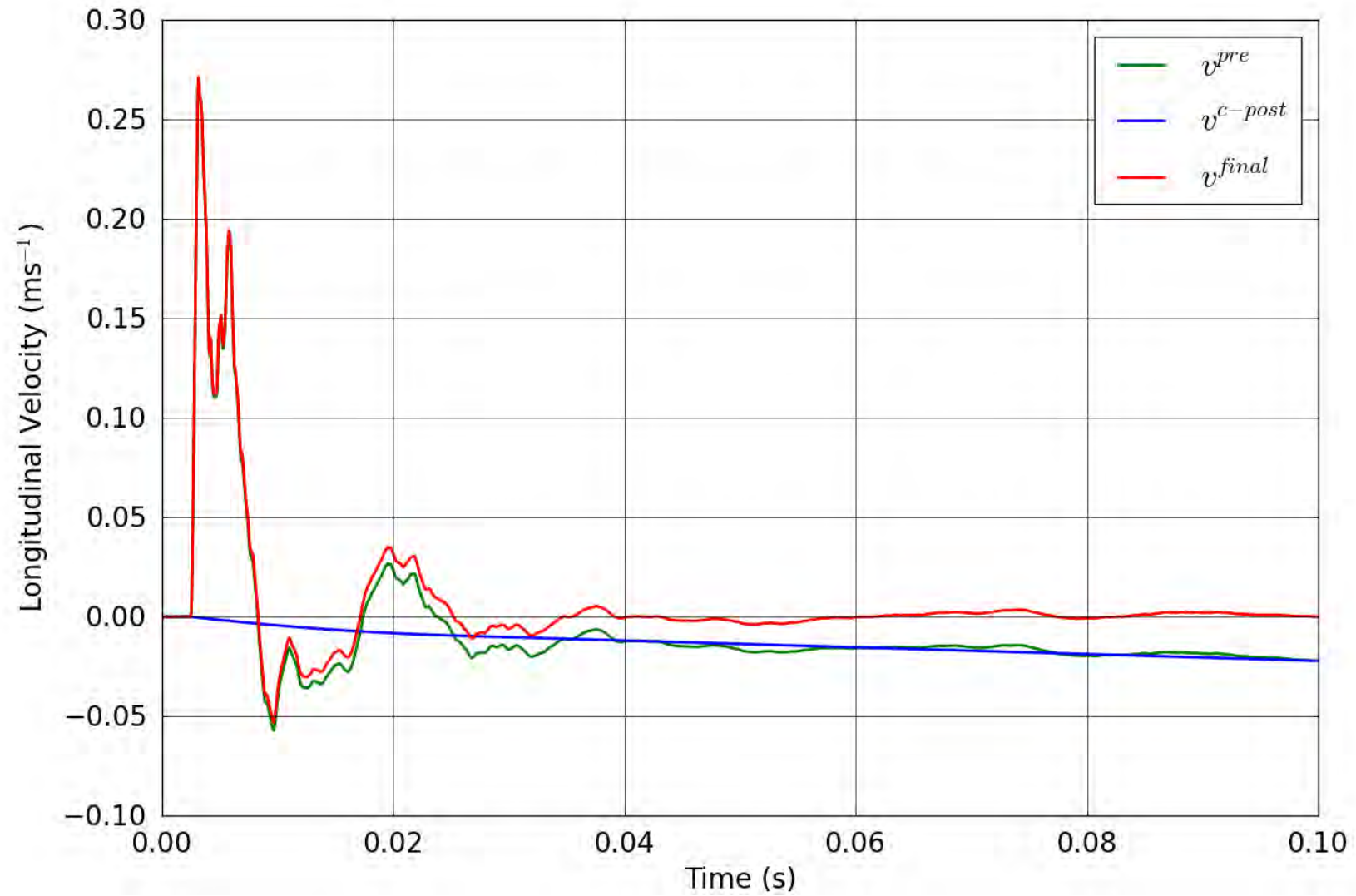


Figure 73. SPE-1 Gauge 3-2-L – Correction of the longitudinal velocity.

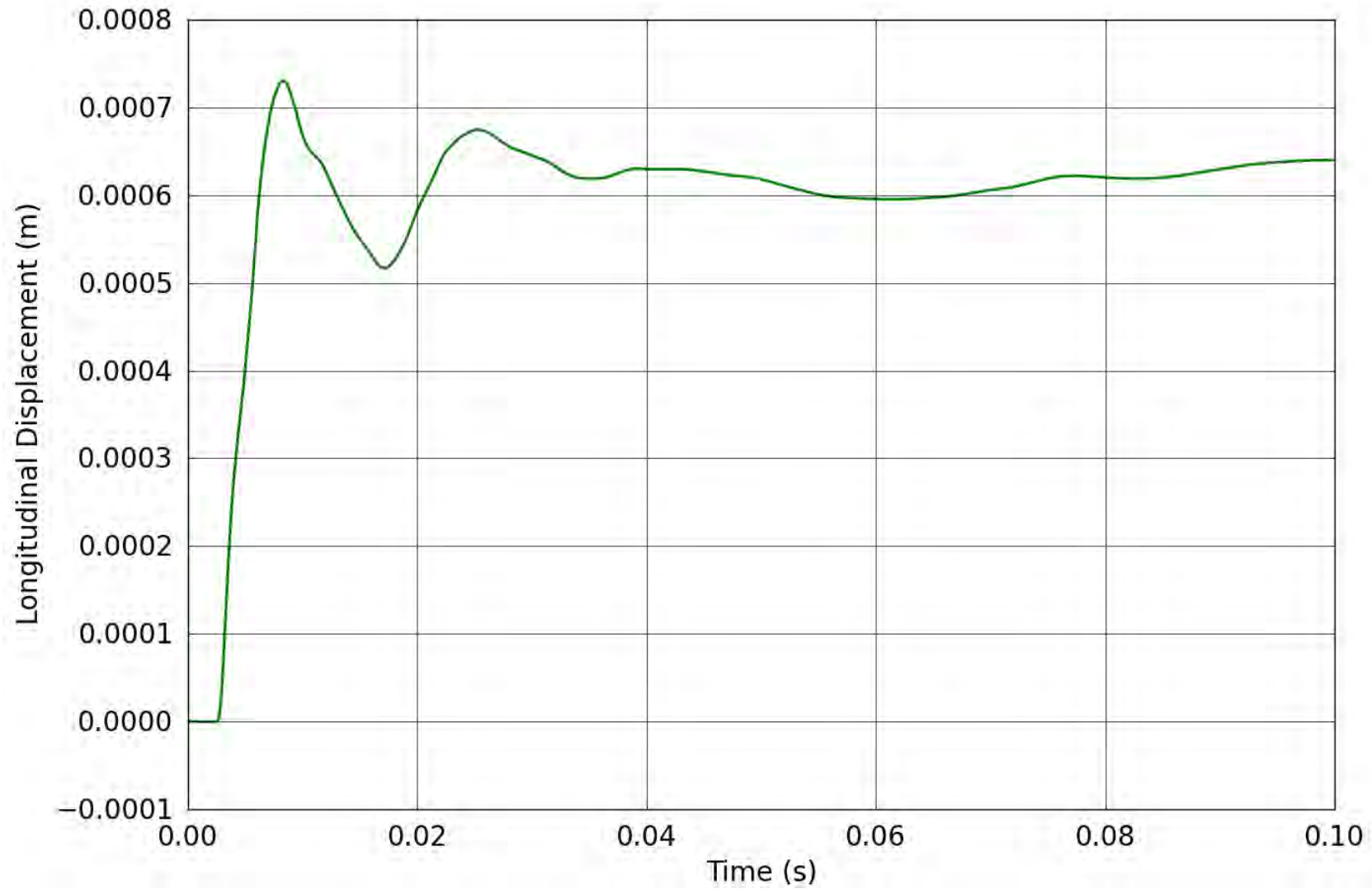


Figure 74. SPE-1 Gauge 3-2-L – Longitudinal displacement obtained from the corrected longitudinal velocity.

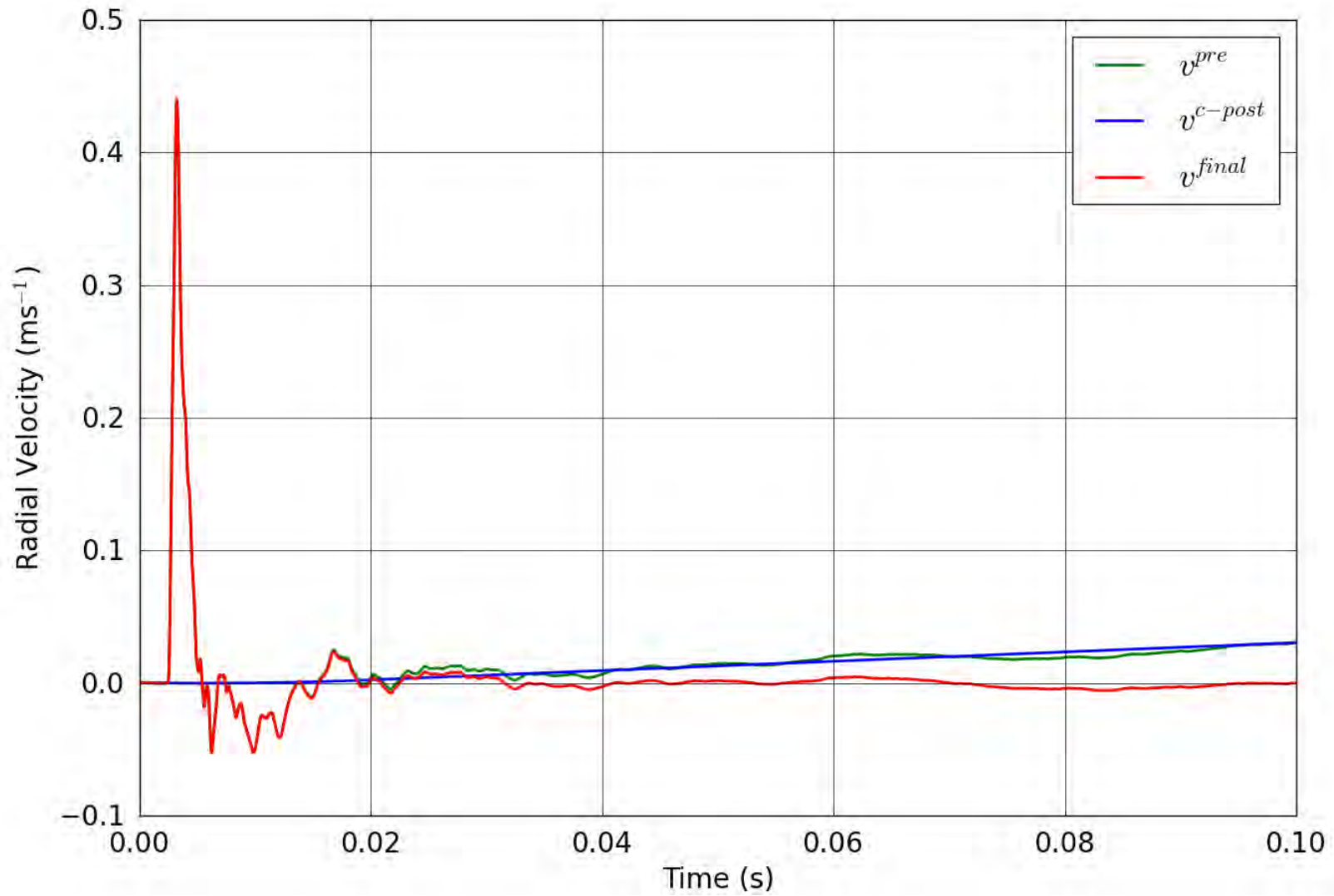


Figure 75. SPE-1 Gauge 3-2-R – Correction of the radial velocity.

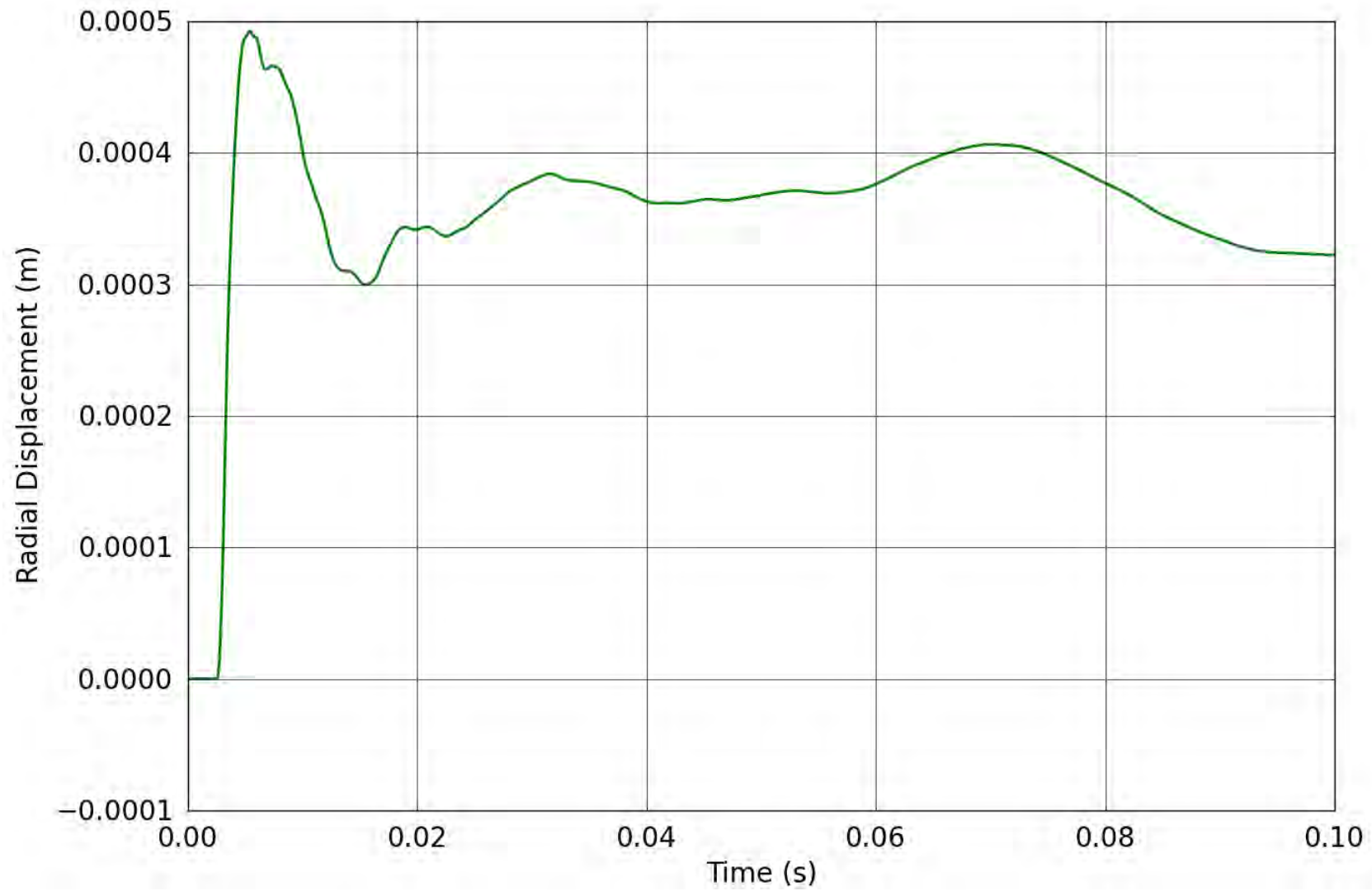


Figure 76. SPE-1 Gauge 3-2-R – Radial displacement obtained from the corrected radial velocity.

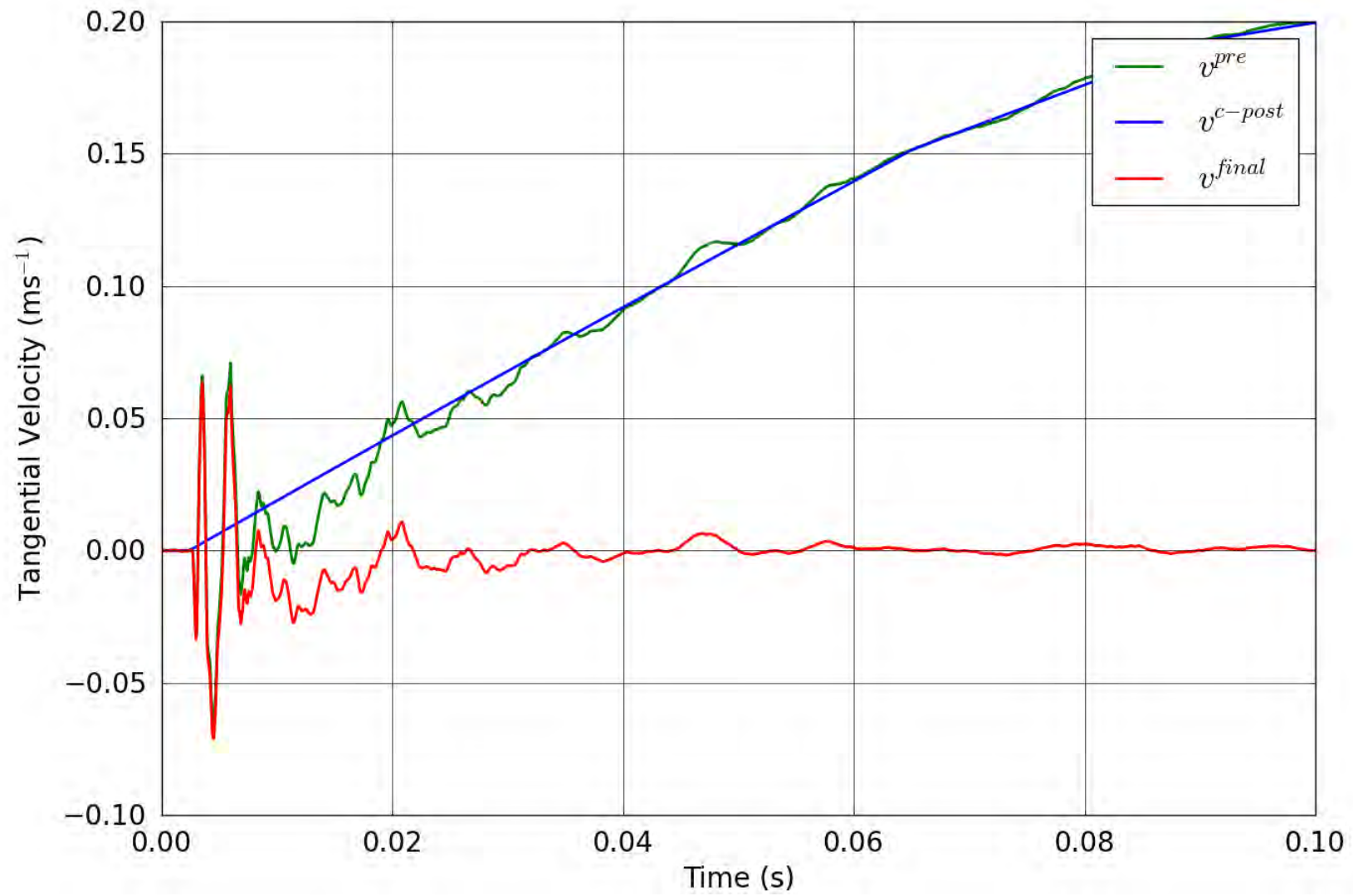


Figure 77. SPE-1 Gauge 3-2-T – Correction of the tangential velocity.

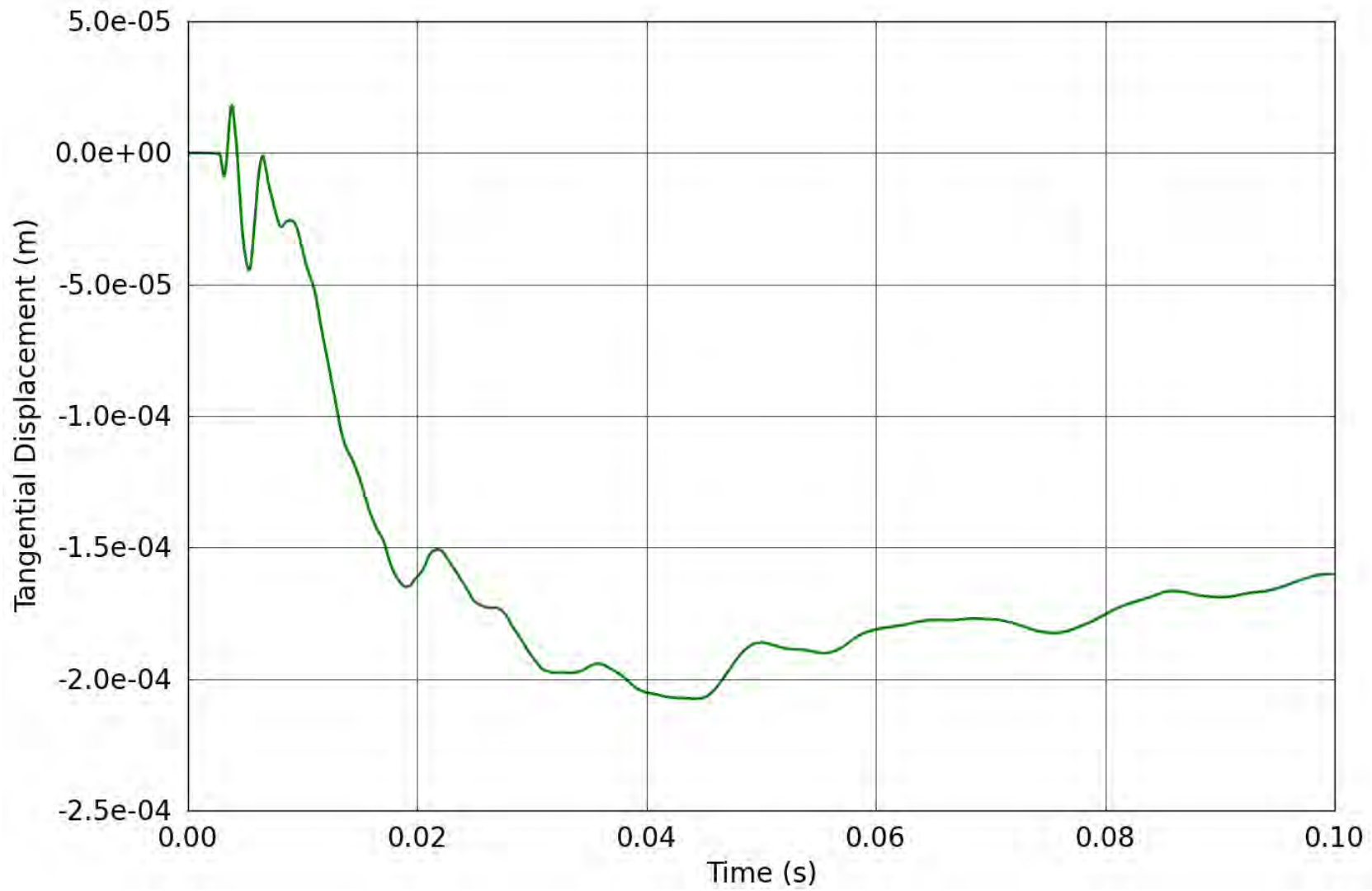


Figure 78. SPE-1 Gauge 3-2-T – Tangential displacement obtained from the corrected tangential velocity.

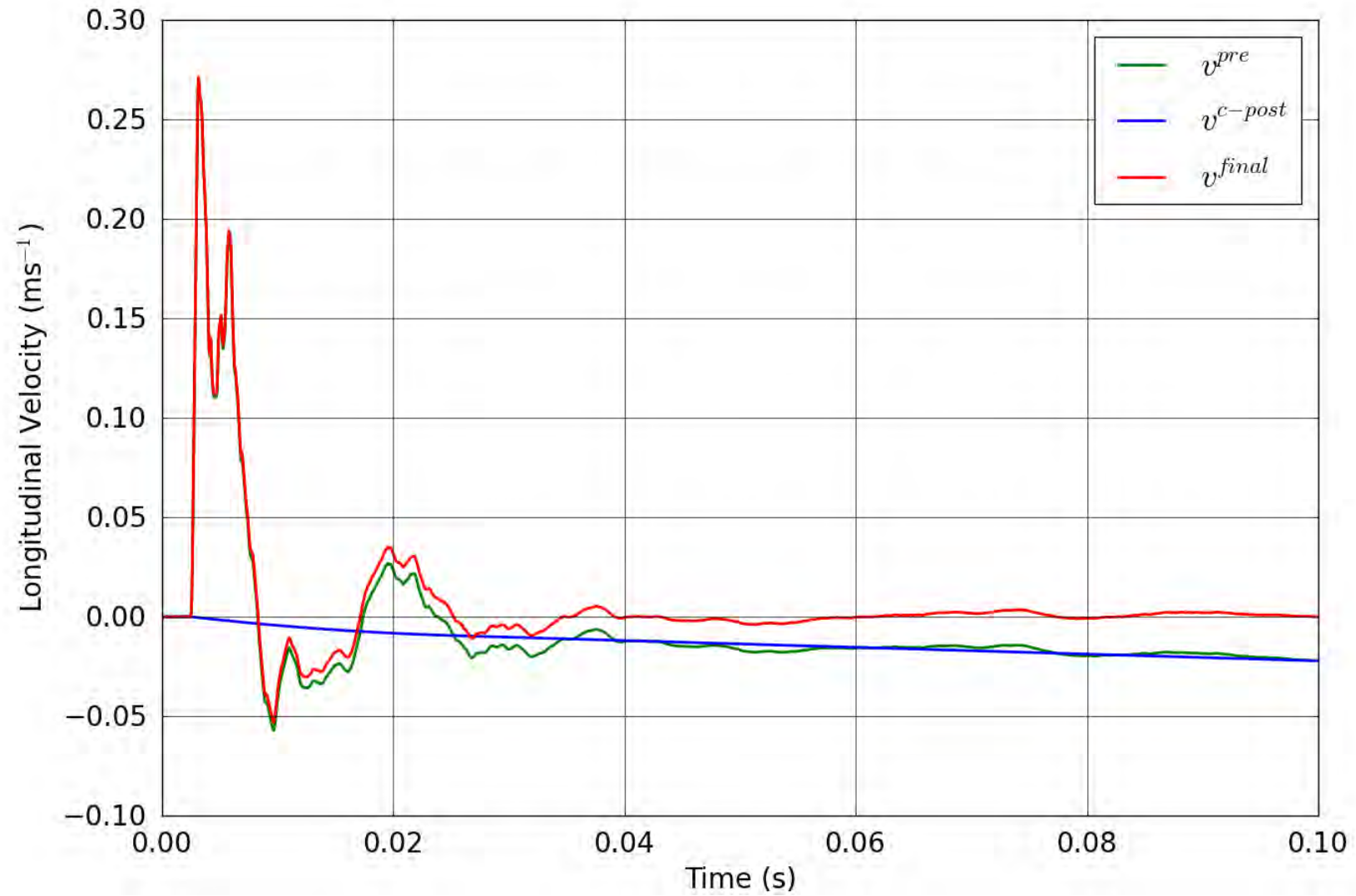


Figure 79. SPE-1 Gauge 3-2-L – Correction of the longitudinal velocity.

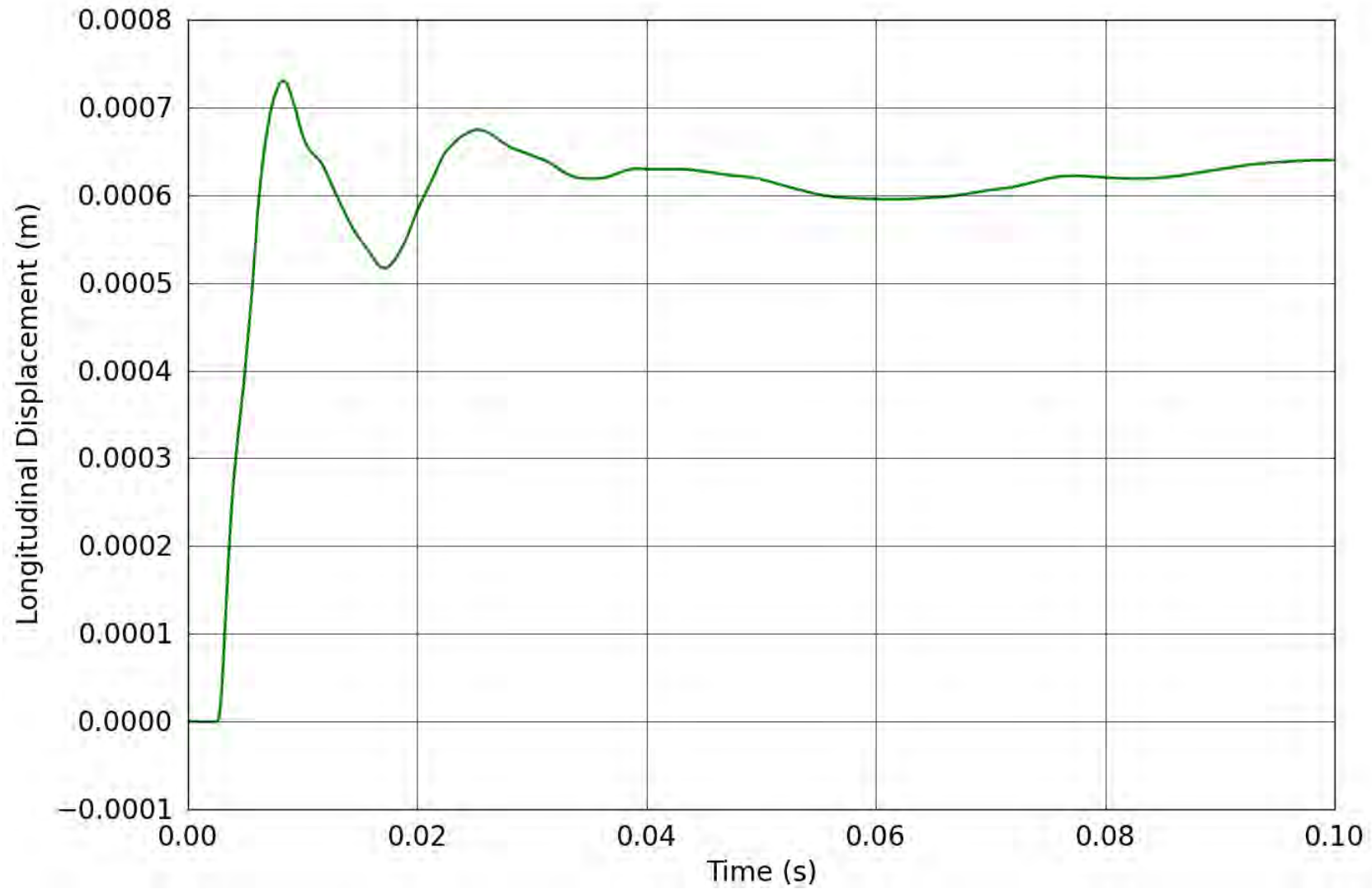


Figure 80. SPE-1 Gauge 3-2-L – Longitudinal displacement obtained from the corrected longitudinal velocity.

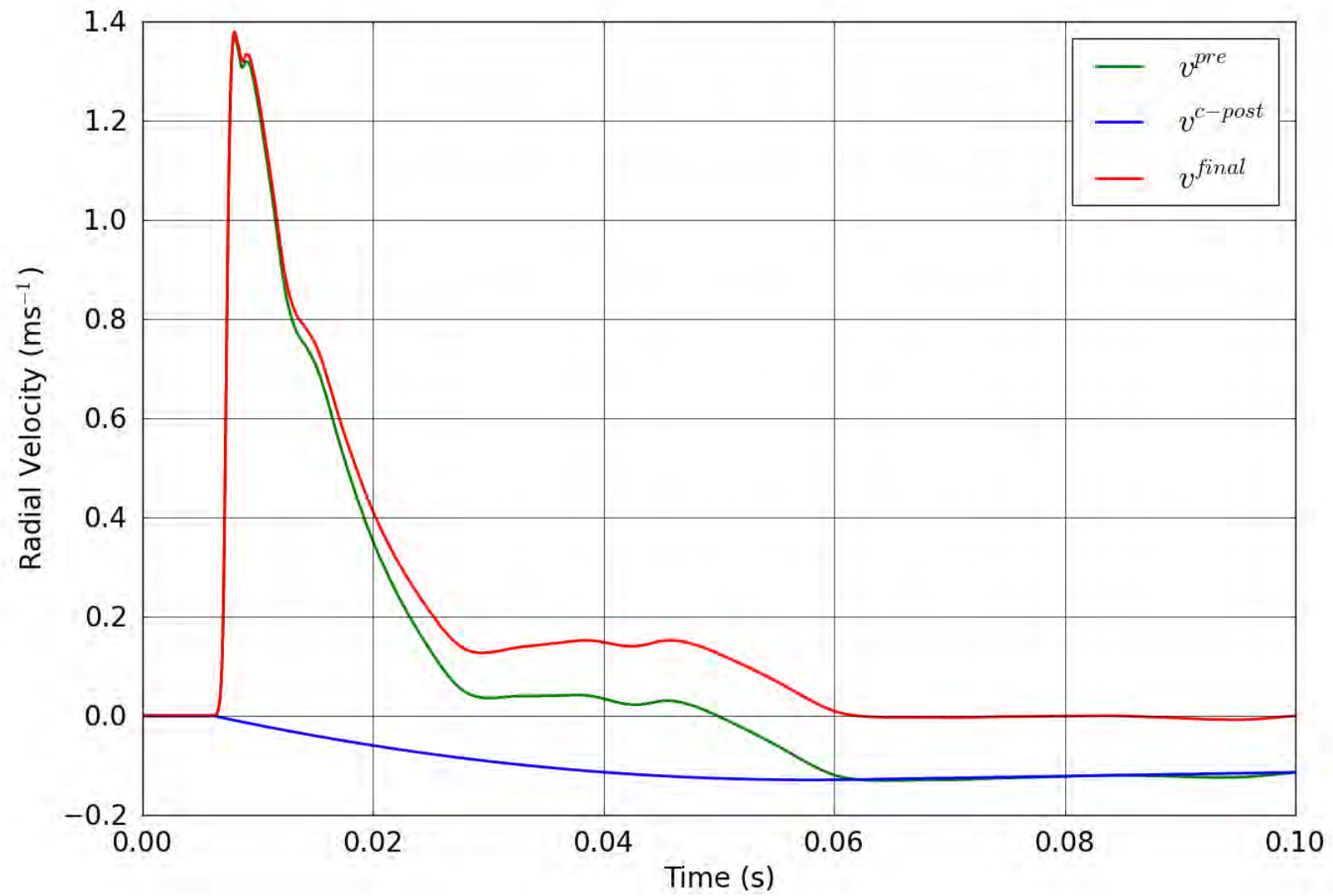


Figure 81. SPE-1 Gauge 3-3-R – Correction of the radial velocity.

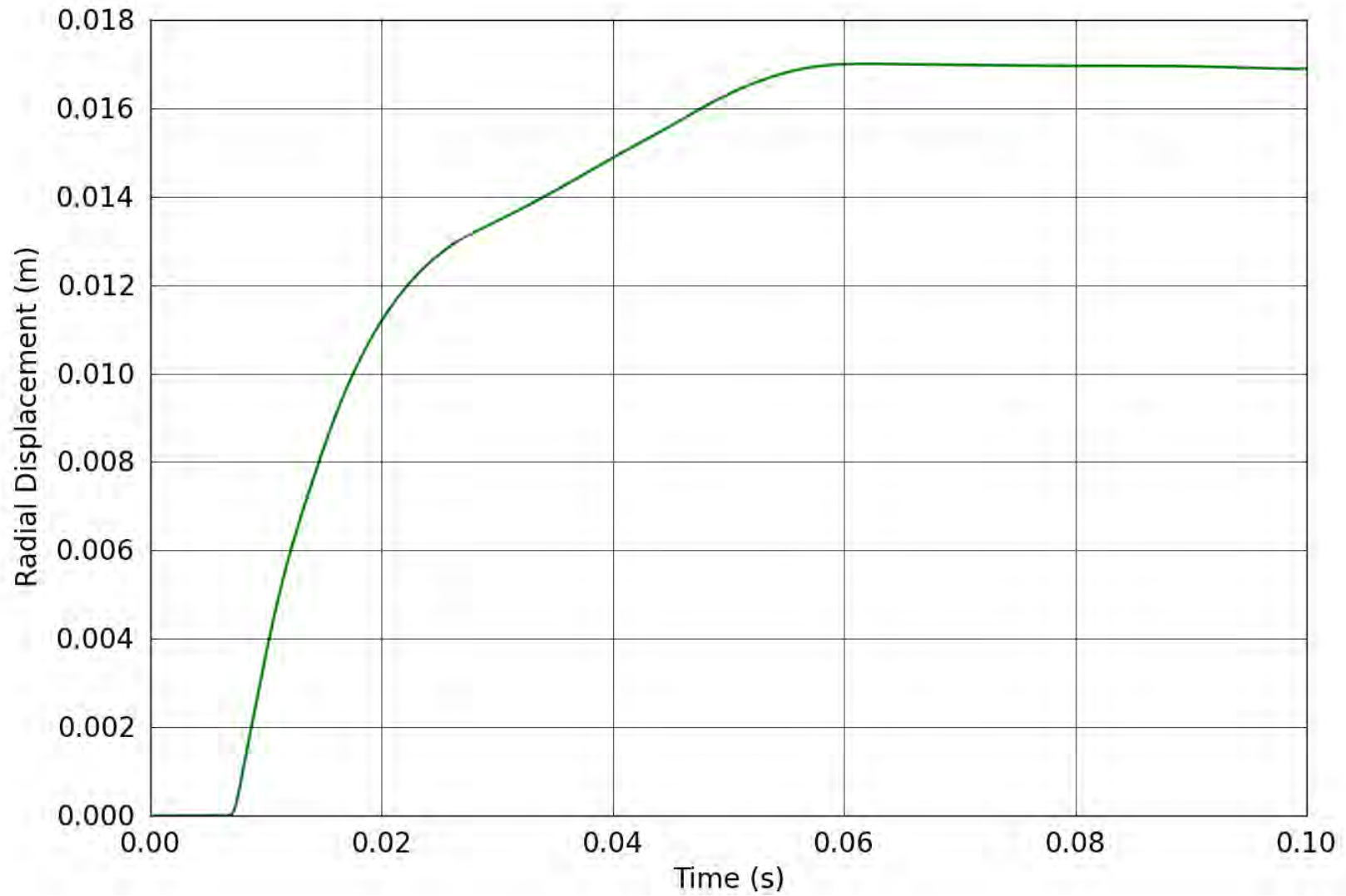


Figure 82. SPE-1 Gauge 3-3-R – Radial displacement obtained from the corrected radial velocity.

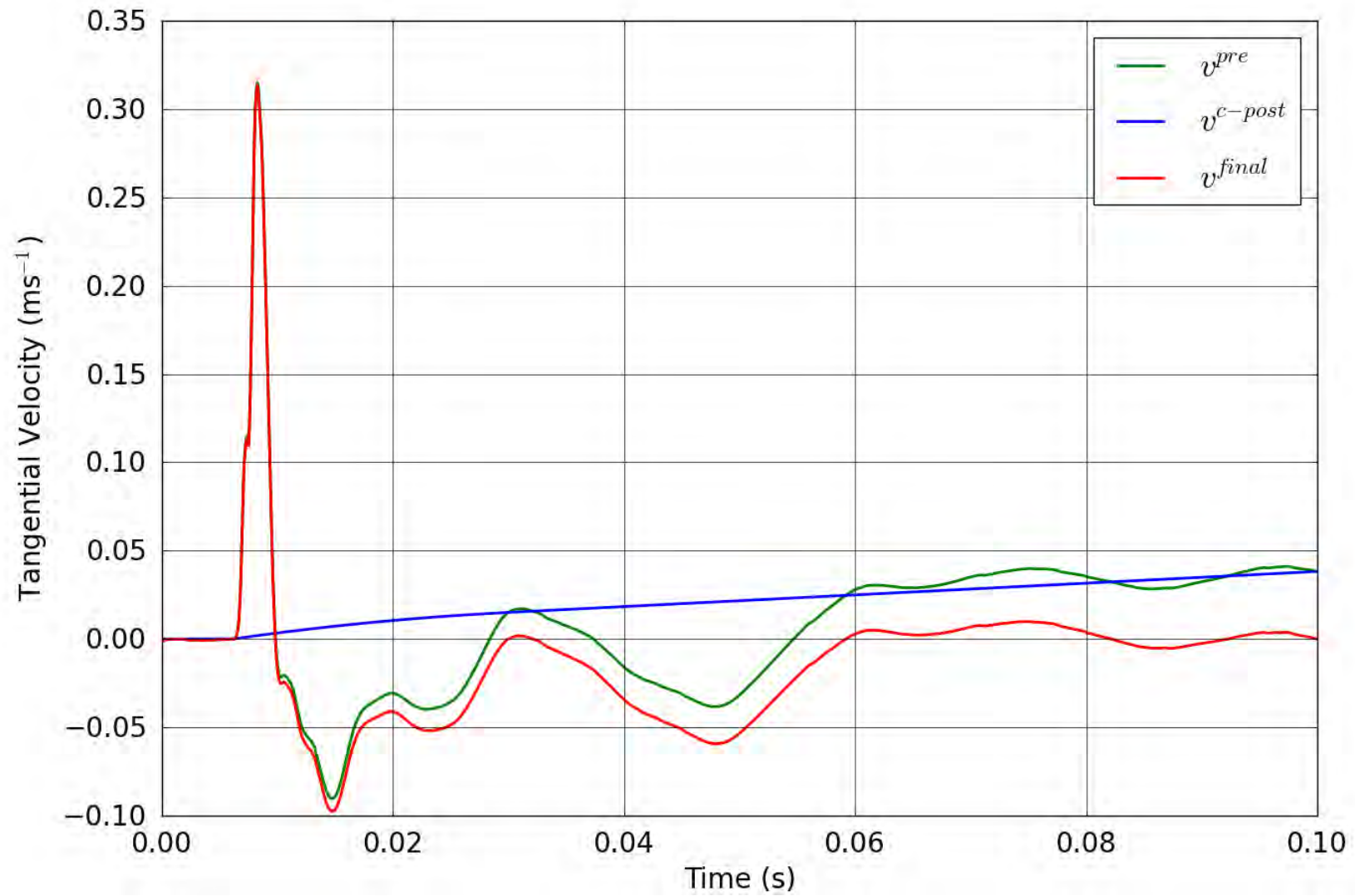


Figure 83. SPE-1 Gauge 3-3-T – Correction of the tangential velocity.

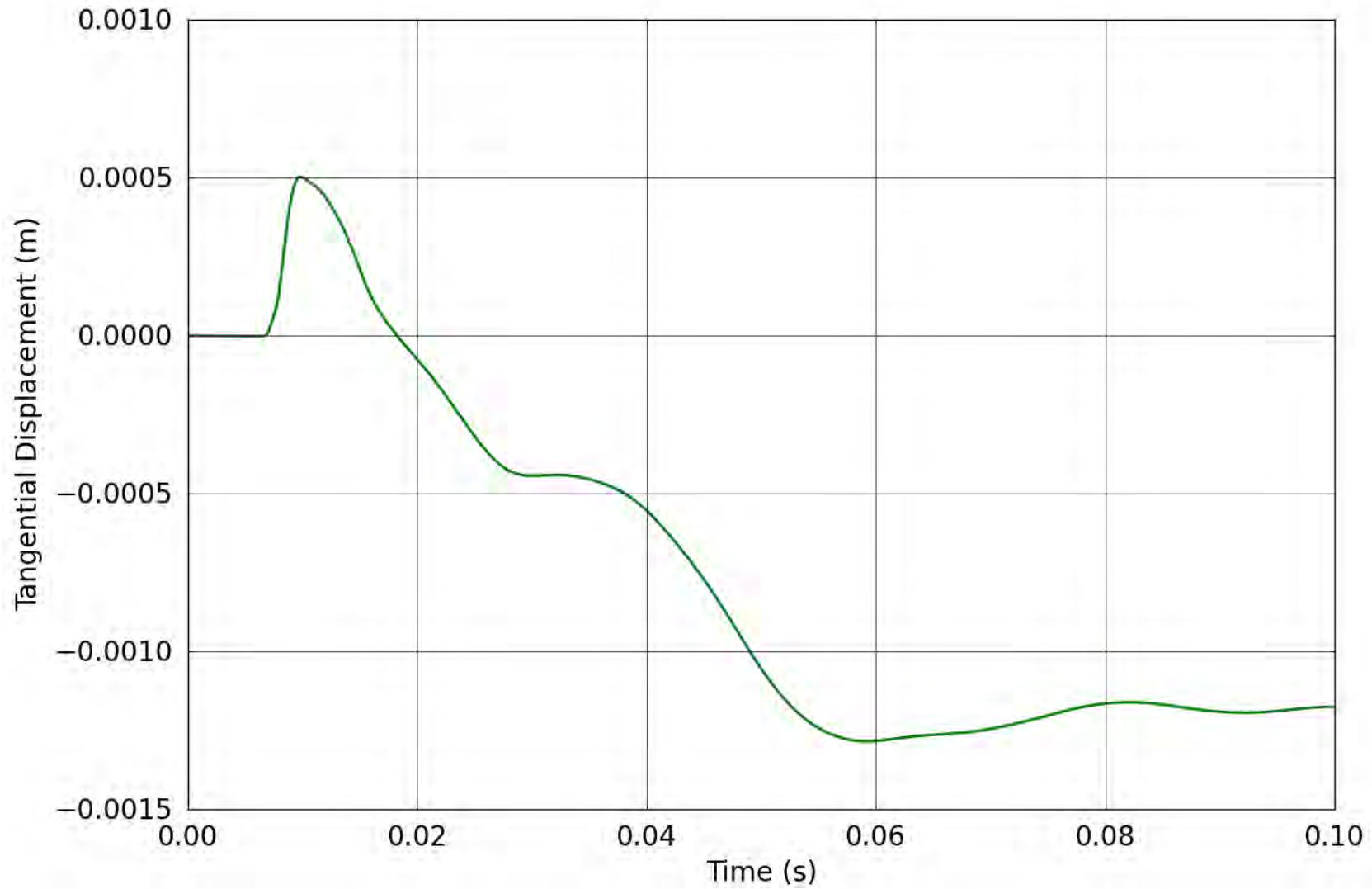


Figure 84. SPE-1 Gauge 3-3-T – Tangential displacement obtained from the corrected tangential velocity.

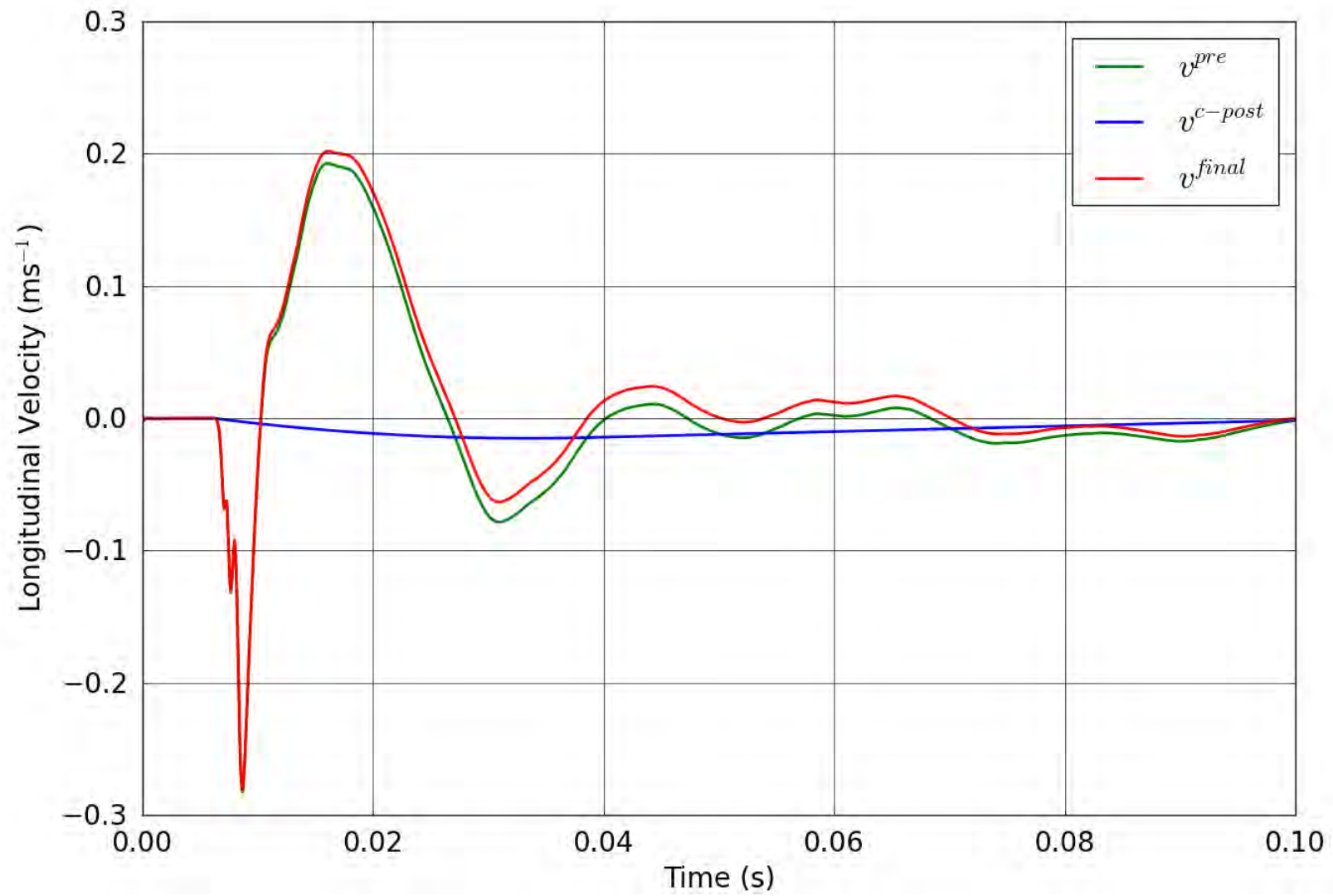


Figure 85. SPE-1 Gauge 3-3-L – Correction of the longitudinal velocity.

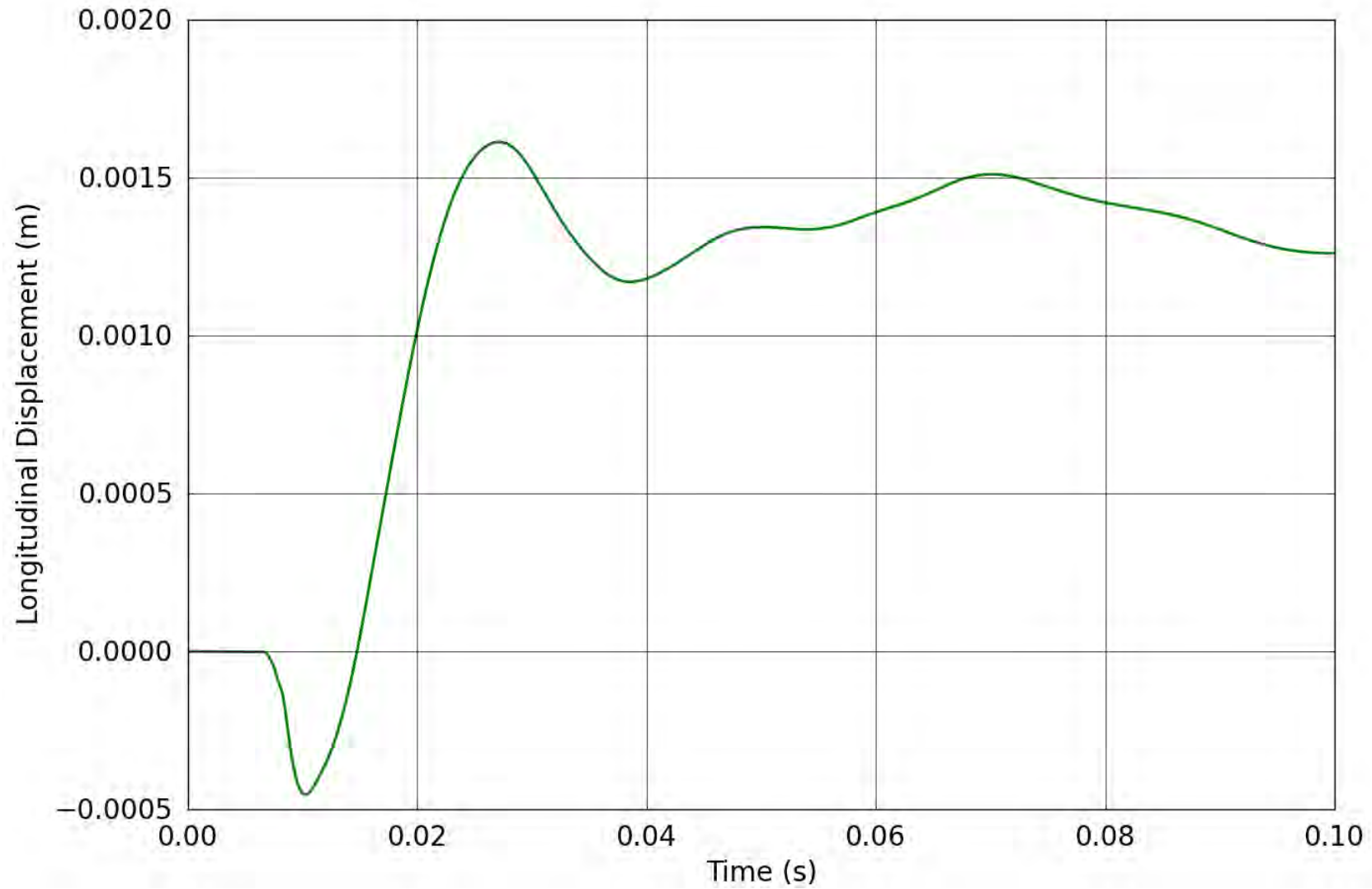


Figure 86. SPE-1 Gauge 3-3-L – Longitudinal displacement obtained from the corrected longitudinal velocity.

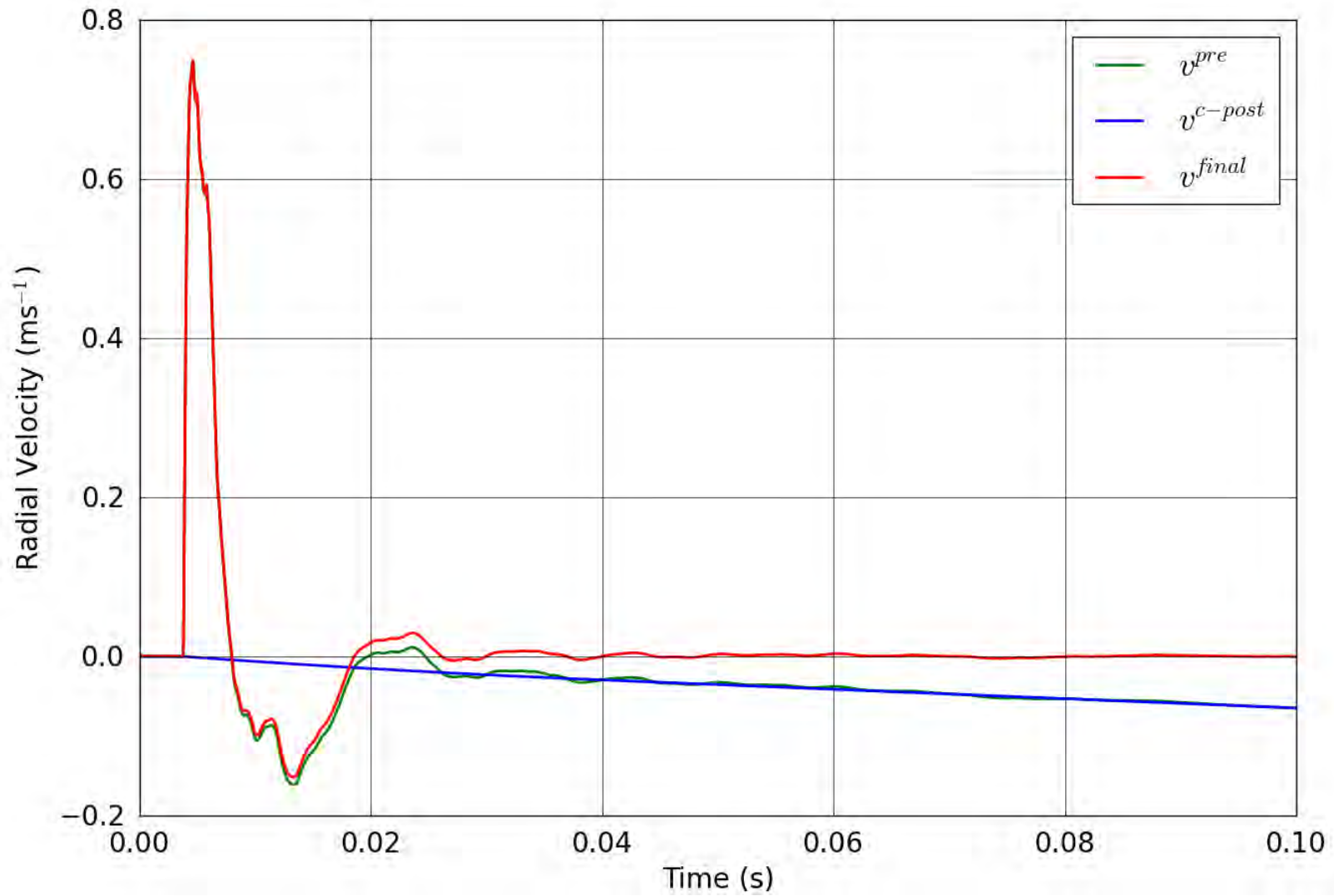


Figure 87. SPE-1 Gauge 4-1-R – Correction of the radial velocity.

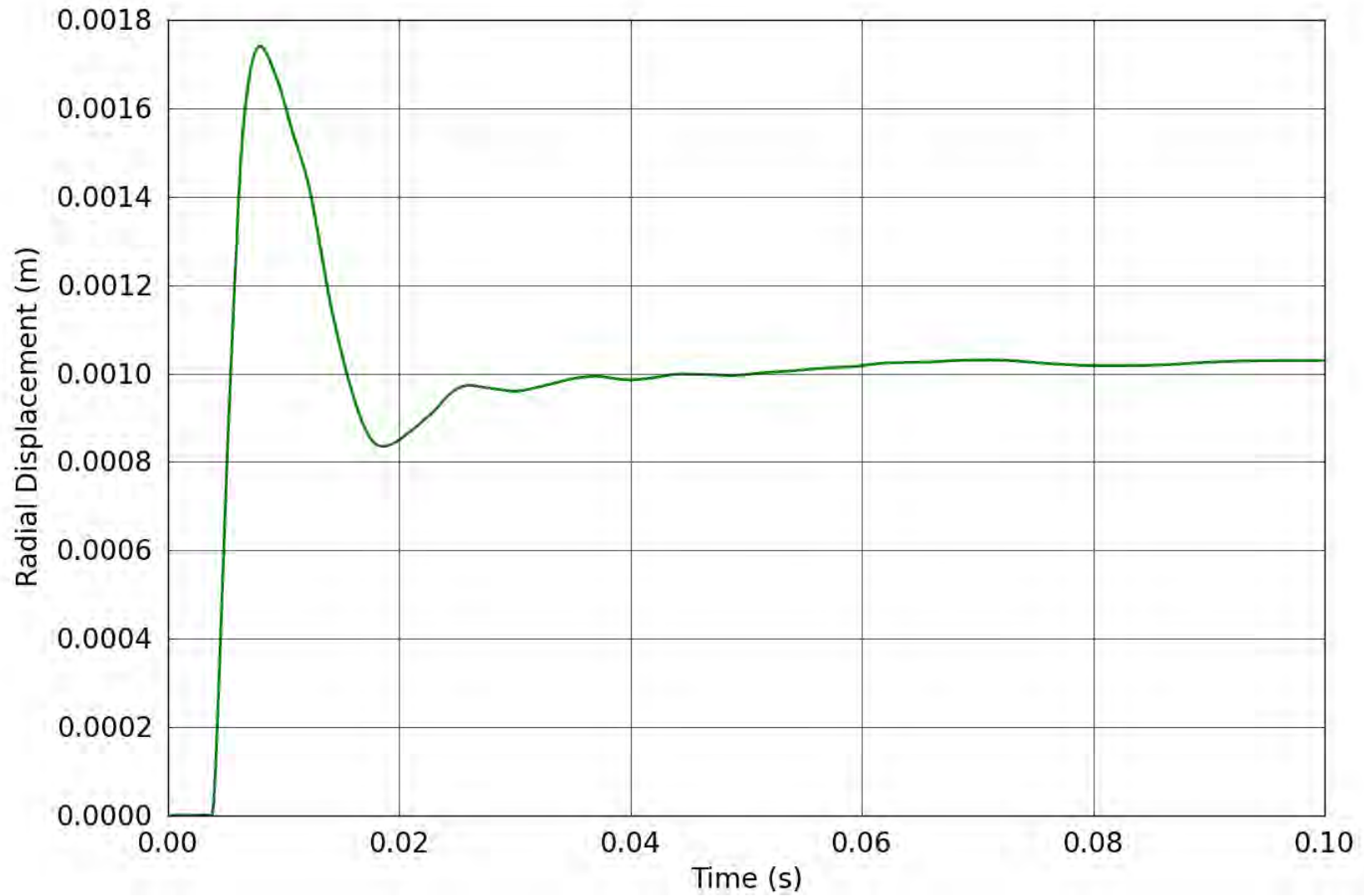


Figure 88. SPE-1 Gauge 4-1-R – Radial displacement obtained from the corrected radial velocity.

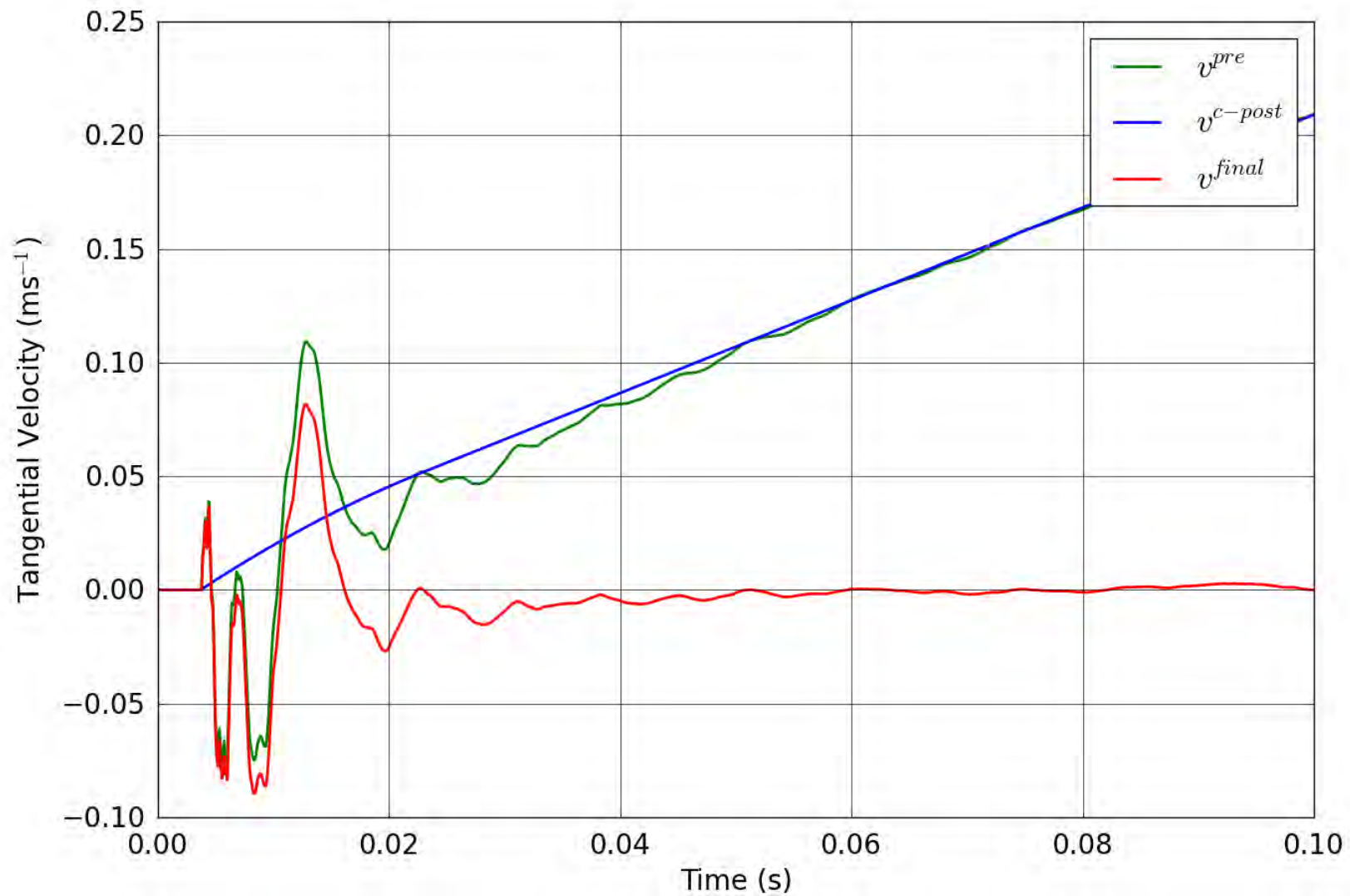


Figure 89. SPE-1 Gauge 4-1-T – Correction of the tangential velocity.

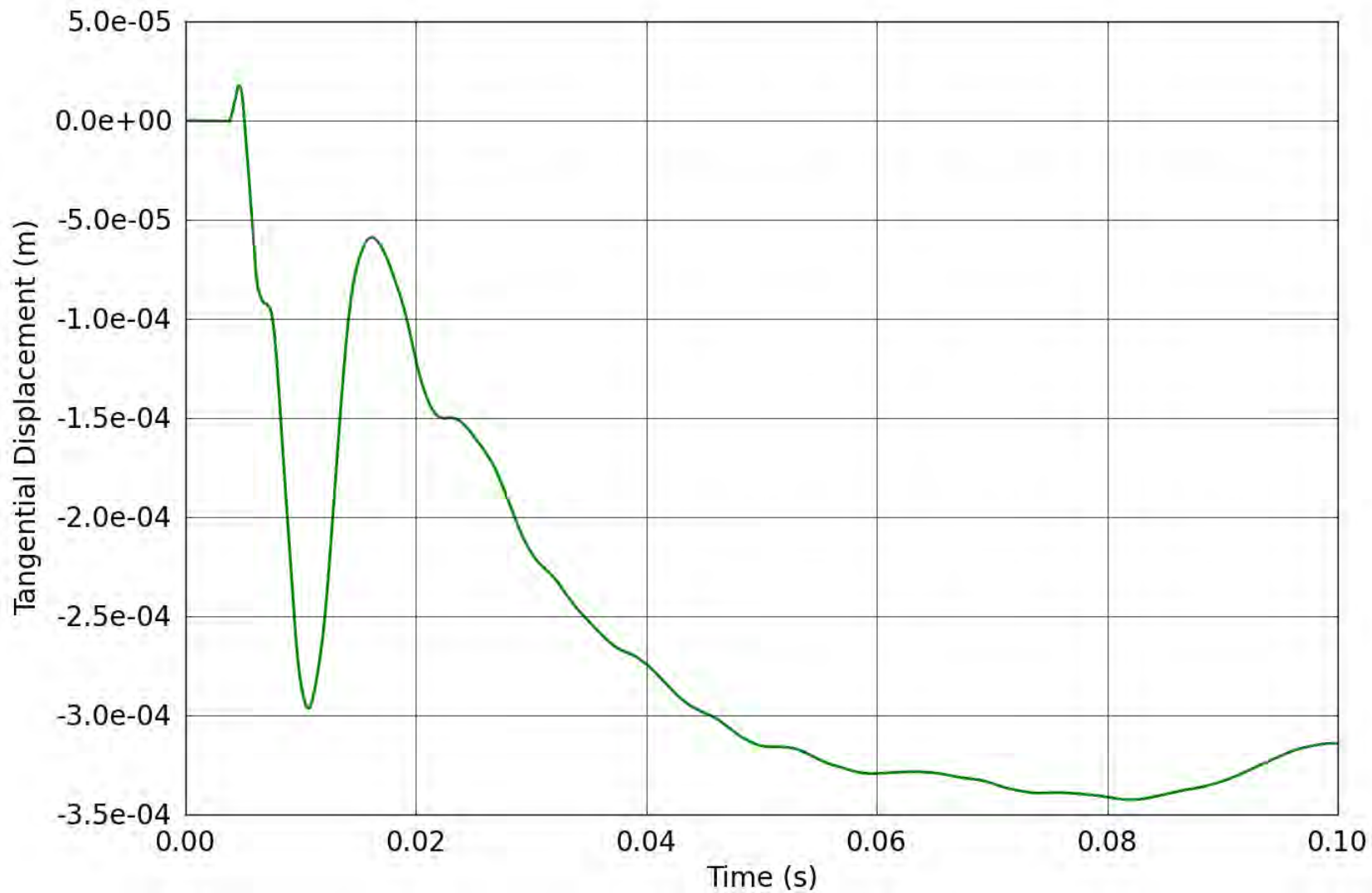


Figure 90. SPE-1 Gauge 4-1-T – Tangential displacement obtained from the corrected tangential velocity.

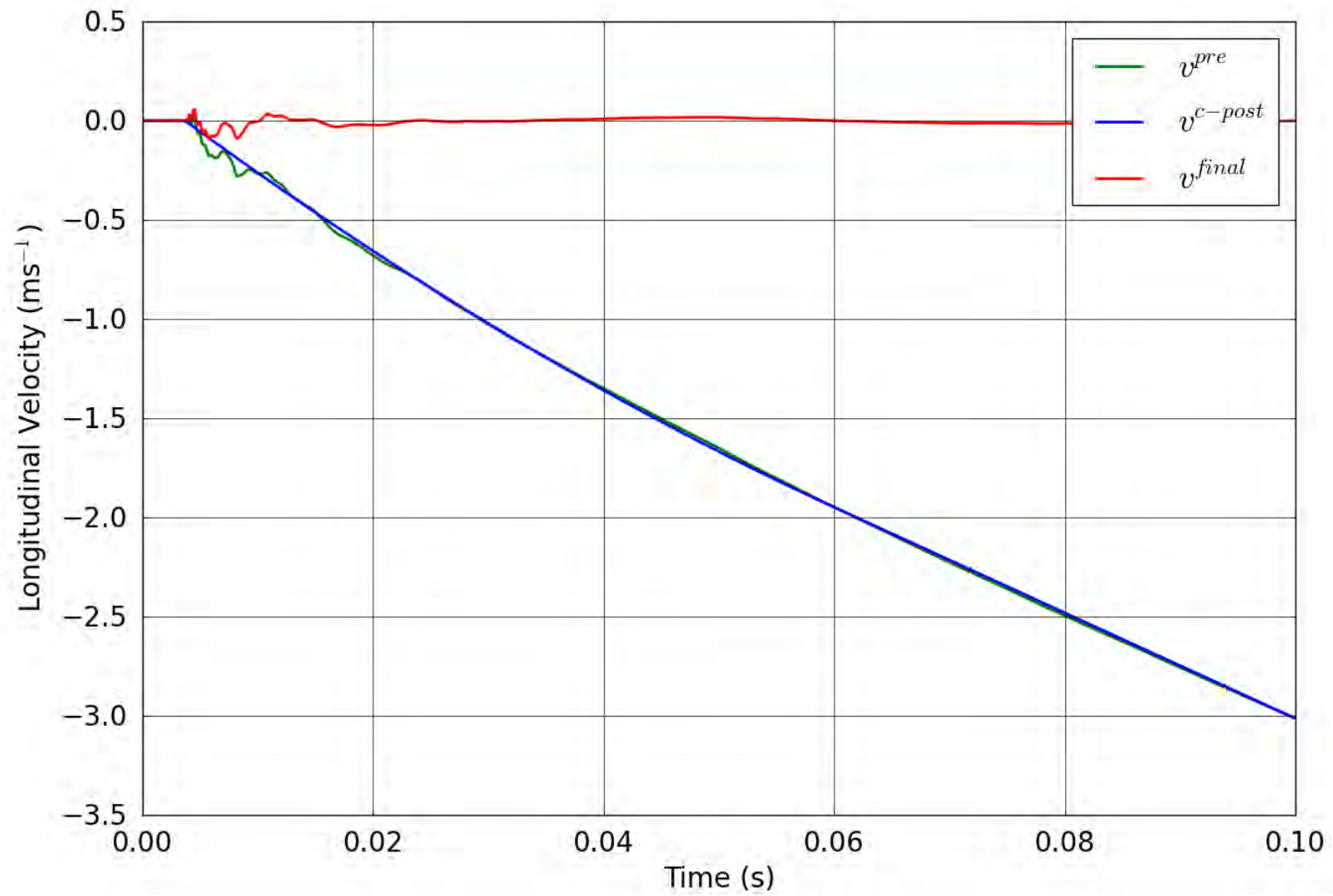


Figure 91. SPE-1 Gauge 4-1-L – Correction of the longitudinal velocity.

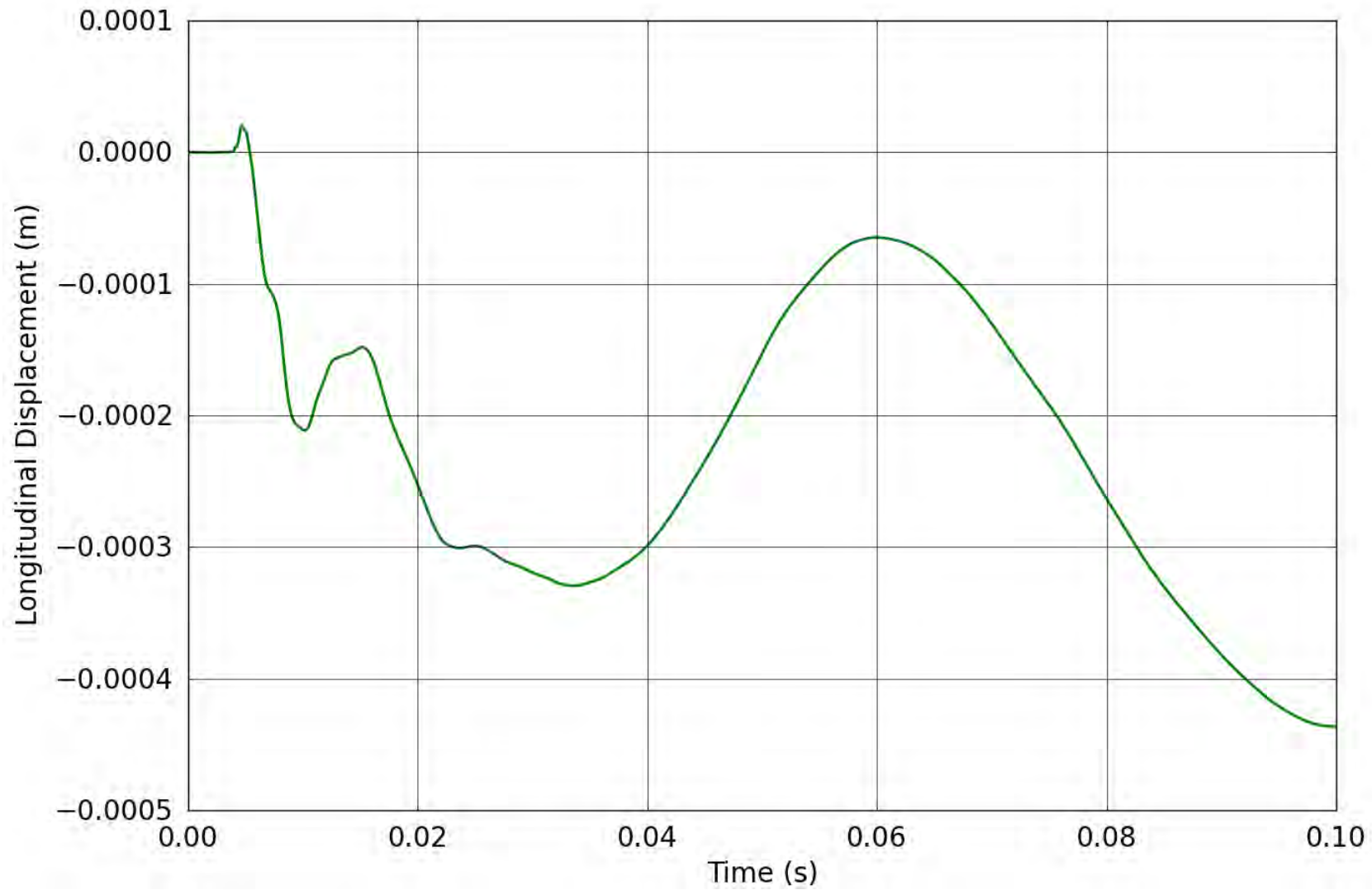


Figure 92. SPE-1 Gauge 4-1-L – Longitudinal displacement obtained from the corrected longitudinal velocity.

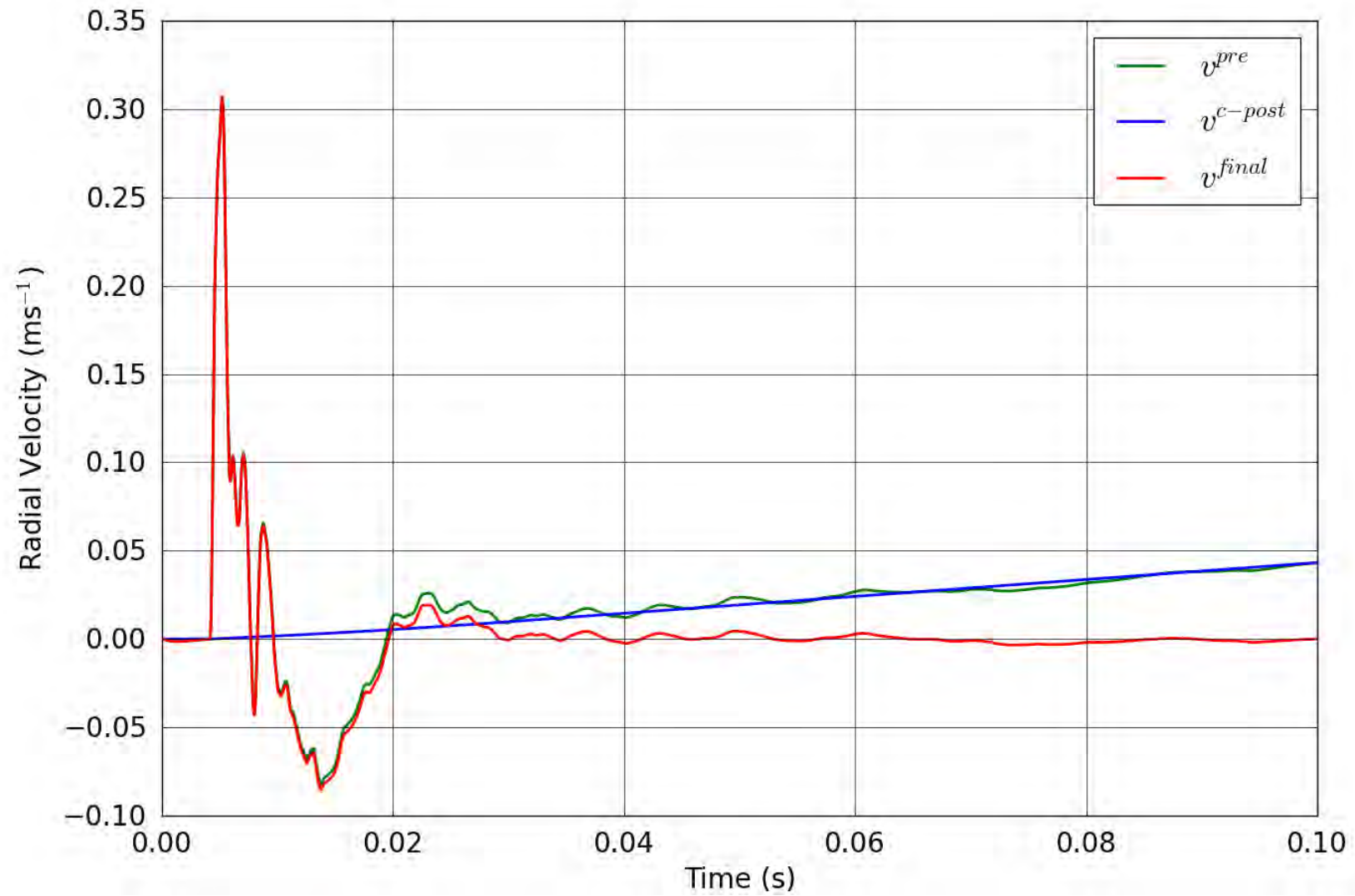


Figure 93. SPE-1 Gauge 4-2-R – Correction of the radial velocity.

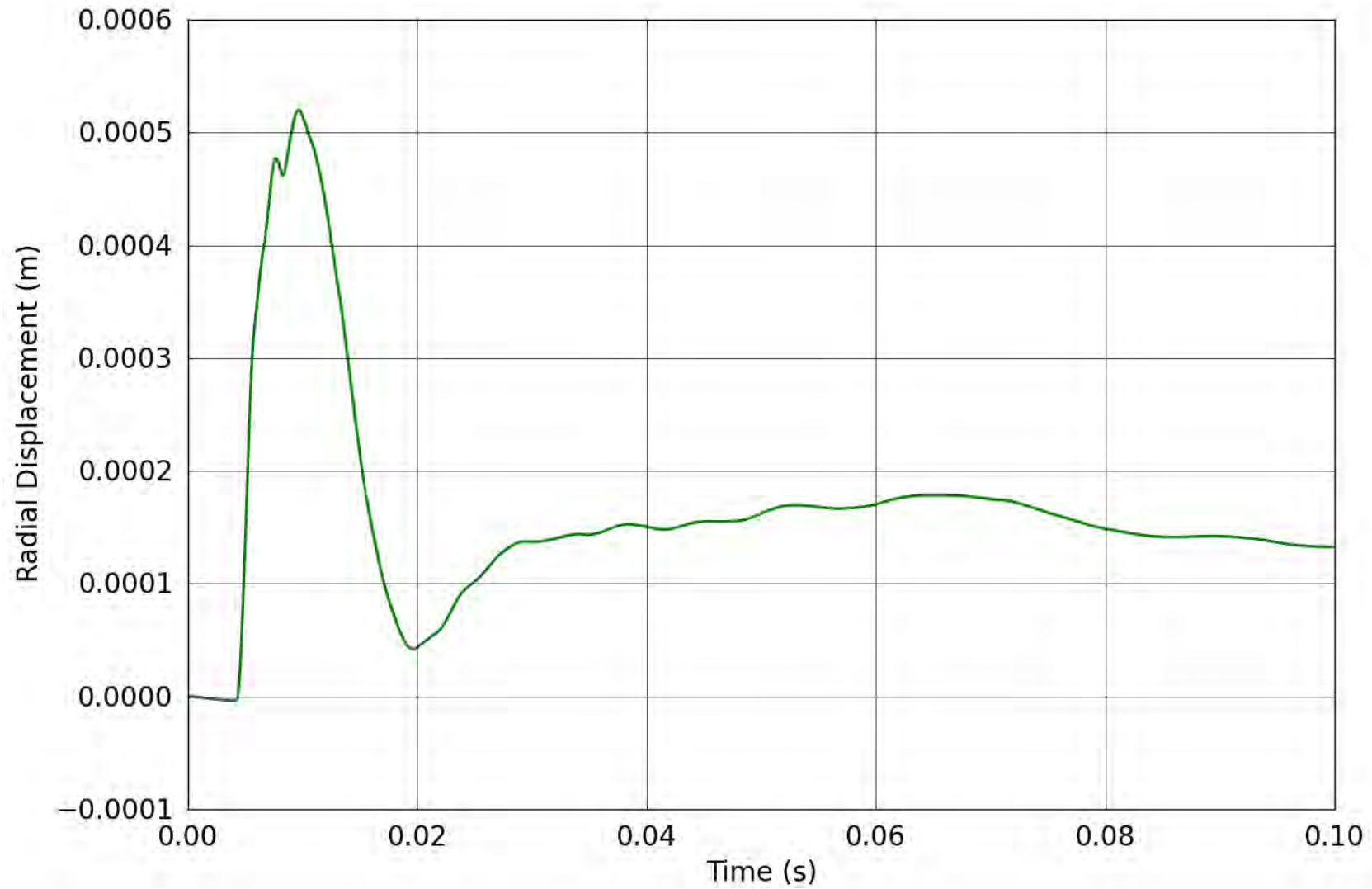


Figure 94. SPE-1 Gauge 4-2-R – Radial displacement obtained from the corrected radial velocity.

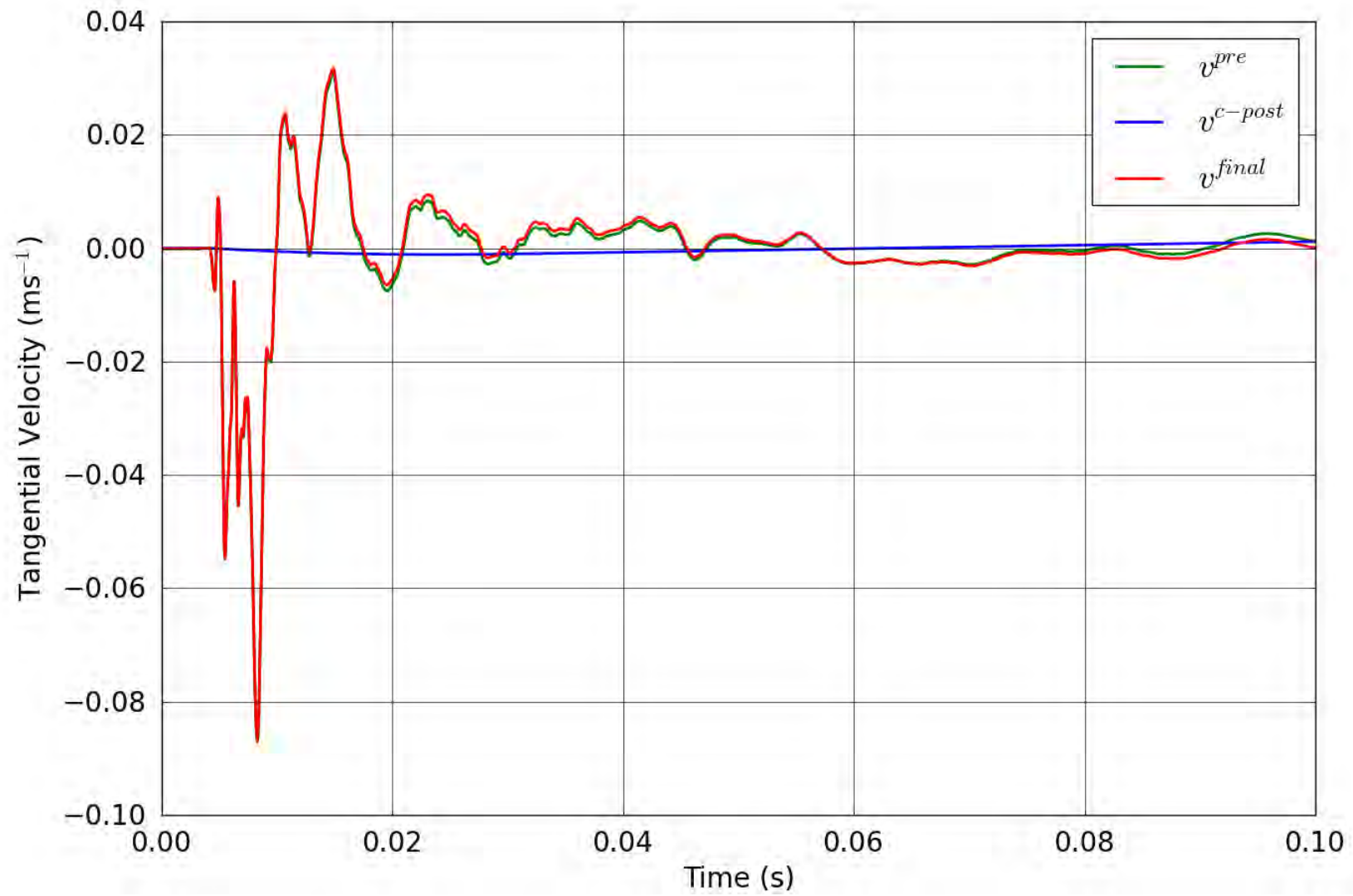


Figure 95. SPE-1 Gauge 4-2-T – Correction of the tangential velocity.

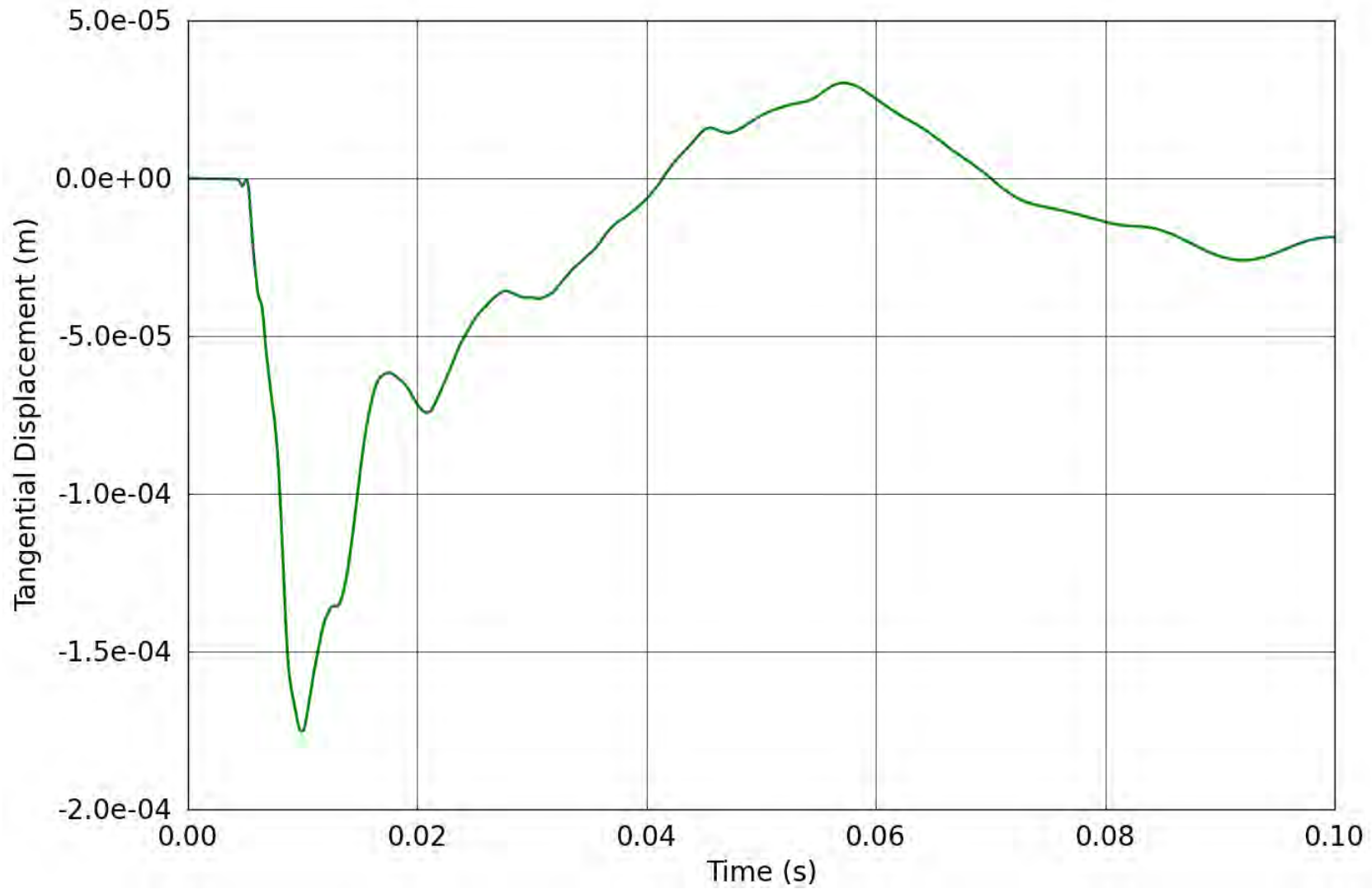


Figure 96. SPE-1 Gauge 4-2-T – Tangential displacement obtained from the corrected tangential velocity.

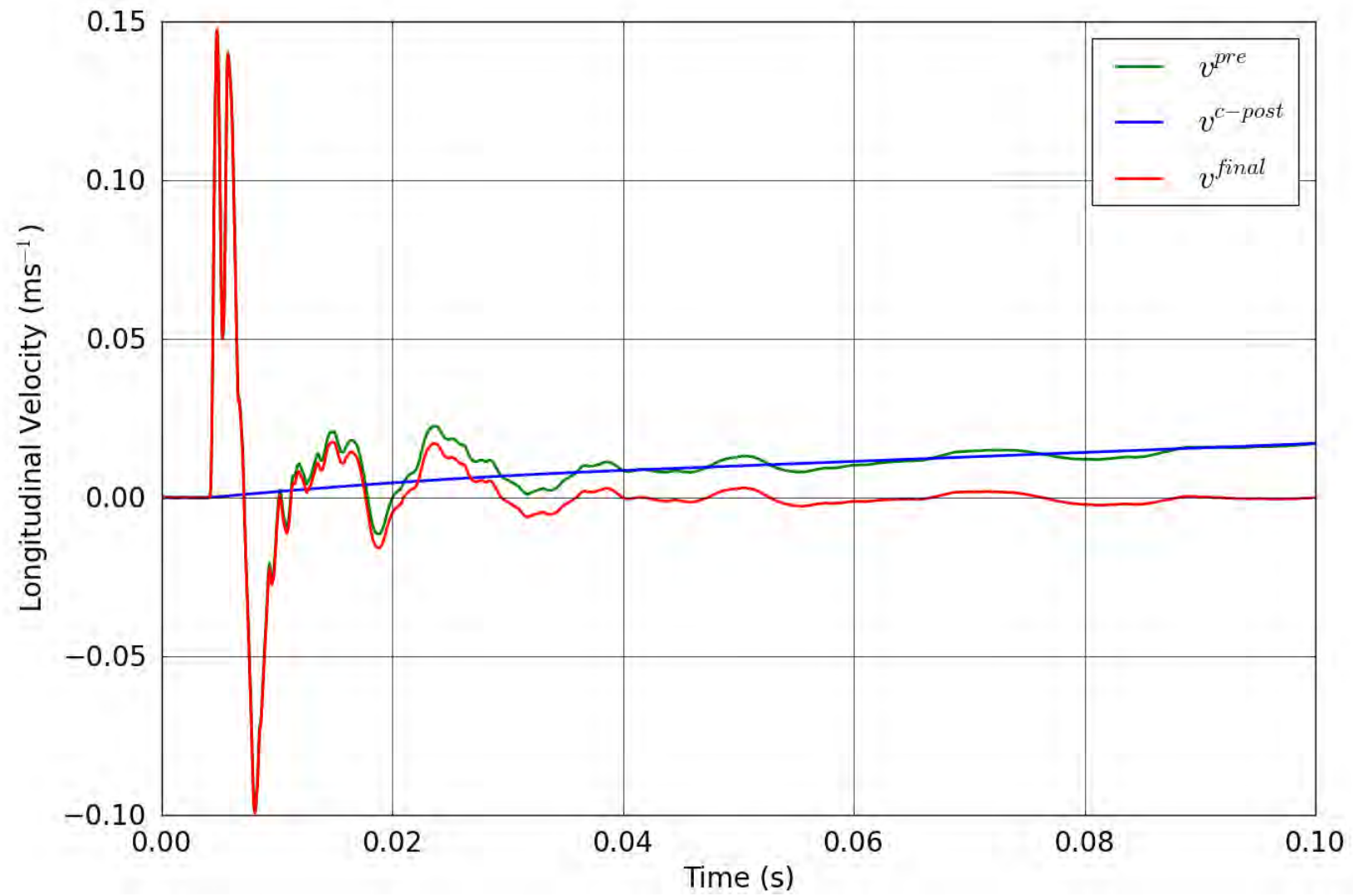


Figure 97. SPE-1 Gauge 4-2-L – Correction of the longitudinal velocity.

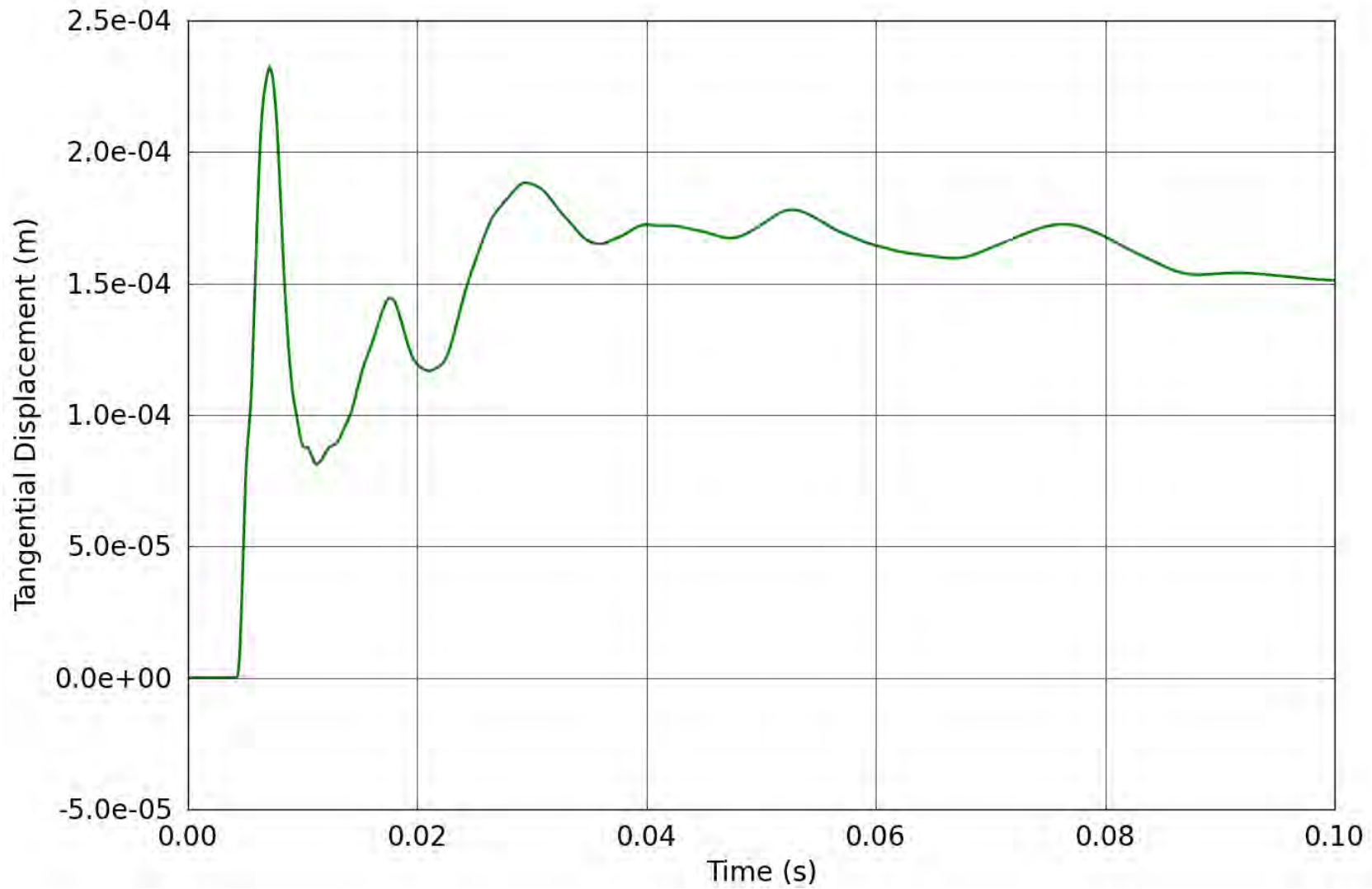


Figure 98. SPE-1 Gauge 4-2-L – Longitudinal displacement obtained from the corrected longitudinal velocity.

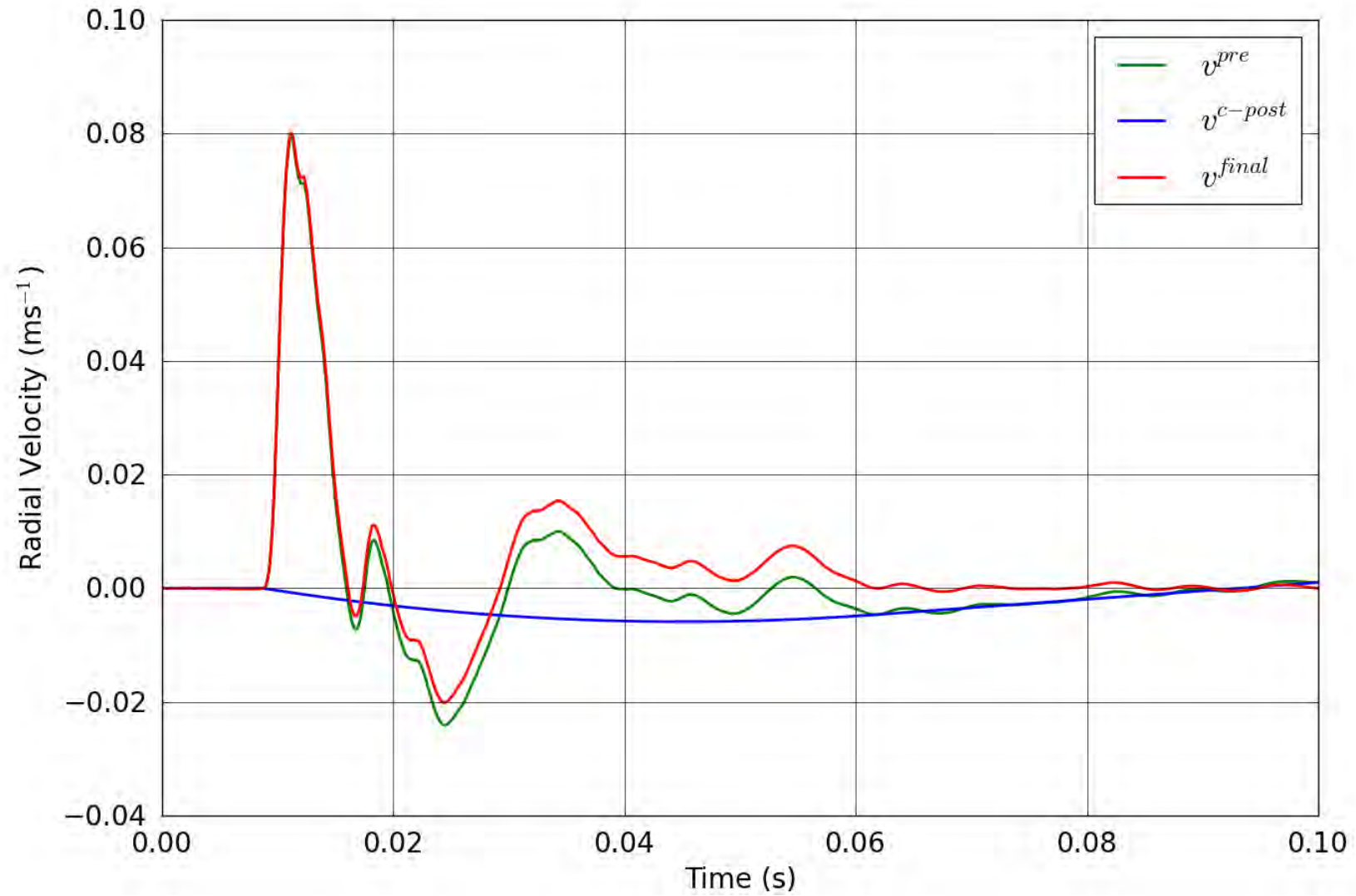


Figure 99. SPE-1 Gauge 4-3-R – Correction of the radial velocity.

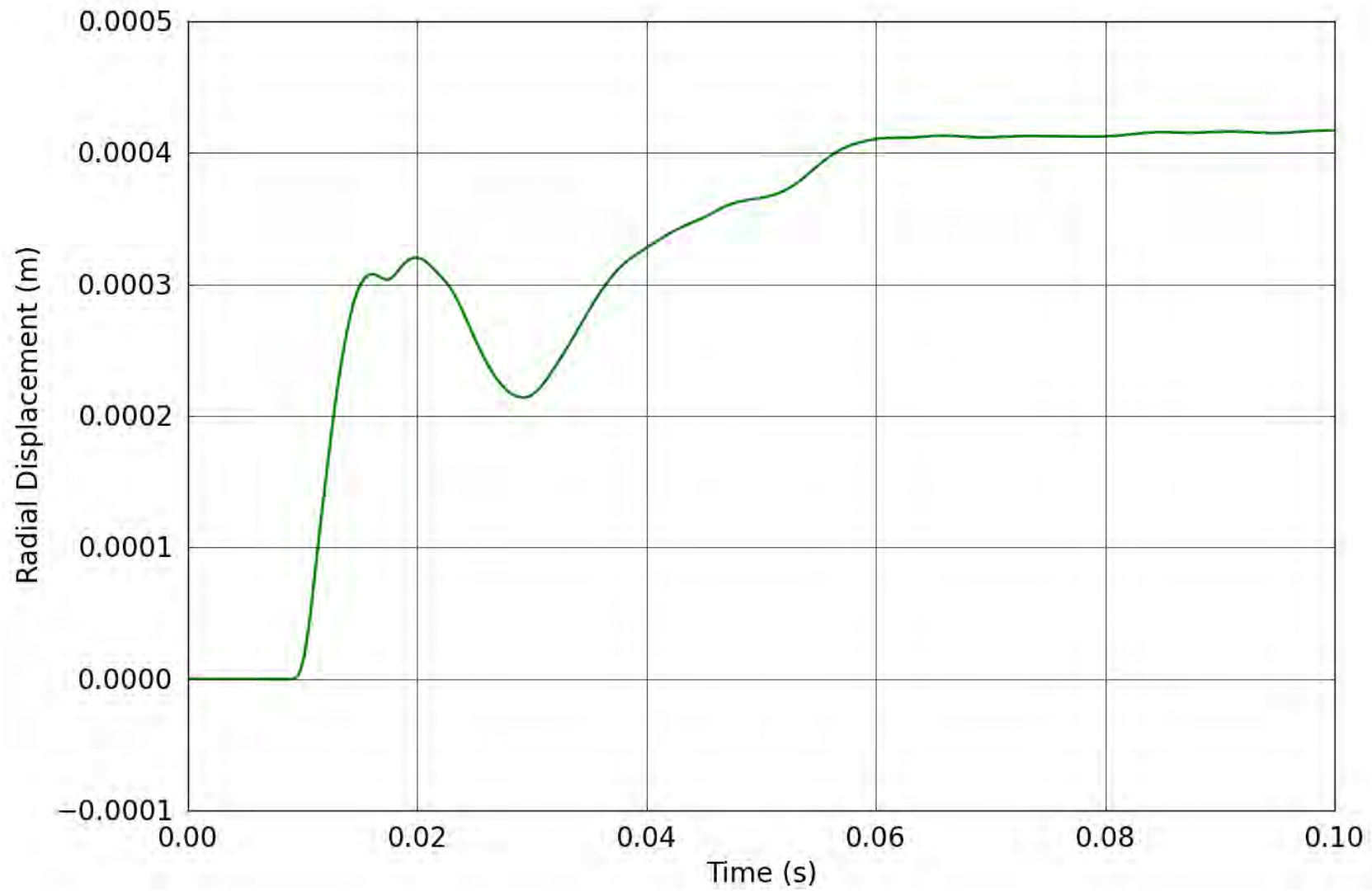


Figure 100. SPE-1 Gauge 4-3-R – Radial displacement obtained from the corrected radial velocity.

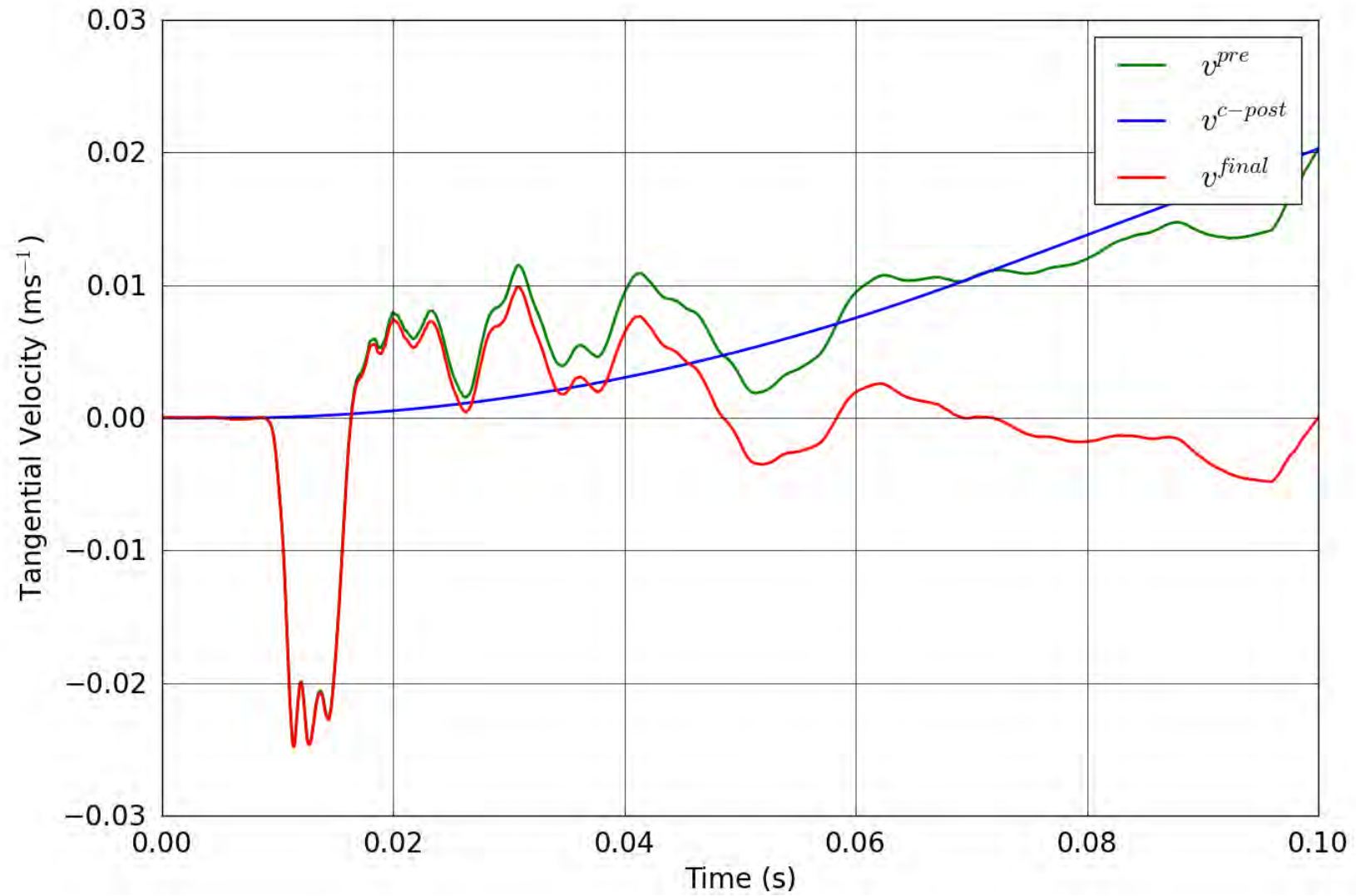


Figure 101. SPE-1 Gauge 4-3-T – Correction of the tangential velocity.

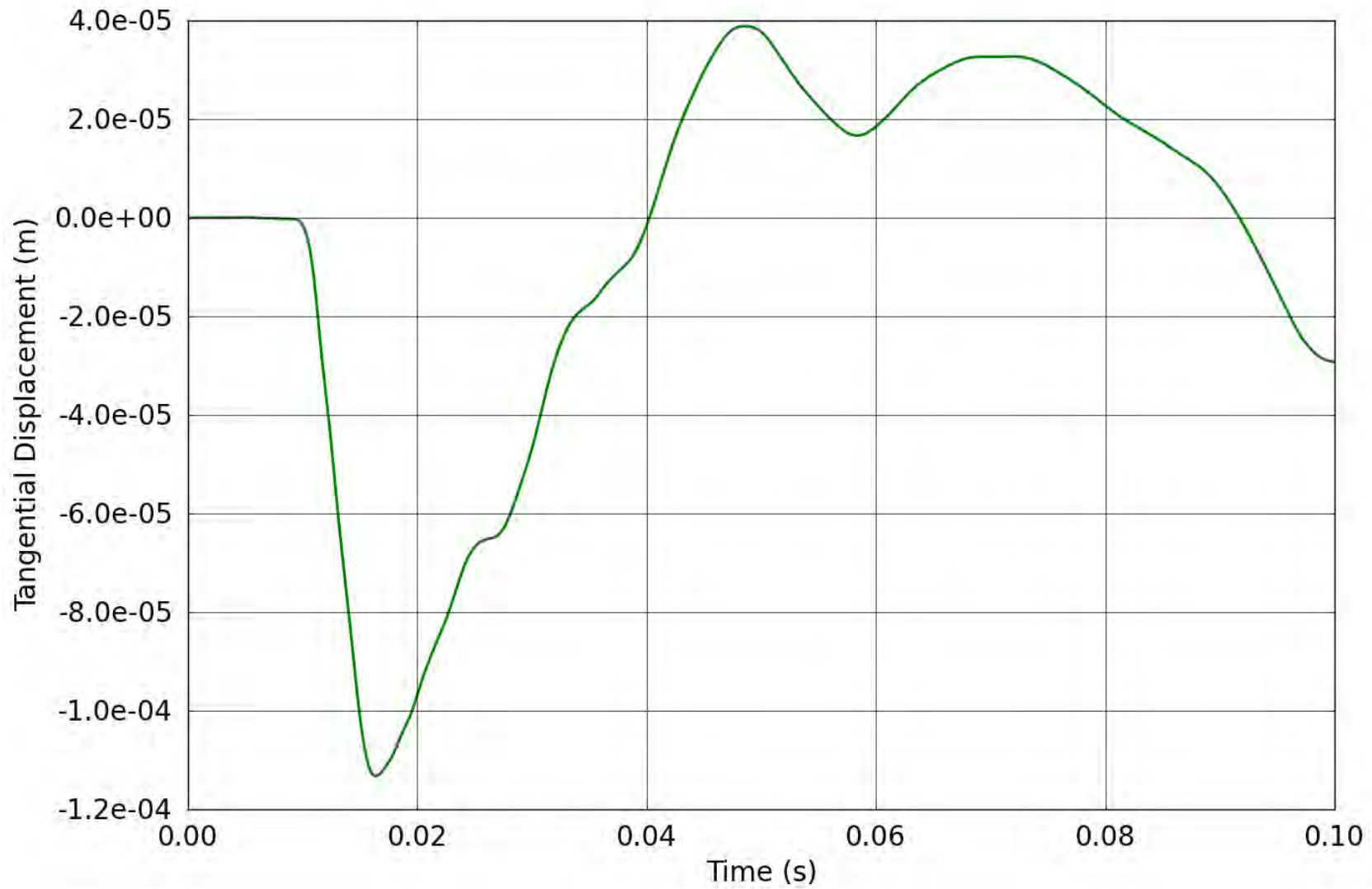


Figure 102. SPE-1 Gauge 4-3-T – Tangential displacement obtained from the corrected tangential velocity.

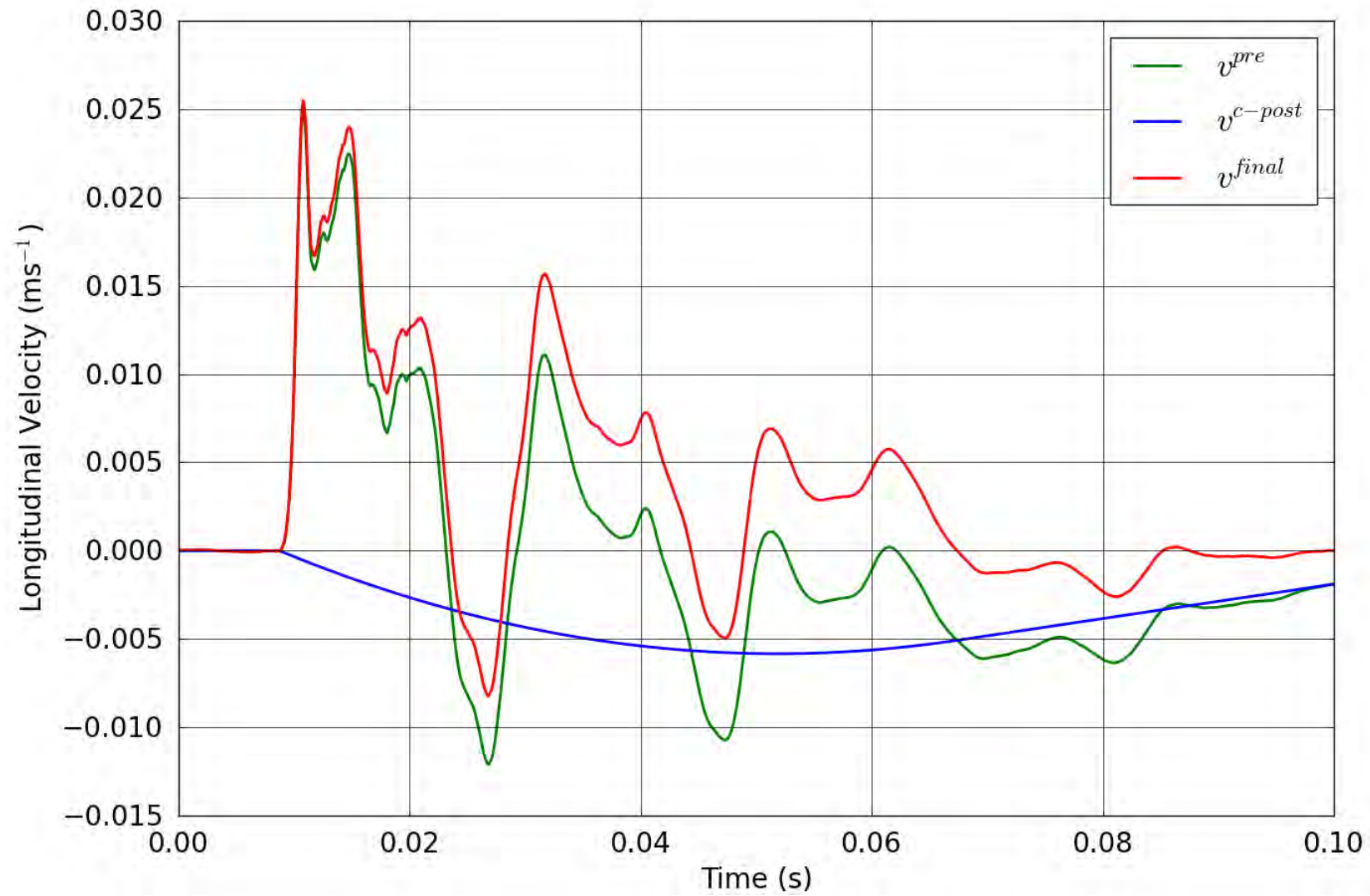


Figure 103. SPE-1 Gauge 4-3-L – Correction of the longitudinal velocity.

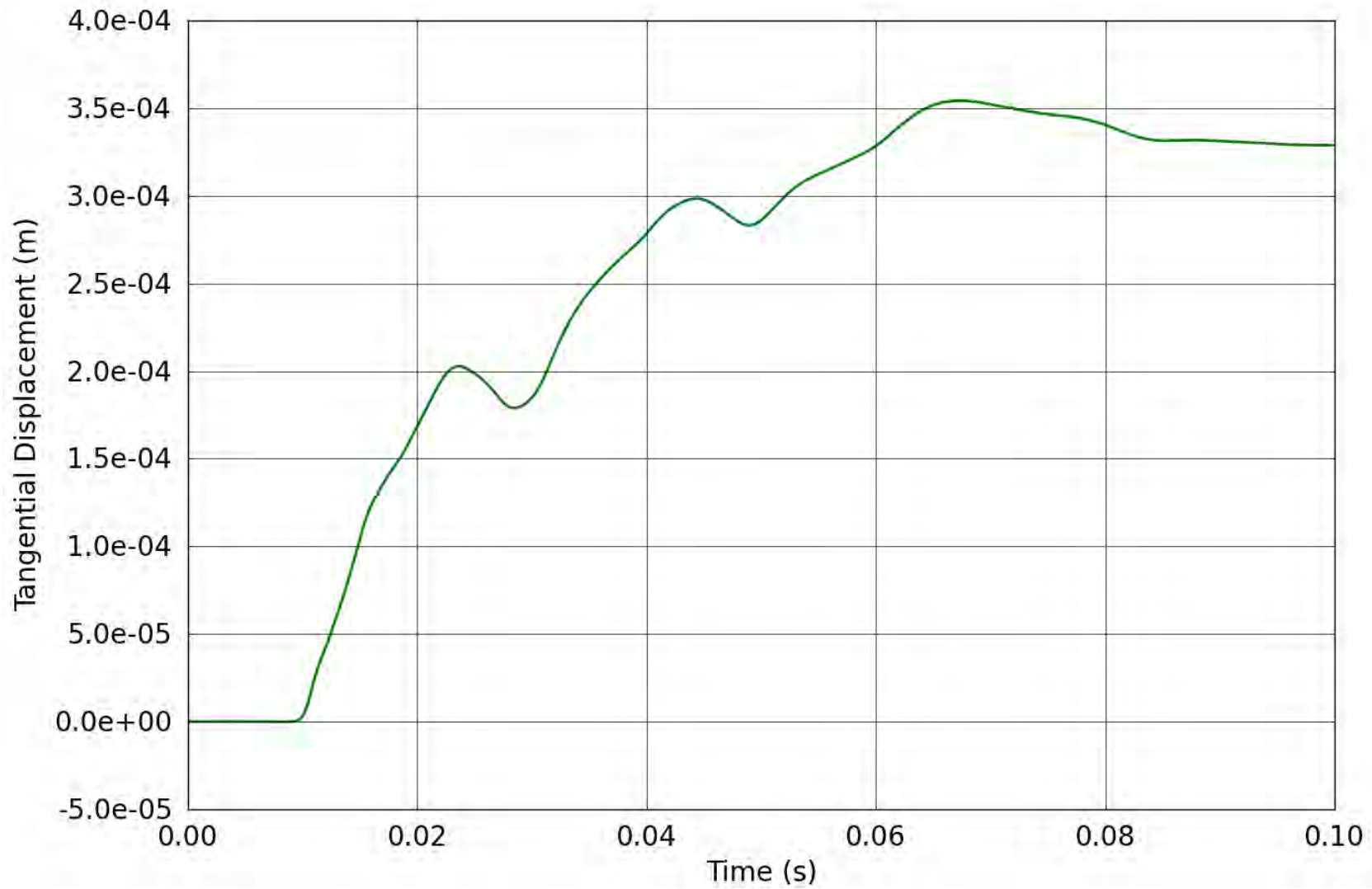


Figure 104. SPE-1 Gauge 4-3-L – Longitudinal displacement obtained from the corrected longitudinal velocity.

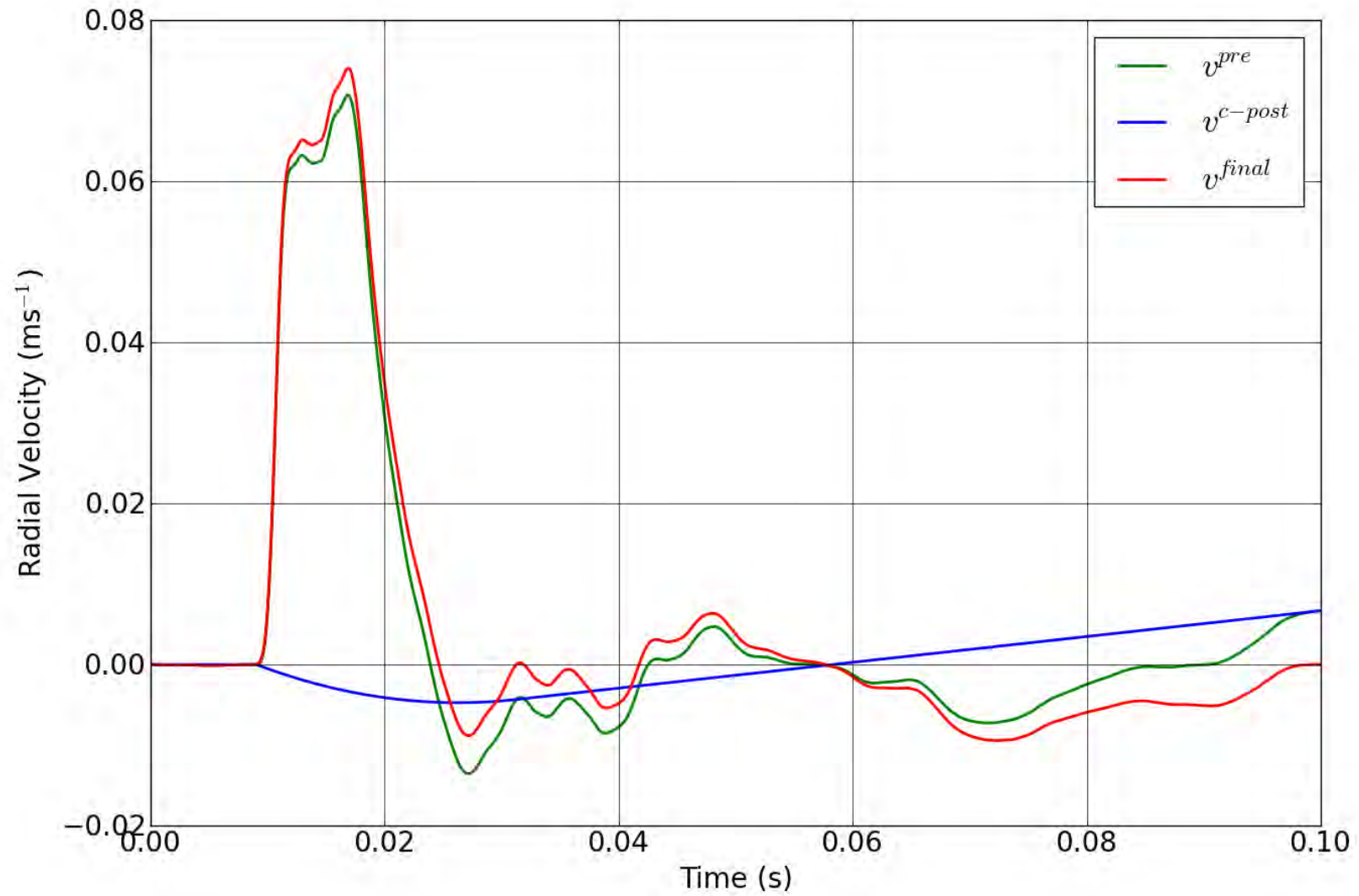


Figure 105. SPE-1 Gauge 5-3-R – Correction of the radial velocity.

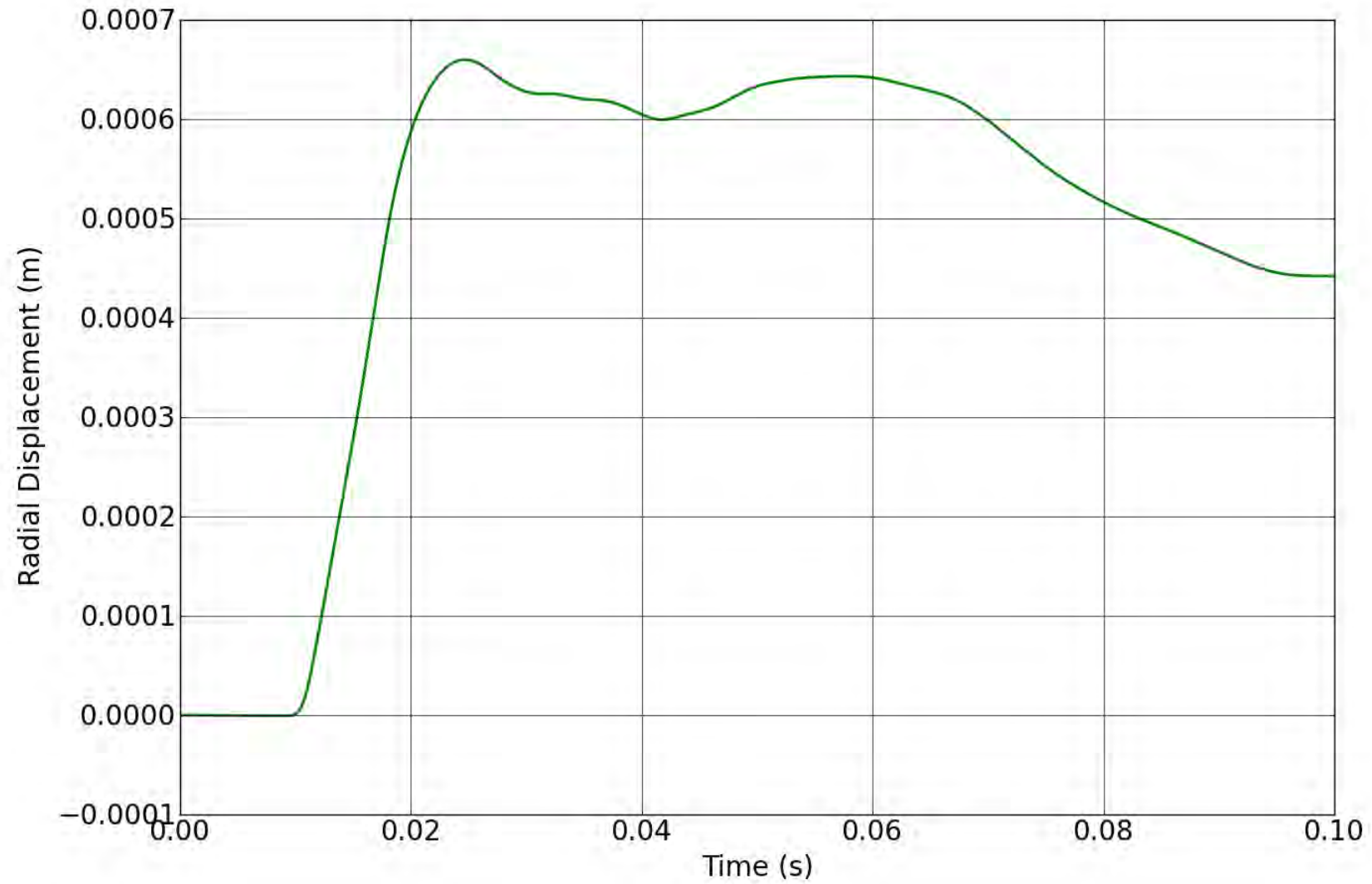


Figure 106. SPE-1 Gauge 5-3-R – Radial displacement obtained from the corrected radial velocity.

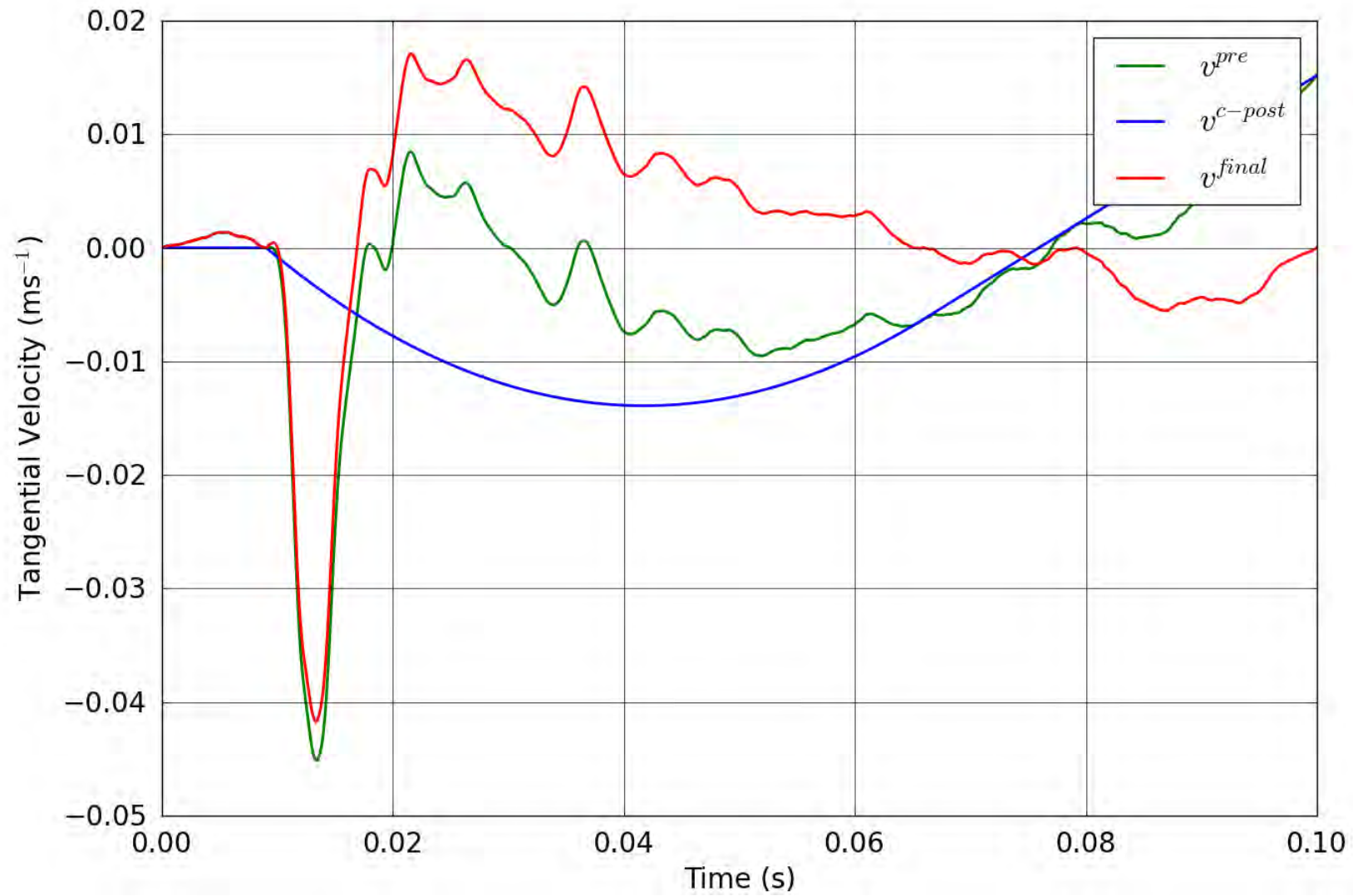


Figure 107. SPE-1 Gauge 5-3-T – Correction of the tangential velocity.

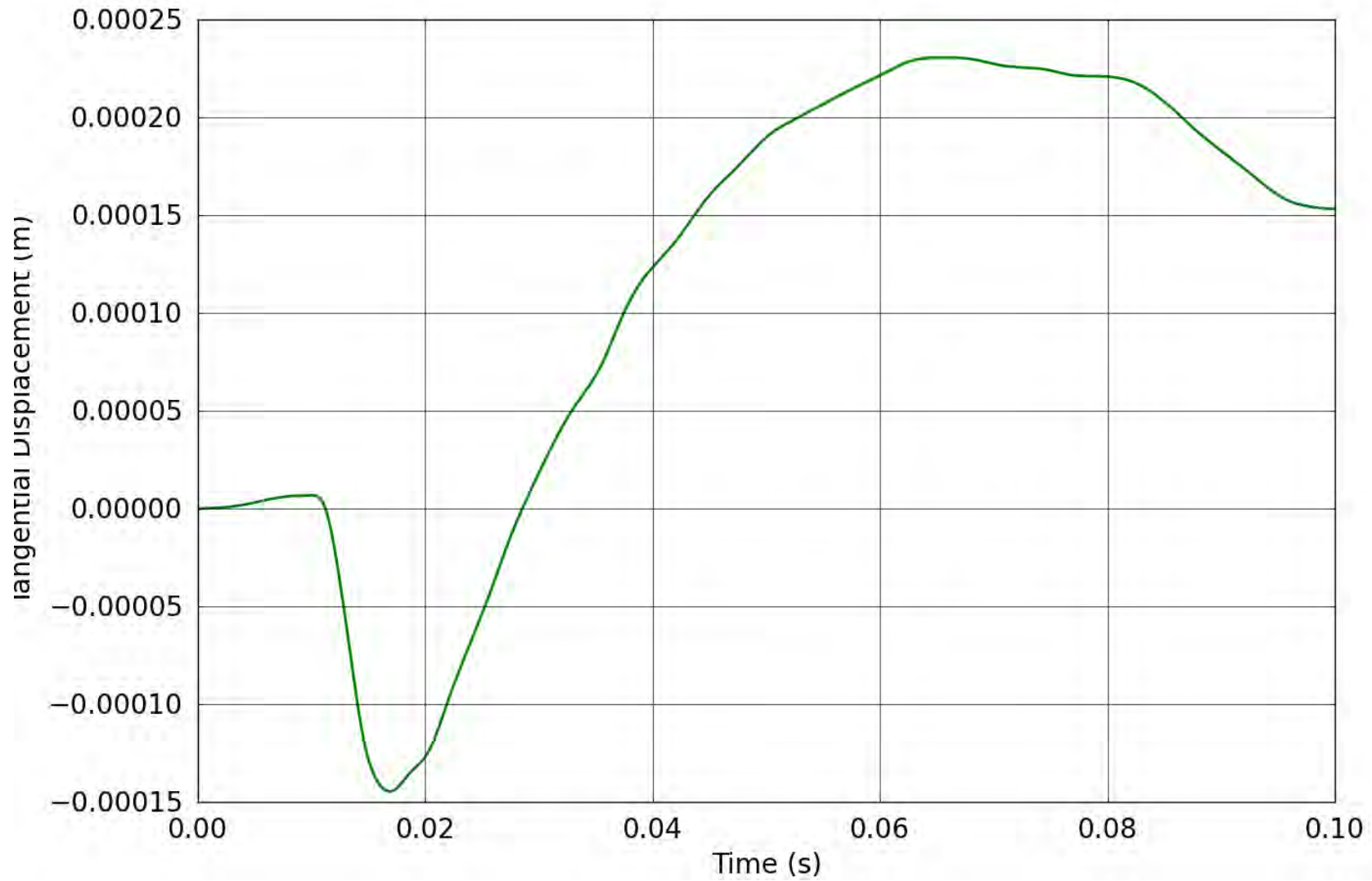


Figure 108. SPE-1 Gauge 5-3-T – Tangential displacement obtained from the corrected tangential velocity.

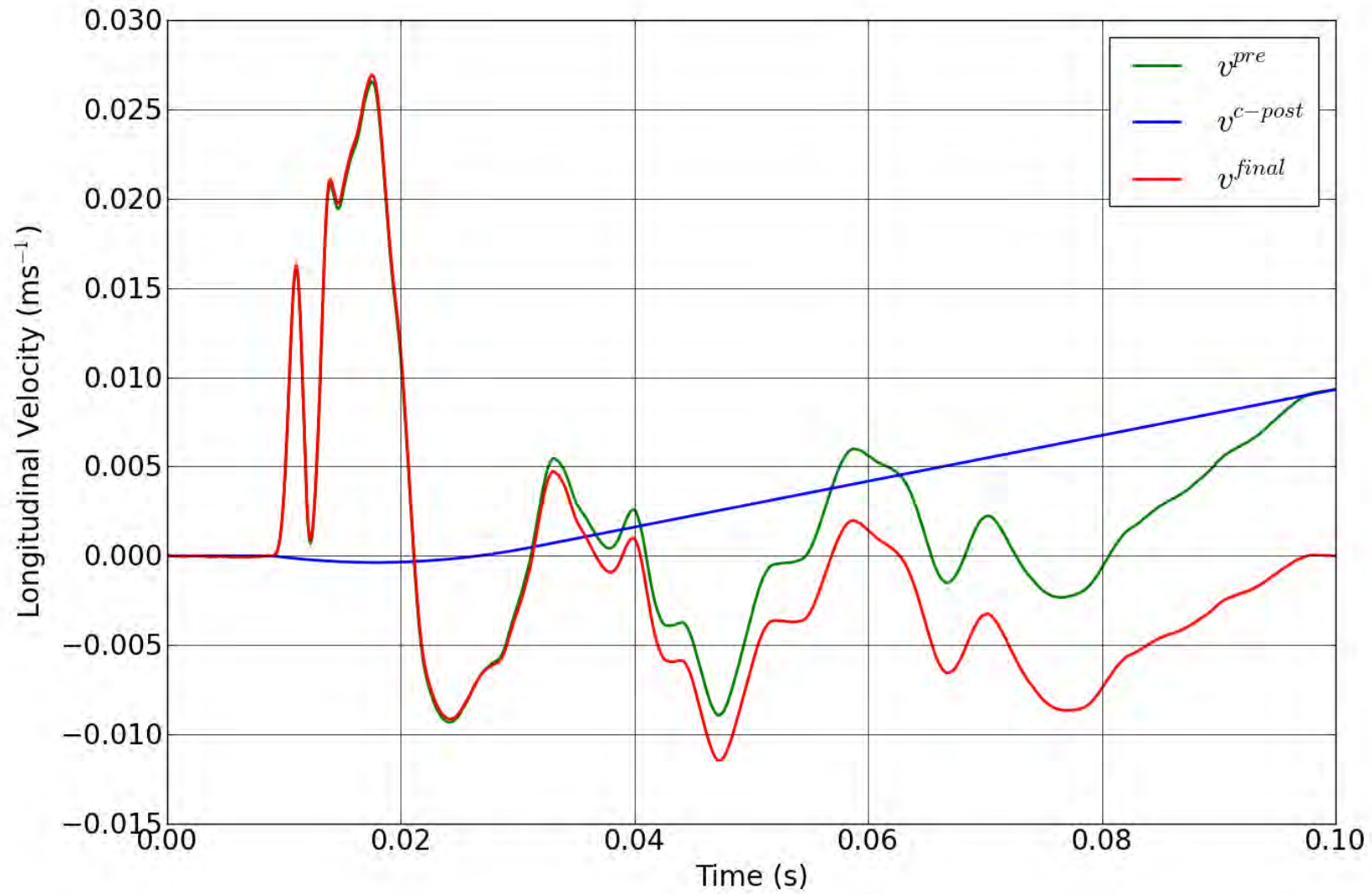


Figure 109. SPE-1 Gauge 5-3-L – Correction of the longitudinal velocity.

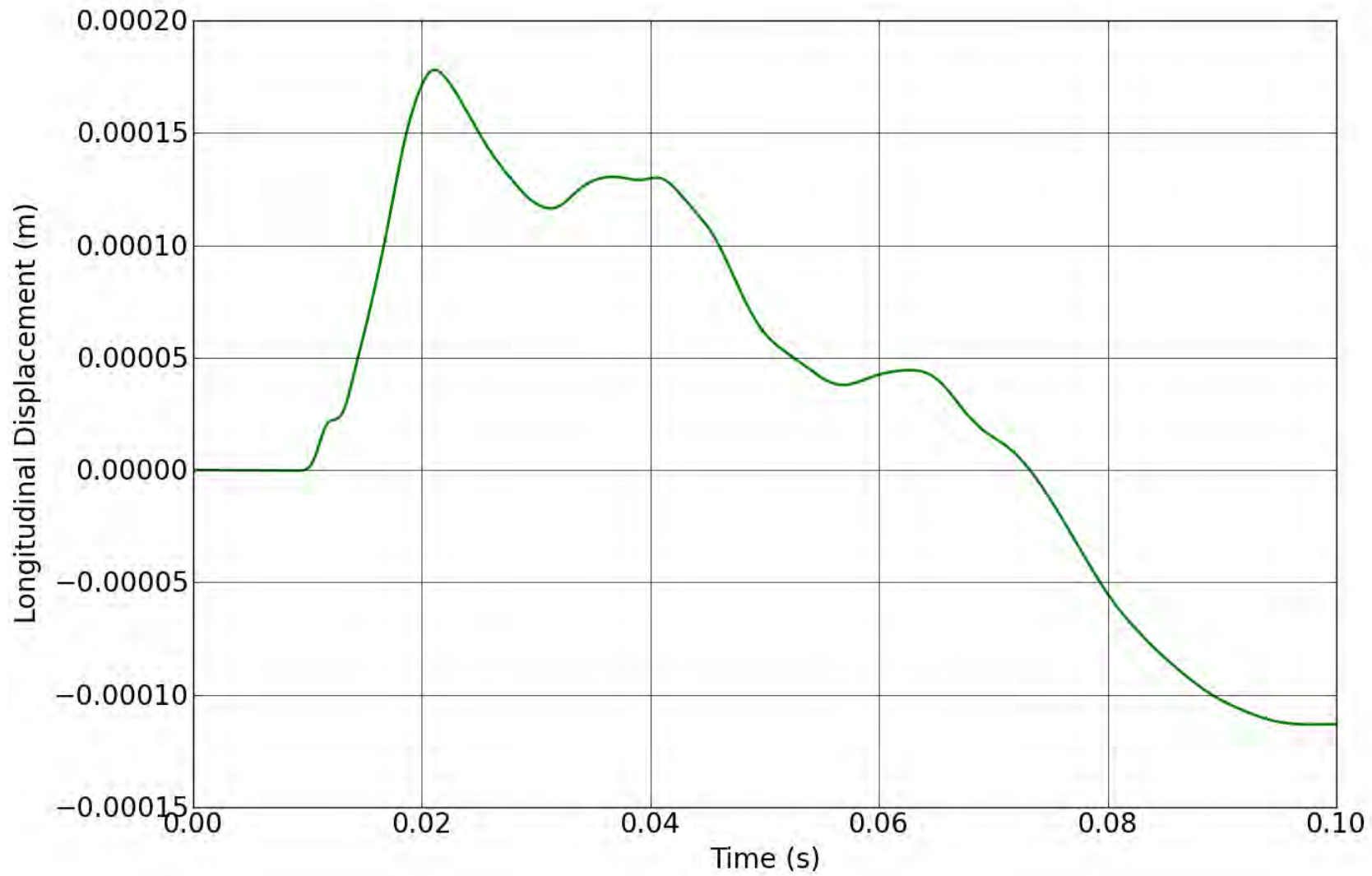


Figure 110. SPE-1 Gauge 5-3-L – Longitudinal displacement obtained from the corrected longitudinal velocity.

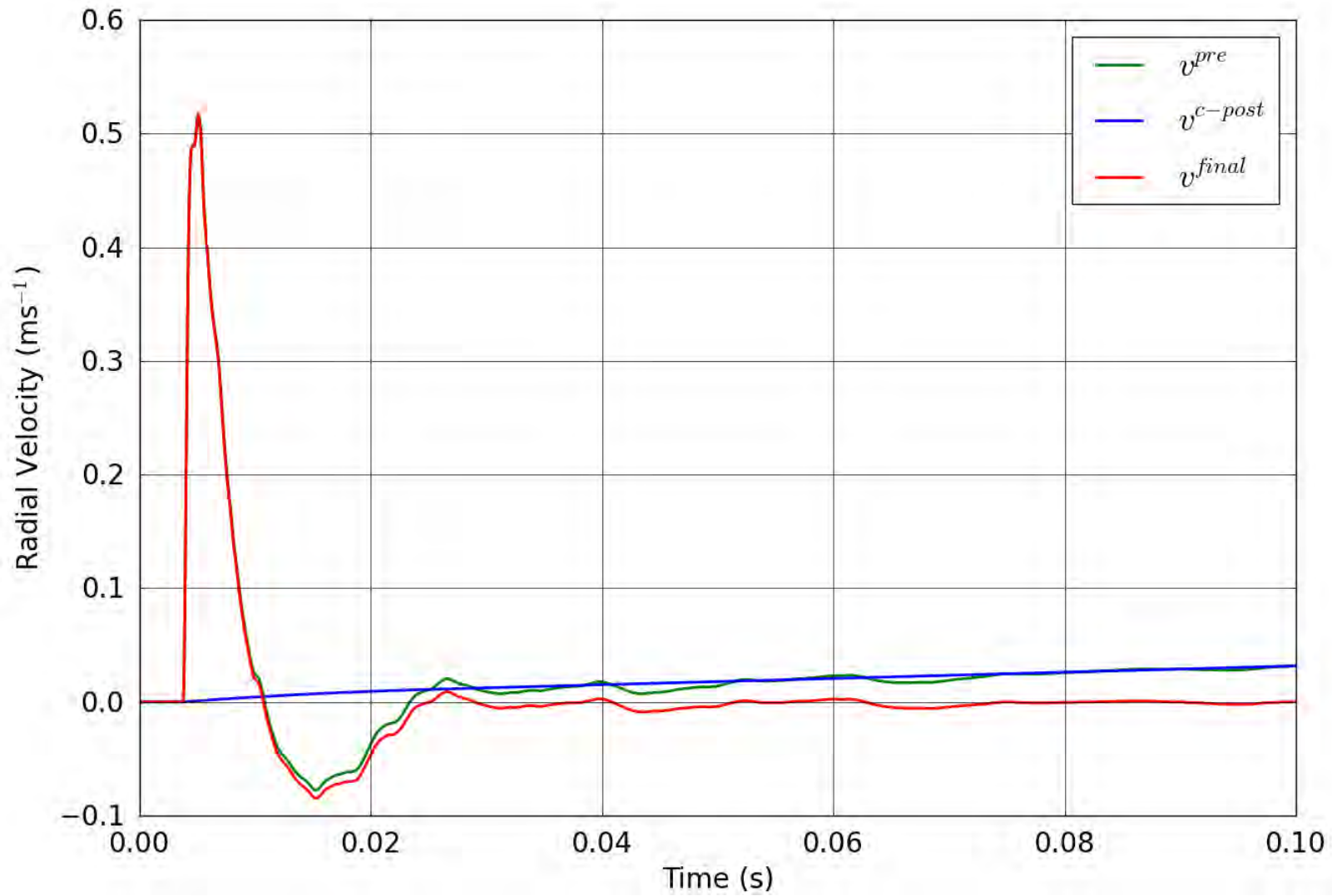


Figure 111. SPE-1 Gauge 6-1-R – Correction of the radial velocity.

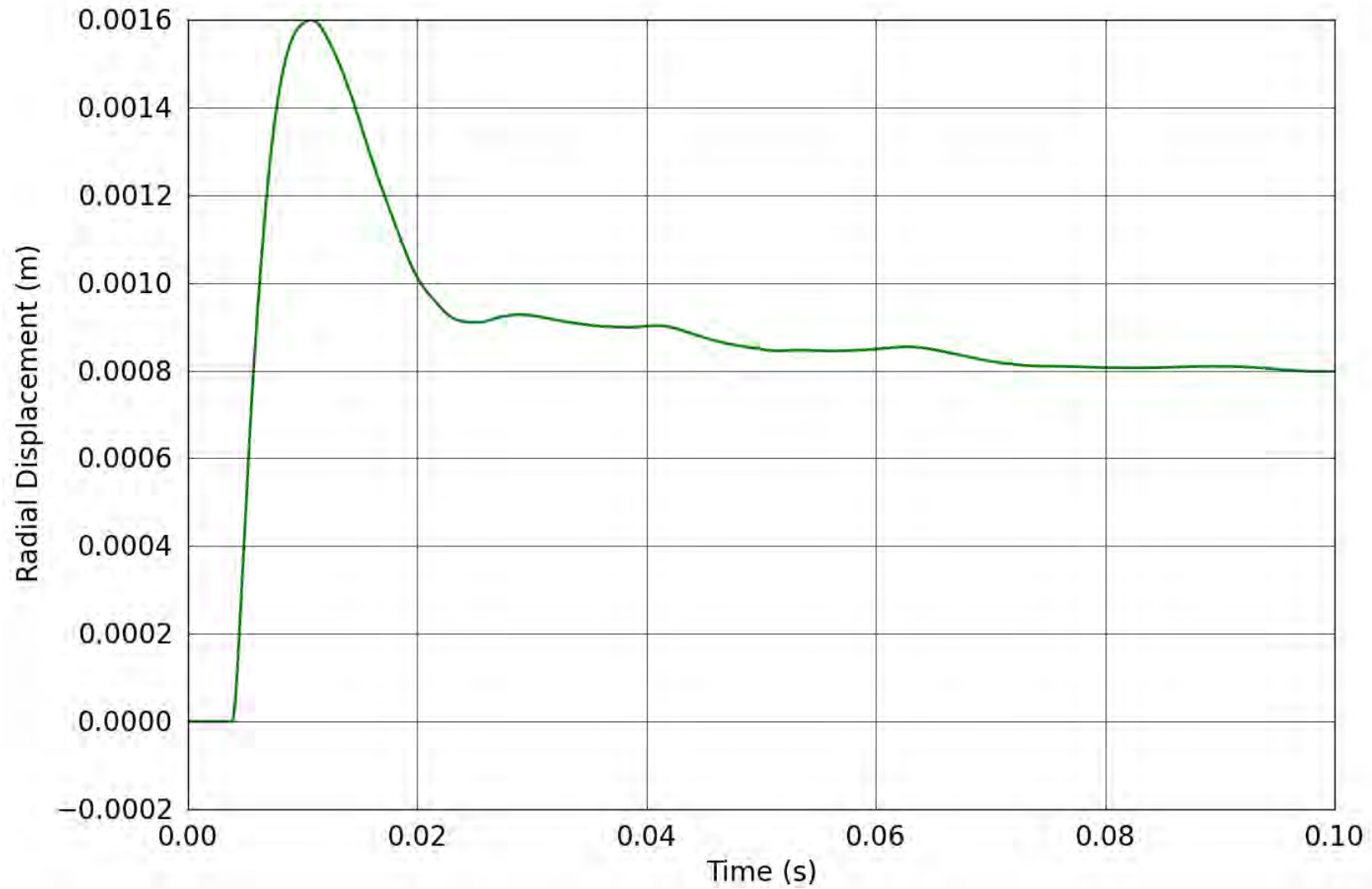


Figure 112. SPE-1 Gauge 6-1-R – Radial displacement obtained from the corrected radial velocity.

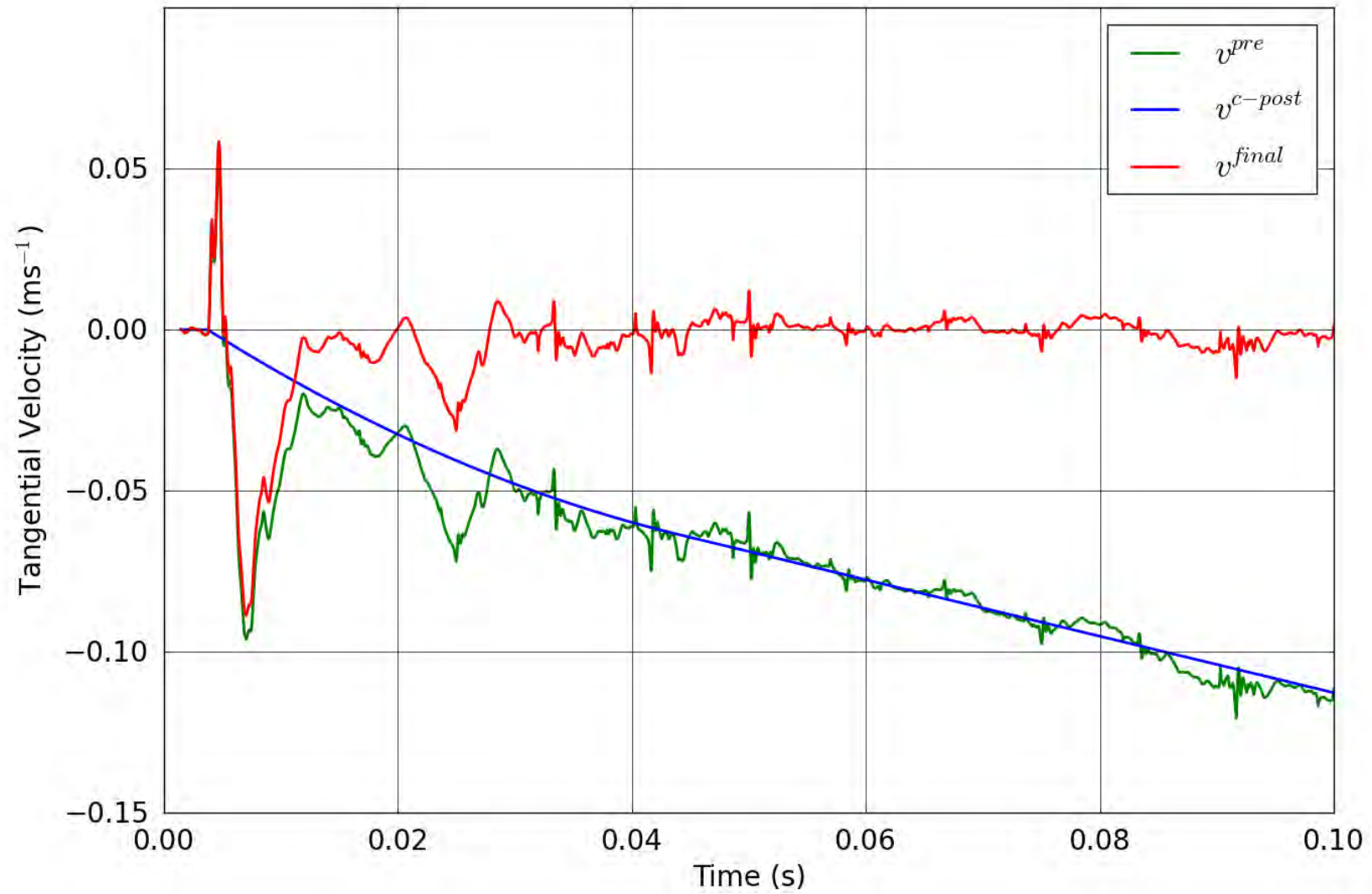


Figure 113. SPE-1 Gauge 6-1-T – Correction of the tangential velocity.

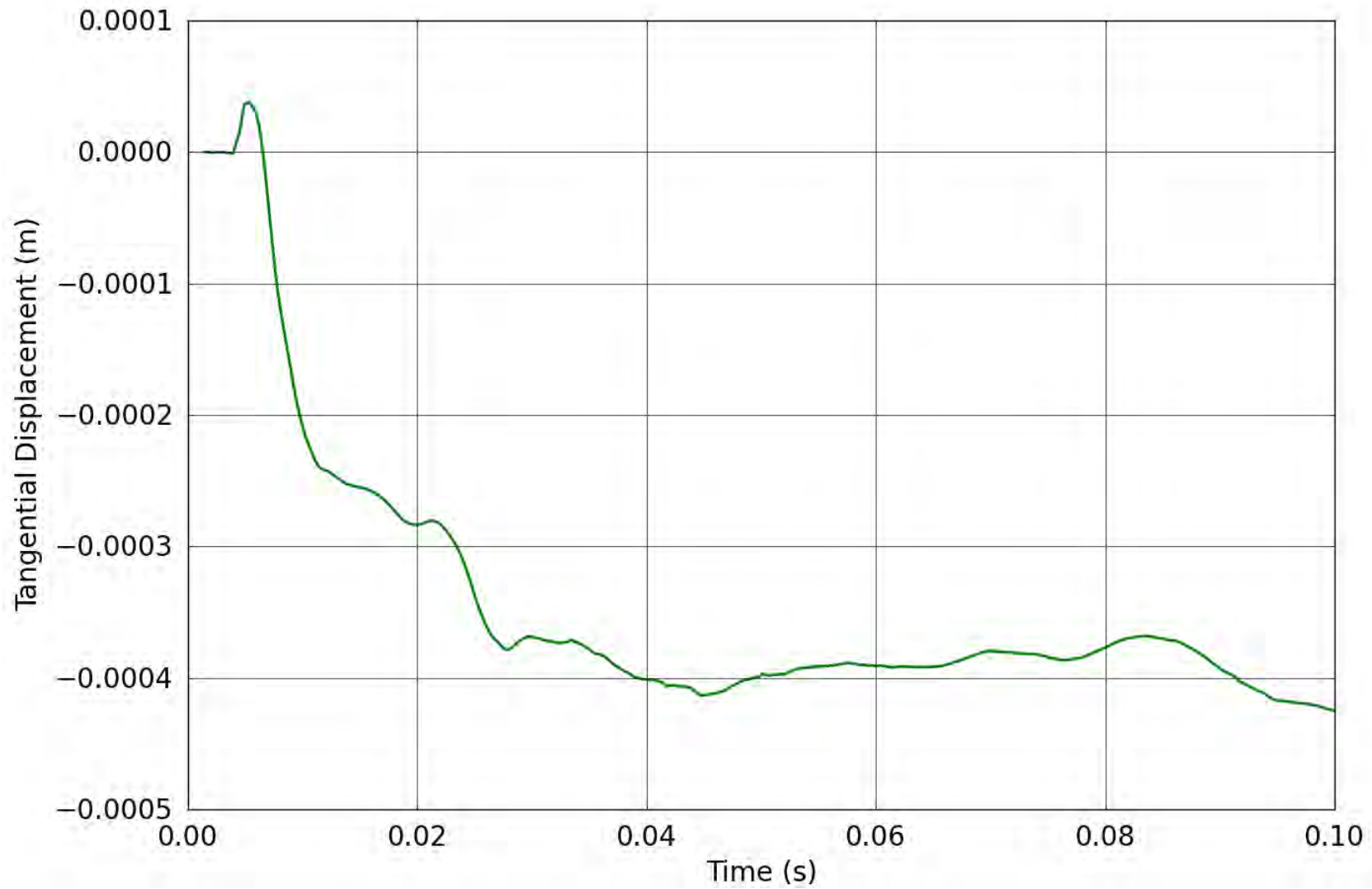


Figure 114. SPE-1 Gauge 6-1-T – Tangential displacement obtained from the corrected tangential velocity.

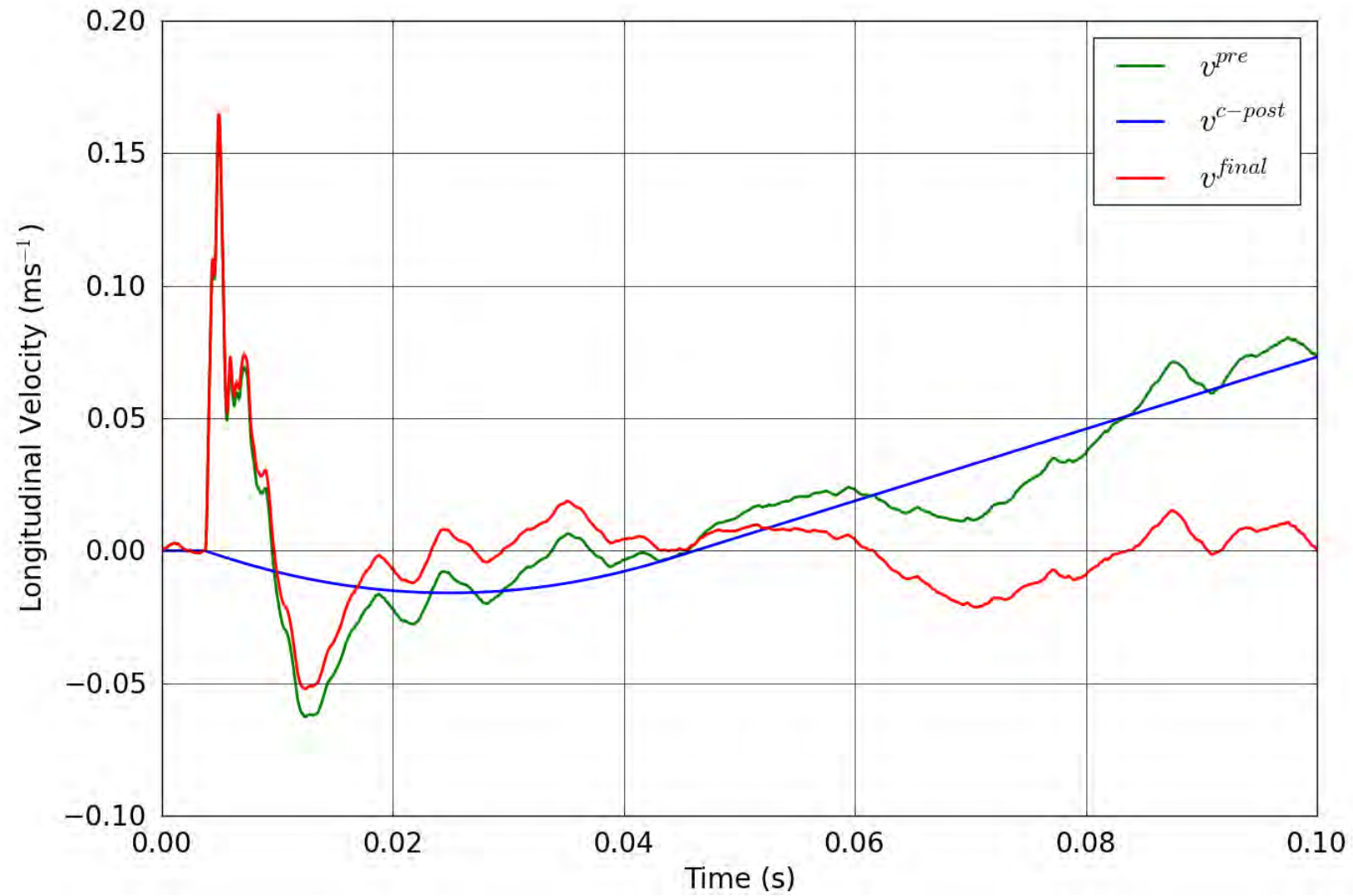


Figure 115. SPE-1 Gauge 6-1-L – Correction of the longitudinal velocity.

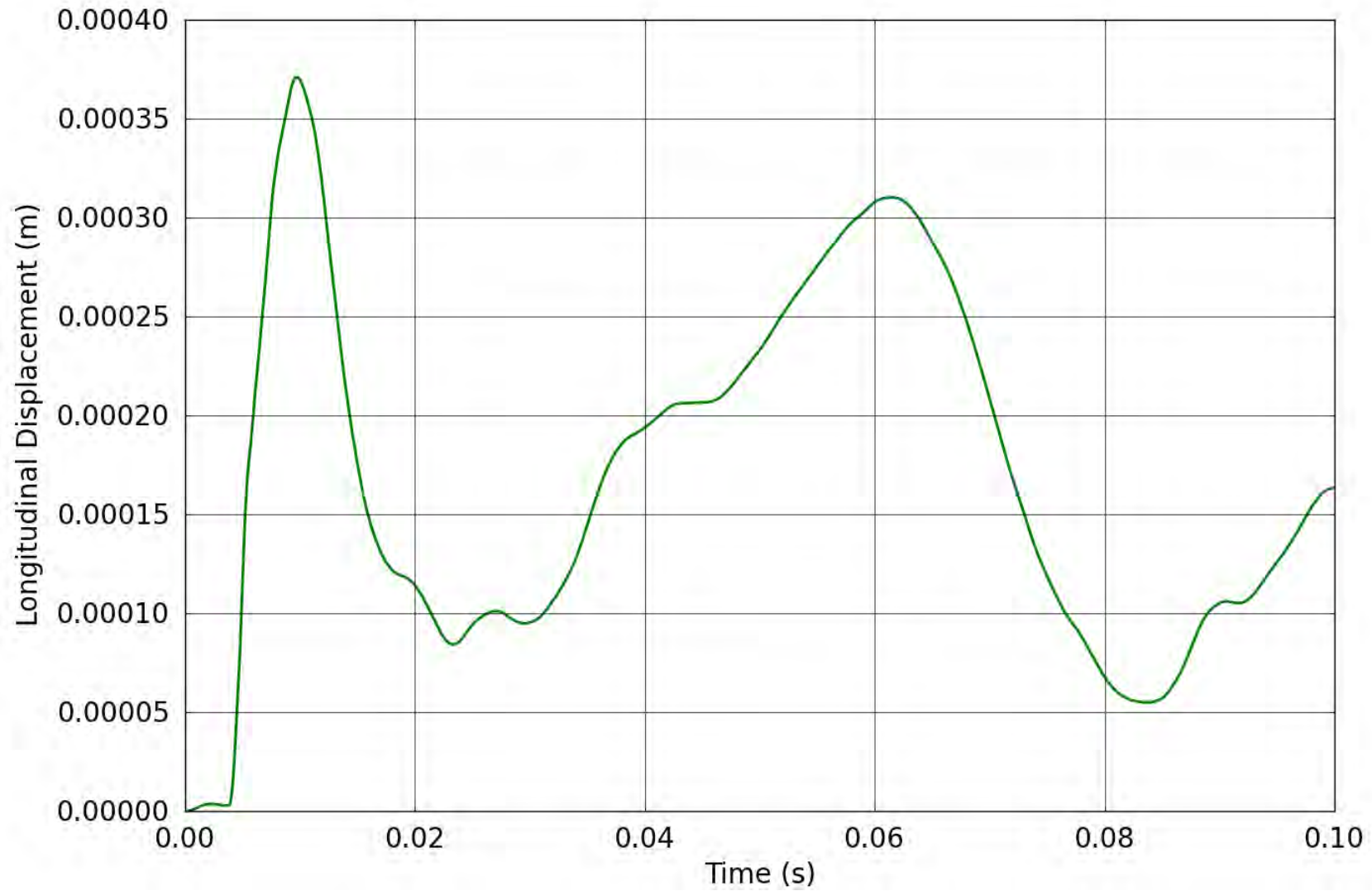


Figure 116. SPE-1 Gauge 6-1-L – Longitudinal displacement obtained from the corrected longitudinal velocity.

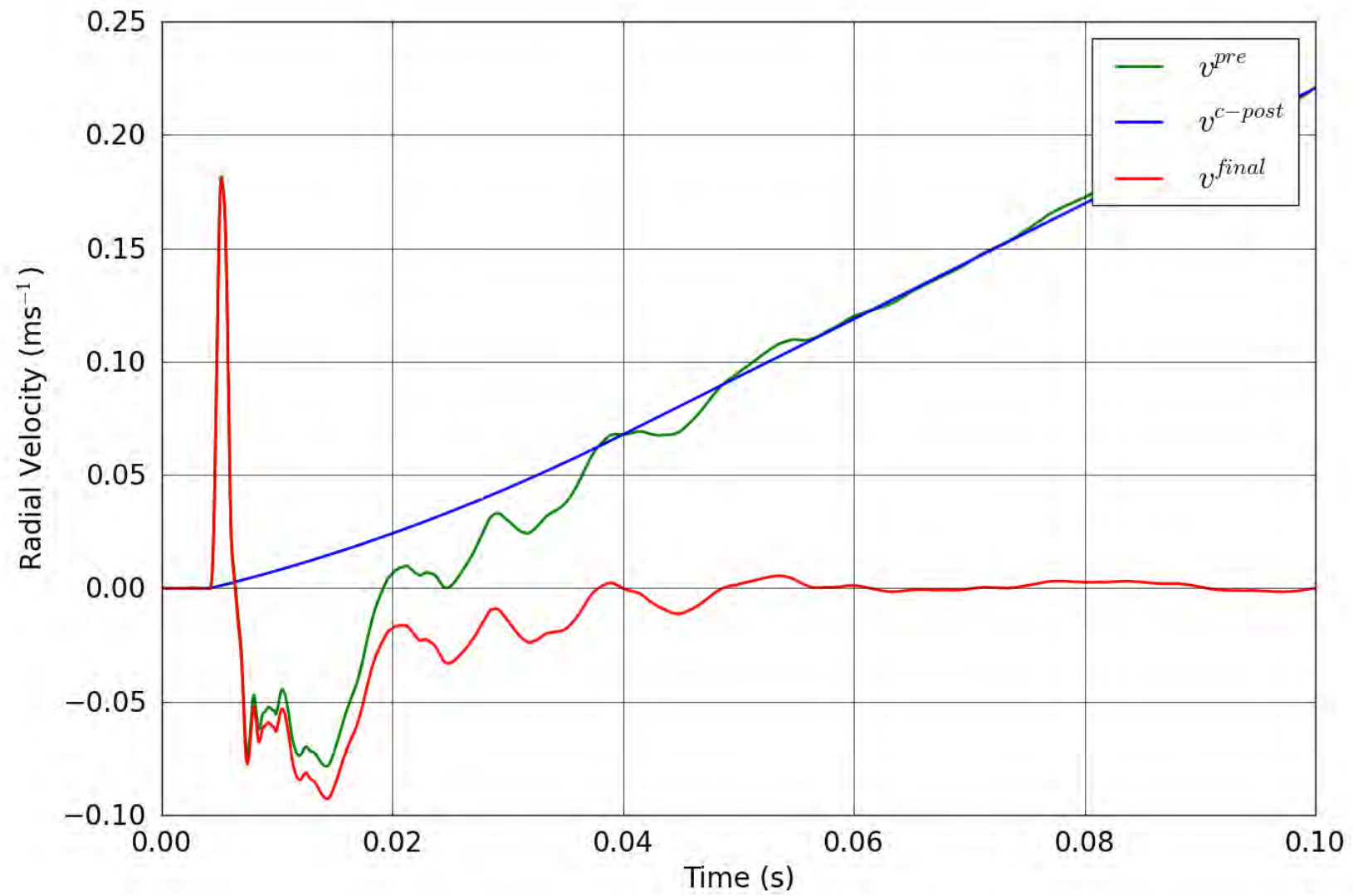


Figure 117. SPE-1 Gauge 6-2-R – Correction of the radial velocity.

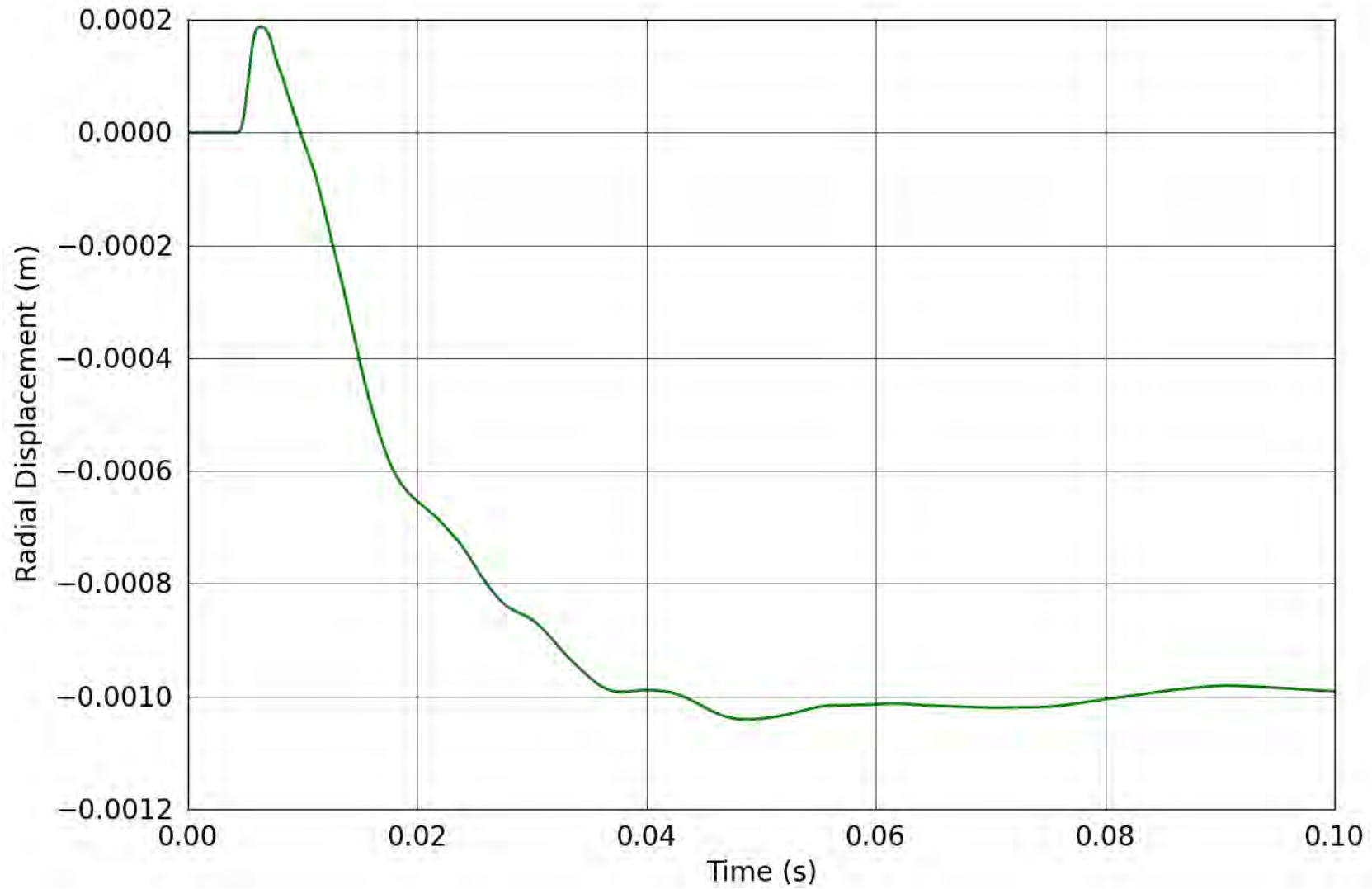


Figure 118. SPE-1 Gauge 6-2-R – Radial displacement obtained from the corrected radial velocity.

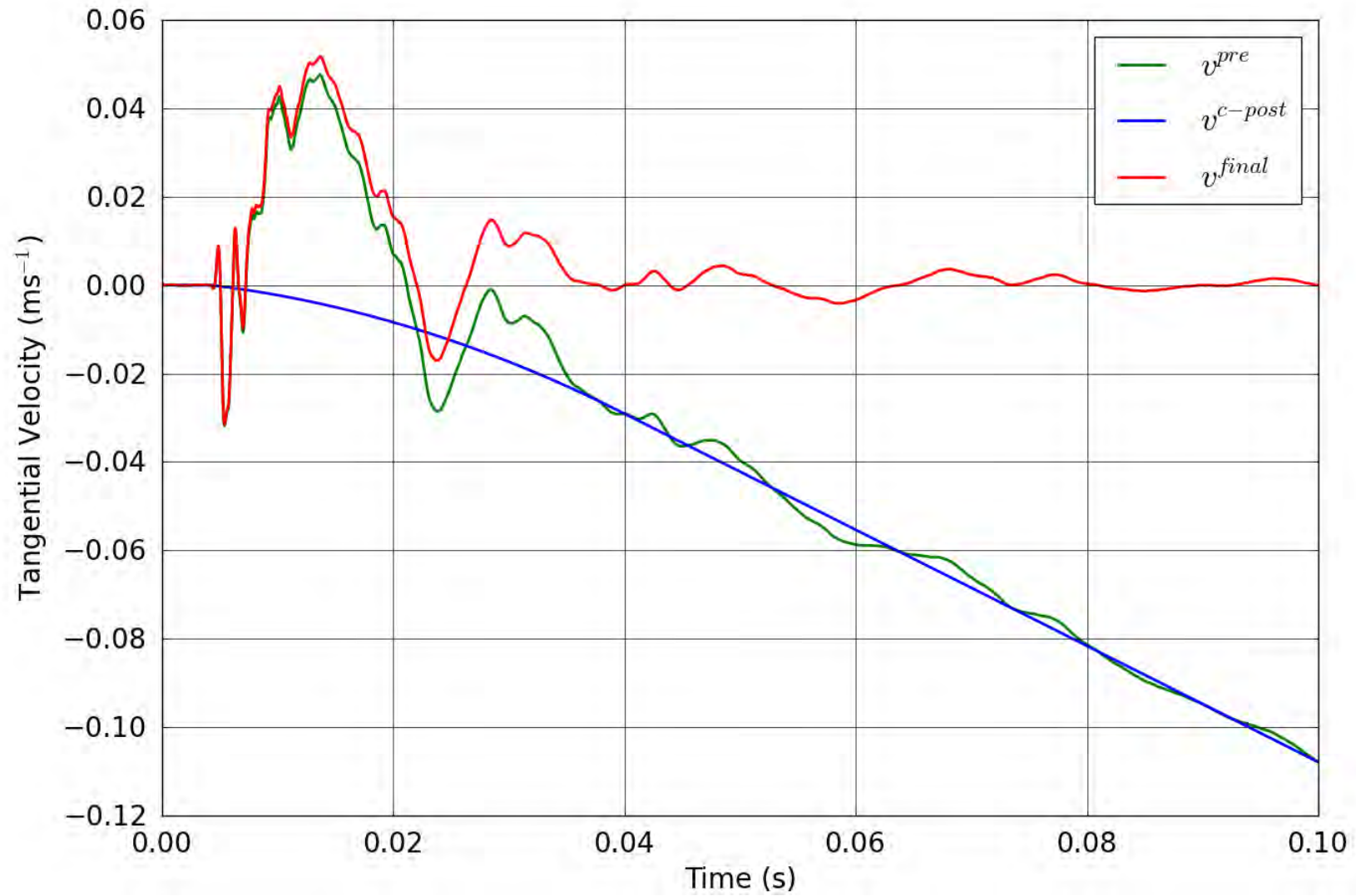


Figure 119. SPE-1 Gauge 6-2-T – Correction of the tangential velocity.

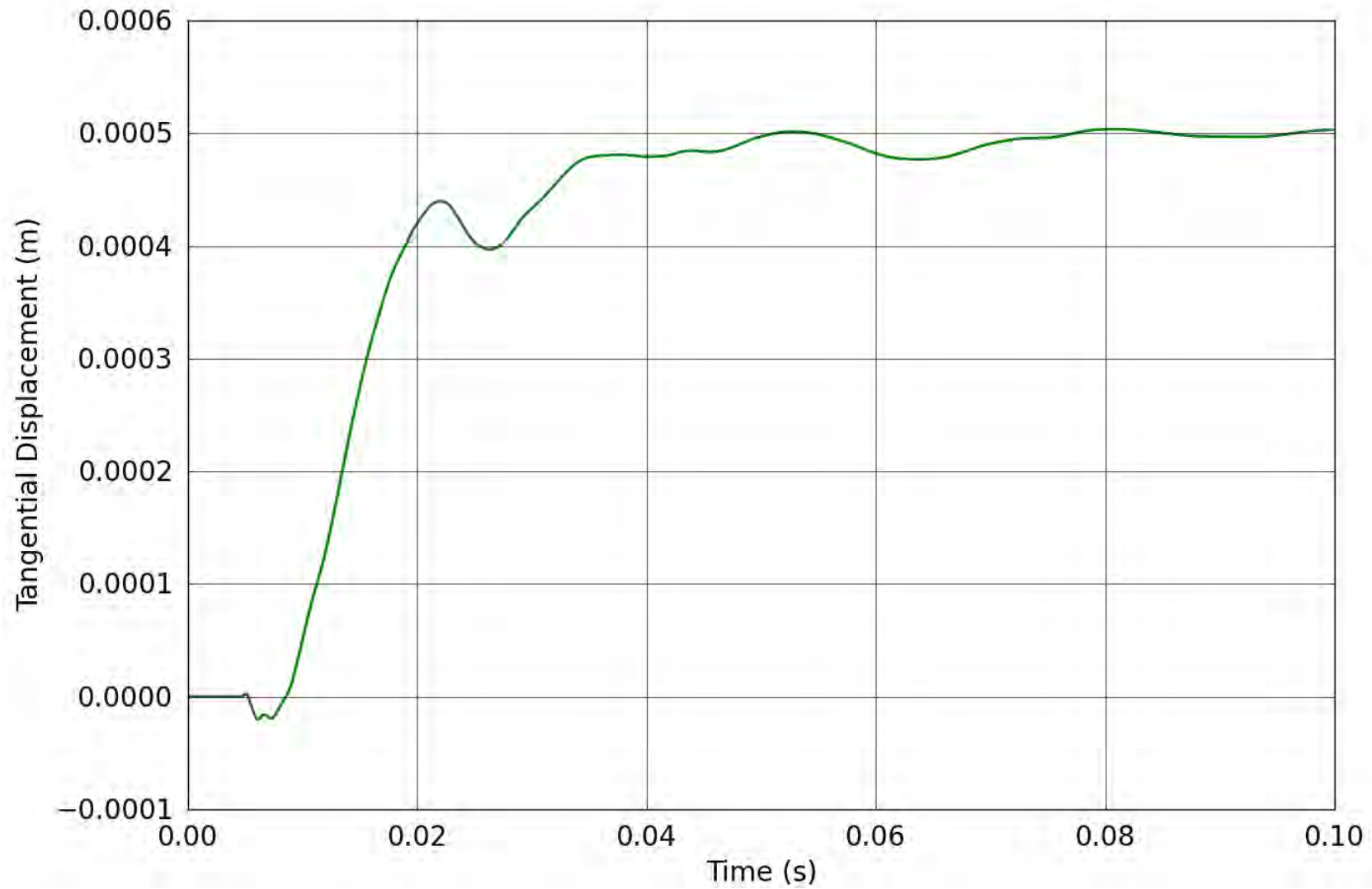


Figure 120. SPE-1 Gauge 6-2-T – Tangential displacement obtained from the corrected tangential velocity.

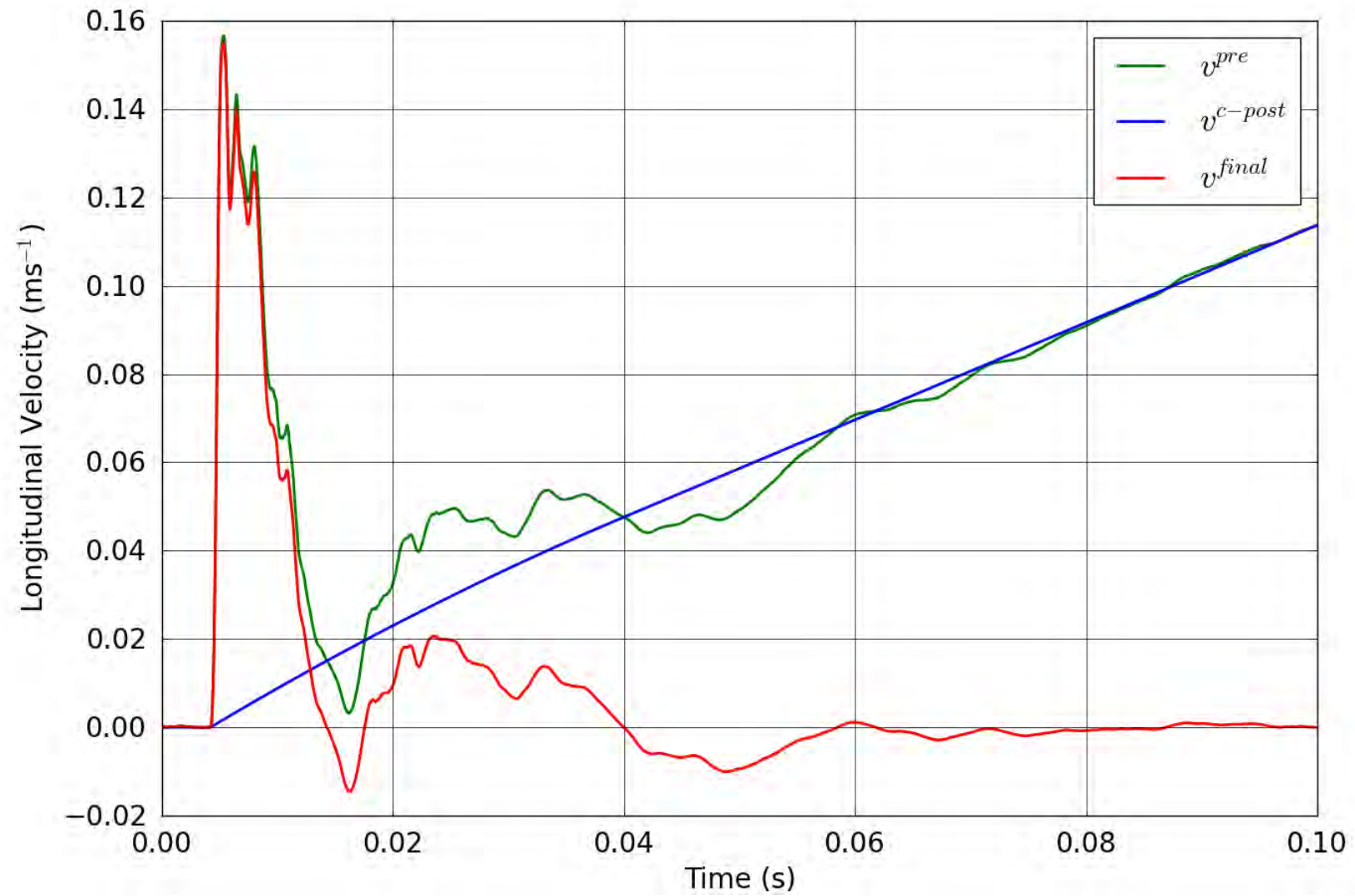


Figure 121. SPE-1 Gauge 6-2-L – Correction of the longitudinal velocity.

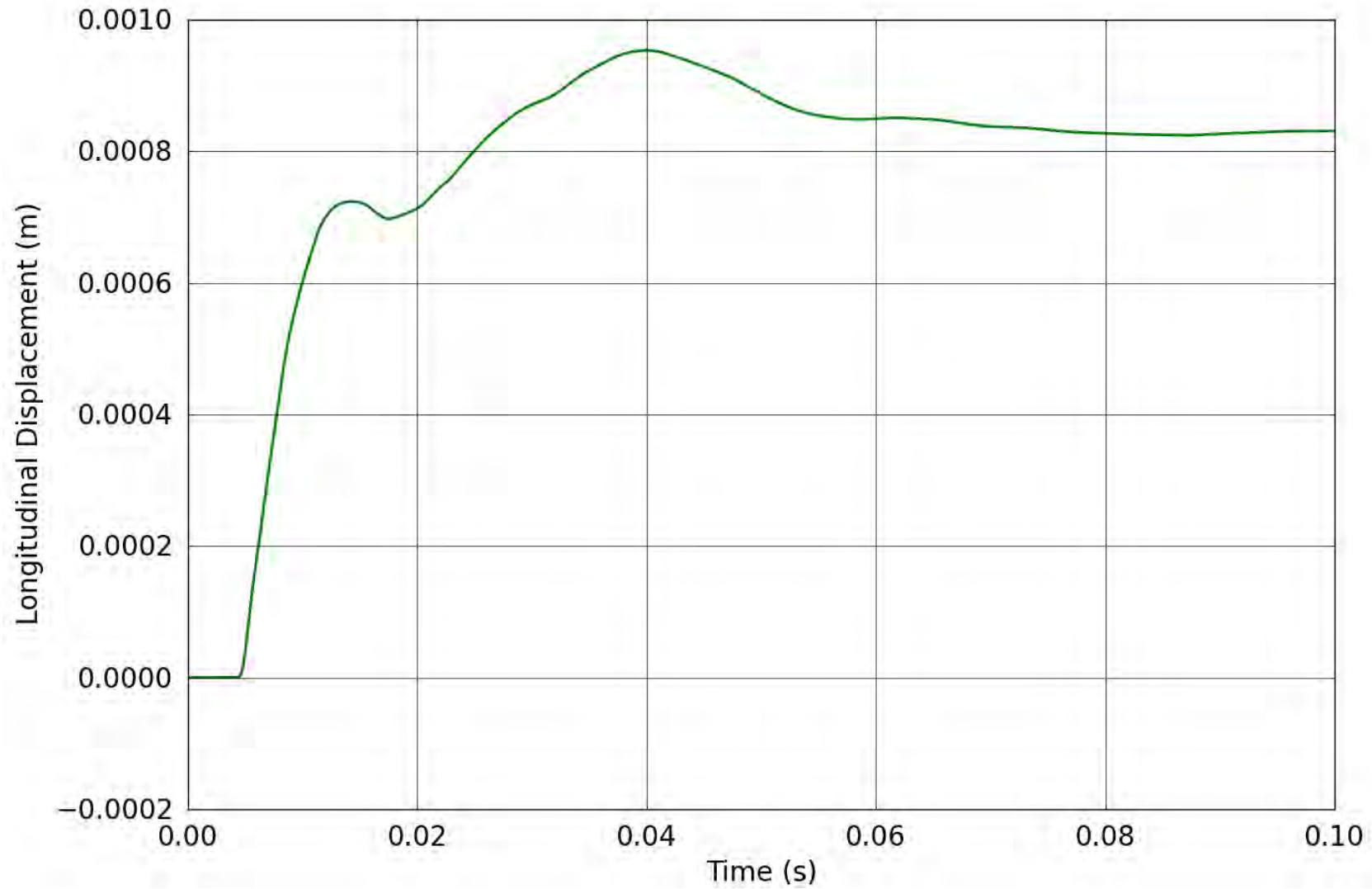


Figure 122. SPE-1 Gauge 6-2-L – Longitudinal displacement obtained from the corrected longitudinal velocity.

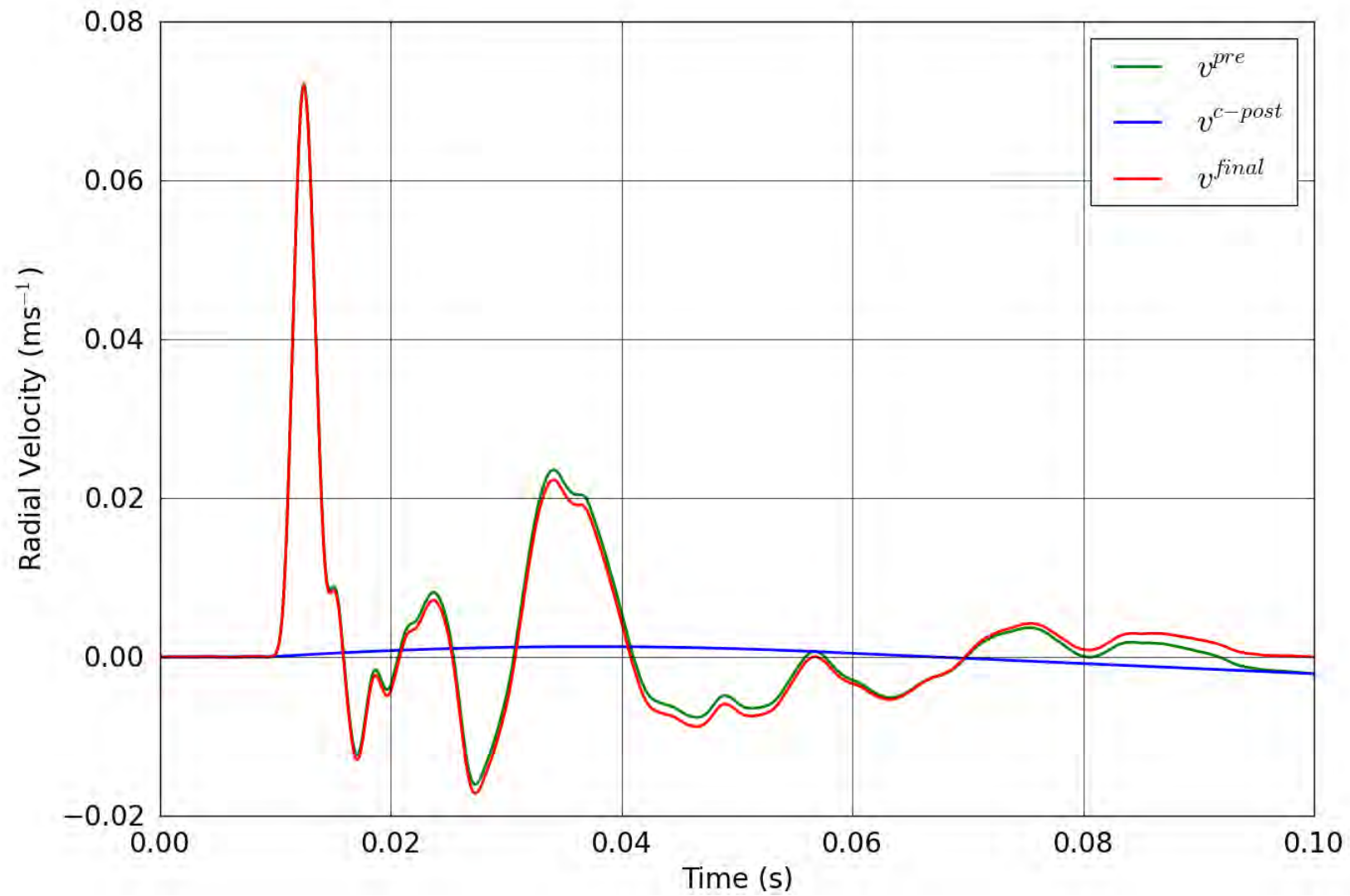


Figure 123. SPE-1 Gauge 6-3-R – Correction of the radial velocity.

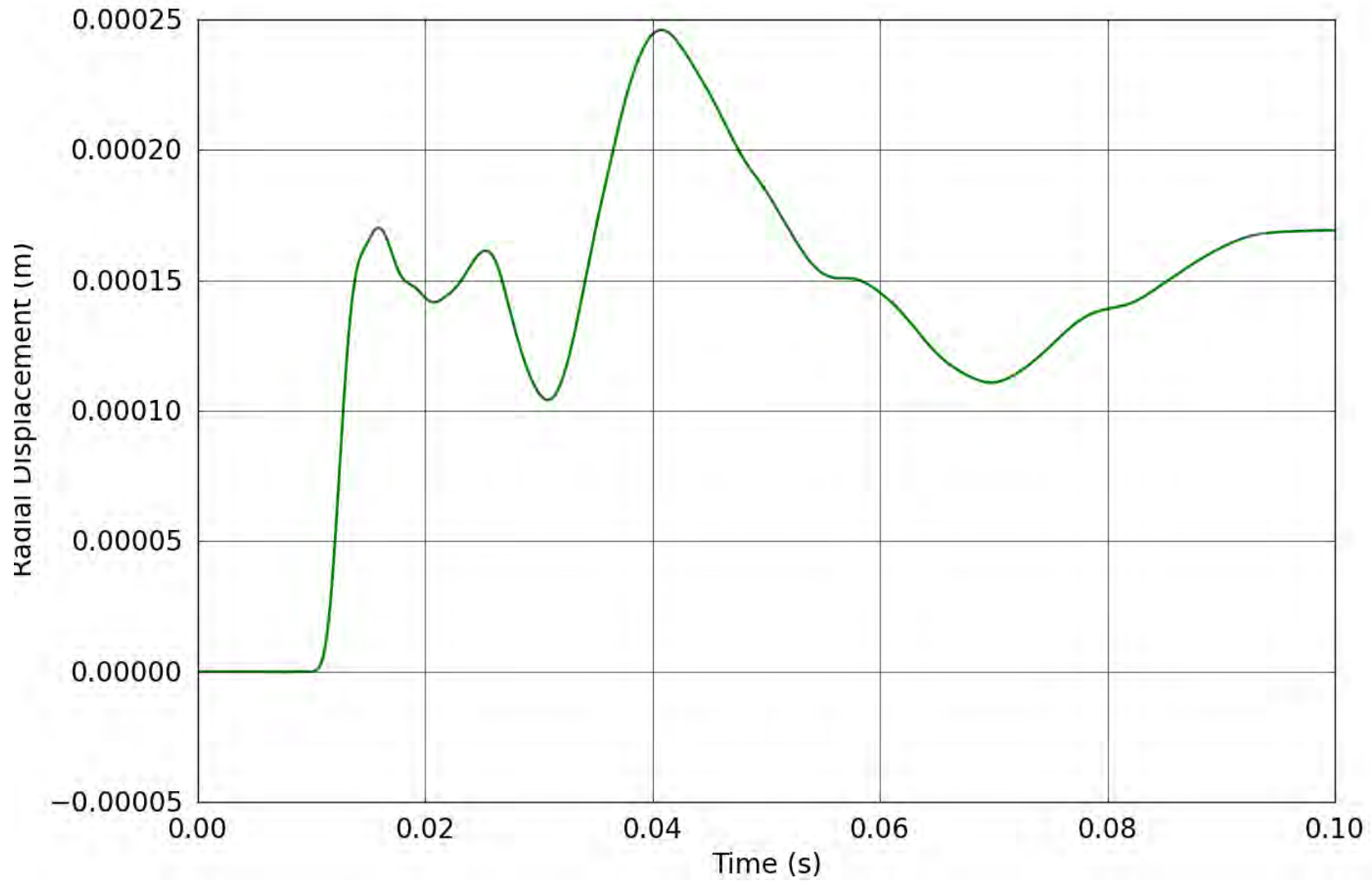


Figure 124. SPE-1 Gauge 6-3-R – Radial displacement obtained from the corrected radial velocity.

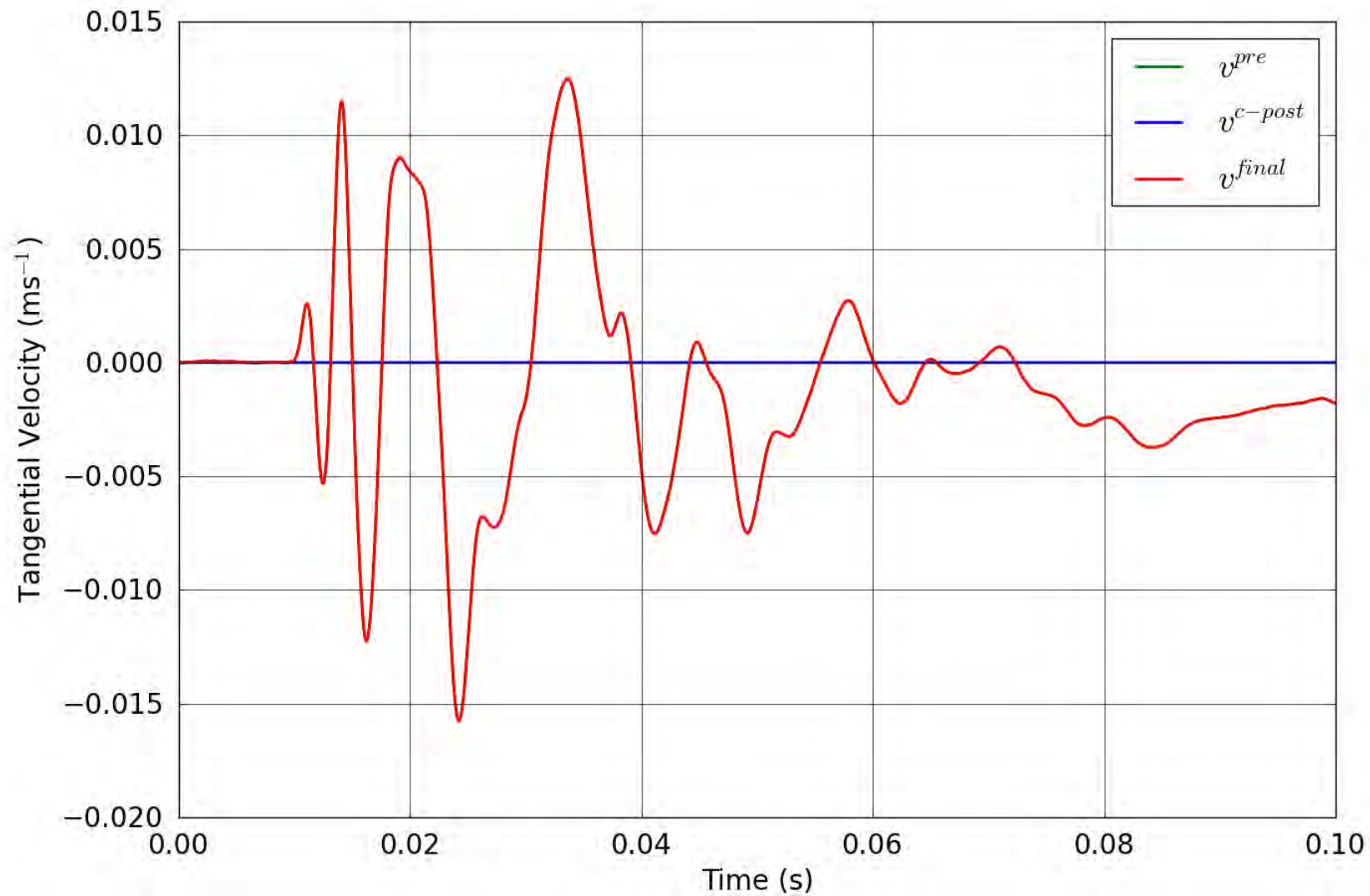


Figure 125. SPE-1 Gauge 6-3-T – Correction of the tangential velocity.

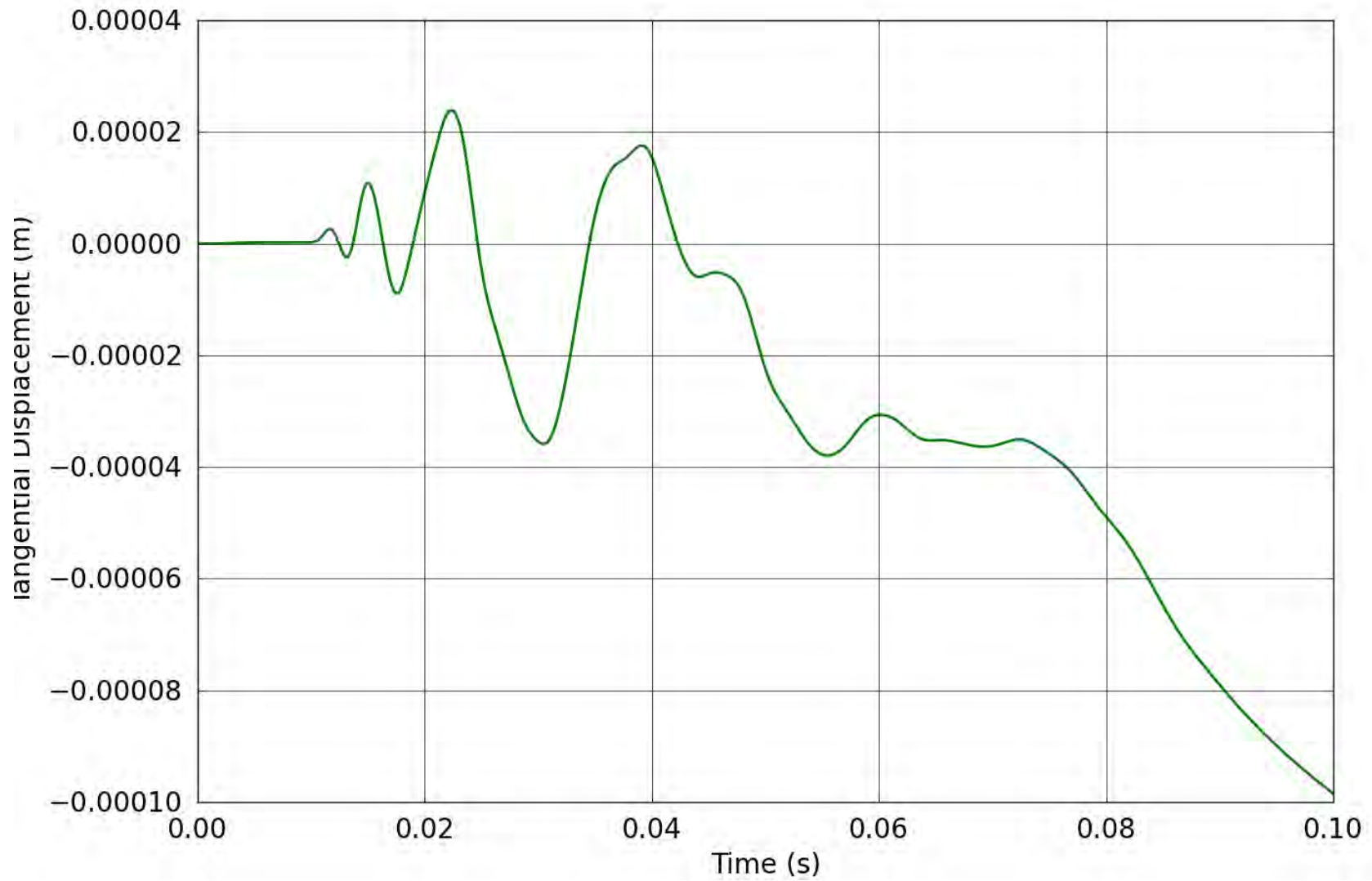


Figure 126. SPE-1 Gauge 6-3-T – Tangential displacement obtained from the corrected tangential velocity.

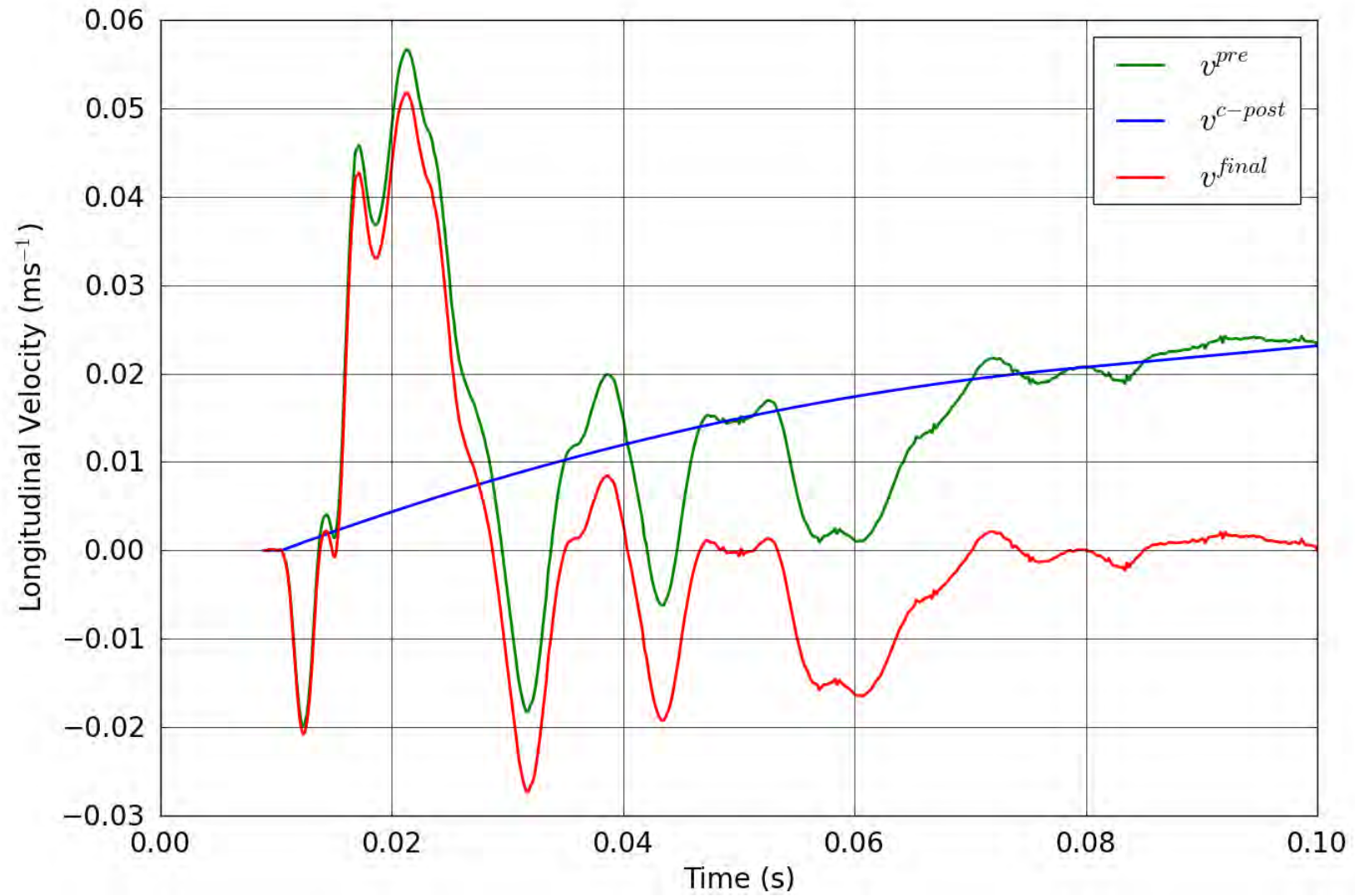


Figure 127. SPE-1 Gauge 6-3-L – Correction of the longitudinal velocity.

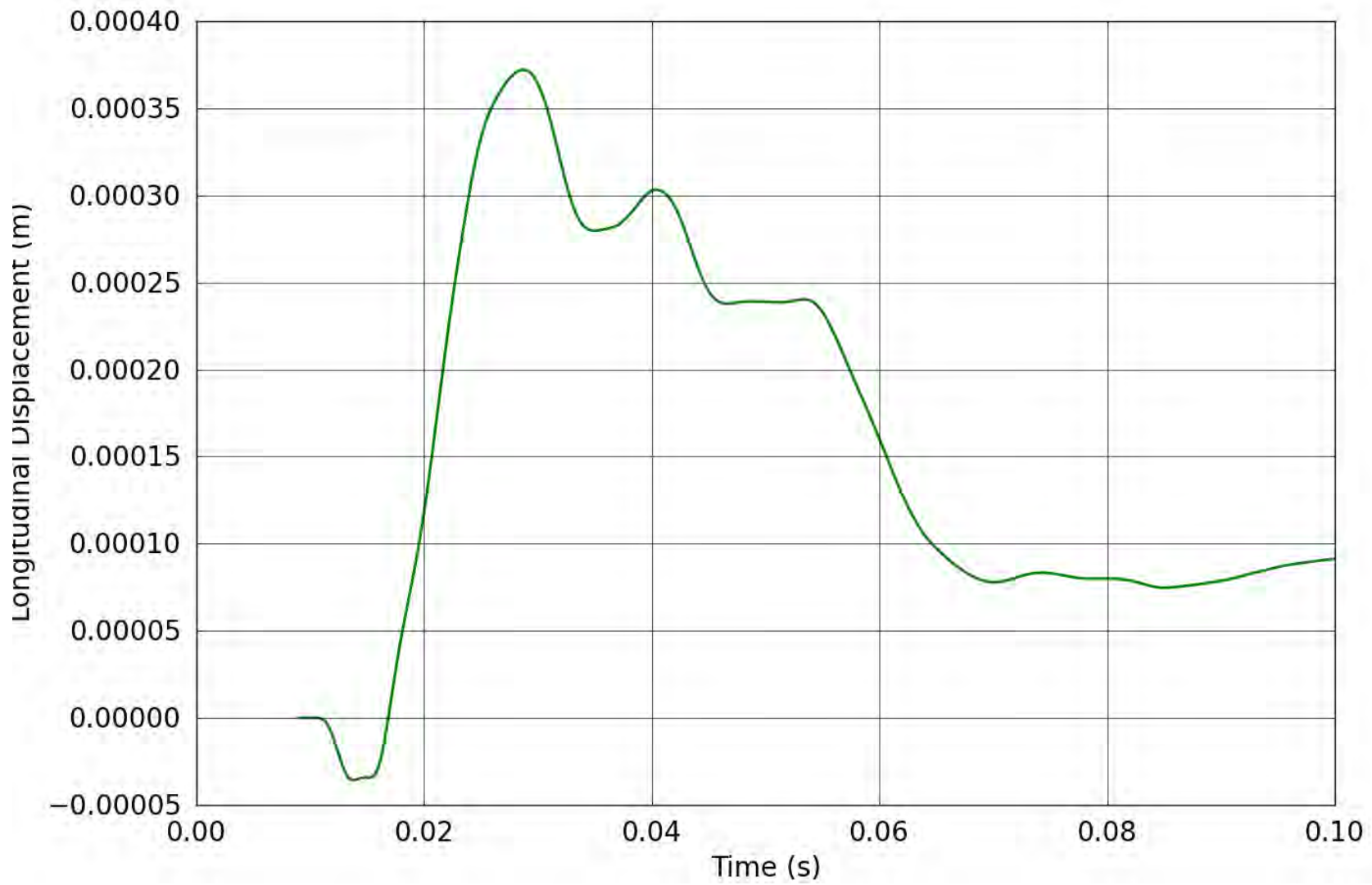


Figure 128. SPE-1 Gauge 6-3-L – Longitudinal displacement obtained from the corrected longitudinal velocity.

3. REFERENCES

1. Jeff Thomsen, SPE Acceleration Component Rotations: Shock Angle Analyses for Holes 1-6 Compared to SPE-3 Holes 7-11, PowerPoint Presentation, Oct. 2012.
2. Jeff Thomsen, SPE Data Acceleration Component Rotation Methodology, PowerPoint Presentation, Oct. 2012.
3. David W. Steedman, Review of Data from Shock Physics Experiments SPE-1, SPE-2 and SPE-3: Data Corrections and Phenomenology Analysis, LA-UR-13-22561, 19 April 2013.
4. Esteban Rougier and Howard J. Patton, Quality assessment of SPE free field data based on reduced displacement potentials, LA-UR-13-20277, PowerPoint Presentation, 16 January 2013.

Appendix 6
Review of Data from Source
Physics Experiment-1:
Data Corrections

Condensed version of Los Alamos National
Laboratory Report LA-UR-22561 (2013)
prepared by D. Steedman

Review of Data from Source Physics Experiment 1: Data Corrections

*The information in this appendix was extracted from
LANL publication LA-UR-13-22561 by D. Steedman*

INTRODUCTION

The NNSA is conducting a series of high explosive (HE) tests – the Source Physics Experiments – at the National Nuclear Security Site (NNSS). These experiments are intended to investigate the generation of geophysical signals from controlled sources. These signals will aid in the development of physics-based models to aid in the discrimination of signals emitted from these and other possible sources, such as earthquakes and clandestine nuclear events.

The SPE events include an array of accelerometers near to the source intended to provide measurements of the strong ground motion, or “near field,” regime. This report coincides with the release of these data for analysts and organizations that are not participants in this program. The report describes the various forms and location of near field data that are available.

DATA

This report coincides with the release of the data package for SPE-1. This includes the raw acceleration-time pairs recorded for all transducers. These data are in the form of time–acceleration pairs and are posted on the project data server. Files are in comma separated variables (csv) format.

This data release includes three additional sets of data histories representing each of three steps of data correction. These included, in successive order, correction for canister rotation, correction for pre-event baseline drift, and correction for baseline drift that occurs during an event. The first of these is a special case that was determined to be needed after a thorough review of data from SPE-1 and two subsequent events, SPE-2 and SPE-3. The other two corrections are standard requirements for acceleration records and were performed after this first correction was applied.

Data Corrections

Gauge Canister Rotations— An explosive event such as SPE-1 will produce a ground shock environment that is expected to follow a well-established theory of outward spherical propagation of compressive shock waves from a cylindrical, or near-spherical, source. Figure 1 provides an example of a set of velocity histories that conform to expectations at the shot depth for SPE-1. Gauge package 6-1 at the 20-m range is dominated by a large outward radial velocity with minor motion in the directions tangential (transverse and longitudinal) to the shock front.

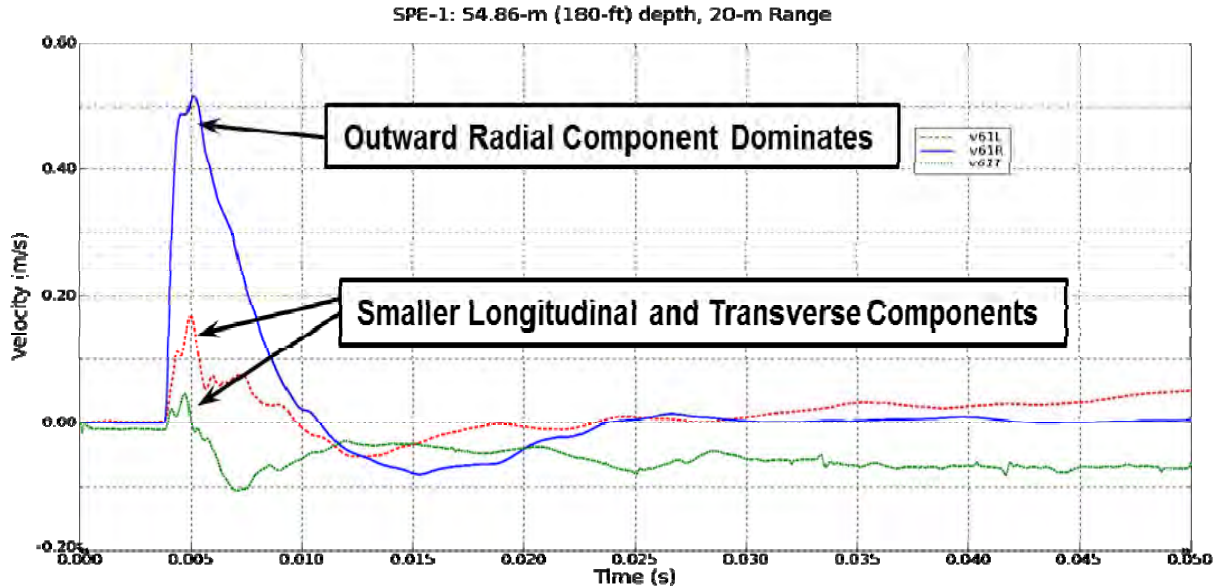


Figure 1: Consistent set of velocity histories for a cylindrical charge: gauge package 6-1.

But a review of other measurements in the SPE-1 set reveals some history sets that are not consistent with expectations. For example, while another gauge package at the same depth and range (*i.e.*, 4-1, Figure 2) shows similarly weak transverse and longitudinal components, the large radial motion is *inward*, or opposite of what one would expect from a compressive, explosively driven shock.

Another problematic response is observed in gauge package 2-1 (Figure 3) at the 10-m range at the shot depth. The radial and transverse components are similar in amplitude for this location. That is different than what is expected (*i.e.*, minor transverse component relative to the radial is expected).

The data from gauge package 3-1 (Figure 4) at the 10-m range at the shot depth is also suspect. The radial measurement in this plot is very low in magnitude and does not have the expected characteristic strong outward phase. On the other hand, the transverse component possesses a strong pulse which, notwithstanding the algebraic sign, possesses the character expected of a radial measurement.

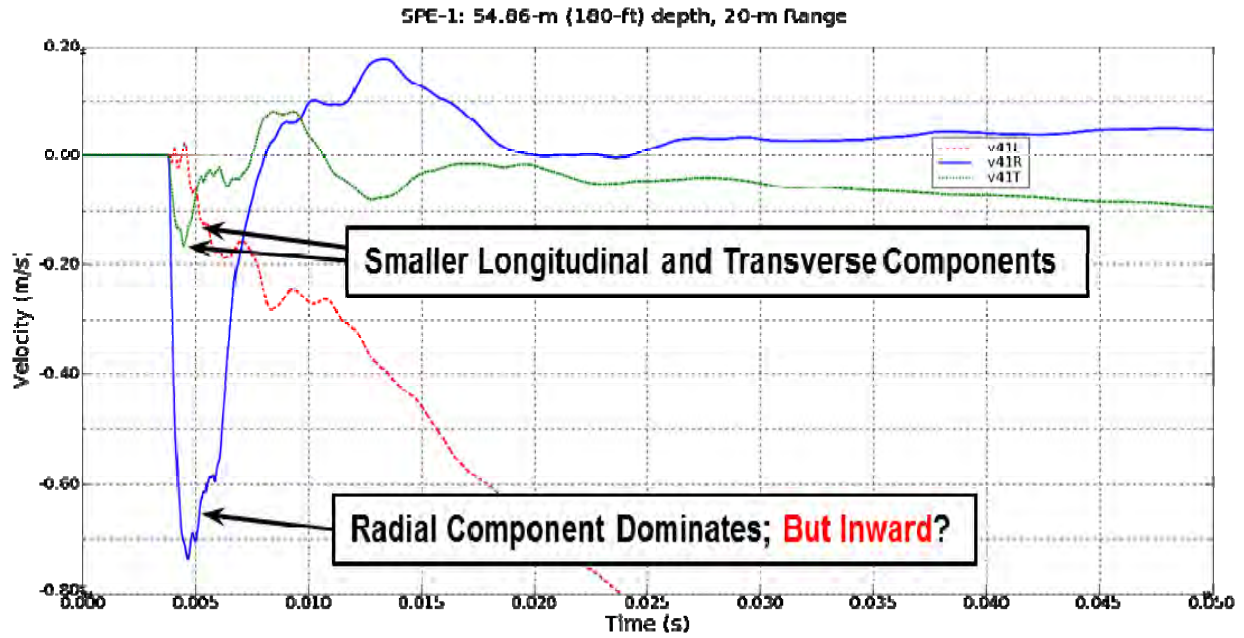


Figure 2: Consistent set of velocity histories for a cylindrical charge except for reversed direction radial: gauge package 4-1.

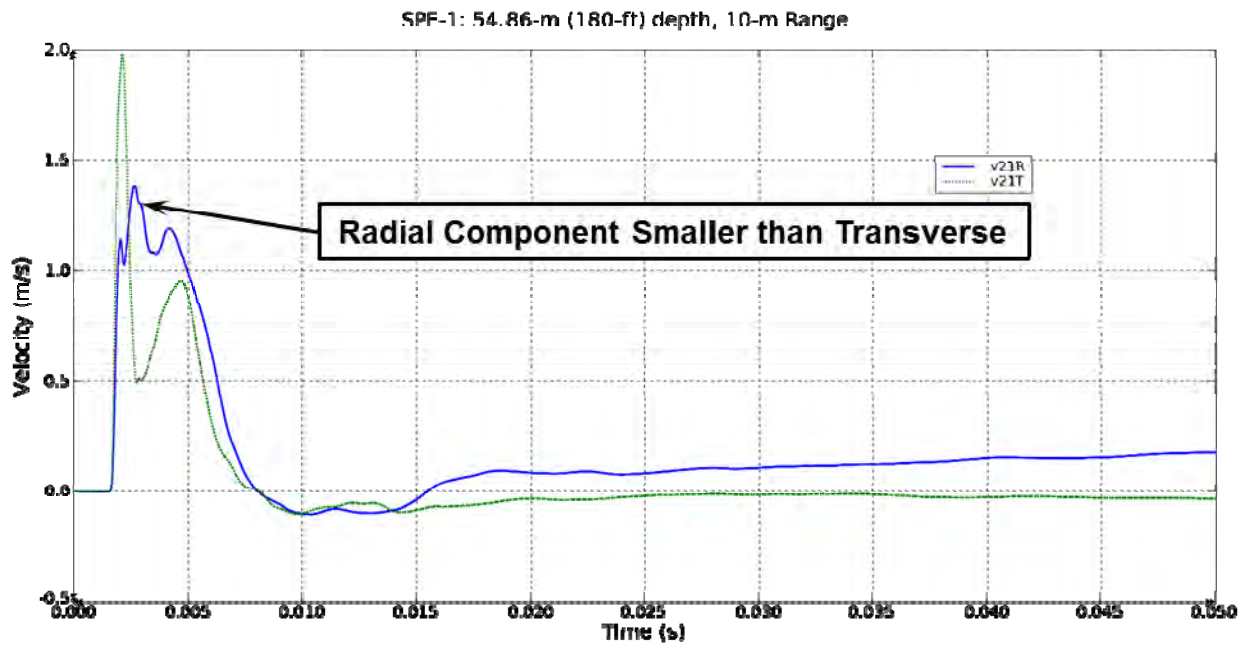


Figure 3: Inconsistent set of velocity histories for a cylindrical charge, including unexpectedly high transverse pulse relative the radial motion: gauge package 2-1.

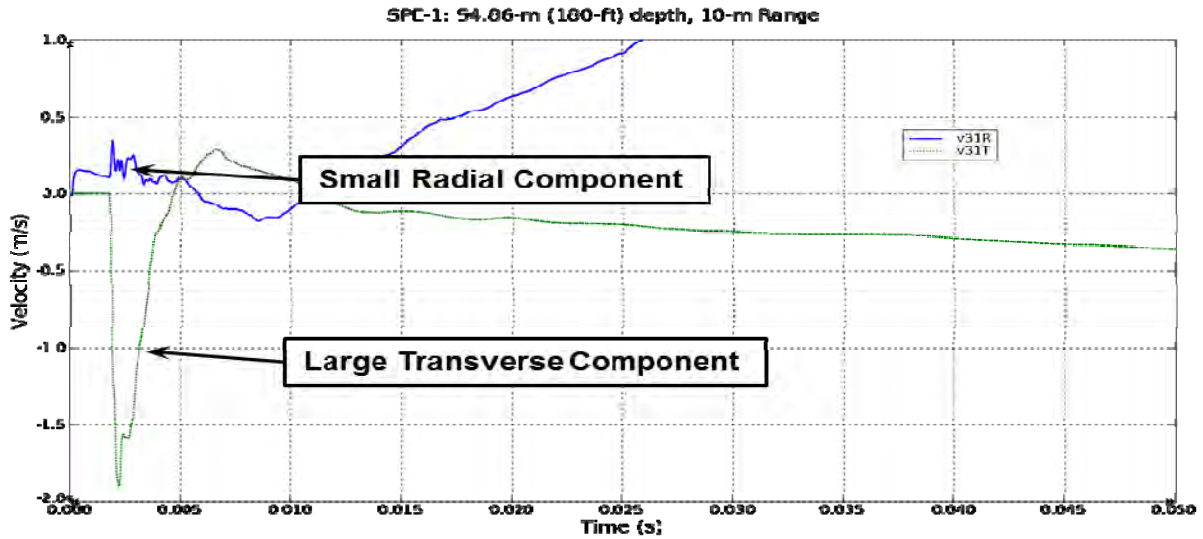


Figure 4: Inconsistent set of velocity histories for a cylindrical charge, including large transverse pulse with limited radial motion: gauge package 3-1.

Figure 3 and Figure 4 were used to illustrate relative response among the components in a given gauge package. Comparisons between data from different gauge packages also provide insight into problems with the gauges. Figure 5 includes one component from each of the gauges at the 10-m range at the shot depth. These are the radial measurement of 1-1 and the transverse components for 2-1 and 3-1 (note that we reversed the sign for the 3-1-T history). The similarity in both magnitude and character between radial and transverse measurements is unexpected. Similarly, the 2-1 radial component is nearly identical to the 1-1 transverse measurement (Figure 6). The fact that some transverse components closely track other radial components is compelling evidence of gauge rotation.

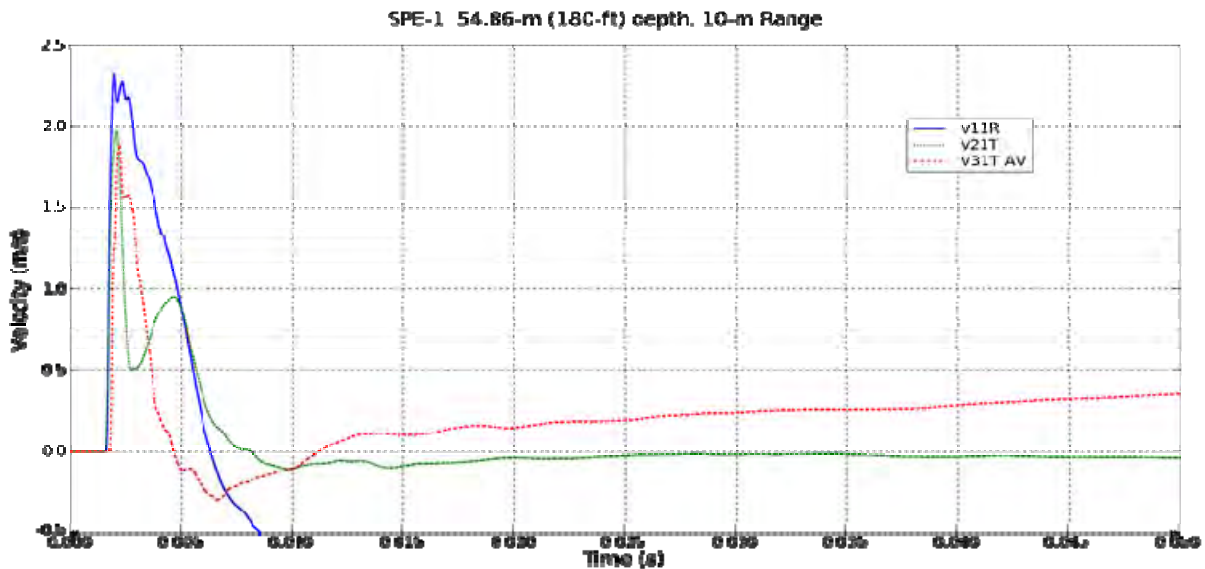


Figure 5: A radial velocity history (1-1) compared to two transverse velocity histories (2-1 and 3-1) at the same range and depth.

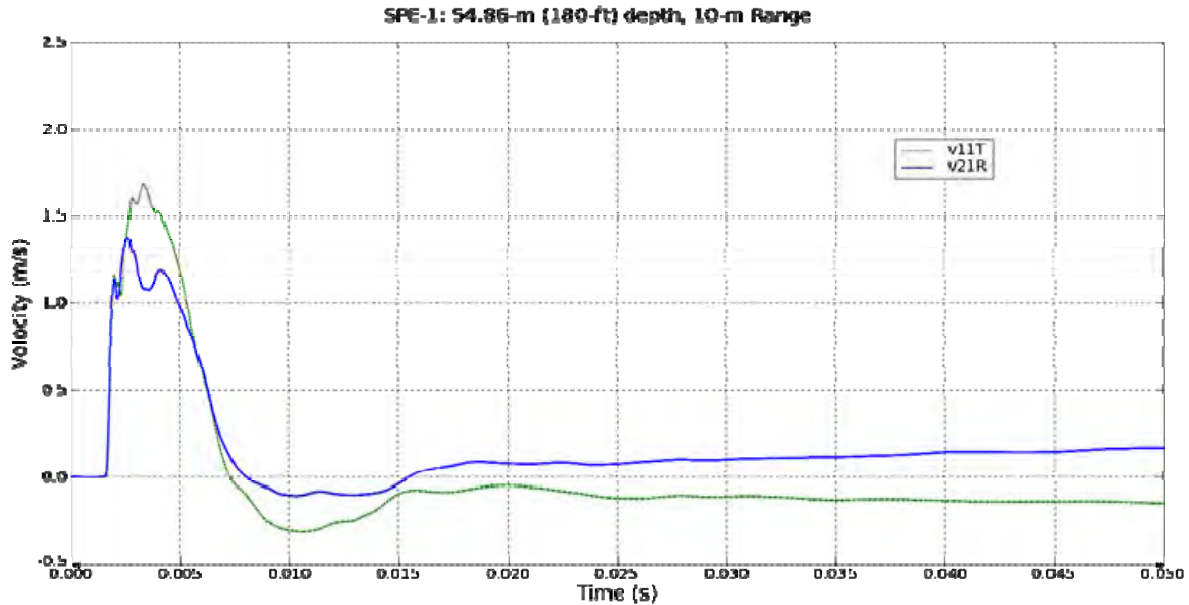


Figure 6: A radial velocity history (2-1) compared to a transverse velocity history (1-1) at the same range and depth.

Similar data anomalies are evident throughout the SPE-1 data set. These anomalies are summarized in a “stop light” chart (Figure 7) where we show all questionable canisters as red. Green represents gauge packages where no apparent anomalies were observed and black represents those locations for which no data were recovered due to inoperable gauges. A significant portion of these data are questionable.



Figure 7: Stop light chart summarizing data anomalies for SPE-1 and SPE-2.

While this report is intended to discuss the release of the SPE-1 data, it is necessary at this point to briefly introduce SPE-2, which is also illustrated in **Error! Reference source not found.** SPE-2 was a

1172-kg SHANFO source placed at the 150-ft depth in hole U15n and fired on 25 October 2011. The same instruments were used to record this event except that some gauges failed during or after SPE-1. Additionally, due to a large gauge loss in hole 1, an identical array of gauges was placed in a new hole 1A drilled nearby to hole 1 (see Figure 8).

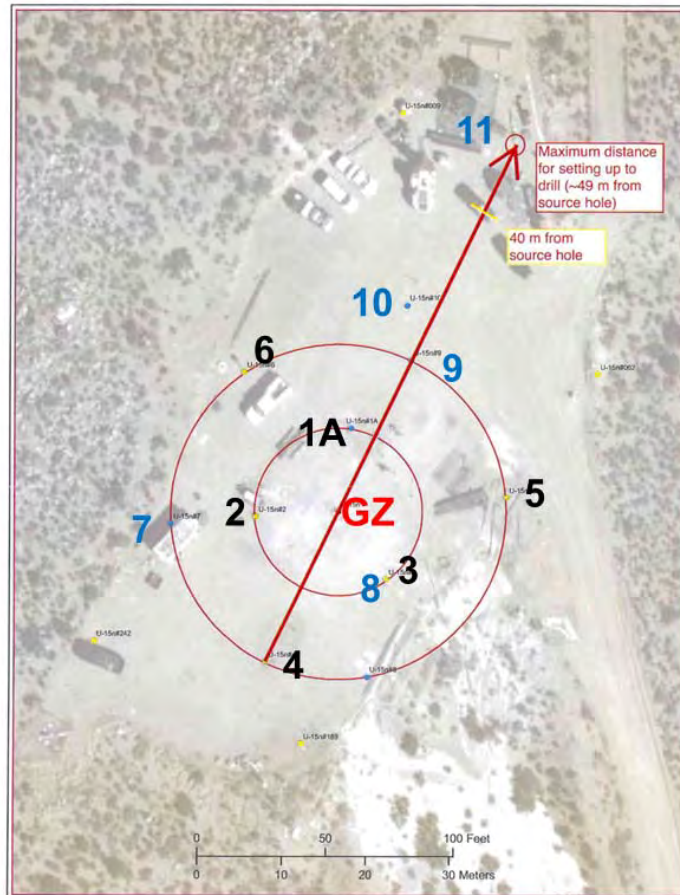


Figure 8: Instrument hole layout for SPE-3.

We will not provide examples here but the anomalies observed in SPE-1 were consistently repeated in SPE-2, as reflected in the second stop light chart in Figure 7. The two charts are consistent between the two events indicating persistence in anomalous behavior.

This includes the fact that that all gauge canisters at the 50-ft depth for both experiments performed as expected. These canisters are nearest to the surface and, thus, would have less opportunity to rotate. Finally, all canisters in the newer hole 1A appeared to yield acceptable data. These replacement gauges were placed with better quality control than the older canisters (Ref. 3).

The reader is referred to Reference 1 and Reference 2 for a comprehensive review of all data from these two events

Based on these observations the test team determined that it would be prudent to include extra gauge canisters for the next test in the series, SPE-3. SPE-3 was slightly smaller (1064.71 kg of SHANFO) than, but placed at the same location as, SPE-2 and fired on 24 July 2012.

These new canisters served two purposes: to provide redundant data for questionable canisters and to fill-in for areas of the test bed where more data coverage was desired. Figure 8 illustrates the layout of these new holes, numbered 7, 8, 9, 10, and 11. Holes 7 and 8 on the 20-m and 10-m rings, respectively, and hole 11, 45 m from the charge hole, had canister depths identical to the older holes; that is, at 50 ft, 150 ft, and 180 ft from the ground surface. Hole 9 on the 20-m ring had canisters at those depths as well as at 90 ft and 120 ft from the ground surface. Hole 10 was a slant hole drilled from the surface location indicated through the SPE-2 charge center, and had a single radial (*i.e.*, in the line of the hole axis) transducer at a distance of 12 m from the charge.

Comparisons between the data from these two events provide adequate evidence into whether some canisters in holes 1 through 6 rotated during placement. For example, Figure 9 presents the data for the radial and transverse transducers (there were no longitudinal transducers active) from canister 6-1 for shots SPE-2 and SPE-3. This canister provides reasonable data in that a large outward radial measurement is accompanied by a relatively small transverse component. The records for both components are consistent between the two events.

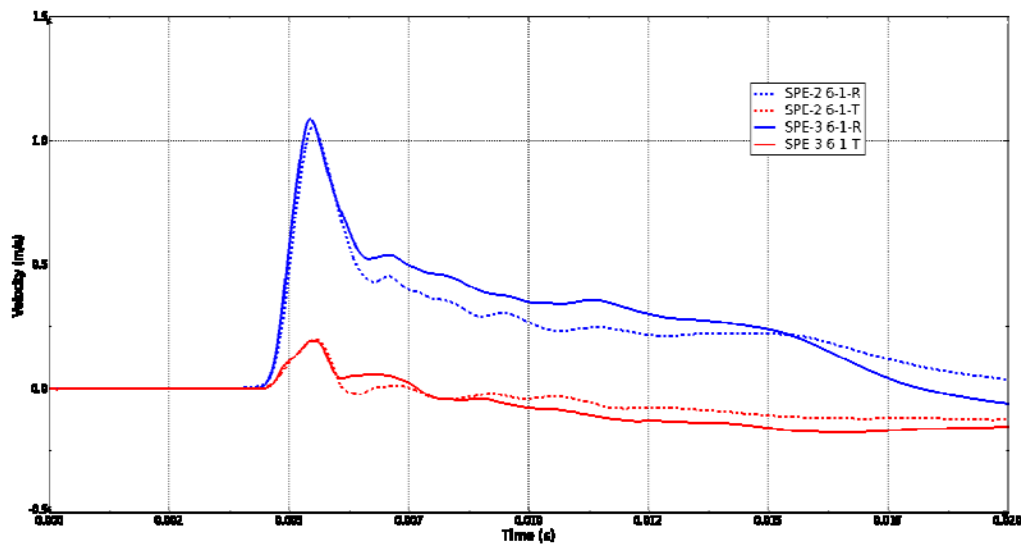


Figure 9: All data components recorded by canister 6-1 from both SPE-2 and SPE-3.

Figure 10 presents the data for these same tests from canister 2-1 where the relative magnitudes between radial and transverse components were previously described to be questionable (Figure 3). As in SPE-1, the transverse component is larger than the radial component which is inconsistent with the response expected. The significant longitudinal component is a reasonable response as the canister is located 45° below the shot point and so the spherically propagating shock will have a significant vertical component. All of the records for canister 2-1 are consistent between the two events.

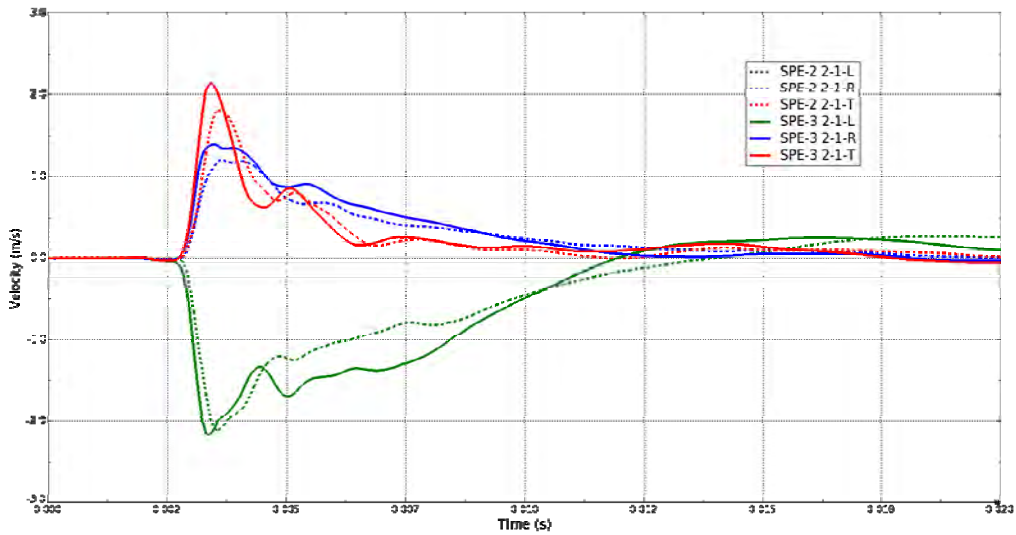


Figure 10: All data components recorded by canister 2-1 from both SPE-2 and SPE-3.

Figure 11 includes SPE-2 and SPE-3 data for canister 6-2 which was dominated completely by the supposed transverse measurement with apparently inconsequential motion in the radial direction. Again, the histories for all transducers are consistent between events but inconsistent with expectations.

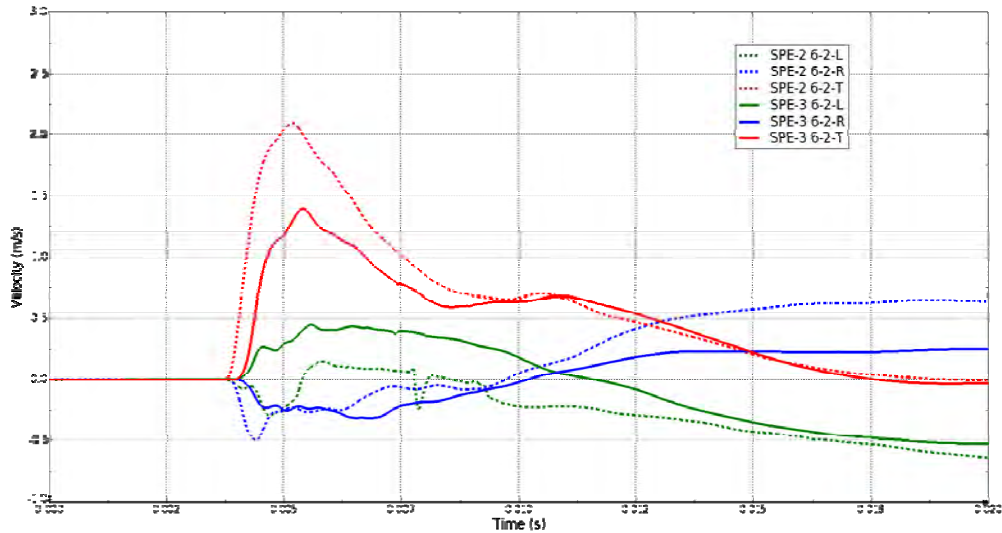


Figure 11: Velocity histories from location 6-2 for SPE-2 and SPE-3.

The above examples used data from three canisters to display consistency between two events with identical locations and nearly identical yields. It is an important observation that one of these (6-1) had reasonable radial-to-transverse component amplitude comparisons while the other two (2-1 and 6-2) provided unexpectedly high transverse magnitudes relative to their respective radial magnitudes. This provides evidence that SPE-3 was a reasonable replication of SPE-2, thus allowing comparisons between

SPE-3 histories from questionable canisters and those from the redundant newer canisters. In other words, the quality of the data from questionable gauges can be judged by the data recovered from the redundant gauges.

For example, reference to Figure 8 reveals that hole 7 was drilled on the 20-m ring on the same radial as hole 2 on the 10-m ring. But while canister 2-1 (Figure 10) appeared to experience questionable transverse-to-radial magnitudes, canister 7-1 (Figure 12) reveals a set of histories that is fully consistent with a shock environment dominated by radial motion (*i.e.*, large radial component accompanied by an insignificant transverse contribution). Canister rotation is a reasonable explanation of the canister 2-1 response.

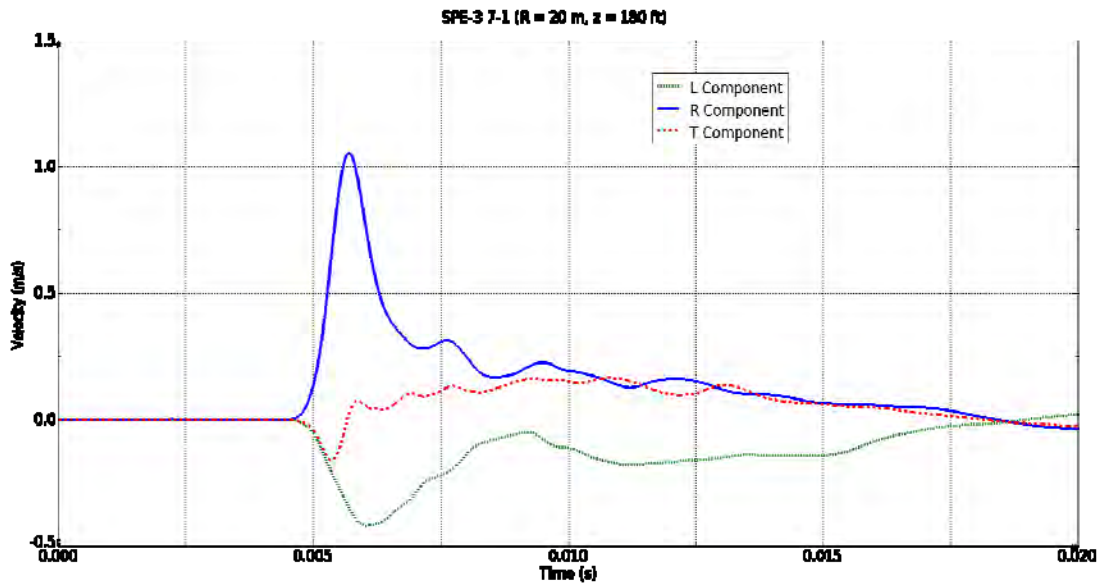


Figure 12: Velocity histories from location 7-1 for SPE-3.

Another example is the comparison in Figure 13 between data from older canister 3-2 and newer canister 8-2 which is nearby on the same radius ring. The 3-2 canister transducers were inoperable for SPE-3 and so those data are from SPE-2; the data at 8-2 are from SPE-3. Other comparisons have already established consistency between those two events, and so comparison between these two nearby canisters is relevant. Specifically, location 3-2 displays uncharacteristically high transverse negative amplitude accompanied by an insignificant radial record. But location 8-2 experienced a high outward radial velocity and a low magnitude transverse velocity. It is unrealistic that the shock environment can change by such a large amount in the short distance between hole 3 and hole 8 and this difference must be explained by rotation of canister 3-2 during installation.

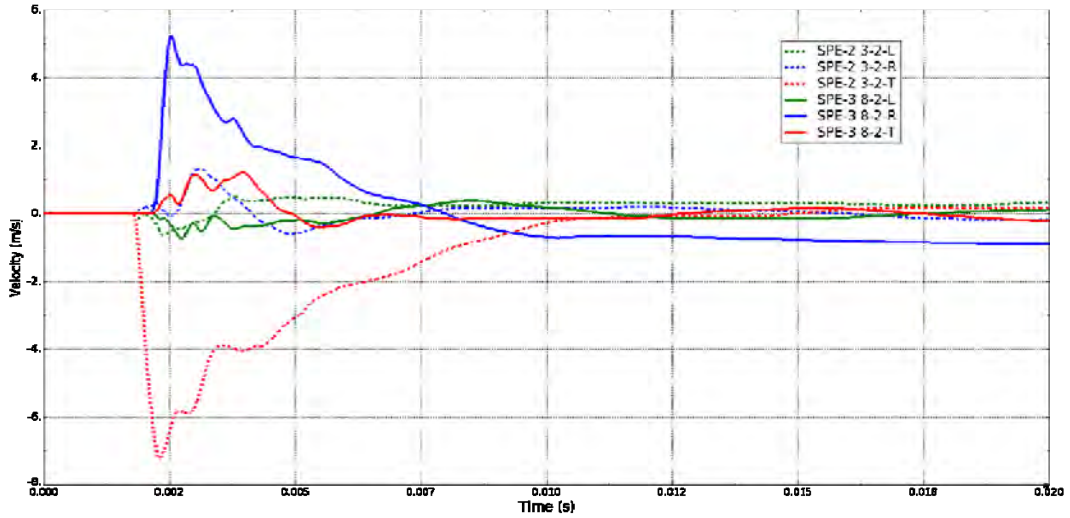


Figure 13: Velocity histories from location 3-2 for SPE-2 and location 8-2 for SPE-3.

Finally, reference to Figure 8 shows that older hole 6 is roughly in the middle of an arc between newer holes 7 and 9 on the 20-m ring. Canister 7-2 (Figure 14) and canister 9-2 (Figure 15) have reasonable relative radial and transverse motions while canister 6-2 (Figure 16) is unreasonable in this respect. It is unlikely that the azimuth to hole 6 would have such a significant difference in the environment relative to the azimuths on either side.

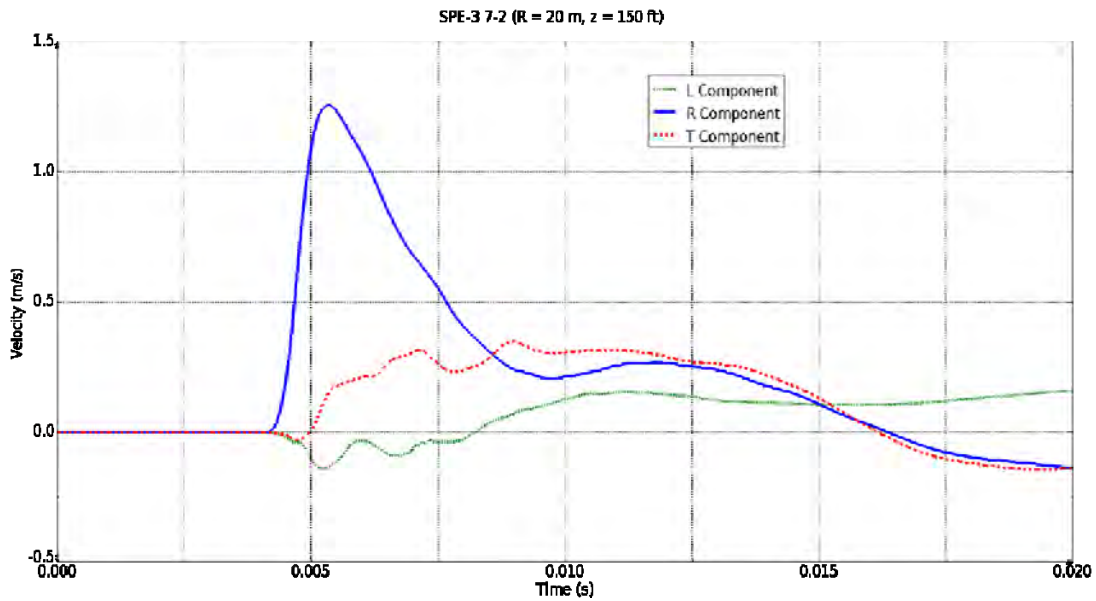


Figure 14: Velocity histories from location 7-2 for SPE-3.

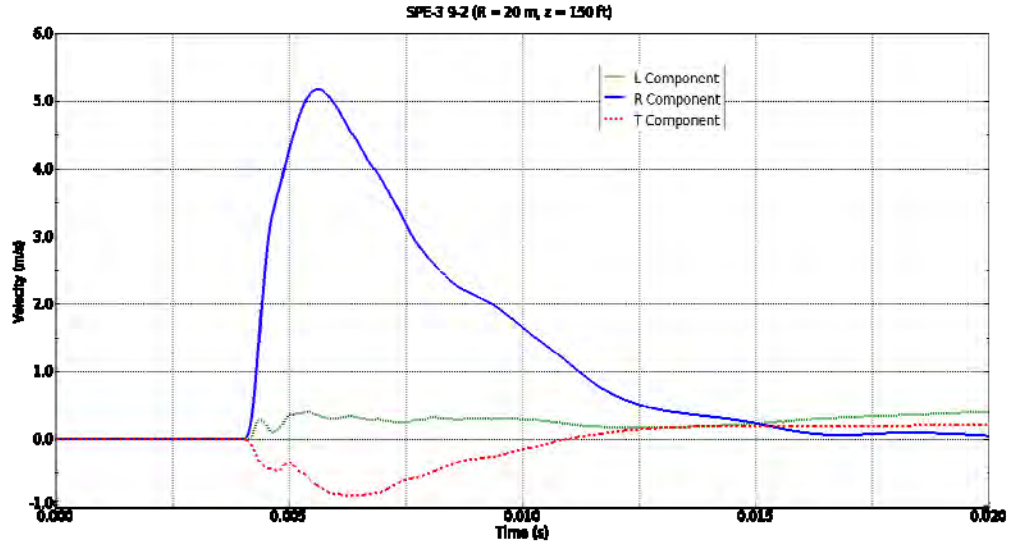


Figure 15: Velocity histories from location 9-2 for SPE-3.

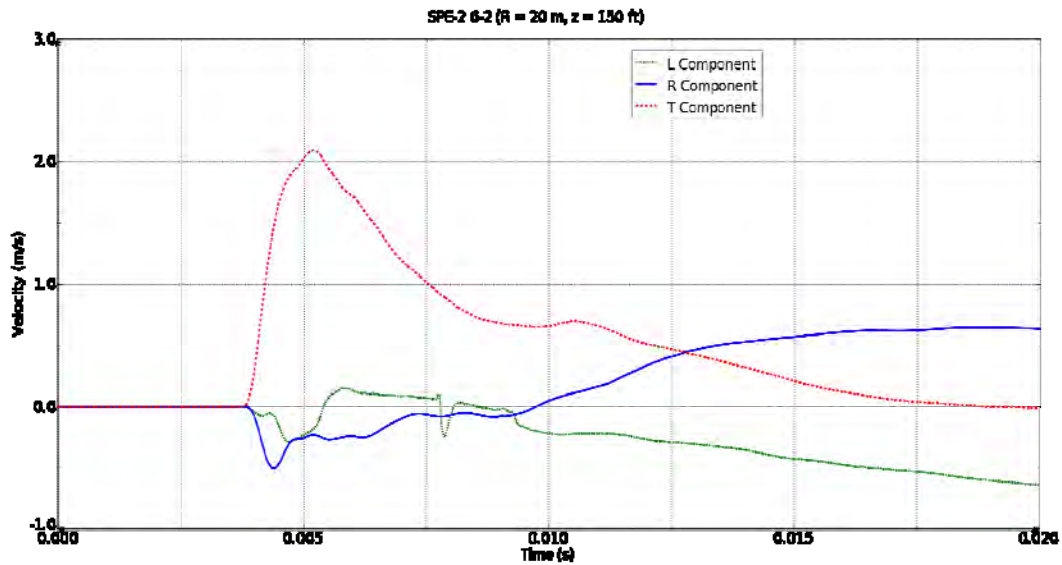


Figure 16: Velocity histories from location 6-2 for SPE-3.

The above discussion reviewed the relative horizontal components of canister histories. The general premise is that for a spherical or cylindrical explosive source the shock environment should be dominated by outward radial motion, with smaller contributions in the orthogonal tangential directions. Reference 4 presents more comparisons of these data that will not be repeated here. Instead, the full SPE-3 data set is summarized by plotting the radial peak velocity vs. the tangential peak velocity for every canister in Figure 17.

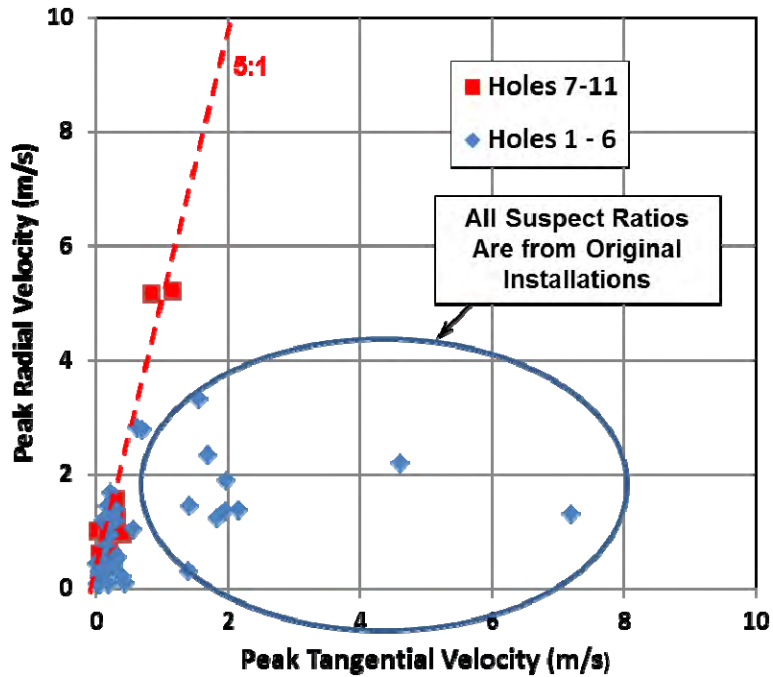


Figure 17: Peak radial velocity vs. peak transverse velocity for all canisters in SPE-3

A fit to the data from only the newer holes suggests that the transverse velocity is about 20% of the radial velocity (*i.e.*, radial is five times the transverse). This is also true of a subset of the older canisters. However, a number of locations have peak transverse velocities that are equal to or greater than the respective peak radial velocity. All of those data points represent older installations. The response of all canisters installed using high quality control (holes 7 through 11) is clearly dominated by radial motion.

A final summary of these data can be seen in Figure 18 which is an updated version of the “stop light” chart shown earlier. It repeats the chart from SPE-2 and includes a similar chart for SPE-3 including both the older and the newer canisters. The figure illustrates: 1) the older gauge response was consistent between the two events and 2) all new gauges provided reasonable data.

These findings were presented in a briefing (Ref. 4) to the SPE Subject Matter Experts (SME) panel and subsequently to the National Center for Nuclear Security (NCNS) Executive Advisory Board (EAB). The recommendation that the radial and transverse data from those gauges be corrected for rotations was accepted by both of these review groups.

Reference 5 describes the correction methodology, while Reference 6 includes the magnitudes of those corrections. Both of these documents are available on the project data server. The records resulting from these corrections are posted on the data server.

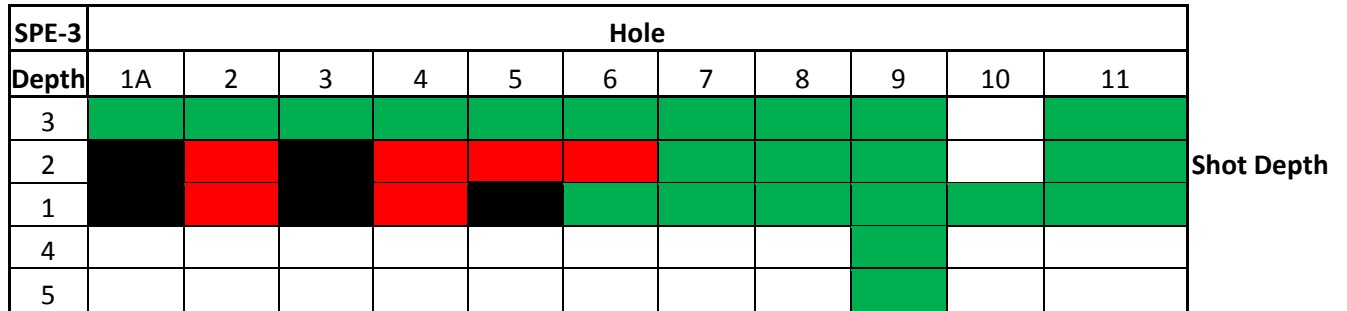


Figure 18: Figure 19: Stop light chart summarizing data for SPE-2 and SPE-3 including new gauge canisters.

Pre-Event Zero-Shift Corrections— When examining data obtained from accelerometers a zero-shift is often observed both prior to and during an event. In a piezoresistive sensor pretest “zero-shifts” may be due to the sensor being out of balance or thermal effects. This type of zero-shift is generally easy to correct as it is normally a uniform shift from what should be zero amplitude; that is, before the shot there should be no motion).

This is typically inconsequential to acceleration character and amplitude. However, velocity is achieved through integration of these acceleration records, and the shift in acceleration can translate into a significant cumulative error. This error can measurably alter the velocity peak amplitude and outward phase to an extent that can change the assessment of the ground shock environment caused by the explosive event.

Consequently, to facilitate analysis of velocity from these records we provide baseline corrected acceleration records for these transducers. These corrections were made by reading the digital data record up to fiducial. As these data should be null, or zero acceleration, the average of these pre-fiducial data is representative of the DC shift. This average value is subtracted from the entire raw data record to generate a new data file for each measurement corrected for zero-shift. Reference 7 describes the magnitudes of shift applied to all data.

Users are welcome to perform their own corrections to the data, or to operate on the uncorrected data as they see fit. We provide corrected data records on the data server to facilitate consistency among analyses. Any alternate approaches to data corrections should be documented by the user. We note

here that the velocity records used to describe the canister rotation analysis in the prior section included zero-shift corrections.

During Event Zero-Shift Corrections— Zero-shifts occurring during an event pose a larger problem and are less tractable than the pre-event zero-shift. Accelerometer data that never returns to baseline, or zero, will result in continually increasing, or decreasing depending on the shift direction, velocity and displacement while, in reality, a static equilibrium state must be achieved. But these shifts are harder to correct.

The shift can reflect several possible phenomena, or combination of phenomena. These include overstressing the piezoelectric crystals, physical movement in the sensor parts, excessive base strain, excessive cable motion, or overloading the signal conditioning. There is not a straight forward way to correct for these phenomena and we recommend caution in accomplishing these corrections and in using the resulting displacements for analysis, such as in the Reduced Displacement Potential (RDP) analysis discussed in Reference 8.

Reference 7 includes a discussion of corrections made for this second drift. Basically, a reasonable estimate was made on the correction required to bring the late-time velocity to a zero-amplitude baseline. Some degree of judgment was required to make these adjustments and so they must be viewed with caution. Nevertheless, an additional set of data with these corrections applied is available on the project data server.

REFERENCES

1. Steedman, D. W., "LANL Review of SPE-2 Near Field Velocity Data," Presented to the SPE SME Data Review, Los Alamos National Laboratory, Los Alamos, NM, January 2012.
2. Steedman, D. W., "Supplement to: LANL Review of SPE-2 Near Field Velocity Data," Presented to SPE Data Review Team, Los Alamos National Laboratory, Los Alamos, NM, January 2012.
3. Shah, K., personal communication, 2011
4. Steedman, D. W., Shah, K., and Hemming, X., "Review of SPE Near Field Accelerometer Data," Presented to the NCNS Executive Advisory Board, 13 September 2012
5. Thomsen, J., "SPE Data Acceleration Component Rotation Methodology," Applied Research Associates, Albuquerque, NM, 22 October 2012.
6. Thomsen, J., "SPE Acceleration Component Rotations: Shock Angle Analyses for Holes 1-6 Compared to SPE-3 Holes 7-11," Applied Research Associates, Albuquerque, NM, 31 October 2012
7. Rougier, E., "SPE-1 Baseline Shift Corrections," Los Alamos National Laboratory, Los Alamos, NM, May 2013.
8. Rougier, E., and Patton, H.J., "Quality Assessment of SPE Free Field Data Based on Reduced Displacement Potentials," LA-UR-13-20277, Los Alamos National Laboratory, Los Alamos, NM, 16 January 2013.